

Dissertation
Graduate School of Systemic Neuroscience,
Ludwig-Maximilians-Universität
München



Graduate School of
Systemic Neurosciences
LMU Munich

Functional characterization of the neural components in *Drosophila* motion detection

Submitted by

Matthias Meier
5th of April 2016



Matthias Meier: Functional characterization of the neural components
in *Drosophila* motion detection,
Dissertation
Graduate School of Systemic Neuroscience,
Ludwig-Maximilians-Universität
München, 2016.

WEBSITE:

<http://www.neuro.mpg.de/>

E-MAIL:

meier.matth@gmail.com

First reviewer (supervisor)
Prof. Dr. Alexander Borst

Second reviewer
PD Dr. Lars Kunz

Date of submission
2016, April, 5th

Date of defense
2016, August, 31st

ABSTRACT

Flies, among many other species mainly rely on visual information to safely navigate through their environment. Behaviors like finding appropriate food sources or potential mates, avoiding obstacles and predators, or simply stabilizing their flight or walking trajectory are executed based on visual cues in their surroundings. Optic flow on the flies' eyes for instance helps them to respond to disturbances caused by external distractors like a gust of wind. In order to do so, the animal has to extract relevant information about the produced optic flow. Calculating features, such as the speed and direction of motion is crucial for their successful compensation. A possible model for the computation of direction selectivity in *Drosophila melanogaster* is based on asymmetric temporal filtering of signals originating from two neighboring photoreceptors in the retina. Wide field neurons in the lobula plate of the fly's optic lobes have long been known to respond in a direction-selective way. The computations in the upstream neuropils that lead to direction selectivity, however, have not yet been described. During my PhD-thesis, I characterized neurons presynaptic to direction-selective lobula plate tangential cells by exploiting the genetic toolbox of the fruit fly in combination with physiological techniques. The use of genetically encoded calcium indicators and two-photon microscopy allowed me to directly investigate response properties of small columnar elements prior to the lobula plate. Expressing neuronal silencers in distinct subtypes of neurons and simultaneously recording from lobula plate tangential cells, I could further probe the contribution of these elements to the computation of direction-selective signals. Combining these techniques with several other methods available in our laboratory, including a behavioral readout of tethered walking flies, optogenetic activation, pharmacology, and modeling, resulted in a total of six publications that comprise this cumulative thesis.

Measuring calcium signals in T₄ and T₅ cells in the first study, established that both populations of neurons exhibit direction-selective response properties. Furthermore, T₄ cells only respond to moving bright edges, whereas T₅ cells encode exclusively dark motion. Silencing the synaptic output of T₄ and T₅ separately, we were able to determine that both lobula plate tangential cell responses as well as the turning behavior of walking flies were impaired only to bright or dark edges, respectively. We thus proposed that the detection of the direction of visual motion must happen either presynaptic to, or on the dendrites of T₄ and T₅ neurons, and that this computation takes place independently for brightness increments and decrements.

The second paper published in 2014 was motivated by an anatomical study that found an asymmetric wiring between L₂ and L₄ cells with the dendrites of Tm₂ in the distal medulla. Using two-photon calcium imaging and neuronal silencing combined with postsynaptic electro-

physiological recordings, we probed the contribution of L4 and Tm2 in the OFF pathway of *Drosophila* motion vision. We found that while Tm2 have small, isotropic, laterally inhibited receptive fields, L4 cells respond to both, small and large field darkening. Blocking the output of both cell types resulted in a strong impairment of OFF motion vision. In contrast to the anatomical prediction, we did not observe any directional effects for either of the cells.

In the third study we used two-photon calcium imaging to investigate spatial and temporal response properties of transmedullary neurons Tm1, Tm2, Tm4, and Tm9 that have been proposed by an anatomical study using electron microscopy to be presynaptic to direction-selective T5 cells. We found that while their spatial properties are largely similar, they differ distinctly in their temporal characteristics, ranging from fast, transient Tm2 and Tm4 cells to intermediate Tm1 and finally to slow, sustained Tm9. Modeling their temporal filters, we could show that combinations of two of the four cell types result in motion detectors with functionally plausible tuning properties. When we tested their contribution to OFF motion vision, by recording visually evoked responses in direction-selective lobula plate tangential cells while silencing the output of single Tm cells, as well as combinations of two cell types, we observed that all of them are involved in the detection of dark edges, albeit to different extents. Taken together, in this study we provided evidence that the computation of direction selectivity on the dendrites of T5 cells is achieved by a complex interaction between Tm1, Tm2, Tm4, and Tm9 cells.

In the fourth paper the cellular mechanisms of the null direction responses found in direction-selective lobula plate tangential cells were characterized. Optogenetic activation of T4 and T5 cells demonstrated that responses in postsynaptic tangential cells consist of a fast excitatory as well as a slower inhibitory component. Through immunostainings we were able to reveal the cholinergic nature of T4 and T5 cells. Pharmacological experiments during recordings from tangential cells confirmed that the excitatory component is mediated by acetylcholine, whereas the inhibition must be accomplished by feedforward mechanisms via – at that time – unidentified neurons.

Measuring *Drosophila's* turning behavior in a paper published in *Neuron* in 2015, we could demonstrate that flies are – similar to humans – susceptible to optical illusions. By supplementing behavioral experiments with genetic silencing techniques, electrophysiological recordings and modeling we could dissect the functional and neural mechanisms underlying this observation. We found that the computation of spatial contrast, rather than absolute luminance forms the basis for a parallel visual pathway that remains functional even in the absence of local motion detectors T4 and T5. Measuring the voltage signals in lobula plate tangential cells indicated that contrast vision, just like motion vision, is mediated by these wide field neurons. Blocking the output of presynaptic columnar neurons that have been shown to be involved in the computation of directional signals in the ON-selective motion pathway also affected responses to contrast stimuli. Hence,

the contrast and motion vision pathways share common elements in the beginning, however diverge into two independent parallel streams.

In the final publication of my thesis, we investigated the functional differences between the ON and the OFF channel of *Drosophila* motion vision. To our surprise, we found that flies that lack one of the two processing streams due to genetic manipulations (blocking either T4 (ON) or T5 cells (OFF)) perform almost equally well in optomotor experiments. *In vivo* calcium imaging and electrophysiological investigations, however, revealed substantial differences in the temporal tuning of the two pathways. Since computational models trained on natural images exhibited similar differences between ON and OFF channels, we concluded that the functional asymmetries between the two channels reflect asymmetries in the distribution of bright and dark features in natural scenes.

ZUSAMMENFASSUNG

Fliegen sind, ähnlich wie viele andere Tierarten, für ihr Überleben hauptsächlich von ihrem Sehsinn abhängig. Für verschiedenste Verhaltensmuster, wie die Suche nach einer Futterquelle, das Vermeiden von Hindernissen und Fressfeinden oder einfach nur um ihre Flug- oder Laufbahn zu stabilisieren, sind visuelle Reize von entscheidender Bedeutung. Optische Flussfelder, die durch Bewegung auf den Augen der Fliegen entstehen, helfen den Insekten dabei auf Störungen von außen, wie beispielsweise einen plötzlichen Windstoß zu reagieren. Zu diesem Zwecke muss die Fliege entscheidende Informationen wie die Geschwindigkeit oder Richtung der Bewegung aus diesen Flussfeldern extrahieren. Ein etabliertes Modell für die Berechnung von richtungsselektiven Signalen basiert auf asymmetrischer Filterung von Signalen, die von zwei benachbarten Photorezeptoren in der Retina der Fliege ausgehen. Großfeldneuronen in der Lobula-Platte, einer Region in den Optischen-Loben von Insekten, reagieren auf visuelle Reize mit richtungsselektiven Signalen. Die Berechnungen in Arealen des Fliegenhirns präsynaptisch zur Lobula-Platte, die für diese gerichteten Antwortigenschaften benötigt werden, sind jedoch bisher noch nicht hinreichend verstanden.

Während meiner Doktorarbeit habe ich Zellen, die den richtungsselektiven Tangentialzellen vorgeschaltet sind, mit Hilfe physiologischer und genetischer Techniken charakterisiert. Mit Zwei-Photonen Mikroskopie und genetisch exprimierbaren Kalzium-Indikatoren konnte ich die Antwortigenschaften von kleinen, kolumnären Elementen im neuronalen Netzwerk des Bewegungsapparates der Fliege direkt untersuchen. Weiterhin konnte ich deren Beteiligung an der Berechnung von gerichteten Signalen ergründen, indem ich die Funktion dieser Zellen durch transgenes einbringen bestimmter Proteine ausschaltete und gleichzeitig die Antworten postsynaptischer Zellen auf bestimmte visuelle Reize charakterisierte. Die Kombination dieser Techniken mit anderen Verfahren wie Verhaltensversuchen, optogenetischer Aktivierung, Pharmakologie und Computer Simulationen resultierte in insgesamt sechs Publikationen, aus denen sich diese kumulative Dissertation zusammensetzt.

In unserer ersten Veröffentlichung beschäftigten wir uns mit zwei Zelltypen, T₄-Zellen, die Medulla und Lobula-Platte miteinander verbinden und T₅-Zellen, welche Verzweigungen sowohl in der Lobula, als auch in der Lobula-Platte vorweisen. Durch das Messen von Kalzium Signalen konnten wir zeigen, dass sowohl T₄-, als auch T₅-Zellen spezifisch auf visuelle Bewegungsreize in eine bestimmte Richtung reagieren. Zusätzlich stellte sich heraus, dass T₄-Zellen ausschließlich auf positive Helligkeitsunterschiede (Licht an, ON) und T₅-Zellen nur auf dunkle Reize (Licht aus, OFF) antworteten. Somit wurde bestätigt, dass auch auf der Ebene der Lobula-Platten-Eingangsneuronen zwei getrennte Signalwege existieren. Indem wir diese bewegungssen-

sitiven Elemente mit Hilfe genetischer Manipulationen aus dem Netzwerk entfernten und gleichzeitig entweder von nachgeschalteten Tangentialzellen ableiteten, oder das Laufverhalten von Fliegen beobachteten, gelang es uns zu beweisen, dass einerseits T₄-Zellen für die Wahrnehmung von ON-Signalen, andererseits T₅-Zellen für die Berechnung von OFF-Signalen von elementarer Bedeutung sind.

Der zweiten Arbeit war eine anatomische Studie vorangegangen, die herausgefunden hatte, dass L₂- und L₄-Zellen in der distalen Medulla asymmetrisch mit Tm₂-Dendriten verbunden sind. Mit Kalzium-Messungen mit einem Zwei-Photonen-Mikroskop und transgener Unterdrückung von synaptischer Signalweitergabe kombiniert mit elektrischen Ableitungen von Tangentialzellen untersuchten wir die Beteiligung von L₄- und Tm₂-Zellen im OFF-spezifischen Netzwerk des Bewegungssehapparates des Fruchtfliege, d.h. die Zellen die für dunkler werdende Reize zuständig sind. Wir fanden, dass Tm₂-Zellen kleine, gleichförmige Rezeptive-Felder haben die durch laterale Hemmung geformt werden, während L₄-Zellen sowohl auf kleine als auch auf große negative Helligkeitsänderungen reagierten. Durch Ausschalten der synaptischen Weiterleitung in beiden Zelltypen konnten wir außerdem feststellen, dass beide für das Zustandekommen gerichteter, OFF-spezifischer Signale in Tangentialzellen benötigt werden, unabhängig der Bewegungsrichtung.

Für die dritte Publikation nutzten wir wiederum Kalzium-Messungen um die räumlichen und zeitlichen Antworteigenschaften der kolumnären Tm₁-, Tm₂-, Tm₄- und Tm₉-Zellen zu charakterisieren. Diese vier Zelltypen wurden in einer anatomischen Studie als Eingangselemente zu T₅ Zellen identifiziert. Wie sich herausstellte ähneln sich die räumlichen Eigenschaften aller vier Zelltypen sehr. Ihre zeitlichen Charakteristika spannen hingegen ein breites Spektrum. Nachdem wir die vier Zeitkonstanten der Zellen durch ein computergeneriertes Modell simuliert hatten, konnten wir feststellen, dass Kombinationen zweier Zellen jeweils in funktionierenden Bewegungsdetektoren resultierten. Als nächstes untersuchten wir die Beteiligung aller Zelltypen an der Berechnung richtungsselektiver Signale auf der Ebene der Lobula-Platte, indem wir synaptische Blocker in Tm-Zellen exprimierten und die Antworten von Tangentialzellen auf visuelle Reize bestimmten. Hierbei fanden wir, dass alle vier Arten von Neuronen, zu unterschiedlichem Ausmaß in den Berechnungen involviert sind. Somit konnten wir in dieser Studie zeigen, dass OFF-spezifische Signale auf den Dendriten von T₅-Zellen durch komplexe Interaktionen von Tm₁-, Tm₂-, Tm₄- und Tm₉-Zellen generiert werden.

Die physiologischen Antworten von richtungssensitiven Tangentialzellen können generell durch zwei Charakteristika beschrieben werden: wenn sie durch Bewegung in ihre Vorzugsrichtung angeregt werden, depolarisieren die Zellen, wohingegen ihr Membranpotential auf visuelle Stimulation in die entgegengesetzte Richtung (Nullrichtung) abnimmt. Die dem Zugrunde liegenden zellulären Mechanismen haben wir in der vierten Studie untersucht. Dabei stellte sich heraus, dass Tangentialzellen bei optogenetischer Aktivierung von T₄- und T₅-Zellen

eine biphasische Reaktion zeigen. Diese besteht aus einer schnellen, exzitatorischen und einer langsameren inhibitorischen Komponente. Antikörperfärbungen von T₄- und T₅-Zellen zeigten, dass beide Neuronenklassen Acetylcholin als Neurotransmitter benutzen. Durch pharmakologische Experimente konnte bestätigt werden, dass der schnelle exzitatorische Anteil der Tangentialzellenantwort durch Acetylcholin ausgelöst wird und die hemmende Komponente über, zu diesem Zeitpunkt unbekannt, Interneuronen vermittelt werden muss.

In einer fünften Publikation beschäftigten wir uns mit der Reaktion von Fruchtfliegen auf optische Illusionen. Genau wie wir Menschen, reagieren auch Fliegen auf visuelle Tricks, die Bewegung suggerieren, selbst wenn sie keine Bewegungsinformation enthalten. Durch Versuche an laufenden *Drosophila*, sowie elektrophysiologischen Experimenten an transgenen Fliegen konnten wir einen Schaltkreis entdecken, der parallel zum Bewegungssehsystem existiert und lokale Kontrastveränderungen misst. Beide neuronalen Netzwerke konvergieren auf der Ebene der Lobula-Platten-Tangentialzellen und teilen sich außerdem einige Eingangselemente. Interessanterweise stellte sich weiterhin heraus, dass T₄- und T₅-Zellen nicht in der Berechnung der Kontrastwahrnehmung beteiligt sind.

Für die letzte Veröffentlichung meiner Dissertation haben wir die Unterschiede zwischen den beiden parallelen Verarbeitungssträngen – für positive (ON) und negative (OFF) Helligkeitsänderungen – des Bewegungssehsystems von Fliegen analysiert. Überraschenderweise fanden wir hierbei, dass der optomotorische Reflex in Fruchtfliegen mit jeweils nur einem funktionierenden System (ON oder OFF) beinahe unverändert gut funktioniert. Durch Kalzium-Messungen und elektrophysiologische Experimente konnten wir jedoch deutliche Unterschiede in der zeitlichen Abstimmung des ON- und des OFF-Kanals aufzeigen. Computersimulationen, welche auf natürliche Szenen trainiert wurden, zeigten ähnliche Unterschiede wie die physiologischen Messungen. Es ist also Wahrscheinlich, dass zeitliche Asymmetrien zwischen ON- und OFF-Detektoren die Verteilung von hellen und dunklen Anteilen in natürlichen Bildern widerspiegeln.

CONTENTS

1	INTRODUCTION	1
1.1	Sensory systems	1
1.2	Visual systems	1
1.3	Motion vision	2
1.4	Tools in neuroscience	4
1.4.1	Physiology	5
1.4.2	<i>Drosophila</i> neurogenetics	6
1.4.3	Mapping neural circuits	7
1.5	The fly visual system	11
1.5.1	Phototransduction	12
1.5.2	The compound eye	12
1.5.3	The optic lobe	14
1.5.4	Motion vision circuit	15
1.6	Concluding remarks	17
2	PUBLICATIONS	19
2.1	A directional tuning map of <i>Drosophila</i> elementary motion detectors	19
2.2	Neural circuit components of the <i>Drosophila</i> OFF motion vision pathway	30
2.3	Comprehensive characterization of the major presynaptic elements of the <i>Drosophila</i> OFF motion detector	44
2.4	Optogenetic and pharmacologic dissection of feedforward inhibition in <i>Drosophila</i> motion vision	72
2.5	Neural mechanisms for <i>Drosophila</i> contrast vision	84
2.6	Asymmetry of <i>Drosophila</i> ON and OFF motion detectors enhances real-world velocity estimation	119
3	DISCUSSION	147
3.1	Algorithmic models for motion detection	147
3.2	Biophysical implementation of local motion detection	149
3.3	Functional significance of parallel processing streams	152
3.4	Cellular mechanisms of motion opponency	153
3.5	Lobula plate and optomotor response	155
3.6	Results in the light of the current literature	158
3.7	Future directions	160
	BIBLIOGRAPHY	163
	INDEX	181

1

INTRODUCTION

1.1 SENSORY SYSTEMS

In order to successfully interact with our environment, we need to be constantly up-to-date about our surroundings. Relevant changes must be reliably detected, processed and the appropriate actions must be initiated. Sensory organs distributed over the body constantly provide our brain with vital multi-modal information. These sensory receptors, triggered by external stimuli are the beginning of an electro-chemical cascade of neuronal processing from the periphery to the central nervous system. Before we even actively perceive a sensation like a smell or a taste the original signals have undergone impressive amounts of computation and filtering at early stages of neural processing. For example, when epithelial cells in the olfactory organs detect minute amounts of chemicals in the air they convey information about their composition and concentration to the olfactory centers of the brain. There, smells can provoke a multitude of responses, reaching from lively, emotional memories ([Herz et al., 2004](#)) to changes in the endocrine system of the body, that result for instance in a sudden desire for Italian cuisine ([Johnson and Wildman, 1983](#); [Yeomans, 2006](#)). The olfactory system, however, adapts very rapidly to persistent stimulation. An initially irritating smell for instance, can sometimes be very hard to detect only a few minutes later.

Sensory systems represent a convenient entry point to study brain functions for several reasons. One common feature shared by all sensory systems is their localization at the periphery of the nervous system and hence their experimental accessibility. In the vertebrate visual system, many highly interesting computations take place at the earliest level of detection, within the retina. The peripheral localization makes it comparatively easy to apply precise artificial stimuli and thereby intentionally trigger neural responses under controlled conditions in a laboratory. Furthermore, even though the computational performance is very elaborate, compared to networks in higher brain areas, like the cerebral cortex, the anatomical complexity of sensory circuits is fairly moderate. It is thus not surprising, that the field of sensory neurobiology is one of the best studied disciplines within neuroscience.

1.2 VISUAL SYSTEMS

Vision is, across many animal species including humans, the primary sensory modality for the execution of manifold behavioral tasks such as orientation in complex environments, social interactions with conspecifics, predator or rival avoidance and adequate food source localization. Sensory receptors extracting visual information are generally

located in the eyes. Across the whole animal kingdom, a vast variety of different eyes have evolved, that can be classified in two groups; compound eyes, as found in crustaceans (e.g. shrimps, lobsters) and insects (e.g. flies, mosquitoes, beetles), and camera eyes that have evolved in parallel in arachnids (e.g. spiders, scorpions, mites), cephalopods (e.g. squids, octopuses) and vertebrates (e.g. fish, birds, mammals) (Land and Nilsson, 2012). The main challenge for visual systems is the transformation of a 3D image onto a two-dimensional array of photoreceptive cells. The neural networks in the mammalian eye accomplish this task through a highly complex parallel organization. The first stage of visual processing takes place in the retina, where light that hits the photoreceptors triggers a biochemical reaction altering their membrane voltage, resulting in a change of transmitter release that can be detected by postsynaptic neurons. In the downstream networks, generally two motifs are found; a parallel, retinotopic arrangement starting with photoreceptor cells that diverge onto approximately ten types of bipolar cells. The bipolar cells ultimately connect to retinal ganglion cells that form the optical nerve linking the retina to higher brain areas. In addition to this parallel organization, lateral interactions are introduced at two stages: horizontal cells shape the responses of photoreceptor and bipolar cells, and amacrine cells act on bipolar cell - ganglion cell connection (for review, see Masland, 2001; Gollisch and Meister, 2010). The ganglion cell signals are subsequently conveyed to higher brain structures, where neuronal ensembles or sometimes single cells extract information about color, texture, or motion of an object (Hadjikhani et al., 1998; Kastner et al., 2000; Hubel and Wiesel, 1968), or even highly complex patterns like faces (Quian Quiroga et al., 2005). These neurons can then signal other neuronal networks to initiate appropriate behavioral actions.

The complex response properties of neurons in higher brain areas give rise to a great variety of interesting scientific questions at different stages of visual processing: Which stimulus triggers which behavioral response? Which cell types are responsible for the initiation of the subsequent behavior? How are neural networks organized to extract the necessary information from a visual scene? However, the enormous complexity of the mammalian brain makes it difficult to address these questions at a circuit level.

Apart from vertebrates, visual processing can be studied in simpler organisms like arthropods. Insects for instance exhibit a number of interesting behaviors triggered by specific visual signals (Hassenstein, 1951; Reichardt and Wenking, 1969; Borst, 1986; Bahl et al., 2013). Additionally, neural networks underlying visual feature extraction can be assessed in intact, living animals with fixed eyes, enabling precise stimulus presentation. Moreover, morphologically and genetically identified cell types allow for the specific manipulation of circuit elements.

1.3 MOTION VISION

One example of feature detection intensely studied in vertebrates and insects alike is motion vision. Insects, with their limited spatial res-

olution, rely heavily on the detection of visual motion. In principle two kinds of motion must be distinguished; object-motion (small field motion) caused by an external cue moving in the visual scene of the observer (for review, see [Nordström, 2012](#)), and ego-motion (wide field motion) generated by movements of the observer through the visual scenery (see [Borst, 2010](#)). In both cases, it is crucial for the observer to detect the direction of motion. Direction-selective neurons exist at several stages of visual processing. In the vertebrate retina, some classes of ganglion cells specifically respond to stimuli moving in one direction but show no response when presented with motion in any other direction ([Barlow et al., 1964](#); [Wässle, 2004](#)). Further downstream the processing cascade, in the primary visual cortex, subsets of neurons exhibit similar response characteristics ([Hubel and Wiesel, 1968](#)). Whether these properties are computed *de novo*, or whether they are inherited from direction-selective cells in the retina is still under debate ([Huberman et al., 2009](#); [Cruz-Martín et al., 2014](#); [Sun et al., 2015](#)). Additionally, the visual systems of many invertebrate species permit elaborate behaviors. When carefully observed with high magnification, in-flight manoeuvres of flies are absolutely breathtaking. During short episodes of conspecific pursuit, male house flies perform acrobatic turns with speeds faster than 2500°s^{-1} ([Land and Collett, 1974](#)). In order to successfully steer towards the target fly and to respond to changes in its flight path, the pursuing fly has to constantly update the information about the position of its target ([Collett and Land, 1978](#)). Extracting, within fractions of a second, important features, like the direction and velocity of moving objects in the visual scene requires a highly specified and efficient neuronal network.

In the 1950's researchers from Tübingen monitored the turning behavior of the beetle *Chlorophanus viridis* on a device they named "Spangenglobus", a spherical y-maze that repeatedly forces the animal to chose between left- or rightward turns (Figure 1a). The beetle was placed inside a rotatable black and white striped cylinder that was used to deliver visual stimuli. Monitoring the visually triggered turning responses of the beetle, Hassenstein and Reichardt observed that the insect would turn with the direction of visual motion ([Hassenstein, 1951](#); [Hassenstein and Reichardt, 1956](#)). The ecological relevance of this behavior, known as optomotor response, can be appreciated when observing an animal in its natural environment. When for instance a fly, flying through a rich visual scenery towards a food source, suddenly becomes distracted from its original path by a gust of wind, it has to correct for this distortion. When the fly experiences acceleration to the left, the image of the world on its eyes

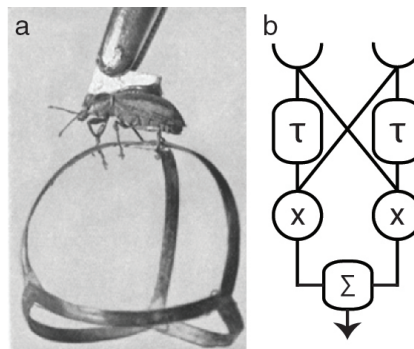


Figure 1. (a) Experimental setup used to extract the turning behavior of a beetle upon visual stimulation (from [Hassenstein, 1951](#)). (b) Schematic representation of a Hassenstein-Reichardt elementary motion detector (HRC) ([Hassenstein and Reichardt, 1956](#))

Optomotor response

is shifted to the right, a phenomenon called optic flow. In order to stay on course, the insect's visual system has to extract this change in optic flow and instantaneously initiate a compensatory movement in the appropriate direction. It is thus absolutely critical to detect the direction of motion based on the movement of the visual scenery. Importantly, photosensitive epithelium cells, the very first stages of the visual systems, do not encode the direction of motion. Hence, direction selectivity must arise through computations within the optic lobe of the brain. The optomotor reflex has been exploited to study the underlying neuronal circuitry, but also develop computational models that can predict such simple behaviors.

*Hassenstein-
Reichardt
Correlator*

Based on their observations in the tethered beetle, Hassenstein and Reichardt proposed an algorithmic model that can compute direction selectivity from two non-directional inputs (Hassenstein and Reichardt, 1956). Their correlation-type motion detector is comprised of two mirror symmetric half-detectors (Figure 1b). Both subunits consist of four stages: first, changes in local luminance are detected by two spatially offset input sites. In a second step these signals are subject to different temporal processing, one input is highpass filtered (direct line), while the signal from the adjacent input site is delayed by a lowpass filter (delayed line, τ). Differential temporal filtering constitutes the basis for a direction-selective signal at the third stage, where both signals interact in a nonlinear way (e.g. through multiplication). Finally, the outputs of both half-detectors are subtracted, resulting in a fully opponent response, where motion in one direction results in a positive and motion in the other directions in a negative signal (Figure 1b, Hassenstein and Reichardt, 1956; Borst, 2014b). Understanding the neuronal implementation of such an elementary motion detector has been an active field of systems neuroscience for over half a century. Only recently, as novel genetic and imaging techniques became available, has significant progress been made.

1.4 TOOLS IN NEUROSCIENCE

Research on *Drosophila melanogaster* began in the early 1900s when Thomas Hunt Morgan identified – without knowledge of genes – the white gene, that is responsible for the production of the typical red pigment in the fly eye (Morgan, 1910). Ever since flies have been subject to anatomical (Cajal and Sánchez, 1915; Fischbach and Dittrich, 1989), genetic (Nüsslein-Volhard and Wieschaus, 1980), and functional (Götz, 1964) investigation (for review see Bellen et al., 2010). In parallel, tools to access the nervous system have steadily improved. Both on the technical side, for instance through the development of new microscopes that improved the optical accessibility of small neurons, as well as on the biological side, where new methods to target genes and proteins multiplied the availability of techniques to visualize (Chalfie et al., 1994) and manipulate single neurons. (Brand and Perrimon, 1993; Kitamoto, 2001).

1.4.1 Physiology

For a very long time, properties of nerves, brain regions and single neurons have been investigated using electrophysiological recordings of membrane voltage (Hodgkin and Huxley, 1952). In the blow fly *Calliphora* many cell types were characterized using intracellular and extracellular recordings with sharp electrodes (Hausen, 1976; Strausfeld and Lee, 1991). Recordings from two or more cells simultaneously enabled the description of connectivity between cells or connections of neurons with downstream nerves (Haag and Borst, 2001; Haag et al., 2004; Kauer et al., 2015). While these approaches worked well for the large nerve cells in the blow fly, recordings with sharp electrodes proved to be difficult at the small scale of *Drosophila* neurons. The whole-cell patch-clamp approach (Sakmann and Neher, 1984) was better suited for this task. Here, a glass electrode with a very fine opening is brought into close vicinity of a neuron under application of a small positive pressure. Once the electrode touches the cell membrane, the pressure is released and minute negative pressure is applied. This causes the cell membrane to become sucked slightly into the opening of the pipette. A so called "giga-Ohm seal" is formed, where the seal between glass capillary and cell membrane strongly increases the electrical resistance. In the next step, a short pulse of negative pressure leads to the detachment of a small patch of membrane into the electrode. The resistance drops and the remaining cell membrane now forms a continuum with the recording electrode, allowing the precise measurement of cellular voltage or current. This technique permitted electrophysiological experiments in some larger cells of the fruit fly's brain (Wilson et al., 2004; Joesch et al., 2008).

Electrophysiology

One technical innovation with an enormous impact on neuroscience was the invention and improvement of electron microscopy. Using electrons instead of photons to probe tissues allowed for pushing the resolution limit far beyond what was possible with optical microscopes (Knoll and Ruska, 1932; Denk and Horstmann, 2004). This innovation promoted the emergence of a new field of neuroscience: connectomics, where neural circuits are described based on dense reconstructions of brain areas (Kim et al., 2014; Takemura et al., 2013; Helmstaedter et al., 2013). In recent years, electron-microscopic studies have provided a new level of insight into the wiring of neuronal circuits. However, information about the connectivity of neurons is by far not enough to understand even primitive neural circuits. The whole neural system of the roundworm *Caenorhabditis elegans* with its 302 neurons, had been reconstructed 30 years ago (White et al., 1986), the function of the circuitry, however, is still subject to investigation. It is therefore indispensable to also probe nervous systems functionally. A milestone for functional imaging – two-photon microscopy – emerged in 1990 (Denk et al., 1990). In a two-photon microscope fluorophores are stimulated with long-wavelength light (~1000nm), that per se does not contain enough energy to trigger fluorescence. Since the laser delivers the excitation with a few femtosecond short pulses, the fluorophores are only excited when two photons coincide within a very short time window. The probability for such an event is only high enough in the focal plane of the laser beam, hence, the z-resolution of such a microscope is

Imaging

very high. Furthermore it circumvents problems of conventional light microscopy, like bleaching, phototoxicity or unspecific photon-noise. Thus, two-photon microscopy greatly improved imaging possibilities in neural systems. However, in order to take advantage of the technological innovations, biological tools needed to be developed.

1.4.2 *Drosophila* neurogenetics

More than a century ago the fruit fly *Drosophila melanogaster* was introduced to the scientific community (see Greenspan, 2008). With its short generation time, small size, relatively modest number of neurons (~250 000, Changeux, 2010) and the recent development of genetic tools, *Drosophila* has become one of the most heavily studied animal species in many disciplines of biology, especially in the field of neuroscience. The fly visual system is particularly suited for the investigation of neural networks, since a great number of theoretical, morphological and physiological studies on closely related fly species as well as the fruit fly itself provide an excellent basis for the deciphering of general functional principles. In the beginning of *Drosophila* research, scientists used x-rays and chemicals to manipulate its DNA (Muller, 1928; Alderson, 1965) and screened for behavioral phenotypes (Benzer, 1967). However, these methods were not very controlled and resulted in random, unpredictable mutations. In order to gain insight into functional principles underlying neuronal circuits it is essential to study the building blocks of the circuitry, single neurons or cell types (for review see Luo et al., 2008). Random mutagenesis is unreliable and unspecific in affecting functions of single cells or defined classes of neurons. Being able to specifically insert pieces of exogenous DNA into the fly's germline created, for the first time, the possibility to more systematically modify the properties of cells. In a pioneering study, Rubin and Spradling (1982) were able to stably insert a new gene into the DNA of a fly. They used mutant flies lacking *rosy*, a gene determining wild-type *Drosophila* eye color. When they injected a vector that contained a transposable element (P-element) carrying the intact *rosy* gene into *Drosophila* embryos, they could rescue the loss-of-function phenotype not only in the injected flies, but also in subsequent generations. This indicates a successful integration of the exogenous gene into the fly's germ-line. However, this technique presents some problems. Since the integration of the P-element happens in random positions of the host DNA, it is possible that it is inserted into encoding areas of the fly's genome which can cause malfunctions of important genes, that may result in off target effects. Moreover the promoters that determine the expression of the downstream genes can not be selected and therefore the cells in which the inserted gene will be expressed cannot be targeted. The biggest disadvantage of this method is that every effector protein has to be inserted *de novo* into the genome.

Gal4-UAS

In the early 1990s, researchers introduced a new binary expression technique to circumvent these issues (Figure 2a, Brand and Perrimon, 1993). The Gal4-UAS system combines two separate strategies to target the expression of any gene of interest to a specific subset of neurons. The yeast transcription factor Gal4, expressed under the control of an

endogenous promoter drives the expression of any protein of interest controlled by the upstream-activation-sequence (UAS). Hence, UAS determines 'what' – which effector – is expressed, and the driver Gal4 defines 'where' this protein is supposed to be present. More recently, the efficiency in creating new fly strains has been considerably improved by the development of a new technique, the so-called ϕ C31 integrase system, that allows for the site-specific insertion of transgenes in the fly genome. Here, an attB donor plasmid containing the transgene is injected into an embryo of a *Drosophila* strain containing an attP-site (Fish et al., 2007; Bischof et al., 2007). This method helped to overcome the issues of random insertion and variable expression level and has supported enormous projects screening for cell type specific Gal4 lines that ultimately resulted in a database containing several thousand publicly available driver lines (Lindsley and Zimm, 1992; Jenett et al., 2012, see also [Bloomington stock collection](#)). Being able to search for distinct strains from a seemingly infinite pool of genetically modified flies created a whole new level of experimental accessibility. A second binary expression method, based on the bacterial DNA-binding protein-operator LexA-op and controlled by the expression of LexA works similarly (Lai and Lee, 2006). With complementary strategies that combine both systems one can target two cell populations independently with two different effectors.

The specificity of Gal4 or LexA driver lines is in some instances not sufficiently high to exclusively target certain subpopulations of neurons or single cell types. Two main intersectional tools help to constrain the expression patterns of driver lines. In the split-Gal4 system (Luan et al., 2006) the Gal4 is separated into two functional subunits, the DNA-binding (DBD) and the transcription-activation (AD) domains, each of which can be expressed under the control of a specific promoter. Neither domain can activate the transcription of a functional Gal4 protein on its own. Only in cells where both are expressed the AD and DBD domains heterodimerize and become transcriptionally competent. Hence, a transgene will only be expressed at the intersection of the expression patterns of both promoters. For example, the combination of driver line A containing populations 1 and 2, and driver line B containing populations 1 and 3 will result in a split-Gal4 line specific for cell population 1. Besides "A and B" strategies, expression patterns of driver lines can also be refined using "A not B" approaches. The combination of Gal4 and the yeast Gal4-inhibitor Gal80 under the control of two different promoters results in transgene expression in cells that only contain Gal4 but not Gal80 (Lee and Luo, 1999; Suster et al., 2004). To profit from these novel transgenic techniques and the large amount of specific driver lines, a number of genetically encoded proteins that specifically manipulate functional properties of neurons in which they are expressed have been engineered.

*Intersectional
strategies*

1.4.3 Mapping neural circuits

In order to characterize neuronal circuits, the functional principles of single elements in these networks need to be understood. The discovery and synthesis of the green fluorescent protein (GFP, Figure 2b,

Shimomura et al., 1962; Chalfie et al., 1994; Heim et al., 1994) enabled scientist to transgenetically label single cells *in vivo* without prior fixation and immunostaining. Using the Gal4-UAS system one can visualize subclasses of neurons in the optic lobe of the fruit fly brain (Figure 2b) and thus probe the specificity of driver lines.

Calcium indicators

Due to their small size, neurons in the brain of *Drosophila* are often inaccessible for electrophysiological recordings. Using light microscopy to observe intracellular calcium levels, a proxy for neuronal activity, can overcome this limitation (2c). When a cell is depolarized, calcium enters the cytosol through voltage-gated calcium channels and calcium influx at the presynapse triggers the fusion of vesicles with the cell membrane which ultimately results in the release of neurotransmitters into the synaptic cleft (Hille, 2001; Grienberger and Konnerth, 2012). Different approaches to engineer genetically encoded calcium indicators have been followed. They are all based on fluorescent proteins equipped with calcium binding domains (Miyawaki et al., 1997). In general, there are two families: ratiometric indicators that consist of two fluorescent proteins linked by a domain, that changes its configuration upon calcium binding. This leads to a fluorescent resonance energy transfer (FRET) between the two fluorophores. Ultimately, the calcium level is read out through a change in the ratio between the emitted light from fluorophore A and fluorophore B (Mank et al., 2006, 2008; Broussard et al., 2014). The second class of calcium indicators are called single wavelength probes where the binding of calcium causes a conformational change in the fluorophore, leading to an increase in photon emission. Consequently, the read-out is the brightness of the indicator (Baird et al., 1999). Today, the most widely used calcium indicators are from the family of single wavelength probes GCaMP (Ohkura et al., 2005; Chen et al., 2013). In order to obtain high spatial resolution, with low tissue damage and acceptable temporal resolution, calcium imaging is often used in combination with two-photon microscopy (Reiff and Borst, 2008; Reiff et al., 2010).

Carefully measuring the response characteristics of neurons can teach us a lot about their physiological contribution to neural networks. However, being able to specifically manipulate their functional properties would dramatically increase the number and type of experiments and could enhance our understanding of whole circuits. For centuries, the importance of regions of the human brain could only be determined through functional impairments occurring in individuals with localized damage from surgery or accidents (e.g. Broca, 1888). Using pharmacology it has been possible to manipulate predetermined brain areas and sometimes even identified subsets of neurons, with the disadvantage of limited temporal and spatial precision. Changing the membrane voltage of neurons with a recording electrode increases temporal accuracy, however, only to a spatially limited extent; i.e. only single or at the best a few cells can be targeted at the same time. Exploiting genetic techniques can overcome both of these issues, enabling the alteration of genetically defined sets of cells, if necessary with high temporal precision.

Silencing neurons

The genetic accessibility of many model systems has initiated the development of tools that allow interference with the function of nerve cells. One way to characterize the role of a network element is by

investigating the effect of removing it from the circuit. There are several tools that allow for a removal of elements from a neural circuit. First, neurons can be killed by expressing apoptotic genes like *reaper* or *hid* (Grether et al., 1995) or by preventing protein synthesis using *ricin A* (Moffat et al., 1992). Second, their output can be permanently blocked by interrupting synaptic communication between neurons (tetanus toxin, Sweeney et al., 1995). Third, the expression of an inwardly rectified potassium channel (Kir2.1, Johns et al., 1999) causes neurons to hyperpolarize, resulting in suppressed excitability. While these tools provide effective and reliable control over the functionality of the targeted cells, the precise timing of activation cannot be determined and their expression is irreversible. In some circumstances, however, it is preferable to reversibly attenuate the activity or the synaptic output of a circuit element for a certain period of time. A dominant-negative version of the gene *shibire*, that encodes an important protein at the presynapse - *dynamin* - can be induced via temperature (Figure 2c). At a permissive temperature ($\sim 25^{\circ}\text{C}$) the reuptake of vesicles from the synaptic cleft, mediated by the GTPase *dynamin*, is still functional. When the ambient temperature is shifted by only a few degrees to a restrictive level of about 31°C the fusion of vesicles with the presynaptic membrane is interrupted, preventing, within a few seconds to minutes, synaptic release, and ultimately silencing the neuron without changing its endogenous properties (Kitamoto, 2001). Lowering the temperature back to permissive levels releases the block effect. Interestingly, in *Drosophila* it has been shown that by exposing flies expressing *shibire^{ts}* to a persistent heat-shock for one hour at an elevated temperature (37°C), the effect becomes long-lasting and the output of the affected cells is suppressed for several hours (Joesch et al., 2010). While this experimental procedure increases the temporal extent of neuronal silencing, it does so at the cost of losing reversibility.

A second approach to probe the connectivity between neural elements in a network is their activation. Classically, connections between neurons have been interrogated using paired recordings from two or more potentially interconnected cells. By injecting current into one cell and recording from another, one can precisely characterize their connection strength and direction. Due to size limitations, unfavorable location or for reasons of efficiency this method is often not feasible. Stimulating or suppressing neurons by other, less invasive and more widespread mechanisms was necessary to improve the circuit mapping. Using temperature, neurons can not only be silenced but also activated. The transient receptor potential cation channel TrpA1 (Hamada et al., 2008; Pulver et al., 2009; Berni et al., 2010) naturally occurs in wild-type flies and is thought to be implicated in temperature sensing (Hamada et al., 2008). Transgenically expressing this channel in the membrane of neurons – for instance using the Gal4-UAS system – allows for temperature mediated excitation. Furthermore, transgenic activators can also be susceptible to chemicals. P2X₂, a cation channel that is activated upon the binding of ATP is used to selectively stimulate genetically identified neurons by application of ATP (Lima and Miesenböck, 2005).

All the tools described above permit the alteration of functional proper-

Activating neurons

Optogenetics

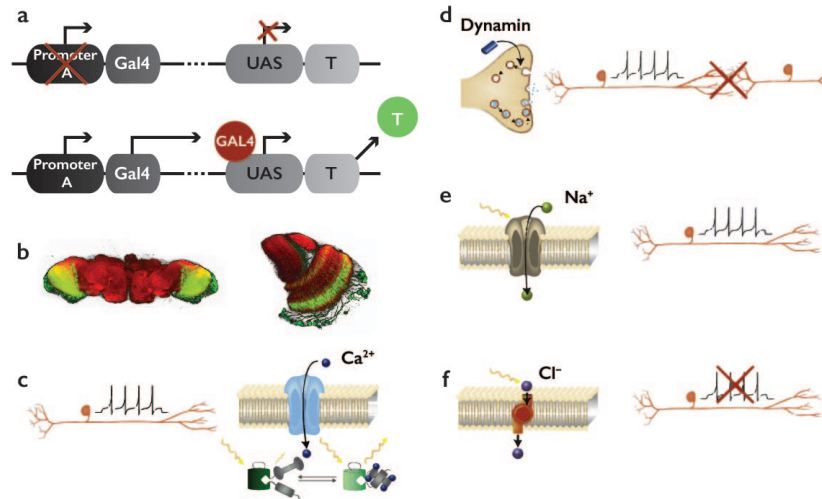


Figure 2. Genetic tools for manipulations in *Drosophila*. (a) The Gal4-UAS system is used to target genetically engineered effectors (UAS) to specific subsets of neurons (Gal4). (b) Transgenic expression of the green fluorescent protein (GFP) enables the visualization of single neurons or cell-types in living animals. E.g. in the optic lobe of the fly brain. (c-f) Genetically encoded effectors. (c) Calcium indicators are used to visualize neuronal activity based on their calcium dynamics. (d) The temperature dependent neuronal silencer *shibire^{ts}* prevents the fusion of synaptic vesicles with the presynaptic membrane and thereby interrupts synaptic communication. (e,f) Optogenetic tools. Light can be used to activate neurons, through channel proteins (e, Channelrhodopsin) or inactivate them via chloride pumps (f, Halorhodopsin). (modified from Borst, 2009; Broussard et al., 2014)

ties of nerve cells in a spatially confined pattern defined by the driver lines used. Nevertheless, the lack of temporal precision in stimulation excludes them for certain applications. The transgenic expression of light-activatable microbial opsins in eucaryotic cells has revolutionized modern neuroscience. The fundamental structure of rhodopsins is largely conserved for all subclasses; they consist of two sub-structures, a light absorbing retinal that is linked to a seven-transmembrane opsin protein. Upon contact with a photon, retinal undergoes isomerization which triggers a conformational change in the connected opsin. In type I rhodopsins found in prokaryotic organisms the photoisomerization of retinal results in the opening of a ion channel, whereas type II rhodopsins from eukaryotes functions as G-protein coupled receptors controlling second-messenger cascades (for review see Fenno et al., 2011). In 2005, the microbial channelrhodopsin (ChR, Figure 2e) was expressed in hippocampal neurons for the first time enabling the activation of nerve cells with millisecond precision, by simply presenting brief flashes of blue light to the tissue (Boyden et al., 2005). Ever since, the field of optogenetics has developed numerous tools for the activation of neurons; improving photo-efficiency (Nagel et al., 2005), increasing speed (Gunaydin et al., 2010), and shifting excitation wavelengths (Lin et al., 2013). One particularly important alteration has been introduced by engineering a version of channelrhodopsin that can be switched on with a short pulse of light (sim10ms) instead

of persistent illumination (Berndt et al., 2009). The slow decay time constant of the channel retains excitation for several seconds, allowing for the presentation of visual stimuli during optogenetic activation without interference of the excitation light with the visual system. Besides excitation, neurons can also be hyperpolarized. Using halorhodopsin (NpHR), a light activated chloride pump derived from *Natromonas pharaonis* (Figure 2f, Schobert and Lanyi, 1982; Zhang et al., 2007), allows for the inhibition of neurons with light at high temporal resolution. Together, channelrhodopsin and halorhodopsin with their variants provide a toolset for the minimal invasive interrogation of neural circuits in living animals. Generally, optogenetic experiments can be applied with two different goals in mind; first, connectivity between cells can be probed in a similar way to classic paired electrophysiological recordings. Activating for instance a subset of neurons expressing channelrhodopsin and measuring resulting changes calcium levels in a second cell type expressing a genetically encoded calcium indicator can provide insight into their connectivity (e.g. Guo et al., 2009; Chuhma et al., 2011). A second application can test the necessity or sufficiency of neural elements for certain behaviors or circuit functions (e.g. Gordon and Scott, 2009; Haikala et al., 2013).

In the 20th century, classical techniques like electrophysiology, neuroanatomy and pharmacology laid the foundation for modern neuroscience. Deciphering the functional principles of neurons, the building blocks of the nervous system and the brain, describing coarse connections between brain regions, and synaptic communication. Recently, an immense number of new techniques have entered the game, dramatically changing large parts of neuroscience. Enormous amounts of data are generated with high throughput, semi-automated image acquisition at modern electron microscopes (Kleinfeld et al., 2011; Helmstaedter et al., 2013; Lichtman et al., 2014), transgenic engineering has opened the door to a whole new world of possibilities to interfere with neuronal networks, and new imaging and stimulation methods allow the observation and manipulation of live and even behaving animals. The fly visual system has been subject to intensive investigation for many years, but only with the genetic toolbox introduced in *Drosophila melanogaster* could a huge step be taken towards fully understanding an entire neural circuit.

1.5 THE FLY VISUAL SYSTEM

In neuroscience, algorithmic models aim to explain, how incoming signals are transformed to produce an observed output. In the visual system, the input signal is a visual stimulus, for example a striped pattern moving from right to left. The output would be a fly turning with the direction of visual motion. The visual system of *Drosophila*, and in particular the circuitry computing motion signals, is especially well suited for investigating neural networks for several reasons. First, stimulus presentation can be controlled in a temporally and spatially precise manner. Accurately timed moving patterns can be presented to the

fly to elicit either behavioral or neural responses. Additionally, closed-loop experiments can be performed, where the responses of the fly influence the presentation of the stimulus, creating a virtual reality environment greatly increasing the stimulus space. The precise stimulus presentation *in vivo* can be problematic in many vertebrate species because of reflexes that cause compensatory eye movements upon visual stimulation (Portugues and Engert, 2009). Second, the morphological structure of the optic lobes is very well described and many cell type specific fly strains enable precise transgenic manipulations. Finally, a well established computational model, the Hassenstein-Reichardt correlator not only predicts the behavioral response of flies to visual motion, but also describes the response characteristics of a class of direction-selective interneurons in the insect brain. Hence, the motion vision system of the fruit fly performs operations that are initiated by a well defined stimulus and result in outputs detectable at several stages of processing.

1.5.1 Phototransduction

The conversion of visual cues, conveyed by photons, into an electrochemical signal is based on a process called phototransduction. In flies, this process takes place in rhabdomeres. Rhabdomeres are comprised of hundreds of thousands of microvilli, each of which contains about 1000 photoactive molecules, called rhodopsins. Rhodopsin is covalently bound to the chromophore 3-hydroxy-11-cis-retinal which upon absorption of a photon is isomerized into all-trans-retinal. This conformational change triggers the conversion of rhodopsin (Rh) into metarhodopsin (M) which leads to the activation of a G-protein coupled cascade that results in the activation of phospholipase C (PLC). PLC hydrolyzes PIP₂ to DAG, IP₃ and a proton. Downstream of PLC, two light-sensitive channels (TRP and TRPL) are activated via yet unknown mechanisms. Their activation leads to calcium and sodium influx, depolarizing the cell membrane (reviewed in Hardie and Raghu, 2001; Hardie and Juusola, 2015). Upon activation, the photoreceptors release the inhibitory neurotransmitter histamine, inhibiting postsynaptic neurons (Sarthy, 1991; Osorio and Bacon, 1994). In contrast, photoreceptors in the vertebrate eye inactivate in response to light, and are depolarized when not illuminated, resulting in a so called 'dark-current' (Yarfitz and Hurley, 1994; Ebrey and Koutalos, 2001).

1.5.2 The compound eye

In contrast to vertebrates, many invertebrate species have compound eyes, consisting of multiple - up to several thousands - optical units, called facets or ommatidia (see Land and Nilsson, 2012). The entirety of the eye of the fruit fly *Drosophila melanogaster*, contains about 800 such units (Ready et al., 1976). The light enters each ommatidium through a lens and is absorbed by the photosensitive pigments in the rhabdoms. A general problem for all visual organs is the trade off between spatial resolution and sensitivity. Increasing the size of each sampling unit or the acceptance angle of each ommatidium increases

the light sensitivity, but at the same time decreases the spatial resolution. In insects, depending on their ecological niche, three different kinds of eyes have evolved; apposition, optic or refracting superposition, and neural superposition eyes (Figure 3). *Drosophila melanogaster*, like all dipteran species have neural superposition eyes. The most important difference between neural superposition and both, apposition and optic superposition eyes is the structure of the rhabdom. That is, while the fly rhabdom consists of eight separate photoreceptors or rhabdomeres, they are fused together in both apposition and optic superposition eyes, forming one light guide that receives information from one point in space.

The apposition eye (Figure 3a), the simplest and most ancient form, is mostly found in diurnal insects. Here, adjacent ommatidia collect information from neighboring points in the visual surrounding. The facets are separated from one another by shield pigments, preventing light from crossing over to the next optic unit and thereby establishing comparatively high spatial resolution. The photoreceptors transmit the visual information in a retinotopic order to the brain. Visual signals originating from neighboring positions in space are detected by neighboring photoreceptors and conveyed to adjacent locations in the optic lobes. This results in a neuronal map that represents the visual scenery in the outside world. However, in this setting, a substantial portion of light is absorbed by the shielding pigment and thus is lost without providing any information. This does not cause problems during high light intensity conditions like bright day light, but strongly impairs visual performance under low light conditions present during dawn and dusk or during the night.

Apposition

Optic superposition eyes (Figure 3b) circumvent this problem by pooling information originating from a larger proportion of visual space enabling insects like moths to be active even during darkness. The increase in light sensitivity however comes with a decrease in spatial acuity. Since the ommatidia are less shielded, light from neighboring facets will elicit responses in photoreceptors facing slightly different areas thereby decreasing spatial resolution.

Optic superposition

Highly visual insects like true flies have developed a sophisticated way to support good spatial resolution conserving high sensitivity during dim light conditions, providing them with an evolutionary advantage of being able to fly also during dusk and dawn, where the visual performance of many predators is compromised. Neural superposition (Figure 3c) eyes are a specialized form of apposition eyes. Each ommatidium in the retina of fruit flies contains eight unfused rhabdomeres, R1-R8 (Figure 3d). R1-R6 are arranged in a hexagonal structure underneath the lens of each facet, while R7 and R8 are stacked on top of each other in the center of the hexagon. As a result of this pattern the photoreceptors face seven different locations in space. While R7 and R8 have been shown to be involved mainly in color discrimination, R1-R6 encode spatial information crucial for motion vision (Yamaguchi et al., 2008). By this configuration, not only do the six outer photoreceptors in one ommatidium face six different positions, but there are also exactly six photoreceptors in six different, adjacent ommatidia that possess identical optical axes. The axons of the six photoreceptors collecting information from the same target are now

Neural superposition

wired up in an extraordinarily precise manner, converging in one cartridge in the brain forming a so-called neuro-ommatidium. Through this redundancy in light detection, neural superposition eyes provide high sensitivity without losing spatial resolution.

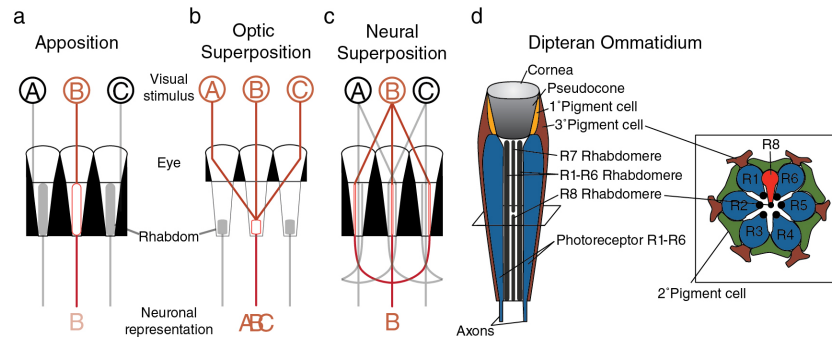


Figure 3. Insect compound eyes. Apposition eyes (a) mostly found in diurnal insects, provide good resolution but require high light levels. Optic superposition (b) provides high sensitivity at the cost of spatial acuity and is mostly found in nocturnal animals. Neural superposition eyes (c) as in flies combine both high sensitivity and good resolution and enable insects to see well under dim light conditions. (d) Vertical (left) and horizontal (right) section through a *Drosophila* ommatidium.

1.5.3 The optic lobe

The visual system of the fly brain is called the 'optic lobe' and consists of four structures; the lamina, the medulla and the lobula complex, comprised of the lobula and lobula plate (Figure 4a). Using Golgi-stainings the first description of the various cell types in the fly optic lobes was published by [Cajal and Sánchez \(1915\)](#). About 50 years later a complete catalog of the majority of cell types in the fly's optic lobe was provided ([Fischbach and Dittrich, 1989](#)).

Lamina

The first neural processing stage of the optic lobes is called lamina. The lamina is made up of repetitive units, called cartridges. Each cartridge represents a single point in space and is therefore also referred to as a neuro-ommatidium. The lamina cartridges receive retinotopic input through achromatic photoreceptors R1-R6 from the retina. The predominant cell types of this neuropil are the lamina monopolar cells L1-L5. Morphological investigations have shown, that L1, L2, and L3 cells receive the majority of their input from photoreceptors R1-R6, while L4 forms reciprocal connections with L2 and only shares a small number of synapses with R6 ([Rivera-Alba et al., 2011](#)). L5 has been shown to receive input from L2, L4 and several lamina interneurons such as an amacrine cell. All five classes of lamina monopolar cells send axonal arbors into distal layers of the subsequent processing stage, the medulla.

Medulla

The next neuropil, involved in early visual processing is the medulla with its ten layers. Here, two main classes of columnar interneurons can be found: about 10 types of medulla intrinsic (Mi) cells and almost 30 subclasses of transmedullary (Tm) neurons (Fischbach and Dittrich, 1989). Mi cells have their dendrites in distal layers of the medulla and send their axons to the proximal medulla. Tm cells receive input from lamina monopolar cells and photoreceptors R7 and R8 in the distal medulla layers 1-5, have, with a few exceptions, an additional ramification in the proximal medulla and terminate in the lobula. In addition to these two types of neurons, TmY cells, connecting medulla, lobula and lobula plate as well as numerous types of amacrine and wide-field neurons have been described. This jungle of interconnected nerve cells has proven very hard to disentangle. Nevertheless, using a combination of light- and electron microscopy, potential circuit layouts could be proposed based on connectivity with presynaptic elements (Fischbach and Dittrich, 1989; Bausenwein and Fischbach, 1992; Takemura et al., 2011).

Lobula complex

The lobula complex, the final stage of neural processing in the optic lobes, consists of two neuropils, the lobula and the lobula plate. The lobula plate and its physiological and anatomical characteristics have been well studied in blow flies (Hausen, 1976; Hengstenberg et al., 1982; Haag and Borst, 1998, 2004). Perpendicular to its columnar organization, the lobula plate is comprised of four structurally distinct layers. Each layer contains a number of wide-field tangential cells. (Figure 4b, Fischbach and Dittrich, 1989; Strausfeld and Lee, 1991). Bushy T-cells, connecting both, medulla (T4) and lobula (T5) with the lobula plate, exist in four subtypes, that send their axons to all four layers of the lobula plate, respectively (Figure 4d). In contradistinction to the lobula plate, the second part of the third neuropil, the lobula is significantly less well studied on a functional level. In general it is comprised of both small columnar neurons as well as large field cells (Fischbach and Dittrich, 1989) that receive their major input through Tm and TmY cells from the medulla. The lobula constitutes an interesting morphological difference between the two input lines to the lobula plate. While T4 cells connect the medulla directly to the four layers of the lobula plate, the second parallel stream takes a detour to the lobula, where T5 cell dendrites reside. While this anatomical peculiarity has been known for a long time, its functional significance remains elusive.

Lobula plate

Lobula

1.5.4 Motion vision circuit

Lobula plate tangential cells are thought to be involved in the initiation of turning behaviors (e.g. Heisenberg et al., 1978). Even though morphologically well described, physiological studies in *Drosophila* remained challenging due to its small size. Deoxyglucose mapping revealed a functional organization which was previously described in

their bigger relatives, showing that the four layers of the lobula plate were active during visual stimulation in the four cardinal directions, respectively (Buchner et al., 1984). Only much later it became possible in *Drosophila* to record from tangential cells. Here, two major groups of lobula plate tangential cells have been described; cells of the horizontal system (HS) that respond preferentially to visual stimuli with horizontal orientations (Schnell et al., 2010), and vertical system (VS) cells that detect vertical motion (Joesch et al., 2008). Both classes of neurons are fully opponent (Figure 4c), i.e. they respond to motion in their preferred direction (PD) with an increase in membrane potential and hyperpolarize when stimulated in the opposite, their anti preferred or null direction (ND). The three HS cells reside in the first layer of the lobula plate and prefer front-to-back motion, while the number of VS cells, that have their dendritic arbors in the fourth layer and are excited by downward motion, has not been finally determined. Unlike in bigger flies like *Calliphora*, where tangential cells in layers 2 and 3 tuned to opposite directions are well characterized (Hausen, 1976; Wertz et al., 2008), descriptions of these neurons are missing in fruit flies. The response characteristics of VS and HS cells are well described by algorithmic models (for review see Borst et al., 2010). The cellular implementation of the necessary computations however is still subject to intense investigation. Anatomical studies proposed the existence of two parallel processing streams via T4 and T5 cells, based on neural connectivity patterns (Bausenwein and Fischbach, 1992). Blocking the synaptic output of both cell types simultaneously rendered lobula plate tangential cells entirely motion insensitive (Schnell et al., 2010). Hence, these two classes of neurons are part of the circuitry responsible for the direction-selective properties of lobula plate tangential cells. Investigating their roles and contributions is part of the content of this dissertation.

Already at an earlier stage of neural processing, in the lamina, the computation of visual motion is implemented, similar to the vertebrate visual system, in two parallel streams for brightness increments and decrements, respectively (Joesch et al., 2010). When blocking the output of lamina monopolar cells L1 and simultaneously recording from downstream direction-selective tangential cells, only responses to bright stimuli (ON edges) were abolished, while dark edge processing was still intact. The exact opposite effect was found when genetically silencing L2 cells, tangential cells still depolarized when stimulated in their preferred direction with bright edges, but exhibited no response to OFF edges.

In a morphological study, Bausenwein and Fischbach (1992) hypothesized that L1 could be connected to T4 via Mi1 cells, while L2 contact T5 via Tm1. In the L2 pathway, Tm1 and Tm2 cells have been shown later by electron microscopy to receive synaptic input from L2 (Takemura et al., 2011). Furthermore an asymmetric connection between L2, L4 and Tm2 cells in the outer medulla could be identified. Tm2 receives input from L2 in its home-column, while L4 connects to two "walking-legs", dendritic proliferations extending posteriorly into neighboring columns. This morphological feature suggested a distinct, potentially directionality-specific role of the L4-Tm2 connection (Takemura et al., 2011). Subsequent investigations revealed two more cell

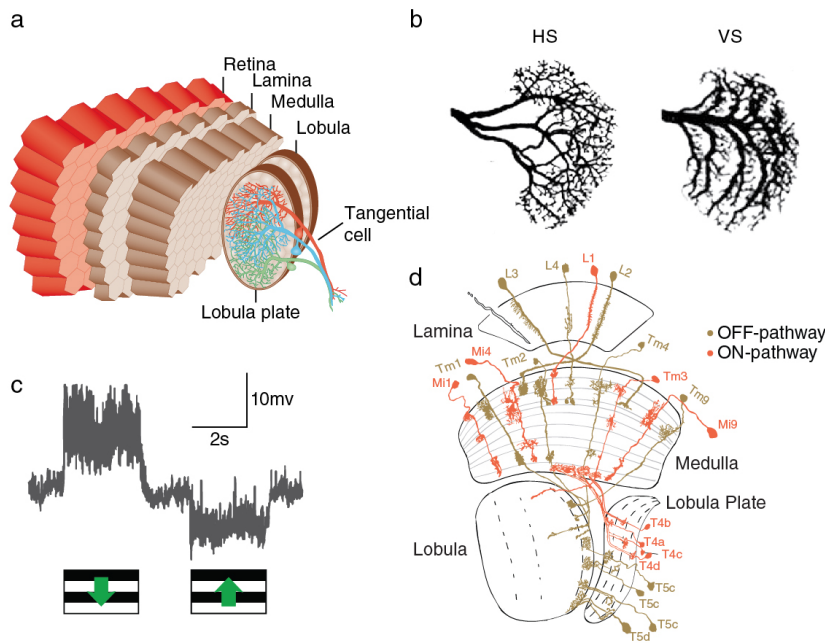


Figure 4. (a) Schematic overview of the nervous system of the fruit fly *Drosophila melanogaster*. (a) Illustration of the optic lobe of a fly. (from [Borst, 2014a](#)). (b) Lobula plate tangential cells of the horizontal (HS) and vertical (VS) system (from [Rajashankar and Shamprasad, 2004](#)). (c) Electrophysiological recordings from a direction-selective vertical system tangential cell. VS cells depolarize to downward motion (PD) and hyperpolarize to visual stimulation in the opposite direction (ND) (modified from [Joesch et al., 2008](#)). (d) Horizontal section through the visual system of *Drosophila*. (modified from [Fischbach and Dittrich, 1989](#)). Presumed OFF pathway elements are depicted in brown, ON pathway candidates in red.

types that are likely to be involved in the computation of moving dark-edges; Tm4 and Tm9 ([Shinomiya et al., 2014](#)). Other than Tm1, Tm2 and Tm4, Tm9 cells are not postsynaptic to L2 or L4, but receive the majority of their input from L3 cells. For the ON-selective pathway, Mi1 and Tm3 have been proposed to play major roles due to their synaptic connectivity to L1 and T4 ([Takemura et al., 2013](#)). Later, Mi4 and Mi9 cells have been added to the potential candidates for the ON pathway of motion vision (Figure 4d, see also [Janelia EM reconstructions](#)). However, without functional studies, the implication in motion detection remains hypothetical.

1.6 CONCLUDING REMARKS

The visual system of the fruit fly is well suited for the analysis of cellular mechanisms underlying functional principles of neuronal networks. The combination of anatomy and physiology, theoretical models and the availability of genetic tools makes this small insect particularly useful. In the course of my PhD thesis, I investigated the neural correlate of an elementary motion detector in the visual system

of *Drosophila*. I used electrophysiological recordings from large field tangential cells in the lobula plate during transgenic silencing of upstream elements to probe the functional relevance of these presynaptic neurons in the computation of direction and contrast selectivity. Furthermore, I characterized the response properties of small, columnar cells in the lamina as well as the medulla using two-photon calcium imaging. Finally, through immunohistochemical stainings, I examined the transmitter systems of T₄ and T₅ cells. The highly collaborative environment of our laboratory allowed my physiological techniques to be complemented by several other approaches, including behavioral observations of walking *Drosophilae*, pharmacology and modeling which resulted in a total of six publications that comprise this cumulative dissertation.

2 | PUBLICATIONS

2.1 A DIRECTIONAL TUNING MAP OF *drosophila* ELEMENTARY MOTION DETECTORS

This paper (Maisak et al., 2013) describes response properties of T4 and T5 cells and characterizes their role in *Drosophila* motion vision. It was published in *Nature* in August 2013.

Bushy T4 cells connect the medulla to the four layers of the lobula plate, while T5 cells provide input from the lobula. Measuring changes in calcium levels in response to moving gratings revealed that each subtype of T4 and T5 cells is tuned selectively to one of four cardinal directions (down, up, left, and right). Moreover, polarity specific stimulation provided evidence that T4 cells are activated only by moving brightness increments (ON edges), whereas T5 cells are susceptible for brightness decrements (OFF edges). Blocking the synaptic output of T4 and T5 cells separately, specifically rendered downstream lobula plate tangential cells insensitive for moving bright and dark edges, respectively. Similar phenotypes could be observed when monitoring the turning behavior of T4 and T5 block flies presented with moving ON and OFF edges. From these experiments we concluded that T4 and T5 cells are motion detectors that process visual information from two parallel pathways.

Summary

The following authors contributed to this work:

Matthew S. Maisak, Jürgen Haag, Georg Ammer, Etienne Serbe, **Matthias Meier**, Aljoscha Leonhardt, Tabea Schilling, Armin Bahl, Gerald M. Rubin, Aljoscha Nern, Barry J. Dickson, Dierk F. Reiff, Elisabeth Hopp, and Alexander Borst

Matthew S. Maisak and Jürgen Haag jointly performed and, together with Alexander Borst, evaluated all calcium imaging experiments. Georg Ammer, Etienne Serbe and **Matthias Meier** recorded from tangential cells. Aljoscha Leonhardt, Tabea Schilling and Armin Bahl performed the behavioral experiments. Gerald Rubin, Barry J. Dickson and Aljoscha Nern generated the driver lines and characterized their expression pattern. Dierk F. Reiff performed preliminary imaging experiments. Elisabeth Hopp helped with programming and developed the PMT shielding for the two-photon microscope. Alexander Borst designed the study and wrote the manuscript with the help of all authors.

Author contribution

This article was highlighted in a number of journals (Flight, 2013; Gilbert, 2013; Masland, 2013; Yonehara and Roska, 2013).

A directional tuning map of *Drosophila* elementary motion detectors

Matthew S. Maisak^{1*}, Juergen Haag^{1*}, Georg Ammer¹, Etienne Serbe¹, Matthias Meier¹, Aljoscha Leonhardt¹, Tabea Schilling¹, Armin Bahl¹, Gerald M. Rubin², Aljoscha Nern², Barry J. Dickson³, Dierk F. Reiff[†], Elisabeth Hopp¹ & Alexander Borst¹

The extraction of directional motion information from changing retinal images is one of the earliest and most important processing steps in any visual system. In the fly optic lobe, two parallel processing streams have been anatomically described, leading from two first-order interneurons, L1 and L2, via T4 and T5 cells onto large, wide-field motion-sensitive interneurons of the lobula plate¹. Therefore, T4 and T5 cells are thought to have a pivotal role in motion processing; however, owing to their small size, it is difficult to obtain electrical recordings of T4 and T5 cells, leaving their visual response properties largely unknown. We circumvent this problem by means of optical recording from these cells in *Drosophila*, using the genetically encoded calcium indicator GCaMP5 (ref. 2). Here we find that specific subpopulations of T4 and T5 cells are directionally tuned to one of the four cardinal directions; that is, front-to-back, back-to-front, upwards and downwards. Depending on their preferred direction, T4 and T5 cells terminate in specific sublayers of the lobula plate. T4 and T5 functionally segregate with respect to contrast polarity: whereas T4 cells selectively respond to moving brightness increments (ON edges), T5 cells only respond to moving brightness decrements (OFF edges). When the output from T4 or T5 cells is blocked, the responses of postsynaptic lobula plate neurons to moving ON (T4 block) or OFF edges (T5 block) are selectively compromised. The same effects are seen in turning responses of tethered walking flies. Thus, starting with L1 and L2, the visual input is split into separate ON and OFF pathways, and motion along all four cardinal directions is computed separately within each pathway. The output of these eight different motion detectors is then sorted such that ON (T4) and OFF (T5) motion detectors with the same directional tuning converge in the same layer of the lobula plate, jointly providing the input to downstream circuits and motion-driven behaviours.

Most of the neurons in the fly brain are dedicated to image processing. The respective part of the head ganglion, called the optic lobe, consists of several layers of neuropile called lamina, medulla, lobula and lobula plate, all built from repetitive columns arranged in a retinotopic way (Fig. 1a). Each column houses a set of identified neurons that, on the basis of Golgi staining, have been described anatomically in great detail^{3–5}. Owing to their small size, however, most of these columnar neurons have never been recorded from electrophysiologically. Therefore, their specific functional role in visual processing is still largely unknown. This fact is contrasted by rather detailed functional models about visual processing inferred from behavioural studies and recordings from the large, electrophysiologically accessible output neurons of the fly lobula plate (tangential cells). As the most prominent example of such models, the Reichardt detector derives directional motion information from primary sensory signals by multiplying the output from adjacent photoreceptors after asymmetric temporal filtering⁶. This model makes a number of rather counter-intuitive predictions all of which have been confirmed experimentally (for review, see ref. 7). Yet, the neurons corresponding to most

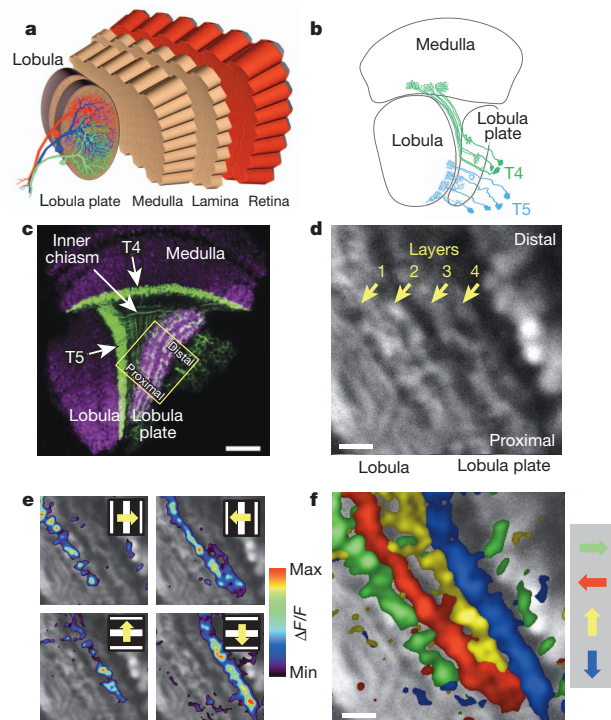


Figure 1 | Directional tuning and layer-specific projection of T4 and T5 cells. **a**, Schematic diagram of the fly optic lobe. In the lobula plate, motion-sensitive tangential cells extend their large dendrites over many hundreds of columns. Shown are the reconstructions of the three cells of the horizontal system²². **b**, Anatomy of T4 and T5 cells, as drawn from Golgi-impregnated material (from ref. 5). **c**, Confocal image of the Gal4-driver line R42F06, shown in a horizontal cross-section (from ref. 10). Neurons are marked in green (Kir2.1-EGFP labelled), whereas the neuropile is stained in purple by an antibody against the postsynaptic protein Dlg. Scale bar, 20 μm . **d**, Two-photon image of the lobula plate of a fly expressing GCaMP5 under the control of the same driver line R42F06. Scale bar, 5 μm . The size and orientation of the image approximately corresponds to the yellow square in **c**. **e**, Relative fluorescence changes ($\Delta F/F$) obtained during 4-s grating motion along the four cardinal directions, overlaid on the greyscale image. Each motion direction leads to activity in a different layer. Minimum and maximum $\Delta F/F$ values were 0.3 and 1.0 (horizontal motion), and 0.15 and 0.6 (vertical motion). **f**, Compound representation of the results obtained from the same set of experiments. Scale bar, 5 μm . Results in **e** and **f** represent the data obtained from a single fly averaged over four stimulus repetitions. Similar results were obtained from six other flies.

¹Max Planck Institute of Neurobiology, 82152 Martinsried, Germany. ²Janelia Farm Research Campus, Ashburn, Virginia 20147, USA. ³Institute of Molecular Pathology, 1030 Vienna, Austria. [†]Present address: Institute Biology 1, Albert-Ludwigs University, 79085 Freiburg, Germany.

*These authors contributed equally to this work.

of the circuit elements of the Reichardt detector have not been identified so far. Here, we focus on a set of neurons called T4 and T5 cells (Fig. 1b) which, on the basis of circumstantial evidence, have long been speculated to be involved in motion detection^{1,8–10}. However, it is unclear to what extent T4 and T5 cells are directionally selective or whether direction selectivity is computed or enhanced within the dendrites of the tangential cells. Another important question concerns the functional separation between T4 and T5 cells; that is, whether they carry equivalent signals, maybe one being excitatory and the other inhibitory on the tangential cells, or whether they segregate into directional- and non-directional pathways¹¹ or into separate ON- and OFF-motion channels^{12,13}.

To answer these questions, we combined Gal4-driver lines specific for T4 and T5 cells¹⁴ with GCaMP5 (ref. 2) and optically recorded the visual response properties using two-photon fluorescence microscopy¹⁵. In a first series of experiments, we used a driver line labelling both T4 and T5 cells. A confocal image (Fig. 1c, modified from ref. 10) revealed clear labelling (in green) in the medulla (T4 cell dendrites), in the lobula (T5 cell dendrites), as well as in four distinct layers of the lobula plate, representing the terminal arborizations of the four subpopulations of both T4 and T5 cells. These four layers of the lobula plate can also be seen in the two-photon microscope when the calcium indicator GCaMP5 is expressed (Fig. 1d). After stimulation of the fly with grating motion along four cardinal directions (front-to-back, back-to-front, upwards and downwards), activity is confined to mostly one of the four layers, depending on the direction in which the grating is moving (Fig. 1e). The outcome of all four stimulus conditions can be combined into a single image by assigning a particular colour to each pixel depending on the stimulus direction to which it responded most strongly (Fig. 1f). From these experiments it is clear that the four subpopulations of T4 and T5 cells produce selective calcium signals depending on the stimulus direction, in agreement with previous deoxyglucose labelling⁸. Sudden changes of the overall luminance evokes no responses in any of the layers (field flicker; $n = 4$ experiments, data not shown). However, gratings flickering in counter-phase lead to layer-specific responses, depending on the orientation of the grating (Supplementary Fig. 1).

The retinotopic arrangement of this input to the lobula plate is demonstrated by experiments where a dark edge was moved within a small area of the visual field only. Depending on the position of this area, activity of T4 and T5 cells is confined to different positions within the lobula plate (Fig. 2a). Consequently, when moving a bright vertical edge horizontally from back to front, activity of T4 and T5 cells is elicited sequentially in layer 2 of the lobula plate (Fig. 2b). These two experiments also demonstrate that T4 and T5 cells indeed signal motion locally. We next investigated the question of where direction selectivity of T4 and T5 cells arises; that is, whether it is already present in the dendrite, or whether it is generated by synaptic interactions within the lobula plate. This question is hard to answer, as the dendrites of both T4 and T5 cells form a dense mesh within the proximal layer of the medulla (T4) and the lobula (T5), respectively. However, signals within the inner chiasm where individual processes of T4 and T5 cells can be resolved in some preparations show a clear selectivity for motion in one over the other directions (Fig. 2c). Such signals are as directionally selective as the ones measured within the lobula plate, demonstrating that the signals delivered from the dendrites of T4 and T5 cells are already directionally selective.

To assess the particular contribution of T4 and T5 cells to the signals observed in the above experiments, we used driver lines specific for T4 and T5 cells, respectively. Applying the same stimulus protocol and data evaluation as in Fig. 1, identical results were obtained as before for both the T4- as well as the T5-specific driver line (Fig. 3a, b). We conclude that T4 and T5 cells each provide directionally selective signals to the lobula plate, in contrast to previous reports¹¹. Thus, both T4 and T5 cells can be grouped, according to their preferred direction, into four subclasses covering all four cardinal directions, reminiscent of ON-OFF ganglion cells of the rabbit retina¹⁶.

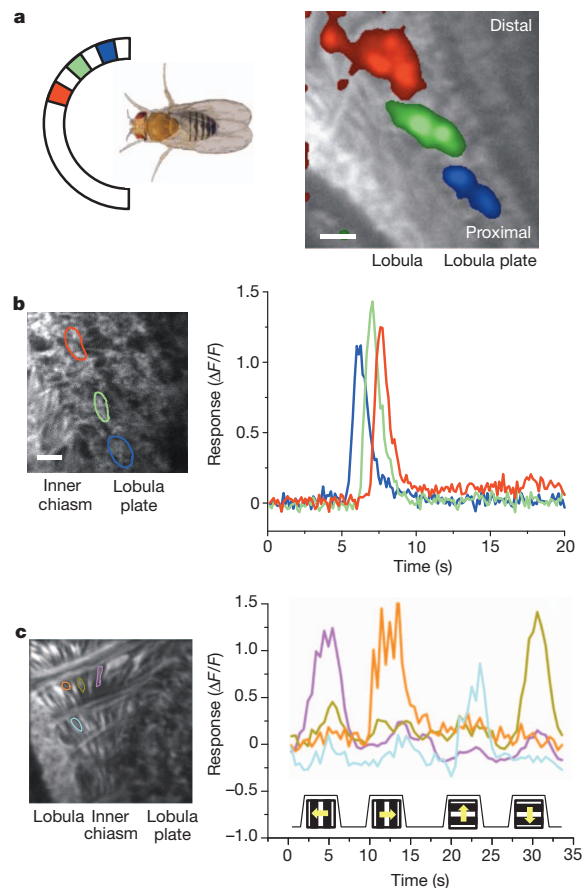


Figure 2 | Local signals of T4 and T5 cells. **a**, Retinotopic arrangement of T4 and T5 cells. A dark edge was moving repeatedly from front-to-back within a 15° wide area at different azimuthal positions (left). This leads to relative fluorescence changes at different positions along the proximal–distal axis within layer 1 of the lobula plate (right). Scale bar, $5\ \mu\text{m}$. Similar results have been obtained in four other flies. **b**, Sequential activation of T4 and T5 cells. A bright edge was moving from back-to-front at $15^\circ\ \text{s}^{-1}$. Scale bar, $5\ \mu\text{m}$. Similar results have been obtained in six other flies. **c**, Signals recorded from individual fibres within the inner chiasm (left) reveal a high degree of direction selectivity (right). Scale bar, $5\ \mu\text{m}$. Similar results were obtained from four other flies, including both lines specific for T4 and T5 cells. Response traces in **b** and **c** are derived from the region of interest encircled in the image with the same colour.

We next addressed whether T4 cells respond differently to T5 cells. To answer this question, we used, instead of gratings, moving edges with either positive (ON edge, brightness increment) or negative (OFF edge, brightness decrement) contrast polarity as visual stimuli. We found that T4 cells strongly responded to moving ON edges, but showed little or no response to moving OFF edges (Fig. 3c). This is true for T4 cells terminating in each of the four layers. We found the opposite for T5 cells. T5 cells selectively responded to moving OFF edges and mostly failed to respond to moving ON edges (Fig. 3d). Again, we found this for T5 cells in each of the four layers. We next addressed whether there are any other differences in the response properties between T4 and T5 cells by testing the velocity tuning of both cell populations by means of stimulating flies with grating motion along the horizontal axis from the front to the back at various velocities covering two orders of magnitude. T4 cells revealed a maximum response at a stimulus velocity of $30^\circ\ \text{s}^{-1}$, corresponding to a temporal frequency of 1 Hz (Fig. 3e). T5 cell responses showed a similar dependency on stimulus velocity, again with a peak at a temporal frequency of

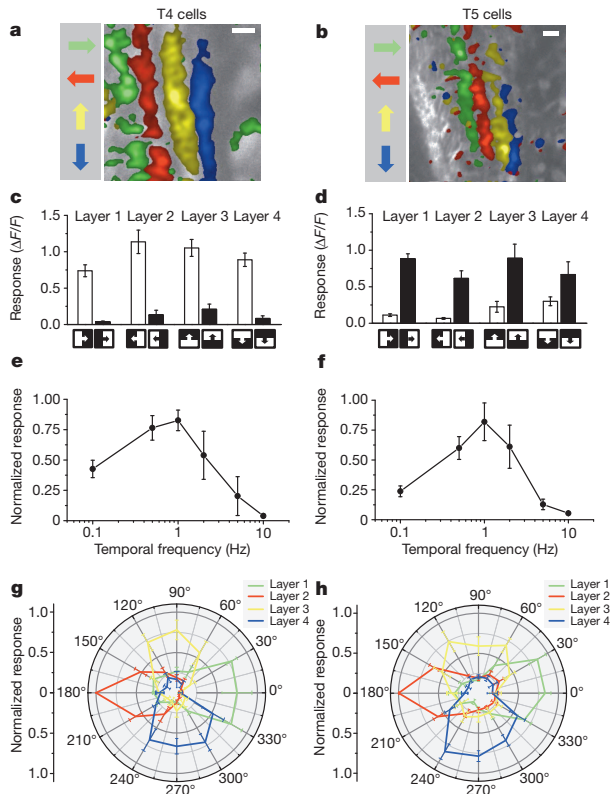


Figure 3 | Comparison of visual response properties between T4 and T5 cells. **a, b**, Relative fluorescence changes ($\Delta F/F$) of the lobula plate terminals of T4 (**a**) and T5 (**b**) cells obtained during grating motion along the four cardinal directions. Results represent the data obtained from a single fly each, averaged over two stimulus repetitions. Scale bars, 5 μm . Similar results have been obtained in ten other flies. **c, d**, Responses of T4 (**c**) and T5 (**d**) cells to ON and OFF edges moving along all four cardinal directions. ON (white) and OFF (black) responses within each layer are significantly different from each other, with $P < 0.005$ except for layers 3 and 4 in T5 cells, where $P < 0.05$. **e, f**, Responses of T4 (**e**) and T5 (**f**) cells to gratings moving horizontally at different temporal frequencies. Relative fluorescence changes were evaluated from layer 1 of the lobula plate and normalized to the maximum response before averaging. **g, h**, Responses of T4 (**g**) and T5 (**h**) cells to gratings moving in 12 different directions. Relative fluorescence changes were evaluated from all four layers of the lobula plate normalized to the maximum response before averaging. Data represent the mean \pm s.e.m. of the results obtained in $n = 8$ (**c**), $n = 7$ (**d**), $n = 6$ (**e**), $n = 7$ (**f**), $n = 6$ (**g**) and $n = 5$ (**h**) different flies. Significances indicated are based on two-sample *t*-test.

1 Hz (Fig. 3f). Thus, there is no obvious difference in the velocity tuning between T4 and T5 cells. As another possibility, T4 cells might functionally differ from T5 cells with respect to their directional tuning width. To test this, we stimulated flies with gratings moving into 12 different directions and evaluated the relative change of fluorescence in all four layers of the lobula plate. Using the T4-specific driver line, we found an approximate half width of $60\text{--}90^\circ$ of the tuning curve, with the peak responses in each layer shifted by 90° (Fig. 3g). No decrease of calcium was detectable for grating motion opposite to the preferred direction of the respective layer. When we repeated the experiments using the T5-specific driver line, we found a similar dependence of the relative change of fluorescence on the stimulus direction (Fig. 3h). We conclude that T4 cells have the same velocity and orientation tuning as T5 cells. The only functional difference we were able to detect remains their selectivity for contrast polarity.

Our finding about the different preference of T4 and T5 cells for the polarity of a moving contrast makes the strong prediction that selective

blockade of T4 or T5 cells should selectively compromise the responses of downstream lobula plate tangential cells to either ON or OFF edges. To test this prediction, we blocked the output of either T4 or T5 cells via expression of the light chain of tetanus toxin¹⁷ and recorded the responses of tangential cells via somatic whole-cell patch to moving ON and OFF edges. In response to moving ON edges, control flies, strong and reliable directional responses were observed in all control flies (Fig. 4a). However, T4-block flies showed a strongly reduced response to ON edges, whereas the responses of T5-block flies were at the level of control flies (Fig. 4b, c). When we used moving OFF edges, control flies again responded with a large amplitude (Fig. 4d). However, the responses of T4-block flies were at the level of control flies, whereas the responses of T5-block flies were strongly reduced (Fig. 4e, f). These findings are reminiscent of the phenotypes obtained from blocking lamina cells L1 and L2 (ref. 13) and demonstrate that T4 and T5 cells are indeed the motion-coding intermediaries for these contrast polarities on their way to the tangential cells of the lobula plate. Whether the residual responses to ON edges in T4-block flies and to OFF edges in T5-block flies are due to an incomplete signal separation between the two pathways or due to an incomplete genetic block in both fly lines is currently unclear.

To address the question of whether T4 and T5 cells are the only motion detectors of the fly visual system, or whether they represent one cell class, in parallel to other motion-sensitive elements, we used tethered flies walking on an air-suspended sphere¹⁸ and stimulated them by ON and OFF edges moving in opposite directions¹⁹. As in the previous experiments, we blocked T4 and T5 cells specifically by selective expression of the light chain of tetanus toxin. During balanced motion, control flies did not show significant turning responses to either side (Fig. 4g). T4-block flies, however, strongly followed the direction of the moving OFF edges, whereas T5-block flies followed the direction of the moving ON edges (Fig. 4h, i). In summary, the selective preference of T4-block flies for OFF edges and of T5-block flies for ON edges not only corroborates our findings about the selective preference of T4 and T5 cells for different contrast polarities, but also demonstrates that the signals of T4 and T5 cells are indeed the major, if not exclusive, inputs to downstream circuits and motion-driven behaviours.

Almost a hundred years after T4 and T5 cells have been anatomically described³, this study reports their functional properties in a systematic way. Using calcium as a proxy for membrane voltage²⁰, we found that both T4 and T5 cells respond to visual motion in a directionally selective manner and provide these signals to each of the four layers of the lobula plate, depending on their preferred direction. Both cell types show identical velocity and orientation tuning which matches the one of the tangential cells^{21,22}. The strong direction selectivity of both T4 and T5 cells is unexpected, as previous studies had concluded that the high degree of direction selectivity of tangential cells is due to a push-pull configuration of weakly directional input with opposite preferred direction^{23,24}. Furthermore, as the preferred direction of T4 and T5 cells matches the preferred direction of the tangential cells branching within corresponding layers, it is currently unclear which neurons are responsible for the null-direction response of the tangential cells. As for the functional separation between T4 and T5 cells, we found that T4 cells selectively respond to brightness increments, whereas T5 cells exclusively respond to moving brightness decrements. Interestingly, parallel ON and OFF motion pathways had been previously postulated on the basis of selective silencing of lamina neurons L1 and L2 (ref. 13). Studies using apparent motion stimuli to probe the underlying computational structure arrived at controversial conclusions: whereas some studies concluded that there was a separate handling of ON and OFF events by motion detectors^{12,25,26}, others did not favour such a strict separation^{19,27}. The present study directly demonstrates the existence of separate ON and OFF motion detectors, as represented by T4 and T5 cells, respectively. Furthermore, our results anatomically confine the essential processing steps of elementary

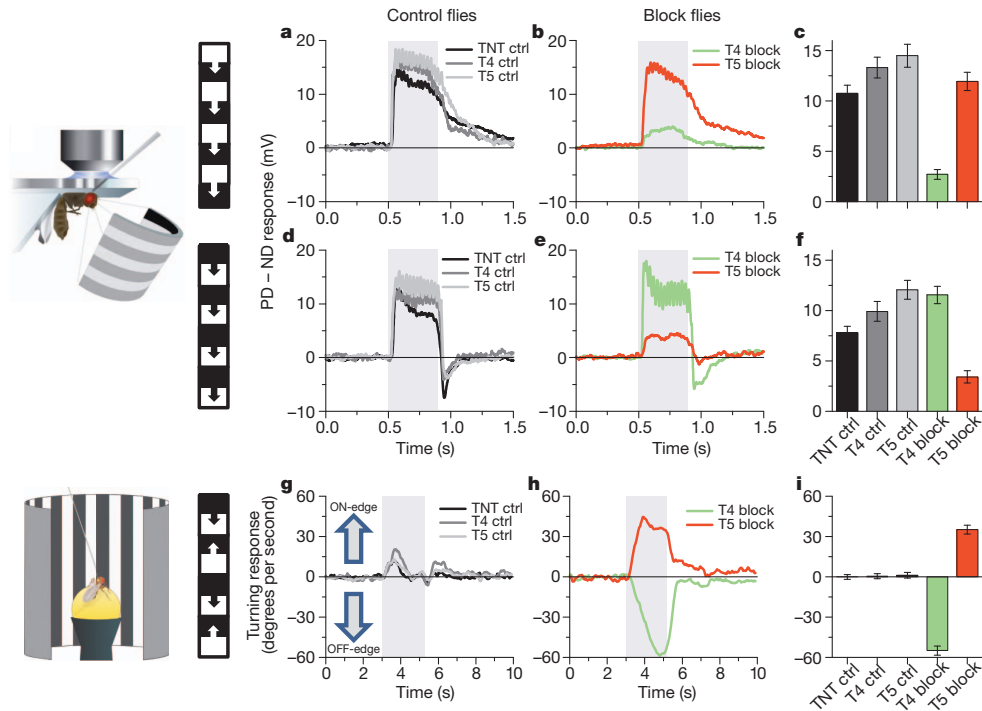


Figure 4 | Voltage responses of lobula plate tangential cells and turning responses of walking flies to moving ON and OFF edges. **a, d,** Average time course of the membrane potential in response to preferred direction motion minus the response to null direction motion (PD – ND response) as recorded in three types of control flies (stimulation period indicated by shaded area). **b, e,** Same as in **a, d,** but recorded in T4-block flies (green) and T5-block flies (red). The stimulus pattern, shown to the left, consisted of multiple ON- (a) or OFF-edges (d). **c, f,** Mean voltage responses (PD – ND) of tangential cells in the five groups of flies. Recordings were done from cells of the vertical²¹ and the horizontal²² system. Because no difference was detected between them, data were pooled. Data comprise recordings from $n = 20$ (TNT control), $n = 12$ (T4 control), $n = 16$ (T5 control), $n = 17$ (T4 block) and $n = 18$ (T5 block) cells. In both T4 and T5-block flies, ON and OFF responses are significantly different

from each other with $P < 0.001$. In T4-block flies, ON responses are significantly reduced compared to all three types of control flies, whereas in T5-block flies, OFF responses are significantly reduced, both with $P < 0.001$. **g,** Average time course of the turning response of three types of control flies to ON and OFF edges moving simultaneously to opposite directions (stimulation period indicated by shaded area). **h,** Same as in **g,** but recorded from T4-block flies (green) and T5-block flies (red). **i,** Mean turning tendency (\pm s.e.m.) during the last second of the stimulation period averaged across all flies within each group. Data comprise average values obtained in $n = 12$ (TNT controls), $n = 11$ (T4 controls), $n = 11$ (T5 controls), $n = 13$ (T4 block) and $n = 12$ (T5 block) flies. Values of T4 and T5-block flies are highly significantly different from zero with $P < 0.001$. Significances indicated are based on two-sample t -test.

motion detection—that is, asymmetric temporal filtering and non-linear interaction—to the neuropile between the axon terminals of lamina neurons L1 and L2 (ref. 28) and the dendrites of directionally selective T4 and T5 cells (Supplementary Fig. 2). The dendrites of T4 and T5 cells might well be the place where signals from neighbouring columns interact in a nonlinear way, similar to the dendrites of starburst amacrine cells of the vertebrate retina²⁹.

METHODS SUMMARY

Flies. Flies used in calcium imaging experiments (Figs 1–3) had the following genotypes: T4/T5 line ($w^-/+;$ $UAS-GCaMP5, R42F06-GAL4/UAS-GCaMP5, R42F06-GAL4$), T4 line ($w^-/+;$ $UAS-GCaMP5, R54A03-GAL4/UAS-GCaMP5, R54A03-GAL4$), T5 line ($w^-/+;$ $UAS-GCaMP5, R42H07-GAL4/UAS-GCaMP5, R42H07-GAL4$). Flies used in electrophysiological and behavioural experiments (Fig. 4) had identical genotypes of the following kind: TNT control flies ($w^+/w^+;$ $UAS-TNT-E/UAS-TNT-E/+;$), T4 control flies ($w^+/w^-;$ $+/+;$ $VT37588-GAL4/+;$), T5 control flies ($w^+/w^-;$ $+/+;$ $R42H07-GAL4/+;$), T4-block flies ($w^+/w^-;$ $UAS-TNT-E/+;$ $VT37588-GAL4/+;$), T5-block flies ($w^+/w^-;$ $UAS-TNT-E/+;$ $R42H07-GAL4/+;$).

Two-photon microscopy. We used a custom-built two-photon laser scanning microscope²⁹ equipped with a $\times 40$ water immersion objective and a mode locked Ti:sapphire laser. To shield the photomultipliers from the stimulus light, two separate barriers were used: the first was placed directly over the LEDs, the second extended from the fly holder over the arena. Images were acquired at a resolution of 256×256 pixels and a frame rate of 1.87 Hz, except where indicated, using ScanImage software³⁰.

Electrophysiology. Recordings were established under visual control using a Zeiss Microscope and a $\times 40$ water immersion objective.

Behavioural analysis. The locomotion recorder was custom-designed according to ref. 18. It consisted of an air-suspended sphere floating in a bowl-shaped sphere holder. Motion of the sphere was recorded by two optical tracking sensors.

Visual stimulation. For calcium imaging and electrophysiological experiments, we used a custom-built LED arena covering 180° and 90° of the visual field along the horizontal and the vertical axis, respectively, at 1.5° resolution. For the behavioural experiments, three 120-Hz LCD screens formed a U-shaped visual arena with the fly in the centre, covering 270° and 114° of the visual field along the horizontal and the vertical axes, respectively, at 0.1° resolution.

Data evaluation. Data were evaluated off-line using custom-written software (Matlab and IDL).

Full Methods and any associated references are available in the online version of the paper.

Received 16 April; accepted 20 May 2013.

- Bausenwein, B., Dittrich, A. P. M. & Fischbach, K. F. The optic lobe of *Drosophila melanogaster* II. Sorting of retinotopic pathways in the medulla. *Cell Tissue Res.* **267**, 17–28 (1992).
- Akerboom, J. *et al.* Optimization of a GCaMP calcium indicator for neural activity imaging. *J. Neurosci.* **32**, 13819–13840 (2012).
- Cajal, S. R. & Sanchez, D. *Contribucion al conocimiento de los centros nerviosos de los insectos* (Imprenta de Hijos de Nicholas Moja, 1915).
- Strausfeld, N. J. *Atlas of an Insect Brain* (Springer, 1976).
- Fischbach, K. F. & Dittrich, A. P. M. The optic lobe of *Drosophila melanogaster*. I. A Golgi analysis of wild-type structure. *Cell Tissue Res.* **258**, 441–475 (1989).

6. Reichardt, W. Autocorrelation, a principle for the evaluation of sensory information by the central nervous system. In *Sensory Communication* (ed. Rosenblith, W. A.) 303–317 (MIT Press and John Wiley & Sons, 1961).
7. Borst, A., Haag, J. & Reiff, D. F. Fly motion vision. *Annu. Rev. Neurosci.* **33**, 49–70 (2010).
8. Buchner, E., Buchner, S. & Buelthoff, I. Deoxyglucose mapping of nervous activity induced in *Drosophila* brain by visual movement. 1. Wildtype. *J. Comp. Physiol. A* **155**, 471–483 (1984).
9. Strausfeld, N. J. & Lee, J. K. Neuronal basis for parallel visual processing in the fly. *Vis. Neurosci.* **7**, 13–33 (1991).
10. Schnell, B., Raghu, V. S., Nern, A. & Borst, A. Columnar cells necessary for motion responses of wide-field visual interneurons in *Drosophila*. *J. Comp. Physiol. A* **198**, 389–395 (2012).
11. Douglass, J. K. & Strausfeld, N. J. Visual motion-detection circuits in flies: Parallel direction- and non-direction-sensitive pathways between the medulla and lobula plate. *J. Neurosci.* **16**, 4551–4562 (1996).
12. Franceschini, N., Riehle, A. & Le Nestour, A. Directionally selective motion detection by insect neurons. In *Facets of Vision* (ed. Stavenha, H.) 360–390 (Springer, 1989).
13. Joesch, M., Schnell, B., Raghu, S. V., Reiff, D. F. & Borst, A. ON and OFF pathways in *Drosophila* motion vision. *Nature* **468**, 300–304 (2010).
14. Pfeiffer, B. D. *et al.* Tools for neuroanatomy and neurogenetics in *Drosophila*. *Proc. Natl Acad. Sci. USA* **105**, 9715–9720 (2008).
15. Denk, W., Strickler, J. H. & Webb, W. W. Two-photon laser scanning fluorescence microscopy. *Science* **248**, 73–76 (1990).
16. Oyster, C. W. & Barlow, H. B. Direction-selective units in rabbit retina: distribution of preferred directions. *Science* **155**, 841–842 (1967).
17. Sweeney, S. T., Broadie, K., Keane, J., Niemann, H. & O’Kane, C. J. Targeted expression of tetanus toxin light chain in *Drosophila* specifically eliminates synaptic transmission and causes behavioral defects. *Neuron* **14**, 341–351 (1995).
18. Seelig, J. D. *et al.* Two-photon calcium imaging from head-fixed *Drosophila* during optomotor walking behavior. *Nature Methods* **7**, 535–540 (2010).
19. Clark, D. A., Bursztyn, L., Horowitz, M. A., Schnitzer, M. J. & Clandinin, T. R. Defining the computational structure of the motion detector in *Drosophila*. *Neuron* **70**, 1165–1177 (2011).
20. Egelhaaf, M. & Borst, A. Calcium accumulation in visual interneurons of the fly: Stimulus dependence and relationship to membrane potential. *J. Neurophysiol.* **73**, 2540–2552 (1995).
21. Joesch, M., Plett, J., Borst, A. & Reiff, D. F. Response properties of motion-sensitive visual interneurons in the lobula plate of *Drosophila melanogaster*. *Curr. Biol.* **18**, 368–374 (2008).
22. Schnell, B. *et al.* Processing of horizontal optic flow in three visual interneurons of the *Drosophila* brain. *J. Neurophysiol.* **103**, 1646–1657 (2010).
23. Borst, A. & Egelhaaf, M. Direction selectivity of fly motion-sensitive neurons is computed in a two-stage process. *Proc. Natl Acad. Sci. USA* **87**, 9363–9367 (1990).
24. Single, S., Haag, J. & Borst, A. Dendritic computation of direction selectivity and gain control in visual interneurons. *J. Neurosci.* **17**, 6023–6030 (1997).
25. Eichner, H., Joesch, M., Schnell, B., Reiff, D. F. & Borst, A. Internal structure of the fly elementary motion detector. *Neuron* **70**, 1155–1164 (2011).
26. Joesch, M., Weber, F., Eichner, H. & Borst, A. Functional specialization of parallel motion detection circuits in the fly. *J. Neurosci.* **33**, 902–905 (2013).
27. Egelhaaf, M. & Borst, A. Are there separate ON and OFF channels in fly motion vision? *Vis. Neurosci.* **8**, 151–164 (1992).
28. Takemura, S. Y., Lu, Z. & Meinertzhagen, I. A. Synaptic circuits of the *Drosophila* optic lobe: the input terminals to the medulla. *J. Comp. Neurol.* **509**, 493–513 (2008).
29. Euler, T., Detwiler, P. B. & Denk, W. Directionally selective calcium signals in dendrites of starburst amacrine cells. *Nature* **418**, 845–852 (2002).
30. Pologruto, T. A., Sabatini, B. L. & Svoboda, K. ScanImage: Flexible software for operating laser scanning microscopes. *Biomed. Eng. Online* **2**, 13 (2003).

Supplementary Information is available in the online version of the paper.

Acknowledgements We thank L. Looger, J. Simpson, V. Jayaraman and the Janelia GECI team for making and providing us with the GCaMP5 flies before publication; J. Plett for designing and engineering the LED arena; C. Theile, W. Essbauer and M. Sauter for fly work; and A. Mauss, F. Gabbiani and T. Bonhoeffer for critically reading the manuscript. This work was in part supported by the Deutsche Forschungsgemeinschaft (SFB 870). M.S.M., G.A., E.S., M.M., A.L., A.Ba and A.Bo are members of the Graduate School of Systemic Neurosciences.

Author Contributions M.S.M. and J.H. jointly performed and, together with A.Bo., evaluated all calcium imaging experiments. G.A., E.S. and M.M. recorded from tangential cells. A.L., T.S. and A.Ba. performed the behavioural experiments. G.R., B.D. and A.N. generated the driver lines and characterized their expression pattern. D.F.R. performed preliminary imaging experiments. E.H. helped with programming and developed the PMT shielding for the two-photon microscope. A.Bo. designed the study and wrote the manuscript with the help of all authors.

Author Information Reprints and permissions information is available at www.nature.com/reprints. The authors declare no competing financial interests. Readers are welcome to comment on the online version of the paper. Correspondence and requests for materials should be addressed to A.Bo. (borst@neuro.mpg.de).

METHODS

Flies. Flies were raised on standard cornmeal-agar medium at 25 °C and 60% humidity throughout development on a 12 h light/12 h dark cycle. For calcium imaging, we used the genetically encoded single-wavelength indicator GCaMP5, variant G, with the following mutations: T302L, R303P and D380Y (ref. 2). Expression of GCaMP5 was directed by three different Gal4 lines, all from the *Janelia Farm* collection¹⁴. Flies used in calcium imaging experiments (Figs 1–3) had the following genotypes: T4/T5 line ($w^-/+;$ *UAS-GCaMP5,R42F06-GAL4/UAS-GCaMP5,R42F06-GAL4*), T4 line ($w^-/+;$ *UAS-GCaMP5,R54A03-GAL4/UAS-GCaMP5,R54A03-GAL4*), T5 line ($w^-/+;$ *UAS-GCaMP5,R42H07-GAL4/UAS-GCaMP5,R42H07-GAL4*). All driver lines were generated by the methods described in ref. 14 and were identified by screening a database of imaged lines, followed by reimaging of selected lines³¹. As homozygous for both the Gal4-driver and the *UAS-GCaMP5* genes, T4 flies also showed some residual expression in T5 cells, and T5 flies also in T4 cells. This unspecific expression, however, was in general less than 25% of the expression in the specific cells. Flies used in electrophysiological and behavioural experiments (Fig. 4) had identical genotypes of the following kind: TNT control flies ($w^+/w^+;$ *UAS-TNT-E/UAS-TNT-E*; $+/+$), T4 control flies ($w^+/w^-;$ $+/+$; *VT37588-GAL4/+*), T5 control flies ($w^+/w^-;$ $+/+$; *R42H07-GAL4/+*), T4-block flies ($w^+/w^-;$ *UAS-TNT-E/+;* *VT37588-GAL4/+*), T5-block flies ($w^+/w^-;$ *UAS-TNT-E/+;* *R42H07-GAL4/+*). *UAS-TNT-E* flies were derived from the Bloomington Stock Center (stock no. 28837) and *VT37588-GAL4* flies were derived from the VDRC (stock no. 205893). Before electrophysiological experiments, flies were anaesthetized on ice and waxed on a Plexiglas holder using bees wax. The dissection of the fly cuticle and exposure of the lobula plate were performed as described previously (for imaging experiments, see ref. 32; for electrophysiology, see ref. 21). Flies used in behavioural experiments were taken from 18 °C just before the experiment and immediately cold-anaesthetized. The head, the thorax and the wings were glued to a needle using near-ultraviolet bonding glue (Sinfony Opaque Dentin) and strong blue LED light (440 nm, dental curing-light, New Woodpecker).

Two-photon microscopy. We used a custom-built two-photon laser scanning microscope³³ equipped with a $\times 40$ water immersion objective (0.80 NA, IR-Achroplan; Zeiss). Fluorescence was excited by a mode locked Ti:sapphire laser (<100 fs, 80 MHz, 700–1,020 nm; pumped by a 10 W CW laser; both Mai Tai; Spectraphysics) with a DeepSee accessory module attached for dispersion compensation control resulting in better pulse compression and fluorescence at the target sample. Laser power was adjusted to 10–20 mW at the sample, and an excitation wavelength of 910 nm was used. The photomultiplier tube (H10770PB-40, Hamamatsu) was equipped with a dichroic band-pass mirror (520/35, Brightline). Images were acquired at a resolution of 256×256 pixels and a frame rate of 1.87 Hz, except in Fig. 2 (7.5 Hz), using the ScanImage software³⁰.

Electrophysiology. Recordings were established under visual control using a $\times 40$ water immersion objective (LumplanF, Olympus), a Zeiss microscope (Axiotech vario 100, Zeiss), and illumination (100 W fluorescence lamp, hot mirror, neutral density filter OD 0.3; all from Zeiss). To enhance tissue contrast, we used two polarization filters, one located as an excitation filter and the other as an emission filter, with slight deviation on their polarization plane. For eye protection, we additionally used a 420-nm LP filter on the light path.

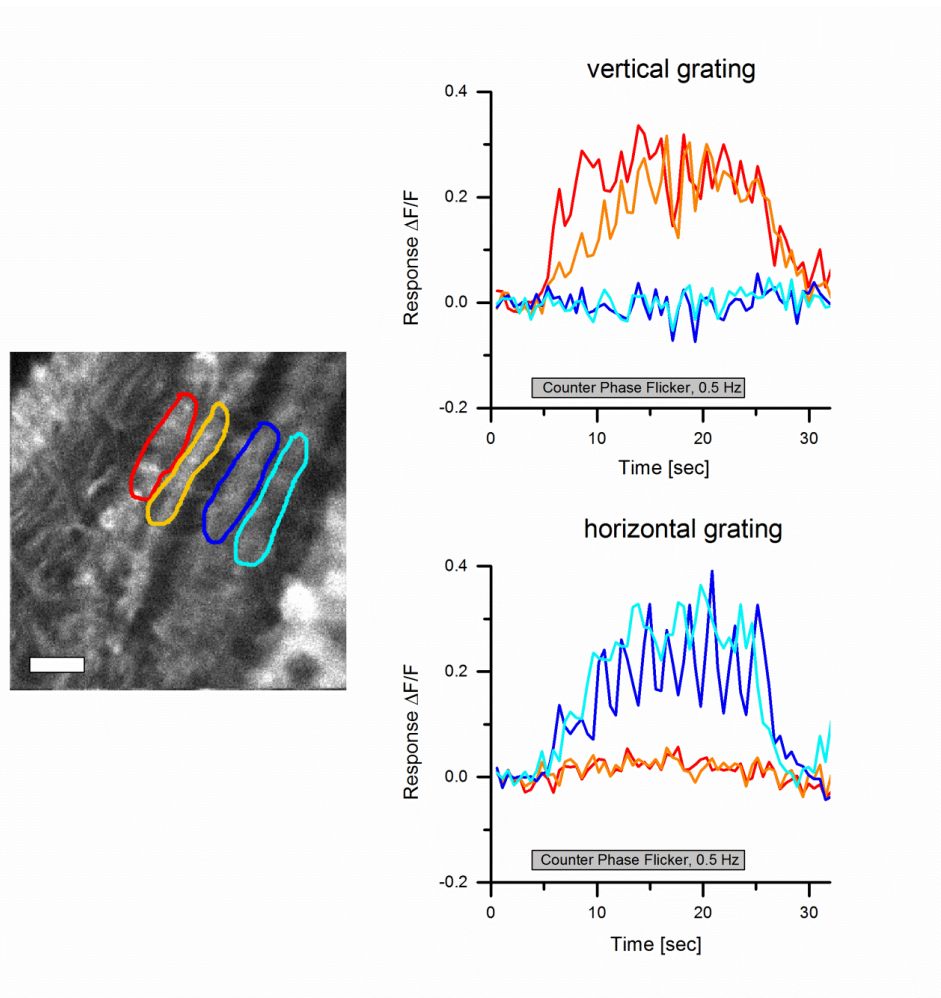
Behavioural analysis. The locomotion recorder was custom-designed according to ref. 18. Briefly, it consists of an air-suspended sphere floating in a bowl-shaped sphere holder. A high-power infrared LED (800 nm, JET series, 90 mW, Roithner Electronics) is located in the back to illuminate the fly and the sphere surface. Two optical tracking sensors are equipped with lens and aperture systems to focus on the sphere behind the fly. The tracking data are processed at 4 kHz internally, read out via a USB interface and processed by a computer at ≈ 200 Hz. This allows real-time calculation of the instantaneous rotation axis of the sphere. A third camera (GRAS-20S4M-C, Point Grey Research) is located in the back which is essential for proper positioning of the fly and allows real-time observation and video recording of the fly during experiments.

Visual stimulation. For calcium imaging and electrophysiological experiments, we used a custom-built LED arena that allowed refresh rates of up to 550 Hz and 16 intensity levels. It covered 180° (1.5° resolution) and 90° (1.5° resolution) of the visual field along the horizontal and the vertical axis, respectively. The LED arena was engineered and modified based upon ref. 34. The LED array consists of 7×4 individual TA08-81GWA dot-matrix displays (Kingbright), each harbouring 8×8 individual green (568 nm) LEDs. Each dot-matrix display is controlled by an ATmega168 microcontroller (Atmel) combined with a ULN2804 line driver (Toshiba America) acting as a current sink. All panels are in turn controlled via an I2C interface by an ATmega128 (Atmel)-based main controller board, which reads in pattern information from a compact flash (CF) memory card. Matlab was used for programming and generation of the patterns as well as for sending the serial command sequences via RS-232 to the main controller board. The

luminance range of the stimuli was $0.5\text{--}33\text{ cd m}^{-2}$. For the calcium imaging experiments, two separate barriers were used to shield the photomultipliers from the stimulus light coming from the LED arena. The first was a spectral filter with transparency to wavelengths > 540 nm placed directly over the LEDs (ASF SFG 10, Microchemicals). The second was a layer of black PVC extending from the fly holder over the arena. Square wave gratings had a spatial wavelength of 30° of visual angle and a contrast of 88%. Unless otherwise stated, they were moving at 30° s^{-1} . Edges had the same contrast and were also moving at 30° s^{-1} . For the experiments shown in Figs 1, 2b and 3, each grating or edge motion was shown twice within a single sweep, resulting in a total of eight stimulation periods. Each stimulus period lasted 4 s, and subsequent stimuli were preceded by a 3-s pause. In the experiment shown in Fig. 2a, a dark edge of 88% contrast was moved for 1 s at 15° s^{-1} from the front to the back at three different positions (22° , 44° , 66° , from frontal to lateral). At each position, edge motion was repeated 15 times. For the experiment shown in Fig. 2b, a bright edge of 88% contrast was moving at 15° s^{-1} from the back to the front, and images were acquired at a frame rate of 7.5 Hz. For the experiments shown in Figs 3e, f, all six stimulus velocities were presented once within one sweep, with the stimulus lasting 4 s, and different stimuli being separated by 2 s. In the experiments shown in Figs 3g, h, a single sweep contained all 12 grating orientations with the same stimulus and pause length as above. For the electrophysiology experiments (Fig. 4a–f), multiple edges were used as stimuli moving simultaneously at 50° s^{-1} . To stimulate cells of horizontal system (HS cells), a vertical, stationary square-wave grating with 45° spatial wavelength was presented. For ON-edge motion, the right (preferred direction, PD) or the left edge (null direction, ND) of each light bar started moving until it merged with the neighbouring bar. For OFF-edge motion, the right or the left edge of each dark bar was moving. To stimulate cells of the vertical system (VS cells), the pattern was rotated by 90° clockwise. For the behavioural experiments (Fig. 4g–i), three 120-Hz LCD screens (Samsung 2233 RZ) were vertically arranged to form a U-shaped visual arena ($w = 31\text{ cm} \times d = 31\text{ cm} \times h = 47\text{ cm}$) with the fly in the centre. The luminance ranged from 0 to 131 cd m^{-2} and covered large parts of the flies' visual field (horizontal, $\pm 135^\circ$; vertical, $\pm 57^\circ$; resolution, $< 0.1^\circ$). The three LCD screens were controlled via NVIDIA 3D Vision Surround Technology on Windows 7 64-bit allowing a synchronized update of the screens at 120 frames per second. Visual stimuli were created using Panda3D, an open-source gaming engine, and Python 2.7, which simultaneously controlled the frame rendering in Panda3D, read out the tracking data and temperature and streamed data to the hard disk. The balanced motion stimulus consisted of a square-wave grating with 45° spatial wavelength and a contrast of 63%. Upon stimulation onset, dark and bright edges moved into opposite directions at 10° s^{-1} for 2.25 s. This stimulation was performed for both possible edge directions and two initial grating positions shifted by half a wavelength, yielding a total of four stimulus conditions.

Data evaluation. Data were evaluated off-line using custom-written software (Matlab and IDL). For the images shown in Figs 1e, f, 2a and 3a, b, the raw image series was converted into four images representing the relative fluorescence change during each direction of grating motion: $(\Delta F/F)_{\text{stim}} = (F_{\text{stim}} - F_{\text{ref}})/F_{\text{ref}}$. The image representing the stimulus fluorescence (F_{stim}) was obtained by averaging all images during stimulation; the image representing the reference fluorescence (F_{ref}) was obtained by averaging three images before stimulation. Both images were smoothed using a Gaussian filter of 10 pixel half-width. For the images shown in Figs 1f and 3a, b, $\Delta F/F$ images were normalized by their maximum value. Then, a particular colour was assigned to each pixel according to the stimulus direction during which it reached maximum value, provided it passed a threshold of 25%. Otherwise, it was assigned to background. The response strength of each pixel was coded as the saturation of that particular colour. For the data shown in Figs 2b, c and 3c–h, the raw image series was first converted into a $\Delta F/F$ series by using the first three images as reference. Then, a region was defined within a raw image, and average $\Delta F/F$ values were determined within that region for each image, resulting in a $\Delta F/F$ signal over time. Responses were defined as the maximum $\Delta F/F$ value reached during each stimulus presentation minus the average $\Delta F/F$ value during the two images preceding the stimulus. For the bar graphs shown in Fig. 4c, f, the average voltage responses during edge motion (0.45 s) along the cell's preferred (PD) and null direction (ND) were calculated. For each recorded tangential cell, the difference between the PD and the ND response was determined, and these values were averaged across all recorded cells. The data shown in Fig. 4g, h were obtained from the four stimulus conditions by averaging the turning responses for the two starting positions of the grating and calculating the mean difference between the turning responses for the two edge directions. For the bar graph shown in Fig. 4i, the average turning response of each fly during the last second of balanced motion stimulation was calculated. These values were averaged across all recorded flies within each genotype.

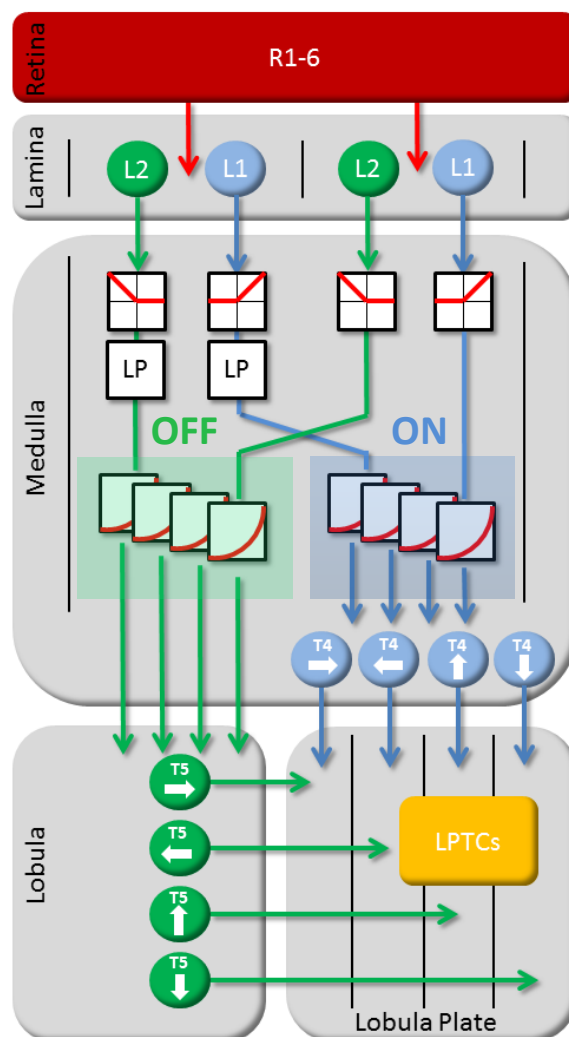
31. Jenett, A. *et al.* A Gal4-driver line resource for *Drosophila* neurobiology. *Cell Rep.* **2**, 991–1001 (2012).
32. Reiff, D. F., Plett, J., Mank, M., Griesbeck, O. & Borst, A. Visualizing retinotopic half-wave rectified input to the motion detection circuitry of *Drosophila*. *Nature Neurosci.* **13**, 973–978 (2010).
33. Euler, T. *et al.* Eyecup scope—optical recording of light stimulus-evoked fluorescence signals in the retina. *Pflüger Arch.* **457**, 1393–1414 (2009).
34. Reiser, M. B. & Dickinson, M. H. A modular display system for insect behavioral neuroscience. *J. Neurosci. Methods* **167**, 127–139 (2008).



Supplemental Fig.1 Responses of T4 and T5 cells to counter-phase flicker. Square-wave gratings (15 deg spatial wavelength and 88% contrast) with vertical (top) and horizontal (bottom) orientation were phase-shifted every second by 180 deg for 20 seconds. Response traces are derived from the region of interest encircled in the image to the left with the same color from a single stimulation period. T4 and T5 cells in layers 1 and 2 only respond to the vertical grating, cells in layers 3 and 4 selectively respond to the horizontal grating. Similar results were obtained in n=4 flies. Scale bar = 5 μ m. Together with the missing response of T4 and T5 cells to full-field flicker, these findings suggest that T4 and T5 cells receive input signals from neurons with different orientation tuning, depending on whether they respond to motion along the horizontal (layers 1 and 2) or the vertical (layers 3 and 4) axis^{1,2}.

1 Pick, B. & Buchner, E. Visual movement detection under light- and dark-adaptation in the fly, *Musca domestica*. *J. Comp. Physiol.* **134**, 45-54 (1979).

2 Srinivasan, M.V. & Dvorak, D.R. Spatial processing of visual information in the movement-detecting pathway of the fly. *J. Comp. Physiol.* **140**, 1-23 (1980).



Supplemental Fig.2 Circuit diagram of the fly elementary motion detector. Visual input from photoreceptors R1-6 is split into parallel pathways, L1 and L2, at the level of the lamina. Two neighboring columns are shown. The outputs from both L1 and L2 are half-wave rectified, such that downstream elements carry information about ON (L1-pathway) and OFF (L2-pathway) signals separately. After temporal low-pass filtering ('LP') the signals from one column, they interact in a supra-linear way with the instantaneous signals derived from the other column. This interaction takes place, separately in both pathways, along all four cardinal directions. Directionally selective signals are carried via T4 and T5 cells to the four layers of the lobula plate where T4 and T5 cells with the same preferred direction converge again on the dendrites of the tangential cells ('LPTCs').

2.2 NEURAL CIRCUIT COMPONENTS OF THE *drosophila* OFF MOTION VISION PATHWAY

In this publication (Meier et al., 2014) we examined the response properties and functional roles of two columnar cell types in the lamina and the medulla. It appeared in *Current Biology* in February 2014.

Summary

Based on morphological evidence, a direction specific role for lamina neurons L4 and transmedullary neurons Tm2 had been proposed. Using two-photon calcium imaging, we probed the functional characteristics of these two cell types. Presenting shifting gratings and edges of either polarity we found that both cell types are excited by brightness decrements moving in any direction. Moreover, while their spatial receptive fields were similar, L4 appeared to integrate dark signals over large areas, whereas Tm2 seemed to be subject to lateral inhibition. Investigating their temporal properties revealed fast, transient kinetics for Tm2 and slower, more sustained responses for L4. We then tested their necessity for the processing of visual motion by recording from motion sensitive lobula plate tangential cells while blocking the synaptic output of either L4 or Tm2. Here, we observed that responses to OFF edges were selectively reduced in both genotypes. From these data we concluded that both L4 and Tm2 cells were crucially involved in the detection of moving dark edges and that they contribute different spatial and temporal filters to this computation.

The following people contributed to this work:

Matthias Meier¹, Etienne Serbe¹, Matthew S. Maisak, Jürgen Haag, Barry J. Dickson, and Alexander Borst

Author contribution

Matthias Meier, Etienne Serbe and Alexander Borst designed the study. **Matthias Meier** and Etienne Serbe performed electrophysiological recordings. **Matthias Meier**, Etienne Serbe, Matthew S. Maisak, and Jürgen Haag performed calcium imaging experiments. Barry J. Dickson provided unpublished Gal4-lines. **Matthias Meier**, Etienne Serbe and Alexander Borst wrote the paper with help of the other authors.

¹ equal contribution

Neural Circuit Components of the *Drosophila* OFF Motion Vision Pathway

Matthias Meier,^{1,3} Etienne Serbe,^{1,3} Matthew S. Maisak,¹ Jürgen Haag,¹ Barry J. Dickson,^{2,4} and Alexander Borst^{1,*}

¹Department of Circuits-Computation-Models, Max Planck Institute of Neurobiology, Am Klopferspitz 18, 82152 Martinsried, Germany

²Research Institute of Molecular Pathology, Dr. Bohr-Gasse 7, 1030 Vienna, Austria

Summary

Background: Detecting the direction of visual motion is an essential task of the early visual system. The Reichardt detector has been proven to be a faithful description of the underlying computation in insects. A series of recent studies addressed the neural implementation of the Reichardt detector in *Drosophila* revealing the overall layout in parallel ON and OFF channels, its input neurons from the lamina (L1 → ON, and L2 → OFF), and the respective output neurons to the lobula plate (ON → T4, and OFF → T5). While anatomical studies showed that T4 cells receive input from L1 via Mi1 and Tm3 cells, the neurons connecting L2 to T5 cells have not been identified so far. It is, however, known that L2 contacts, among others, two neurons, called Tm2 and L4, which show a pronounced directionality in their wiring.

Results: We characterized the visual response properties of both Tm2 and L4 neurons via Ca²⁺ imaging. We found that Tm2 and L4 cells respond with an increase in activity to moving OFF edges in a direction-unselective manner. To investigate their participation in motion vision, we blocked their output while recording from downstream tangential cells in the lobula plate. Silencing of Tm2 and L4 completely abolishes the response to moving OFF edges.

Conclusions: Our results demonstrate that both cell types are essential components of the *Drosophila* OFF motion vision pathway, prior to the computation of directionality in the dendrites of T5 cells.

Introduction

The computation of motion is imperative for fundamental behaviors such as mate or prey detection, predator avoidance, and visual navigation. In the fruit fly *Drosophila*, motion cues are processed in the optic lobe, a brain area comprised of the lamina, medulla, lobula, and lobula plate, each arranged in a columnar, retinotopic fashion. Whereas photoreceptors respond to motion in a nondirectional way, wide-field tangential cells of the lobula plate depolarize to motion in their preferred direction (PD) and hyperpolarize to motion in the opposite or null direction (ND) [1, 2]. These direction-selective responses are well characterized by a mathematical model, the so-called Reichardt detector. In this model, signals from neighboring photoreceptors are multiplied after asymmetric

temporal filtering [3–5]. Due to the anatomical complexity and miniscule size of the columnar neurons of the optic lobe, identification of the neural elements of the motion detection circuit has long proven difficult.

In agreement with previous suggestions based on costratification of Golgi-stained columnar cells [6, 7] and cell-unspecific activity labeling using the deoxyglucose method [8], recent studies identified two parallel motion processing streams, one leading from lamina neuron L1 via T4 cells and the other from lamina neuron L2 via T5 onto the dendrites of the tangential cells [9, 10]. Within each pathway, four subpopulations of T4 and T5 cells are tuned to one of the four cardinal directions (front to back, back to front, upward, or downward), providing direction-selective signals to four different sublayers of the lobula plate [11, 12]. Here, they become spatially integrated on the dendrites of tangential cells [12, 13]. The two pathways are functionally segregated with regard to their selectivity for contrast polarity: the L1 pathway is selectively responsive to the motion of brightness increments (ON pathway), while the L2 pathway responds selectively to the motion of brightness decrements (OFF pathway) [10, 12, 14–16]. These findings suggest that important processing steps of motion computation take place between the axon terminals of L1/L2 and the output regions of T4/T5.

For the ON pathway, a recent connectomic EM study of the fly medulla [17] not only identified two neurons, Mi1 and Tm3, as the most prominent postsynaptic targets of L1, but also showed that these cells make up for more than 90% of all input synapses on the dendrites of T4 cells. Most interestingly, the innervation of Tm3 and Mi1 on a single T4 cell is asymmetric, consistent with the preferred direction of the T4 cell, i.e., the lobula plate layer where it terminates. Because connectomic analysis has not yet reached the lobula, where the dendrites of T5 cells reside [6], the connectivity for the OFF pathway is known only within the lamina and the medulla [17–22]. Here, several cell types have been found to be postsynaptic to L2 [17, 18], i.e., L4, Tm1, and Tm2. Tm1 and Tm2 both receive synaptic input from L2 in the second layer of the medulla [17, 18] projecting to the first layer of the lobula. Within the lamina, L4 sends its processes into three neighboring columns, one into its “home” column and two into the two neighboring posterior columns [19, 20]. Within each of these columns, L4 forms reciprocal connections with L2 and with the processes of those L4s originating from other columns [19–22]. In its home column, L4 receives additional synaptic input from a lamina amacrine cell, as well as from photoreceptor R6 [21, 22], which might explain why blocking synaptic output from L2 leaves the visual responses of L4 intact [23]. Within the medulla, L4 synapses onto three Tm2 cells, one located in the home column and two in the adjacent columns located posterior in visual space [17, 18] (Figure 1A; for illustration purposes, only two neighboring columns are depicted). Based on their connectivity and anatomical layout, there are two plausible hypotheses for these cells’ role in the motion detection circuit. First, Tm2 could exhibit a directional tuning for OFF motion from the front to the back, as suggested by the asymmetrical wiring between L4 and Tm2 [18]. Alternatively, Tm2 could act as one of the two input arms of the elementary OFF motion detector. In this case, Tm2 would reveal a preference for moving

³These authors contributed equally to this work

⁴Present address: Janelia Farm Research Campus, 19700 Helix Drive, Ashburn, VA 20147, USA

*Correspondence: borst@neuro.mpg.de



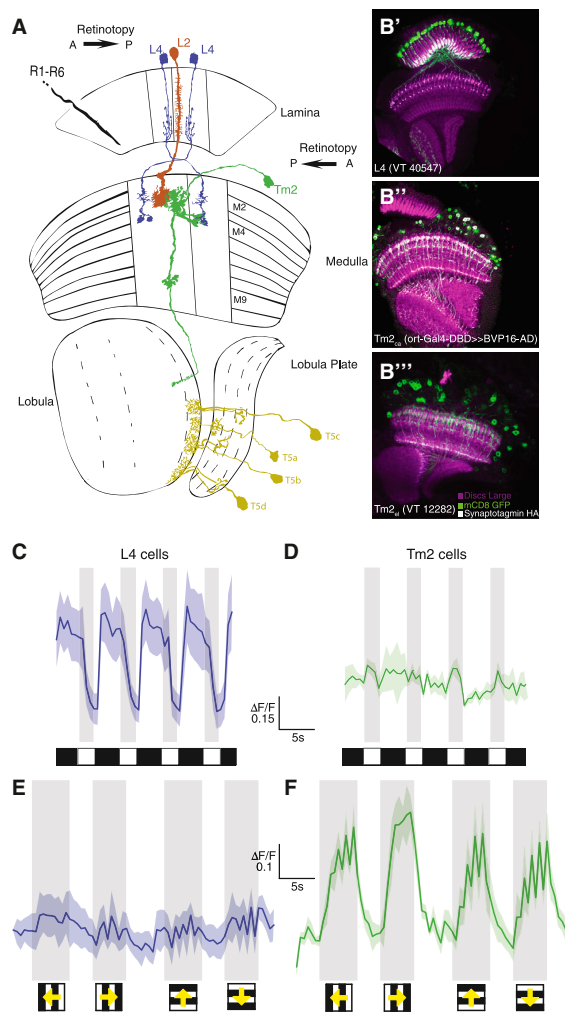


Figure 1. Wiring Diagram and Basic Response Properties of L4 and Tm2
 (A) Photoreceptors (R1–R6) synapse onto the lamina monopolar cells L2 (red) and L4 (blue). These two cell types are connected in an intercolumnar and reciprocal manner in the lamina. Both give input to the transmedulla neuron Tm2 (green) in their home column. Additionally, two L4 cells from posterior columns are presynaptic to Tm2, with axonal output regions coinciding with T5 dendrites in the lobula. Adapted and modified from [6, 18].
 (B) Confocal images of the Gal4-driver lines used in this study, shown in horizontal cross-sections. Neurons are marked in green (mCD8-GFP expression), neuropils in magenta (antibody against Dlg), and synaptic output regions in white (antibody against HA, bound to synaptotagmin). L4 (B') and Tm2_{ca} (B'') lines were used for Ca²⁺ imaging. L4 (B') and Tm2_{el} (B''') lines were used for blocking experiments.
 (C and D) Average relative change of fluorescence in response to four full-field flicker stimuli in L4 (C; n = 7) and Tm2 (D; n = 5) terminals (±SEM).
 (E and F) Mean responses of L4 (E; n = 7) and Tm2 (F; n = 8) to square-wave gratings moving in all four cardinal directions at 30° s⁻¹.
 (C–F) Grey-shaded areas indicate the stimulation period. For Tm2, responses to vertical motion are slightly but significantly smaller than to horizontal motion (p < 0.015).

OFF edges, but its responses would be nondirectional; direction selectivity would only arise after a multiplicative interaction of the two input signals on the dendrites of T5 cells.

Functional analysis using behavioral readouts during selective blockade of L4 arrived at controversial conclusions: while one study found no impairment of motion-dependent behavior after silencing of L4 [23], another study observed a specific deficit in L4 block flies to detect motion from the front to the back, consistent with the first of the above hypotheses, as well as to detect moving OFF edges, consistent with the second hypothesis [24].

To probe these cells' specificity for OFF motion and their potential direction selectivity, we analyzed the visual response properties of Tm2 and L4 using Ca²⁺ imaging. Both Tm2 and L4 are excited exclusively by moving OFF edges, albeit in a non-directional way. Both cells have a bell-shaped receptive field with a half width of approximately 5°. While L4 exhibits rather linear spatial integration properties and responds to changes in full-field luminance, Tm2 becomes inhibited by stimuli of increasing size. To investigate the participation of L4 and Tm2 in motion processing, we recorded the motion responses from wide-field tangential cells, instead of using a behavioral readout. When synaptic output from either Tm2 or L4 was blocked, responses of LPTCs to moving OFF edges are eliminated, demonstrating their crucial role in the OFF pathway of *Drosophila* motion vision.

Results

To investigate the visual response properties of L4 and Tm2, we used cell-specific Gal4 driver lines. To verify these lines' specificity, we drove the expression of membrane-bound GFP and the hemagglutinin (HA)-tagged presynaptic marker protein synaptotagmin. We then antibody stained against GFP and HA, allowing us to compare the labeling with the branching as known from Golgi studies (GFP), as well as to determine the synaptic output layers (synaptotagmin). The L4 line shows specific expression of GFP within the optic lobe that is characteristic for this cell. Synaptotagmin staining of the line indicates synaptic output in the distal portion of the lamina and the second and fourth layer of the medulla, which is in agreement with previous Golgi and electron microscopy studies (Figure 1B') [6, 17, 18]. Both of our Tm2 driver lines showed a specific, Tm2-characteristic expression within the optic lobe and similar synaptotagmin staining, labeling the ninth layer of the medulla and the first layer of the lobula (Figures 1B'' and B'''). The strong synaptotagmin staining in the first layer of the lobula suggests that this is also an output region of Tm2 where it could provide input to T5.

Visual Response Properties of L4 and Tm2

To optically record from these cells using two-photon microscopy [25], we used the Tm2_{ca} and L4 driver lines and crossed them with UAS-GCaMP5. To investigate how whole-field brightness changes are encoded in the terminals of both L4 and Tm2, we presented four spatially uniform bright pulses of light, each lasting for 2 s, interleaved by 4 s, and measured the change in fluorescence of individual L4 terminals in the second layer of the medulla and Tm2 terminals in the first layer of the lobula. In L4, the activity follows the full-field luminance in an almost tonic way, such that the lowest brightness level leads to the strongest response (Figure 1C). In contrast to L4, Tm2 does not respond to full-field luminance changes (Figure 1D). In order to test whether direction selectivity is already

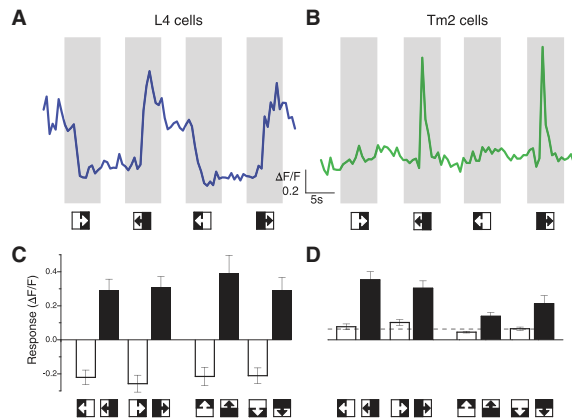


Figure 2. L4 and Tm2 Responses to Moving Edges
(A and B) Single-cell response traces of L4 (A) and Tm2 (B) to horizontally moving edges of either polarity. Stimulation period is indicated by the shaded area.
(C and D) Mean responses of L4 (C; $n = 10$) and Tm2 (D; $n = 12$) to ON (white bars) and OFF (black bars) edges moving at 30° s^{-1} . Chance response level is indicated by the dashed line (see the [Experimental Procedures](#)). Error bars indicate \pm SEM. For Tm2, responses to OFF edges moving in the vertical direction are significantly smaller than those for the horizontal direction ($p < 0.01$).
See also [Figure S3](#).

present at the level of Tm2 or L4, we presented square-wave gratings moving in the four cardinal directions (back to front, front to back, upward, and downward). L4 responds with only small modulations in activity to square-wave motion ([Figure 1E](#)). In striking difference to L4, Tm2 responds strongly to gratings moving in all directions. Contradicting the hypothesis based on the asymmetric wiring in the medulla [18], Tm2 shows no directional preference, responding to gratings moving in all directions in a similar way, albeit with a somewhat smaller amplitude to vertical than to horizontal motion ([Figure 1F](#)).

Anatomical evidence has implicated both Tm2 and L4 as being postsynaptic to L2 and, thus, as potential elements in the OFF motion pathway [17, 18]. Therefore, we tested their sensitivity to the contrast polarity of moving edges. We presented either bright or dark edges, each moving in all four cardinal directions. Interestingly, L4 and Tm2 respond with quite different dynamics, as exemplified in single-cell traces in response to horizontal edge motion ([Figures 2A and 2B](#)). In L4, when an OFF edge passes the fly's visual field, the activity transiently increases settling at a plateau level that persists until the subsequent ON edge arrives. The ON edge strongly reduces L4's activity. Hence, L4 encodes moving edges with a persistent DC component, which is superimposed by a small transitory peak ([Figure 2A](#)). In contrast to L4, Tm2 responds solely with a fast, transient increase in activity to moving OFF edges ([Figure 2B](#)). When probed with moving ON and OFF edges in all directions, L4 responds to moving OFF edges equally in all four directions, primarily with a persistent change in activity. If L4's activity is at an elevated level, it becomes reduced by an ON edge ([Figures 2A and 2C](#)). As does L4, Tm2 responds to OFF edges moving in all four directions. However, in contrast to L4, Tm2 responds to moving OFF edges with a pronounced transient increase in activity. Tm2 does not respond at all to moving ON edges ([Figures 2B and 2D](#)).

To measure the receptive fields of Tm2 and L4, we periodically presented a dark vertical bar of 4.5° width on a bright background at different azimuthal positions and measured the response of both cells as defined by the difference between the relative fluorescence during bar presentation and the response level before ([Figures 3A and 3B](#)). L4 responded most strongly when the bar was within a window of about $\pm 5^\circ$ around a position, leading to maximal response ([Figure 3A](#)). The average sensitivity profile, obtained after aligning the results from different cells with respect to their maximum, closely resembles a bell-shaped Gaussian with a half width of $\sim 5^\circ$. Tm2 responded to such stimuli in a similar way: again, maximum responses were elicited in a rather small window of about 10° widths, with no significant responses to stimulation outside this window ([Figure 3B](#)). In order to examine the spatial integration properties of L4 and Tm2, on a bright background, we presented a dark, vertical bar, increasing in size and centered at the position of a cell's maximum response. Based on L4's receptive field derived from the previous experiment and assuming linear spatial integration, we expected the responses to strongly increase with increasing bar width until approximately 10° and plateau thereafter. The response of L4 to small bar widths is consistent with this expectation; however, the response of L4 even increases when the bar width changes from 25° to 50° without any sign of saturation ([Figure 3C](#)). For Tm2, considering the data from the previous experiment ([Figure 3B](#)) and the fact that Tm2 doesn't respond to full-field flicker ([Figure 1D](#)), we expected a rather different spatial integration property. Indeed, Tm2 responses differ strongly from those of L4, displaying a maximum response to a bar of 4.5° and then decreasing rapidly as the bar becomes wider ([Figure 3D](#)). This implicates the existence of lateral inhibition, shaping the receptive field properties of Tm2.

In addition to the spatial response properties of these cells, their temporal dynamics are also of interest. Using the line-scan mode of the two-photon microscope, we measured single terminals of both cell types in response to flickering dark bars of 4.5° width at a temporal resolution of 480 Hz. As can be expected from their full-field flicker and edge responses, L4 and Tm2 responded with considerably different temporal dynamics. L4 reached its maximal response level approximately 100 ms after stimulus onset. At the end of the dark bar presentation, the fluorescence in L4 was still approximately 50% of the maximum response ([Figure 3E](#)). Tm2 responded with comparable rise times—reaching maximum response levels 100 ms after stimulus onset—but decayed much faster than L4. At the end of the bar presentation, Tm2 responses had decayed to 20% of their maximum value ([Figure 3F](#)). Note that all data obtained from Ca^{2+} imaging in layer 1 of the lobula are consistent with data from M9 (data not shown).

Motion Responses after Blocking L4 or Tm2

Our results from Ca^{2+} imaging of Tm2 and L4 cells revealed that none of these cells exhibit a preference for grating or edge motion in any direction. However, both cells become selectively excited by brightness decrease, as expected from being postsynaptic to L2. In order to assess their participation in motion processing, we blocked synaptic output of either Tm2 or L4 by expressing shibire [27] and recorded the responses of lobula plate tangential cells to moving ON and OFF edges (data from horizontal system [HS] and vertical system [VS] cells were pooled). Control flies of identical genotype but not subjected to a temperature shift showed strong and

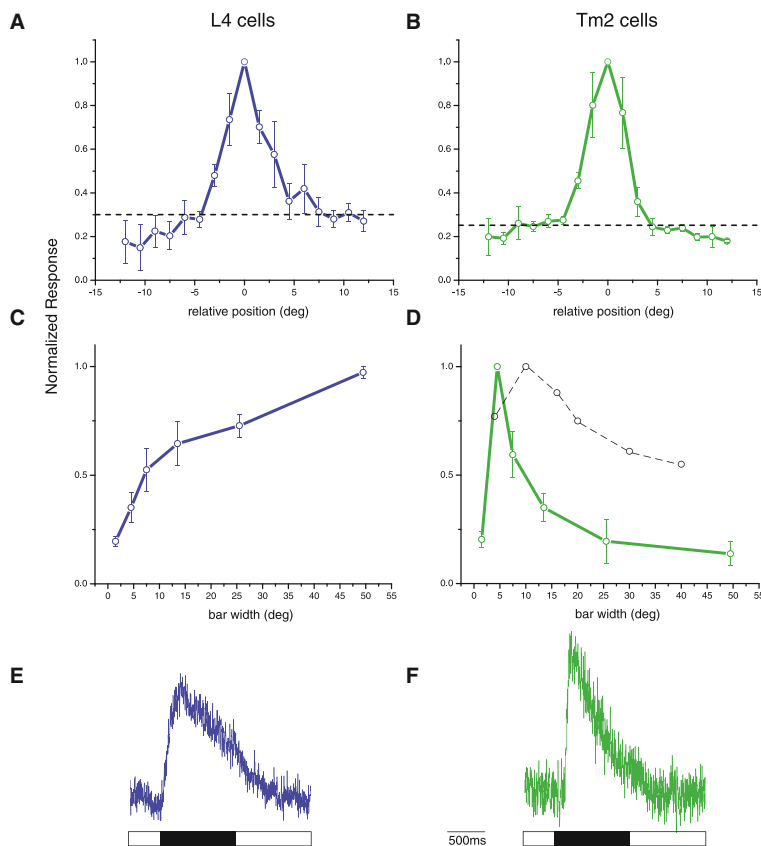


Figure 3. Response Characteristics of L4 and Tm2 Cells upon Stimulation with Flickering Bars

(A and B) Ca^{2+} response of L4 (A; $n = 5$) and Tm2 (B; $n = 5$) to 4.5°-wide, dark, vertical bars appearing and disappearing at various positions (shifted by 1.5°) on a bright background at a frequency of 0.5 Hz. Graphs were normalized to the position of the maximum response. Chance response level is indicated by the dashed line (see the [Experimental Procedures](#)). Error bars indicate \pm SEM.

(C and D) Normalized Ca^{2+} response of L4 (C; $n = 7$) and Tm2 (D; $n = 5$) cells to dark, vertical bars of increasing size (bar widths: 1.5°, 4.5°, 7.5°, 13.5°, 25.5°, and 49.5°). For comparison, L2 responses from [26] are indicated as a dashed line in (D).

(E and F) Ca^{2+} response of a single L4 (E; 50 sweeps) and Tm2 (F; ten sweeps) cell (in arbitrary units) stimulated by a 4.5°-wide dark bar for 1 s, recorded at 480 Hz. The duration of the stimulation is indicated by the black bar below.

See also [Figure S3](#).

responses between control and block flies is shown in [Figure S1](#) (available online). All of these findings are reminiscent on the results of previous studies in which either L2 or T5 cells were blocked, leading to a selective loss of tangential cell responses to OFF edges [10, 12].

We also tested the responses of L4 and Tm2 block flies to grating motion ([Figure S2](#)). As expected from the above results and the assumption that T4 and T5 cells contribute to the grating response with about equal weight, grating responses to horizontal and to vertical

reliable directional responses to both ON and OFF edges, depolarizing by about 8 mV during motion in the preferred direction and hyperpolarizing by about 5 mV during motion in the null direction of the tangential cells (black and gray traces in [Figures 4A–4D](#)). When L4 cells were blocked, the responses to ON edges moving along the preferred as well the null direction were almost indistinguishable from those in control flies (blue traces in [Figures 4A](#) and [4C](#)). However, the responses to OFF edges were severely reduced, both for preferred-direction and for null-direction motion (blue traces in [Figures 4B](#) and [4D](#)). When Tm2 was blocked, tangential cells responded strongly to ON edges moving along the preferred direction of the cells, but the response to null direction had less than half of the amplitude as compared to control flies (green traces in [Figures 4A](#) and [4C](#)). For OFF edge motion, a similar result was obtained as for L4 block flies: Again, the response to motion along both the preferred and the null directions was almost completely abolished (green traces in [Figures 4B](#) and [4D](#)). Using the time average of the difference between the preferred- and null-direction response as a measure, the results can be summarized as follows ([Figures 4E](#) and [4F](#)): blocking synaptic output from L4 cells leaves the ON edge responses unaffected, but strongly and highly significantly reduces the OFF edge response (blue bars, compared to black bars); and blocking synaptic output from Tm2 cells reduces the ON edge responses somewhat, but abolishes the OFF edge response completely (green bars, compared to gray bars). A detailed comparison of preferred- and null-direction

motion in L4 and Tm2 block flies are found to be at roughly half of the amplitude as in control flies. However, consistently in HS and VS cells, the null-direction response is compromised more strongly than is the preferred-direction response. While this might indicate a direction-specific contribution of L4 and Tm2 at first sight, it can be readily explained by a slightly elevated threshold of the inhibitory input to the tangential cells. We therefore conclude that both L4 and Tm2 cells represent essential, nondirectional components of the OFF motion pathway in *Drosophila*.

Discussion

Our results reveal that L4 and Tm2 cells are necessary components for the computation of OFF motion signals. In line with this notion, we find both L4 and Tm2 neurons being excited preferentially by moving OFF edges. Furthermore, we demonstrate that direction selectivity does not occur at the level of L4 or Tm2 cells, but is rather computed downstream of Tm2, presumably in the dendrites of T5 cells.

Contrast Polarity and Direction Sensitivity

Using full-field flicker and moving edges of single contrast polarity, we measured the basic response characteristics of both L4 and Tm2 cells. L4 cells receive their main input from L2 in the lamina, where they form reciprocal, cholinergic connections [18, 21]. In agreement with previous studies [23, 28], we observed a decrease in Ca^{2+} when stimulating

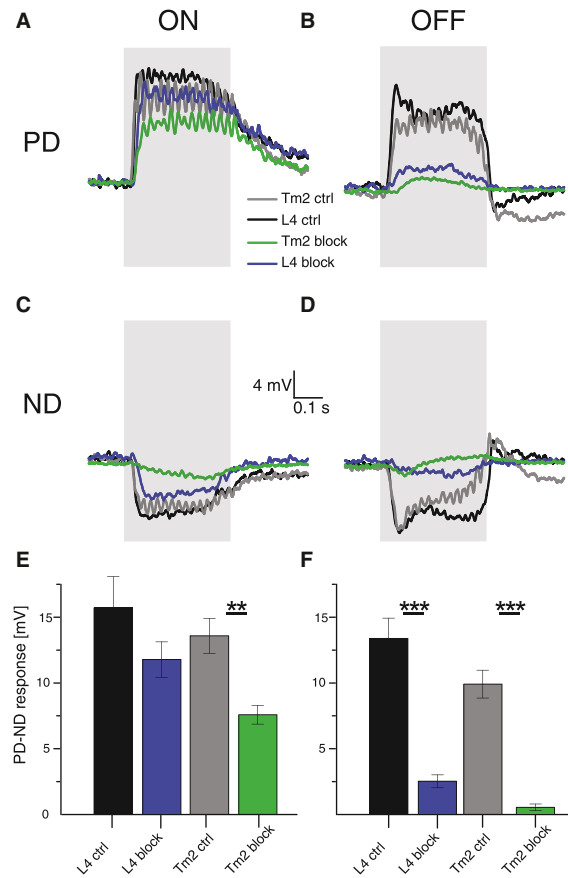


Figure 4. Voltage Responses of Lobula Plate Tangential Cells to Moving ON and OFF Edges

(A–D) Average time course of the membrane potential in response to ON (A and C) and OFF (B and D) edges moving along the preferred (PD; A and B) and null (ND; C and D) direction as recorded in two types of control flies (gray and black), as well as in flies in which synaptic output from L4 (blue) or Tm2 (green) cells was blocked. The stimulation period is indicated by the shaded area.

(E and F) Mean voltage responses (PD – ND) to ON (E) and OFF (F) edges of tangential cells in all four groups of flies. Recordings were done from HS [2] and VS [1] cells. HS cells have front to back as their PD and back to front as their ND; VS cells have downward as their PD and upward as their ND. Since no difference was detected between HS and VS cells, data from both cell types were pooled. L4 control data are from nine cells (four HS, five VS) in two flies, L4 block data are from ten cells (three HS, seven VS) in two flies, Tm2 control data are from 14 cells (six HS, eight VS) in eight flies, and Tm2 block data are from 11 cells (five HS, six VS) in five flies. In L4 block flies, ON responses are nonsignificantly different from control flies, whereas OFF responses are highly significantly reduced. In Tm2 block flies, ON responses are significantly different from control flies, and OFF responses are highly significantly reduced. * $p < 0.05$, ** $p < 0.001$, *** $p < 0.0001$, tested using two-tailed t tests against their controls. Error bars indicate \pm SEM. See also Figures S1–S3.

L4 with brightness increments and an increase of Ca^{2+} when presenting light decrements. Assuming an excitatory connection between L2 and L4, these results are consistent with data that have been described for L2 [23, 26, 29]. The temporal response characteristics of L4, however, differ substantially from those observed in L2 by the existence of a sustained

component in L4, which is not seen in L2. This discrepancy is in agreement with the finding that L4 receives input from photoreceptors, both directly from R6 and indirectly via the lamina amacrine cell, in addition to the input from L2 [22]. Tm2 receives its main input from L2. In agreement with this notion, we observed an increased Ca^{2+} signal in response to brightness decrements and no response to brightness increments. The transient nature of the signal and its selectivity for OFF edges parallels the reported findings for the Ca^{2+} signal in the terminal region of L2 [15, 29], suggesting that half-wave rectification in the L2 terminal represents the biophysical mechanism for OFF selectivity within the L2 pathway [29]. In contrast to L2, L4, and previous electrophysiological recordings in the calliphorid ortholog of Tm2 [28], Tm2 cells in *Drosophila* do not show any response to full-field luminance changes of either polarity. This finding indicates the existence of an inhibitory subregion of the receptive field. It also argues against the hypothesis that intercolumnar L4 connections onto Tm2 might implement a pooling of excitatory neighboring signals [18]. Furthermore, the observed nondirectional responses of both L4 and Tm2 allow us to rule out the hypothesis that the asymmetrical wiring between L4 and Tm2 could implement direction selectivity [18]. This passes the emergence of direction selectivity to the postsynaptic neurons—presumably T5—that have been shown to exhibit a precise directional tuning [12].

Receptive Field Properties

Stimulation with dark bars at different positions and increasing widths revealed the receptive field properties of L4 and Tm2 cells. We could demonstrate that the spatial sensitivity distribution for excitatory input to both cells exhibits comparable characteristics in the azimuthal extent when probed by small bars. However, it differs significantly in response to larger objects. Here, the response of L4 cells increases with the size of the visual stimulus, and thus varies distinctly from the center-surround receptive field described in L2 [26]. This is a further indication for a contribution of additional inputs to L4, e.g., via wide-field amacrine cells. As is shown by a linear receptive field model—an isotropic Gaussian inhibitory center with a half width σ of 2° and a spatially constant excitatory surround—even a minute excitatory surround contribution, undetectable by local stimulation, is sufficient to account for the increase in response with increasing stimulus size (Figure 5E). Tm2, in contrast, seems to be inhibited by large objects, since their response decreases dramatically when stimulated with bars wider than 4.5° . With Ca^{2+} as a proxy for membrane voltage, this inhibitory surround has not been detected by the stimulation with small bars at such lateral positions, either because intracellular Ca^{2+} does not decrease with membrane hyperpolarization or because the Ca^{2+} indicator does not report these low concentrations. Compared to L2 [26], surround inhibition seems to be much more pronounced in Tm2 (L2 responses from [26] are indicated as dashed line in Figure 3D). Tm2 cells lack every response to objects larger than 25° , indicating the existence of further lateral inhibition at the level of Tm2 that leads to a sharpening of their receptive field, probably via wide-field amacrine cells. In order to quantitatively reproduce Tm2 responses to bars of increasing width and moving gratings, we modeled the receptive field of Tm2 as the difference of two Gaussians with a half width σ of 2° horizontally and 4° vertically for the inhibitory center and of 10° horizontally and 20° vertically for the excitatory surround. This combination resulted in a maximum local surround excitation that amounted

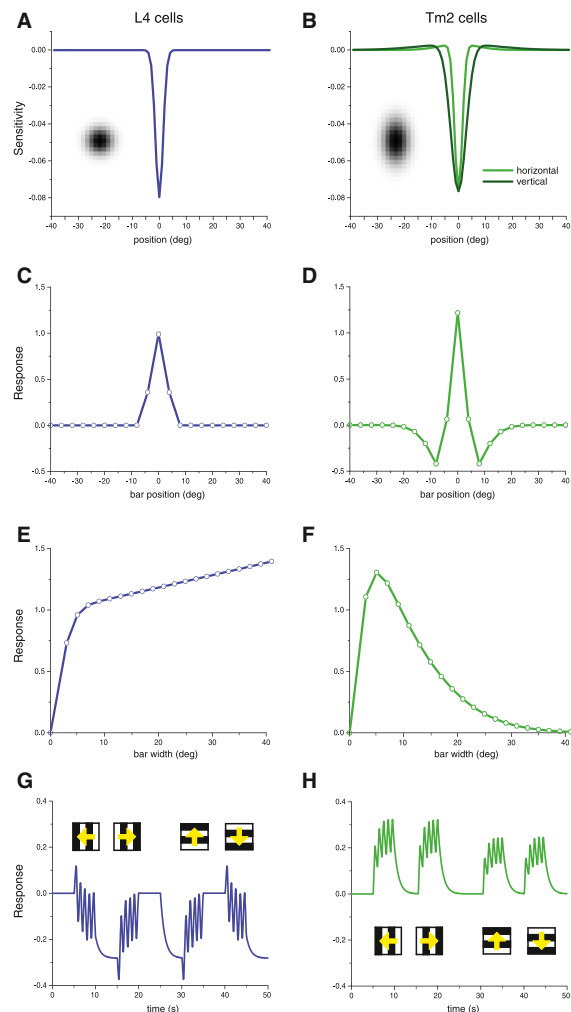


Figure 5. Model Simulations of L4 and Tm2 Receptive Fields
(A and B) Sensitivity profile across the receptive field of L4 (A) and Tm2 (B). The insets show a magnified view of the 2D receptive field, with each pixel corresponding to one $1^\circ \times 2^\circ$ of visual space.
(C and D) Responses of L4 (C) and Tm2 (D) to a 7° -wide bar as a function of bar position.
(E and F) Responses of L4 (E) and Tm2 (F) to a bar, centered in the receptive field, as a function of bar width.
(G and H) Responses of L4 (G) and Tm2 (H) to a grating (spatial wavelength = 20°) moving at a temporal frequency of 1 Hz along four orthogonal directions. Responses were obtained by low-pass filtering ($\tau = 1$ s) of original signals from L4 and half-wave rectifying signals from Tm2.
See also Figure S3.

to only 3% of the peak center inhibition, but nevertheless was able to fully reproduce the strong decrease of the response of Tm2 with increasing bar width seen in the experiments (Figures 5B and 5F). A further interesting difference between L4 and Tm2 appears in their responses to moving square wave gratings: while L4 responses remain at rest, at best being slightly modulated at the temporal frequency of the local luminance changes (Figure 1E), Tm2 responses build up during grating motion with temporal modulations riding on

top (Figure 1F). As shown by model simulations, these differences are readily explained by the half-wave rectified response property of Tm2, but not in L4, assuming a temporal integration of the membrane potential either by intracellular Ca^{2+} and/or the buffering of the indicator (Figures 5G and 5H). Furthermore, assuming a slight anisotropy of the receptive field of Tm2 as explained above (Figure 5B), similar to what has been reported for L2 [26], the simulation results for grating motion are consistent with the somewhat smaller response amplitude of Tm2 to vertical than to horizontal motion (Figure 5H). Note, however, that the anisotropy of the Tm2 receptive field was not directly measured.

L4 and Tm2 Are Crucial OFF Pathway Elements

To test the role of L4 and Tm2 in motion detection in *Drosophila*, we blocked their synaptic output and recorded from tangential cells of the lobula plate. Unlike a behavioral study by Silies and colleagues that shows only mild reductions in responses to OFF motion stimuli when blocking L4 [23], we observed a strong impairment of tangential cell responses for OFF motion. This difference might be explained by differing expression levels of Gal4 in L4 fly lines: in the same study, silencing L4 in two different fly lines caused significantly different effects of responses toward opposing edges [23]. In another study, Tuthill and colleagues tested the effect of blocking all lamina neurons individually on turning behavior of flying *Drosophila* [24]. In agreement with our results, blocking L4 resulted in a selective impairment of the turning responses to OFF versus ON edges. In response to grating motion from the front to the back, these flies also exhibited a response reduction to about 50% of control level, as is expected from our data (Figures 4, S1, and S2). However, the same flies reacted with the same amplitude as control flies to grating motion from the back to the front. Since the behavioral response to back-to-front motion is much smaller than that to front-to-back motion, the residual tangential cell response might be sufficient to generate normal behavioral output under these conditions. Our results show that L4 is necessary for OFF motion signals in tangential cells (Figure 4). The same effect was observed when Tm2 was blocked. Blocking and Ca^{2+} imaging experiments match, because no direction-specific defect could be detected. This speaks in favor of the hypothesis that blocking Tm2 corresponds to the disruption of one input element to the Reichardt detector. L4, on the other hand, as one of the major input elements to Tm2 [18], seems to be needed either for a proper functioning of L2, or in conjunction with L2 to successfully evoke signals in Tm2. Our data also show a reduction in the responses of tangential cells in Tm2 block flies to ON stimuli, especially in the cells' null direction (Figure 4). This decrease of the ON response could be caused by disruption of a potential tonic input of Tm2 to the ON pathway via L5 [17, 18] or via its arborization in medulla layer 9. Together with the spatiotemporal response properties of Tm2 reported above, the following conclusions can be drawn regarding motion processing in the OFF pathway: (1) The narrow receptive field of Tm2 (Figure 3B) with a half width of about 5° indicates input from only a single optical cartridge. This is significantly smaller than the "anatomical receptive field," as reported in Takemura et al. [17] for Tm3, one of the inputs to the T4 cells, and thus might represent an interesting difference between the ON and the OFF motion pathway. (2) The strong surround inhibition we see in Tm2 (Figure 3D) readily explains the missing responses to field flicker stimuli that was observed in T5 cells

[12]. (3) The rather transient response of Tm2 (Figures 2B and 3F) makes it a candidate for the fast (i.e., high-pass filtered) input to the motion detection mechanism in the postsynaptic dendrite of T5 cells. This is all the more true since the calcium indicator is expected to slow down the signal significantly: thus, the membrane potential response in Tm2 will certainly be even faster. As a caveat, however, no data on Tm1 neurons exist so far to compare with. (4) The fact that blocking Tm2 abolishes the OFF response in the tangential cells for all stimulus directions (Figures 4B, 4D, and 4F) suggests that Tm2 serves as input element for all four types of T5 cells tuned to the four cardinal directions.

In summary, we thus conclude that L4 and Tm2 are essential OFF motion processing elements in the fly visual system that are not directionally selective. Consequently, direction selectivity in the OFF pathway is likely to arise at the level of the T5 dendrites.

Experimental Procedures

Flies

Flies were raised on standard cornmeal-agar medium with 12 hr light/12 hr dark cycles, 25°C, and 60% humidity. For Ca²⁺ imaging, we used the genetically encoded indicator GCaMP5 [30] driven by two different Gal4 lines with the following genotypes: Tm2_{ca} line (*w⁻;ort-Gal4-DBD,N9A >> BVP16-AD;UAS-GCaMP5*), provided by Chi-Hon Lee [31], and L4 line (*w⁻;UAS-GCaMP5;VT40547-Gal4*, VDRC stock number 200265). Cell-specific block effects in electrophysiological experiments were accomplished using UAS-shibire^{ts} [27]. Fly lines with the following genotypes were used for electrophysiological recordings: L4 line (*shi^{ts}/+;+;shi^{ts}/VT40547-Gal4*, VDRC stock number 200265) and Tm2_{el} line (*shi^{ts}/+;+;shi^{ts}/VT12282-Gal4*, VDRC stock number 203097). Expression and specificity of driver lines were investigated using a combination of membrane tethered GFP and synaptotagmin-hemagglutinin (courtesy of Andreas Prokop) [32, 33]. Fly lines had the following genotypes: Tm2_{ca} line (*w⁻;UAS-SYT-HA,UAS-mCD8-GFP/ort-Gal4-DBD,N9A >> BVP16-AD;+*), Tm2_{el} line (*w⁻;UAS-SYT-HA,UAS-mCD8-GFP/+;VT12282-Gal4/+*), and L4 line (*w⁻;UAS-SYT-HA,UAS-mCD8-GFP/+;VT40547-Gal4/+*). The Tm2_{ca} line had a higher Gal4 expression level than did the Tm2_{el} line. The Tm2_{el} line, however, showed a more specific expression pattern. Detailed descriptions of preparation and experiments are found in [29] for Ca²⁺ imaging and in [1] for electrophysiology.

Immunohistochemistry and Confocal Imaging

Immunostainings were performed as described in [2]. As primary antibodies (1:200) we used mouse anti-discs large (DLG, Developmental Studies Hybridoma Bank), rabbit anti-GFP-Alexa488 conjugate (Molecular Probes), and rat anti-hemagglutinin (Roche). For visualization, we used the following secondary antibodies (1:200 in PBT): goat anti-mouse Alexa 568, goat anti-rat Alexa 568 (Molecular Probes), and goat anti-mouse Alexa 647 (Rockland Immunochemicals). Brains were mounted (IMM, Ibbidi) and optically sectioned in the horizontal plane with a Leica SP5 confocal microscope. For documentation, single sections were processed in ImageJ 1.46r (NIH).

Electrophysiology

The recording protocol was adapted from [1]. In addition, the glial sheet was digested locally by application of a stream of 0.5 mg/ml collagenase IV (GIBCO) through a cleaning micropipette (~5 µm opening) under polarized light contrast.

Two-Photon Microscopy and Visual Stimulation

Two-photon microscopy and visual stimulus presentation were performed as described in [12]. Square-wave gratings had a spatial wavelength of 30° of visual angle and a contrast of 88%, moving at either 30° s⁻¹ or 60° s⁻¹. Edges had the same contrast and were moving at 30° s⁻¹. For the experiments shown in Figures 1 and 2, each grating or edge motion was shown twice within a single sweep, each lasting 4 s. Subsequent stimuli were preceded by a 3 s pause. For the experiments shown in Figures 3A and 3B, we flickered 4.5°-wide vertical dark bars on a bright background at 0.5 Hz at 10 different positions. The position yielding maximum response was set to 0°. The responses were normalized and plotted depending on their distance to the peak response. For Figures 3C and 3D, vertical dark

bars, increasing in size, were flickered at the peak response position. The responses were normalized to the peak response. For Figures 3E and 3F, a 4.5° vertical dark bar was flickered for 1 s on a bright background (line scan, averaged trace, ten repetitions). For the experiments shown in Figure 4, multiple edges were used as stimuli moving simultaneously at 60° s⁻¹. For stimulation of HS cells, a vertical, stationary square-wave grating with 45° spatial wavelength was presented. For ON edge motion, the right (PD) or the left (ND) edge of each light bar started moving until it merged with the neighboring bar. For OFF edge motion, the right or the left edge of each dark bar was moving. For stimulation of VS cells, the pattern was rotated by 90°. A collection of all stimuli is presented as space-time plots in Figure S3.

Data Evaluation

Data were evaluated offline using custom written software (MATLAB) and Origin (OriginLab). For evaluation of the Ca²⁺ imaging data, the raw image series was first converted into a relative fluorescence change (ΔF/F) series using the first five images as reference. Then a region was defined within a raw image and average ΔF/F values were determined within that region for each image, resulting in a ΔF/F signal over time. The Ca²⁺ signal traces in Figures 1C–1F were obtained by calculation of the average ΔF/F signal over trials and flies, with shading indicating the SEM. For the bar graphs in Figure 2C, the average signals of three frames before stimulus onset were subtracted from the mean response within the three last images of edge motion. For Figure 2D, the average Ca²⁺ signal of three images prior to visual stimulation (reference value) was subtracted from the maximum response during each stimulus presentation. The dashed line was calculated by subtraction of the reference value from a maximum, obtained without visual stimulation (chance response level). The graphs in Figures 3A and 3B show the average signal (maximum – minimum of peaks, five presentations) to flickering bars normalized to the maximum response. Again, the dashed line represents chance level. The voltage traces in Figures 4A–4D were obtained by averaging of the responses of all cells upon visual stimulation with multiple edges of either polarity in the four cardinal directions. For the bar graphs in Figures 4E and 4F, the responses during edge motion (0.375 s) along the preferred and null direction were subtracted (PD – ND). The mean PD – ND responses were subsequently averaged across all cells, with error bars representing the SEM.

Supplemental Information

Supplemental Information includes three figures and can be found with this article online at <http://dx.doi.org/10.1016/j.cub.2014.01.006>.

Acknowledgments

We thank Chi-Hon Lee and Andreas Prokop for providing us with fly lines; David Soll for the DLG-antibody; Johannes Plett for designing and engineering the LED arena and for technical support; Christian Theile, Wolfgang Essbauer, and Michael Sauter for fly work; Romina Kutlesa for stainings; and Aljoscha Leonhardt, Elisabeth Hopp, and Georg Ammer for constructive discussions and help with programming.

Received: October 22, 2013

Revised: November 29, 2013

Accepted: January 3, 2014

Published: February 6, 2014

References

1. Joesch, M., Plett, J., Borst, A., and Reiff, D.F. (2008). Response properties of motion-sensitive visual interneurons in the lobula plate of *Drosophila melanogaster*. *Curr. Biol.* 18, 368–374.
2. Schnell, B., Joesch, M., Forstner, F., Raghu, S.V., Otsuna, H., Ito, K., Borst, A., and Reiff, D.F. (2010). Processing of horizontal optic flow in three visual interneurons of the *Drosophila* brain. *J. Neurophysiol.* 103, 1646–1657.
3. Hassenstein, B., and Reichardt, W. (1956). Systemtheoretische Analyse der Zeit-, Reihenfolgen- und Vorzeichenauswertung bei der Bewegungspersonen des Rüsselkäfers *Chlorophanus*. *Z. Naturforsch.* B 11b, 513–524.
4. Reichardt, W. (1987). Computation of optical motion by movement detectors. *J. Comp. Physiol. A* 161, 533–547.

5. Borst, A., and Euler, T. (2011). Seeing things in motion: models, circuits, and mechanisms. *Neuron* 71, 974–994.
6. Fischbach, K., and Dittrich, A. (1989). The optic lobe of *Drosophila melanogaster*. I. A Golgi analysis of wild-type structure. *Cell Tissue Res.* 258, 441–475.
7. Bausenwein, B., Dittrich, A.P.M., and Fischbach, K.F. (1992). The optic lobe of *Drosophila melanogaster*. II. Sorting of retinotopic pathways in the medulla. *Cell Tissue Res.* 267, 17–28.
8. Bausenwein, B., and Fischbach, K.F. (1992). Activity labeling patterns in the medulla of *Drosophila melanogaster* caused by motion stimuli. *Cell Tissue Res.* 270, 25–35.
9. Rister, J., Pauls, D., Schnell, B., Ting, C.Y., Lee, C.H., Sinakevitch, I., Morante, J., Strausfeld, N.J., Ito, K., and Heisenberg, M. (2007). Dissection of the peripheral motion channel in the visual system of *Drosophila melanogaster*. *Neuron* 56, 155–170.
10. Joesch, M., Schnell, B., Raghu, S.V., Reiff, D.F., and Borst, A. (2010). ON and OFF pathways in *Drosophila* motion vision. *Nature* 468, 300–304.
11. Buchner, E., Buchner, S., and Bülthoff, I. (1984). Deoxyglucose mapping of nervous activity induced in *Drosophila* brain by visual movement. *J. Comp. Physiol.* 155, 471–483.
12. Maisak, M.S., Haag, J., Ammer, G., Serbe, E., Meier, M., Leonhardt, A., Schilling, T., Bahl, A., Rubin, G.M., Nern, A., et al. (2013). A directional tuning map of *Drosophila* elementary motion detectors. *Nature* 500, 212–216.
13. Schnell, B., Raghu, S.V., Nern, A., and Borst, A. (2012). Columnar cells necessary for motion responses of wide-field visual interneurons in *Drosophila*. *J. Comp. Physiol. A Neuroethol. Sens. Neural Behav. Physiol.* 198, 389–395.
14. Eichner, H., Joesch, M., Schnell, B., Reiff, D.F., and Borst, A. (2011). Internal structure of the fly elementary motion detector. *Neuron* 70, 1155–1164.
15. Clark, D.A., Bursztyn, L., Horowitz, M.A., Schnitzer, M.J., and Clandinin, T.R. (2011). Defining the computational structure of the motion detector in *Drosophila*. *Neuron* 70, 1165–1177.
16. Joesch, M., Weber, F., Eichner, H., and Borst, A. (2013). Functional specialization of parallel motion detection circuits in the fly. *J. Neurosci.* 33, 902–905.
17. Takemura, S.Y., Bharioke, A., Lu, Z., Nern, A., Vitaladevuni, S., Rivlin, P.K., Katz, W.T., Olbris, D.J., Plaza, S.M., Winston, P., et al. (2013). A visual motion detection circuit suggested by *Drosophila* connectomics. *Nature* 500, 175–181.
18. Takemura, S.Y., Karuppururai, T., Ting, C.-Y., Lu, Z., Lee, C.-H., and Meinertzhagen, I.A. (2011). Cholinergic circuits integrate neighboring visual signals in a *Drosophila* motion detection pathway. *Curr. Biol.* 21, 2077–2084.
19. Braitenberg, V., and Debbage, P. (1974). A regular net of reciprocal synapses in the visual system of the fly, *Musca domestica*. *J. Comp. Physiol.* 90, 25–31.
20. Strausfeld, N.J., and Campos-Ortega, J.A. (1973). The L4 monopolar neurone: a substrate for lateral interaction in the visual system of the fly *Musca domestica* (L.). *Brain Res.* 59, 97–117.
21. Meinertzhagen, I.A., and O’Neil, S.D. (1991). Synaptic organization of columnar elements in the lamina of the wild type in *Drosophila melanogaster*. *J. Comp. Neurol.* 305, 232–263.
22. Rivera-Alba, M., Vitaladevuni, S.N., Mishchenko, Y., Lu, Z., Takemura, S.Y., Scheffer, L., Meinertzhagen, I.A., Chklovskii, D.B., and de Polavieja, G.G. (2011). Wiring economy and volume exclusion determine neuronal placement in the *Drosophila* brain. *Curr. Biol.* 21, 2000–2005.
23. Silies, M., Gohl, D.M., Fisher, Y.E., Freifeld, L., Clark, D.A., and Clandinin, T.R. (2013). Modular use of peripheral input channels tunes motion-detecting circuitry. *Neuron* 79, 111–127.
24. Tuthill, J.C., Nern, A., Holtz, S.L., Rubin, G.M., and Reiser, M.B. (2013). Contributions of the 12 neuron classes in the fly lamina to motion vision. *Neuron* 79, 128–140.
25. Denk, W., Strickler, J.H., and Webb, W.W. (1990). Two-photon laser scanning fluorescence microscopy. *Science* 248, 73–76.
26. Freifeld, L., Clark, D.A., Schnitzer, M.J., Horowitz, M.A., and Clandinin, T.R. (2013). GABAergic lateral interactions tune the early stages of visual processing in *Drosophila*. *Neuron* 78, 1075–1089.
27. Kitamoto, T. (2001). Conditional modification of behavior in *Drosophila* by targeted expression of a temperature-sensitive shibire allele in defined neurons. *J. Neurobiol.* 47, 81–92.
28. Douglass, J.K., and Strausfeld, N.J. (1995). Visual motion detection circuits in flies: peripheral motion computation by identified small-field retinotopic neurons. *J. Neurosci.* 15, 5596–5611.
29. Reiff, D.F., Plett, J., Mank, M., Griesbeck, O., and Borst, A. (2010). Visualizing retinotopic half-wave rectified input to the motion detection circuitry of *Drosophila*. *Nat. Neurosci.* 13, 973–978.
30. Akerboom, J., Chen, T.-W., Wardill, T.J., Tian, L., Marvin, J.S., Mutlu, S., Calderón, N.C., Esposti, F., Borghuis, B.G., Sun, X.R., et al. (2012). Optimization of a GCaMP calcium indicator for neural activity imaging. *J. Neurosci.* 32, 13819–13840.
31. Ting, C.-Y., Gu, S., Guttikonda, S., Lin, T.-Y., White, B.H., and Lee, C.-H. (2011). Focusing transgene expression in *Drosophila* by coupling Gal4 with a novel split-LexA expression system. *Genetics* 188, 229–233.
32. Löhner, R., Godenschwege, T., Buchner, E., and Prokop, A. (2002). Compartmentalization of central neurons in *Drosophila*: a new strategy of mosaic analysis reveals localization of presynaptic sites to specific segments of neurites. *J. Neurosci.* 22, 10357–10367.
33. Robinson, I.M., Ranjan, R., and Schwarz, T.L. (2002). Synaptotagmins I and IV promote transmitter release independently of Ca(2+) binding in the C(2)A domain. *Nature* 418, 336–340.

Current Biology, Volume 24

Supplemental Information

Neural Circuit Components of the

***Drosophila* OFF Motion Vision Pathway**

Matthias Meier, Etienne Serbe, Matthew S. Maisak, Jürgen Haag, Barry J. Dickson, and Alexander Borst

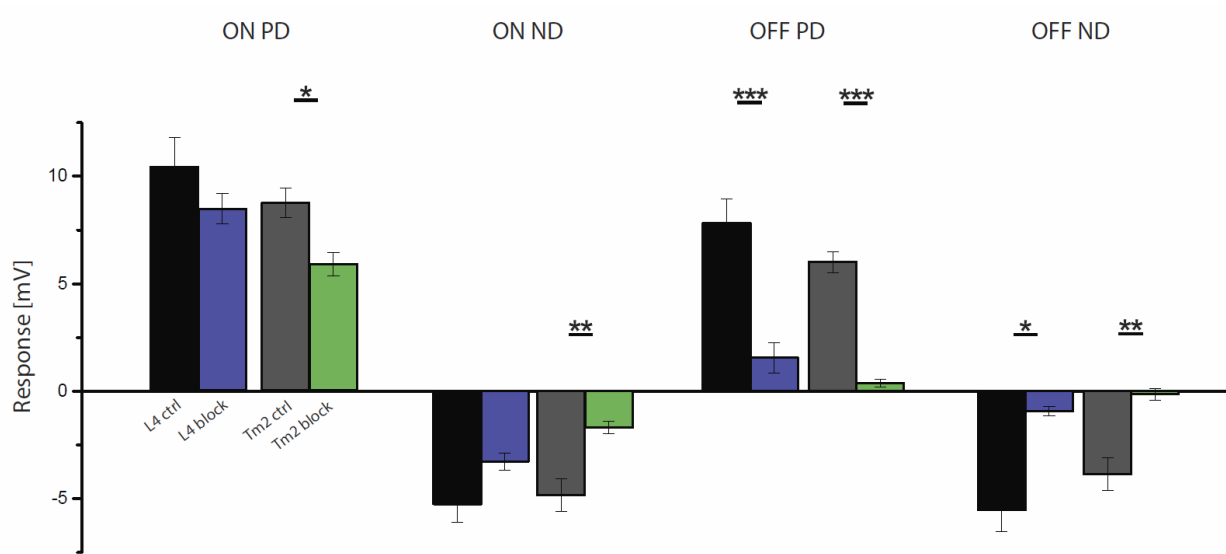


Figure S1: Detailed comparison of preferred (PD) and null (ND) direction responses to moving ON (left) and OFF (right) edges between L4 control and L4 block flies, and between Tm2 control and Tm2 block flies. As in Figure 4, data are pooled from HS and VS cells. L4 control data are from 9 cells (4 HS, 5 VS) in 2 flies, L4 block data from 10 cells (3 HS, 7 VS) in 2 flies, Tm2 control data from 14 cells (6 HS, 8 VS) in 8 flies, Tm2 block data from 11 cells (5 HS, 6 VS) in 5 flies. * $p < 0.05$, ** $p < 0.001$, *** $p < 0.0001$, tested using two-tailed t tests against their controls. Error bars denote \pm SEM. Related to Figure 4.

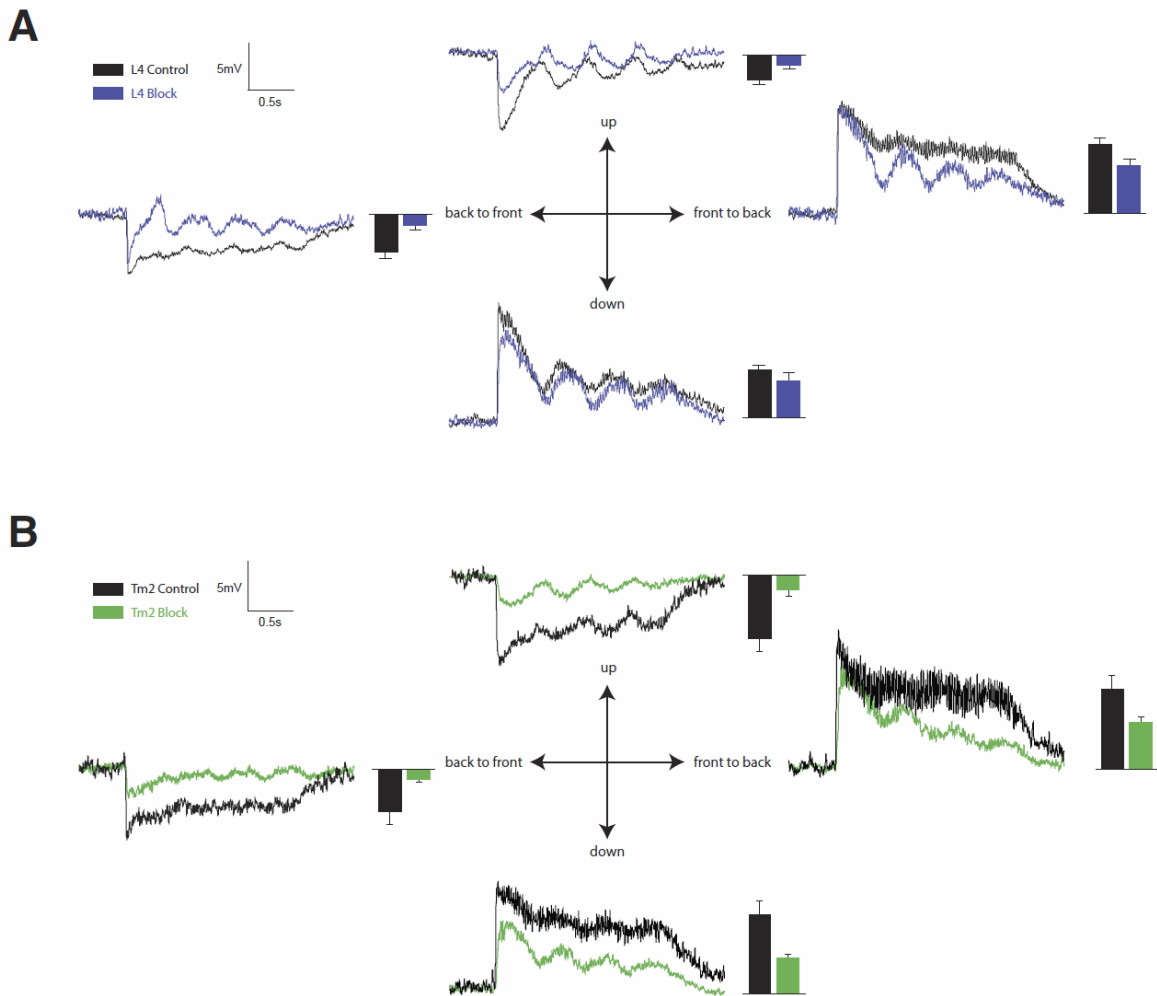


Figure S2: Responses to moving gratings of L4 control and L4 block flies (**A**) and of Tm2 control and Tm2 block flies (**B**). Data for horizontal motion are from HS cells, for vertical motion from VS cells. L4 control data are from 40 cells (21 HS, 19 VS) in 15 flies, L4 block data from 31 cells (12 HS, 19 VS) in 12 flies. Tm2 control data are from 14 cells (6 HS, 8 VS) in 7 flies, Tm2 block data from 11 cells (6 VS, 5 HS) in 5 flies. Error bars denote \pm SEM. Gratings had a spatial wavelength of 30 deg and were moving at 60 deg/s resulting in a temporal frequency of 2 Hz. Related to Figure 4.

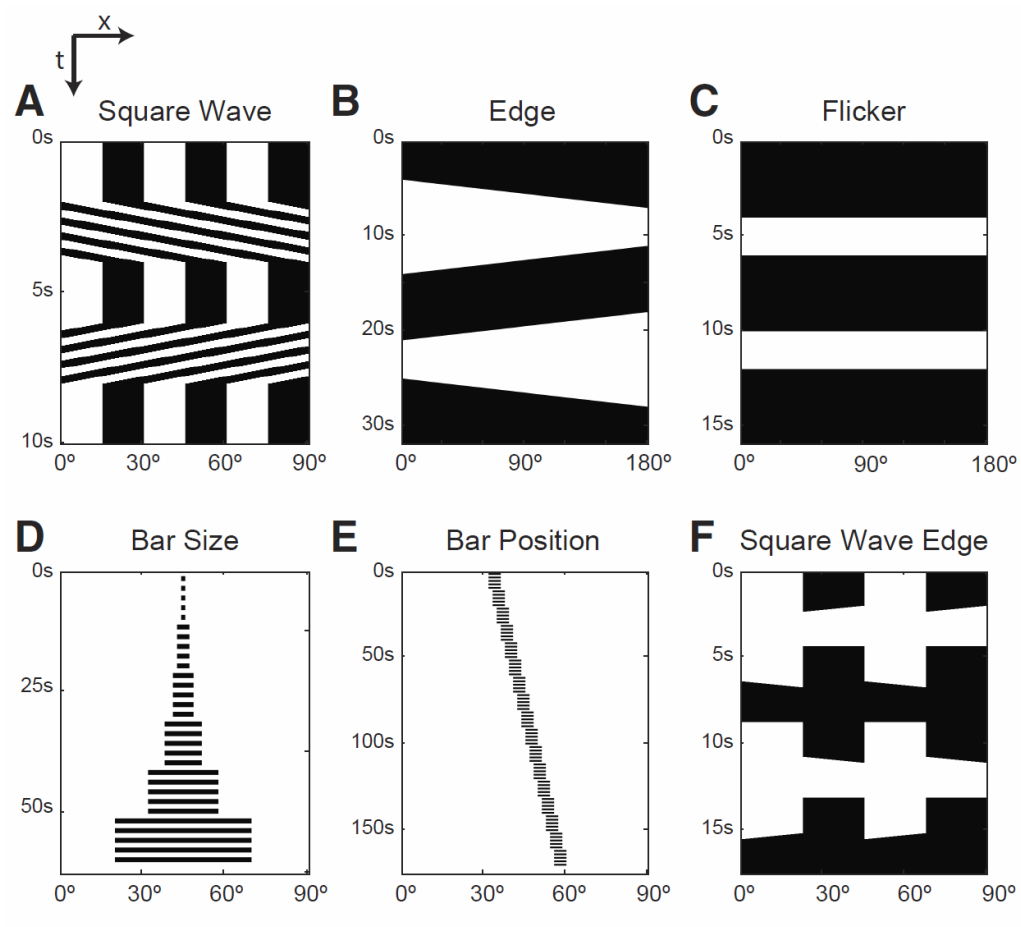


Figure S3: Space-time (xt) plots of all visual stimuli used in the study. Related to Figures 2-5.

2.3 COMPREHENSIVE CHARACTERIZATION OF THE MAJOR PRESYNAPTIC ELEMENTS OF THE *drosophila* OFF MOTION DETECTOR

In this study (Serbe et al., 2016) we characterized the response properties and tested the necessity of four columnar cell types presynaptic to dark-selective T5. It was published in *Neuron* in February 2016.

Summary

Using two-photon calcium imaging, we probed temporal and spatial characteristics of presumed OFF pathway cells Tm₁, Tm₂, Tm₄, and Tm₉. All of the four columnar cell types have small, isotropic receptive fields, shaped by lateral inhibition. Their temporal response profiles differ substantially. Tm₂ and Tm₄ provide fast, transient signals best described by band-pass filters with small time constants, Tm₁ exhibit intermediate band-pass characteristics, while the slow responses of Tm₉ cells appear to be solely low-pass filtered. Modeling elementary motion detectors by employing the measured time constants resulted in tuning curves similar to physiological measurements. Measuring direction selectivity in lobula plate tangential cells, we found all four cells to be involved to different degrees in the detection of moving brightness decrements. Simultaneous silencing of binary combinations of Tm cells eliminated complete redundancy of individual elements. Repeating the silencing experiments, now monitoring the turning behavior of tethered walking flies, in principle confirmed these findings. We furthermore observed an interesting nonlinear relation between tangential cell signals and behavioral output.

The following authors contributed to this work:

Etienne Serbe¹, **Matthias Meier**¹, Aljoscha Leonhardt, and Alexander Borst

Author contribution

Etienne Serbe, **Matthias Meier**, and Alexander Borst designed the study. **Matthias Meier** and Etienne Serbe performed calcium imaging and electrophysiological recordings. Aljoscha Leonhardt performed behavioral experiments. Aljoscha Leonhardt and Alexander Borst performed modeling experiments. **Matthias Meier** and Etienne Serbe wrote the paper with help of the other authors.

This article was featured in a preview in the same issue of *Neuron*. **Four to Foxtrot: How Visual Motion is Computed in the Fly Brain** (Tuthill and Borghuis, 2016)

¹ equal contribution

Comprehensive Characterization of the Major Presynaptic Elements to the *Drosophila* OFF Motion Detector

Highlights

- All *Drosophila* OFF motion pathway Tm cells are activated by brightness decrements
- None of the four cell types are direction selective
- Tm1, Tm2, Tm4, and Tm9 display a variety of temporal filter properties
- The four Tm cells are involved in OFF motion processing to different degrees

Authors

Etienne Serbe, Matthias Meier, Aljoscha Leonhardt, Alexander Borst

Correspondence

serbe@neuro.mpg.de (E.S.),
mmeier@neuro.mpg.de (M.M.)

In Brief

Serbe et al. use calcium imaging, electrophysiology, and behavior to assess the roles of columnar elements in the OFF motion vision pathway of *Drosophila*. Here, the complex interaction of four cell types shapes the flies' responses to motion stimuli.

Comprehensive Characterization of the Major Presynaptic Elements to the *Drosophila* OFF Motion Detector

Etienne Serbe,^{1,2,*} Matthias Meier,^{1,2,*} Aljoscha Leonhardt,¹ and Alexander Borst¹

¹Max-Planck-Institute of Neurobiology, Am Klopferspitz 18, 82152 Martinsried, Germany

²Co-first author

*Correspondence: serbe@neuro.mpg.de (E.S.), mmeier@neuro.mpg.de (M.M.)

<http://dx.doi.org/10.1016/j.neuron.2016.01.006>

SUMMARY

Estimating motion is a fundamental task for the visual system of sighted animals. In *Drosophila*, direction-selective T4 and T5 cells respond to moving brightness increments (ON) and decrements (OFF), respectively. Current algorithmic models of the circuit are based on the interaction of two differentially filtered signals. However, electron microscopy studies have shown that T5 cells receive their major input from four classes of neurons: Tm1, Tm2, Tm4, and Tm9. Using two-photon calcium imaging, we demonstrate that T5 is the first direction-selective stage within the OFF pathway. The four cells provide an array of spatiotemporal filters to T5. Silencing their synaptic output in various combinations, we find that all input elements are involved in OFF motion detection to varying degrees. Our comprehensive survey challenges the simplified view of how neural systems compute the direction of motion and suggests that an intricate interplay of many signals results in direction selectivity.

INTRODUCTION

Extracting the direction of visual motion is an essential operation for most animals to successfully perform tasks like navigation, prey capture, predator avoidance, and mating. Correlation-type motion detectors represent a class of algorithmic models that achieve direction selectivity by multiplying signals from two adjacent photoreceptors after asymmetric temporal filtering (Figure 1A; Hassenstein and Reichardt, 1956). In various vertebrate and invertebrate species, this is realized separately for brightness increments (ON) and decrements (OFF; Werblin and Dowling, 1969; Joesch et al., 2010; Borst and Euler, 2011). In the mouse retina, for example, direction selectivity in OFF-type starburst amacrine cells is proposed to arise from spatially offset bipolar cell input (Kim et al., 2014). These cells exhibit temporally diverse calcium (Baden et al., 2013) and glutamate release signals (Borghuis et al., 2013). In *Drosophila melanogaster*, photoreceptor signals are processed in a retinotopic way within

the four neuropils of the optic lobe, called lamina, medulla, lobula, and lobula plate (Figure 1B). In the lobula plate, wide-field tangential cells respond to motion stimuli in a fully opponent, direction-selective manner: they depolarize to motion along their preferred direction (PD) and hyperpolarize to motion along the opposite or null direction (ND; Joesch et al., 2008; Schnell et al., 2010). Tangential cells receive excitatory cholinergic input from two types of neurons, called T4 and T5 cells (Mauss et al., 2014). They were first described via Golgi stainings (Cajal and Sánchez, 1915) and exist in four subtypes, depending on their projection layer in the lobula plate (Figure 1B; Fischbach and Dittrich, 1989). Genetically silencing both cell types turns tangential cells motion insensitive and walking flies motion blind (Schnell et al., 2012; Bahl et al., 2013). Each of the four subtypes responds only to either brightness increments (ON for T4) or decrements (OFF for T5), moving in one of the four cardinal directions (front to back, back to front, upward, and downward). Blocking either T4 or T5 results in selectively diminished responses of lobula plate tangential cells to ON and OFF stimuli, respectively (Maisak et al., 2013). The splitting of ON and OFF signals starts at the level of lamina monopolar cells, which receive direct input from photoreceptors. L1 signals feed into the ON pathway; L2–L4 signals feed into the OFF pathway (Joesch et al., 2010, 2013; Clark et al., 2011; Eichner et al., 2011; Takemura et al., 2011; Silies et al., 2013; Meier et al., 2014). Electron microscopy reconstructions identified the primary interneurons that connect lamina monopolar cells to the dendrites of T4 and T5 cells. L1 synapses mainly onto the medulla intrinsic neuron Mi1 and onto the transmedulla neuron Tm3, which both contact T4 cells (Takemura et al., 2013). In the OFF pathway, reciprocally connected L2 and L4 cells (Rivera-Alba et al., 2011) connect to Tm1, Tm2, and Tm4 cells while L3 cells synapse onto Tm9 cells (Figure 1B; Takemura et al., 2013). These four Tm cells have been described as cholinergic and collectively account for nearly 90% of T5 input synapses, with Tm2 being the numerically dominant input (~33%), followed by Tm9 (~22%), Tm1 (~20%), and Tm4 (~13%; Takemura et al., 2011; Shinomiya et al., 2014). Calcium imaging and electrophysiological recordings revealed that Tm1 and Tm2 respond to OFF stimuli with transient activation, independent of the direction of motion (Meier et al., 2014; Strother et al., 2014; Behnia et al., 2014). Their dynamic properties, estimated using a white-noise stimulus, revealed an offset in peak response times of 13 ms. This led to the suggestion that Tm1 and Tm2 cells form the

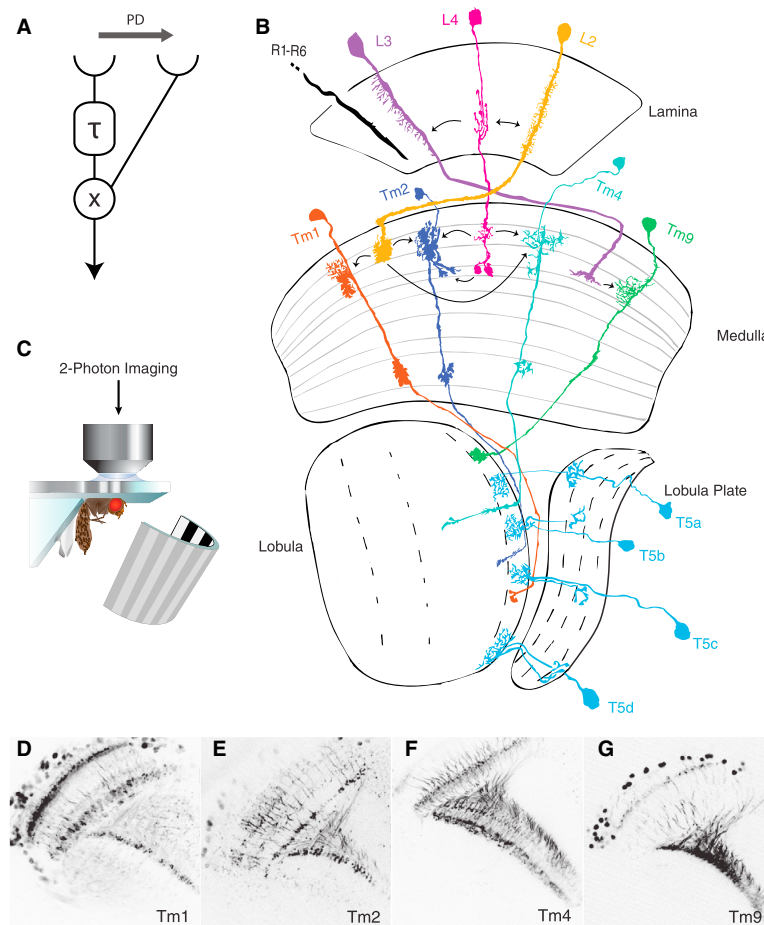


Figure 1. The OFF Pathway of *Drosophila* Motion Vision

(A) Schematic representation of a subunit of a Hassenstein-Reichardt correlator tuned to rightward motion (preferred direction, PD). Signals from two spatially offset inputs are multiplied (\times) after one of them has been temporally delayed by a low-pass filter with the time constant τ .

(B) Wiring diagram of the proposed OFF pathway neurons. Photoreceptors R1–R6 project onto interconnected lamina monopolar cells L2 (yellow), L3 (purple), and L4 (magenta). The L2–L4 sub-pathway consists of transmedullary neurons Tm2 (dark blue) and Tm4 (cyan). L3 contacts Tm9 cells (green). Tm1 (orange) only receives input via L2 (yellow). All four Tm cells project into the lobula, giving input to the four subtypes of T5 (light blue). Arrows indicate synaptic contacts between cell types. (Modified from Fischbach and Dittrich, 1989.)

(C) Experimental setup for two-photon calcium imaging.

(D–G) Contrast-inverted maximum intensity z projections of two-photon image stacks through the optic lobe of flies expressing GCaMP6f in Tm1 (D), Tm2 (E), Tm4 (F), and Tm9 (G) cells.

two input lines of an OFF elementary motion detector (Behnia et al., 2014). Indeed, blocking Tm2 cells strongly reduces the responses of tangential cells to moving dark edges (Meier et al., 2014). Whether Tm1 is equally critical has not been clarified; neither have the roles of the other two input neurons, Tm4 and Tm9. We therefore set out to explore the response properties and necessity of all four major inputs to T5 cells, which constitutes a crucial step toward a mechanistic understanding of how direction selectivity is computed in the OFF pathway of *Drosophila*.

First, we performed two-photon calcium imaging (Figure 1C) to assess the visual response properties of all major T5 inputs, including direction selectivity, response dynamics, and receptive fields. Second, we blocked the synaptic output of single-cell types, as well as combinations of two-cell types, using *shibire^{ts}* (Kitamoto, 2001) and analyzed responses of tangential cells and walking flies to visual motion stimuli. Our results demonstrate that all four Tm cell types are activated by brightness decrements, irrespective of the direction of motion, confirming the notion that T5 cells are the first direction-selective cells within the OFF pathway (Maisak et al., 2013;

Fisher et al., 2015). Their responses revealed substantially different temporal dynamics. Blocking their synaptic output individually and in combination exclusively impaired OFF motion vision, though by different magnitudes. Combinatorial blocking of two Tm cell types resulted in an increased reduction of the OFF motion response. These data do not map easily onto classical models of motion detection involving two input

RESULTS

Response Properties of Tm1, Tm2, Tm4, and Tm9 Cells

To directly examine the response properties of Tm cells, we expressed calcium indicator GCaMP5 (Akerboom et al., 2012) under the control of cell-type-specific Gal4 lines (Brand and Perrimon, 1993). We manually chose regions of interest that corresponded to single axonal terminals in the lobula where T5 dendrites are located (Figures 1D–1G) and determined the fluorescence change during visual stimulation. First, we characterized the calcium responses of T5's presynaptic elements by presenting edges of both polarities (ON and OFF edges) moving in the four cardinal directions. With these visual stimuli, we addressed two questions: First, are neurons upstream of T5 cells direction selective? Second, do they exhibit rectified responses with respect to the contrast polarity of the stimulus? In agreement with previous studies (Meier et al., 2014; Strother et al., 2014; Behnia et al., 2014), we found that Tm1 and Tm2 cells

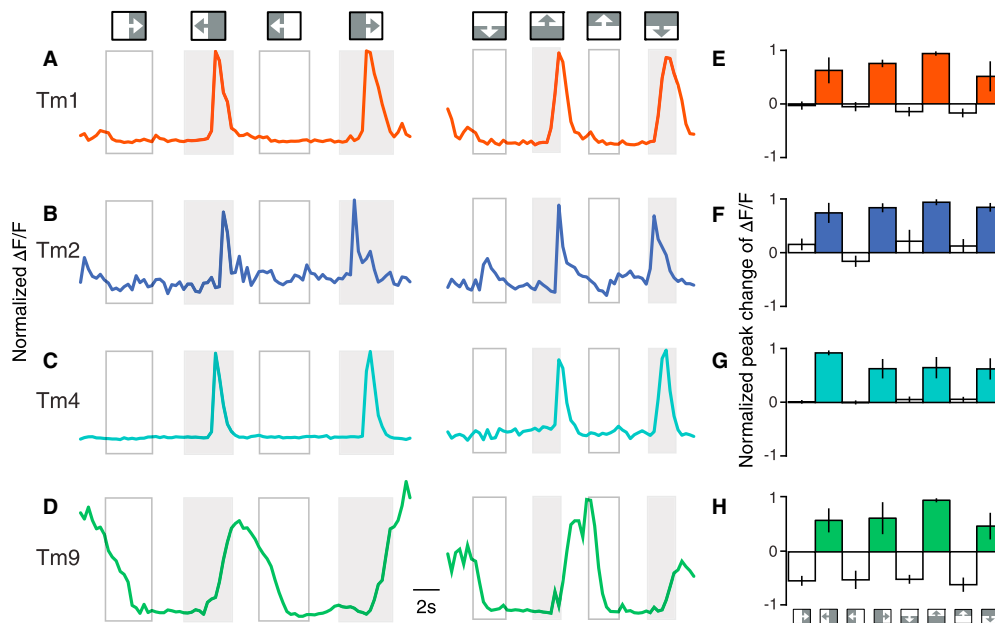


Figure 2. OFF Edges Activate Tm Cells Irrespective of the Direction of Motion

(A–D) Normalized $\Delta F/F$ calcium responses of single Tm1 (A), Tm2 (B), Tm4 (C), and Tm9 (D) cells. Flies were visually stimulated with ON and OFF edges moving horizontally (left panel) and vertically (right panel). Empty boxes indicate stimulation periods of ON edge motion; gray boxes indicate stimulation periods of OFF edge motion. Directions and polarity of edge motion are illustrated by little boxes on top. Between stimulations, luminance levels remain constant; i.e., after presentation of OFF edges, the stimulation device remains dark until the subsequent ON stimulus. After presentation of ON edges, the arena remains bright. (E–H) Average normalized peak changes in calcium signals during edge presentation. Stimuli are represented at the bottom of (H). Tm1 (E; $n = 11$ cells in $N = 11$ flies), Tm2 (F; $n = 8$, $N = 8$), Tm4 (G; $n = 9$, $N = 9$), and Tm9 (H; $n = 8$, $N = 8$). Error bars indicate \pm SEM. See also Figure S7.

respond to moving brightness decrements (OFF edges) with a transient increase in calcium, independent of the direction of motion. In this experiment, neither Tm1 nor Tm2 cells showed any response when stimulated with moving brightness increments (ON edges; Figures 2A and 2B). Tm4 cells exhibited similar characteristics with short increases of activity when stimulated with OFF edges moving along all four cardinal directions (Figure 2C). The calcium levels of Tm9, however, changed more tonically, inversely following the local luminance level: when presented with a moving ON edge, the cell's initial calcium level dropped, and it only increased when a dark edge was moved through the fly's visual field (Figure 2D). Again, this was true for all four directions. To quantify the calcium responses to moving edges—and to detect increases, as well as decreases—we calculated the extremum (maximum or minimum) of the derivative of the fluorescence change for each stimulus (Figures 2E–2H). This demonstrated that all transmedullary neurons, anatomically identified to be presynaptic to T5, are not themselves direction selective and respond with increased activity to visual stimulation with dark edges. The response kinetics of the different Tm cells, however, looked qualitatively different. To more precisely characterize the temporal properties of Tm cells and to investigate whether the four cell types exhibit rectified responses with respect to contrast polarity, we increased the temporal resolution of the scanning microscope from 1.8 to 480 Hz by

acquiring data from a single line through one axonal arbor in the lobula. Moreover, we expressed a faster calcium indicator, GCaMP6f (Chen et al., 2013), in the Tm cells. We used a 4.5° -wide, dark, vertical bar appearing and disappearing on a bright background for seven durations (50, 75, 125, 225, 425, 825, and 1,625 ms). All four Tm cells responded with an increase in calcium levels to local brightness decrements (Figures 3A–3D). Consistent with the edge stimulation results, this set of experiments revealed a broad range of response kinetics for the four Tm cell types. Furthermore, we observed a drop in calcium signaling upon stimulus offset. Based on these observations, we simulated their responses by fitting a three-stage filter model to the mean calcium traces (Figure 3E). Within this model, inputs were first linearly high-pass filtered (τ_{HP}), then rectified by setting negative values to zero, and finally low-pass filtered (τ_{LP}). Using this simple model, we were able to reproduce the measured calcium dynamics and estimate filter time constants for each cell type from the observed responses (Figures 3F–3I). In agreement with the data from the stimulation with moving edges, the four cell types could be classified in three groups: fast, transient Tm2 ($\tau_{HP} = 0.36$ s and $\tau_{LP} = 0.1$ s; Figures 3B and 3G) and Tm4 ($\tau_{HP} = 0.25$ s and $\tau_{LP} = 0.2$ s; Figures 3C and 3H), intermediate Tm1 ($\tau_{HP} = 1.23$ s and $\tau_{LP} = 0.23$ s; Figures 3A and 3F), and tonic Tm9 ($\tau_{LP} = 0.63$ s; Figures 3D and 3I). In contrast to the other cell types, the slow dynamics of Tm9 responses were best predicted

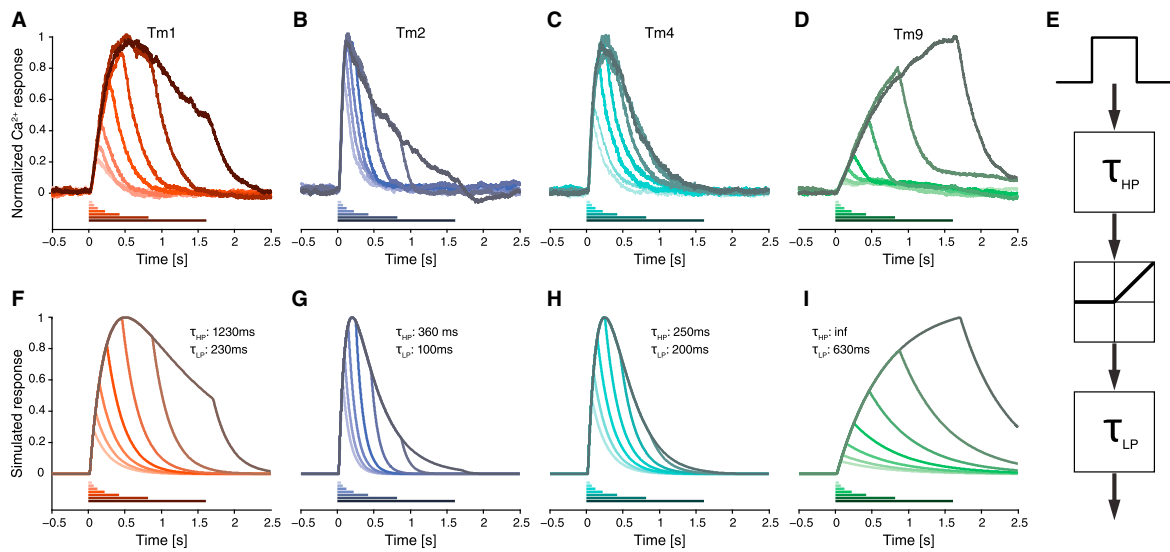


Figure 3. Temporal Tm Cell Response Properties

(A–D) Normalized $\Delta F/F$ calcium responses of Tm1 (A; $n = 32$, $N = 5$), Tm2 (B; $n = 38$, $N = 5$), Tm4 (C; $n = 26$, $N = 3$), and Tm9 (D; $n = 44$, $N = 4$), obtained by line scans through individual axonal arbors. Flies were presented with a 4.5° -wide, dark, vertical bar appearing on a bright background for seven periods: 50, 75, 125, 225, 425, 825, and 1,625 ms. Color-coded bars at the bottom of the graphs indicate the duration of stimulus presentation.

(E) Simulation procedure. The input signals were high-pass filtered (τ_{HP}), rectified, and low-pass filtered (τ_{LP}). Filter time constants are indicated in each panel. (F–I) Simulated responses of Tm1 (F), Tm2 (G), Tm4 (H), and Tm9 (I) obtained by using the indicated time constants for the low-pass and high-pass filtering. For Tm9, no high-pass filtering was applied.

See also [Figures S1](#) and [S7](#).

by a pure low-pass filter. Also, prolonging the period of stimulus presentation to 2 and 4 s supported the finding that Tm9 cells respond tonically to visual stimulation with dark bars ([Figure S1](#)). To exclude that calcium buffering caused the slow dynamics of the Tm9 responses, we repeated the experiments using flies heterozygous for Gal4 and upstream activating sequence (UAS)-GCaMP6f to reduce expression levels of GCaMP. Here, we obtained the same results. In summary, the preceding results demonstrate that Tm1, Tm2, Tm4, and Tm9 are directionally unselective and thus confine the computation of direction selectivity in the OFF pathway to the dendrites of T5 cells. Furthermore, our data indicate that Tm cells provide a variety of temporal filters, ranging from fast, transient Tm2 and Tm4 over intermediate Tm1 to slow and sustained Tm9 cells.

Receptive Field Characteristics of Tm1, Tm2, Tm4, and Tm9

Current models for motion detection are based on the spatio-temporal correlation of input signals. It is thus crucial to characterize receptive field sizes and spatial integration properties of columnar neurons. To probe the receptive fields of the four Tm cells, we recorded changes in fluorescence at a lower temporal resolution of 1.8 Hz. Because our previous experiments ([Figures 2](#) and [3](#)) had revealed that all four cell types respond to changes in local luminance, we stimulated flies with 4.5° -wide, dark, vertical bars flickering on a bright background with 0.5 Hz at different azimuthal positions, each shifted by 1.5° . All

four Tm cells tested with this stimulus exhibited similar receptive field sizes, ranging from 4.2° to 5.5° of half-width ([Figures 4A–4E](#)). We next used horizontal bars and presented them at different elevations. Again, we found comparable receptive field sizes with half-widths between 3.9° and 4.2° ([Figure 4E](#)). From this, we conclude that Tm1, Tm2, Tm4, and Tm9 cells have small isotropic receptive fields. The size of the measured receptive fields approximately corresponded to the visual acceptance angle of one neuro-ommatidium ([Götz, 1964](#); [Land, 1997](#)), which indicates that the main activation of Tm cells is restricted to visual information detected by only one ommatidium. Stimulating the fly's eye in consecutive steps along the azimuth with terminals of several adjacent Tm9 cells in focus nicely revealed the retinotopic organization of columnar elements projecting from the medulla to the lobula ([Movie S1](#)). Next, we investigated spatial integration properties by centering a flickering dark, vertical bar at the position of maximal excitability of individual Tm cells. After each period of stimulation, we increased the width of the bar. All four cell types showed maximum responses when stimulated with bars of a 4.5° to 7.5° width but decreased activity when presented with stimuli spanning larger areas in visual space ([Figures 4F–4I](#)). Hence, all cells seem to be subject to lateral inhibition, preventing them from responding to wide-field flicker. The responses of Tm9 cells diverged from the other cell types for full-field stimulation (180° azimuth): while the calcium response levels elicited by flicker between a 13.5° and a 67.5° width were small, the response to full-field darkening amounted

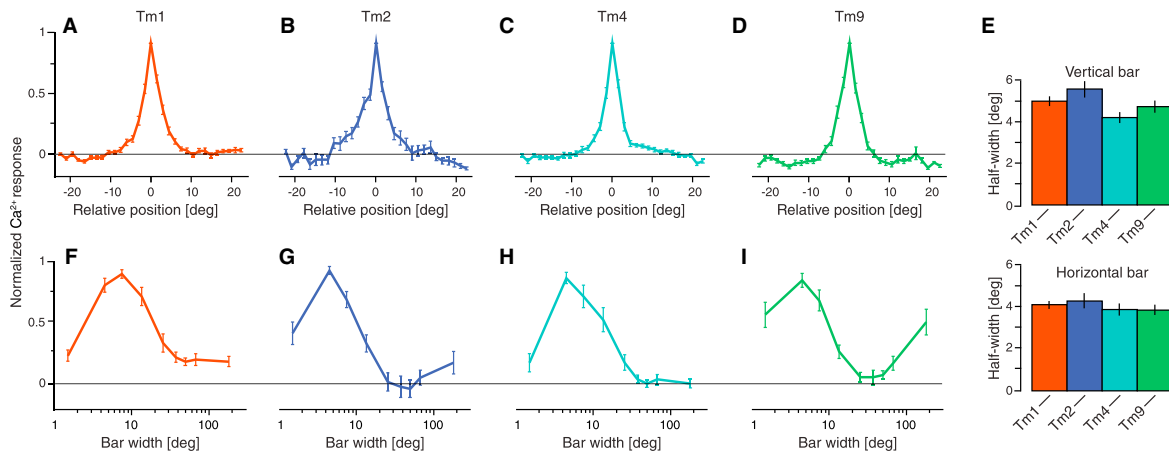


Figure 4. Receptive Field Properties of Tm Cells

(A–D) Spatial receptive fields measured by normalized calcium responses of Tm1 (A; $n = 45$, $N = 10$), Tm2 (B; $n = 29$, $N = 8$), Tm4 (C; $n = 30$, $N = 5$), and Tm9 (D; $n = 31$, $N = 8$) to 4.5°-wide, dark, vertical bars appearing and disappearing at various positions (shifted by 1.5°) on a bright background at a frequency of 0.5 Hz. (E) Quantification of receptive field half-width for vertical bars (top panel) and horizontal bars (bottom panel). Tm1 ($n = 37$, $N = 8$), Tm2 ($n = 26$, $N = 6$), Tm4 ($n = 20$, $N = 3$), and Tm9 ($n = 24$, $N = 3$).

(F–I) Spatial integration properties measured by normalized calcium responses of Tm1 (F; $n = 15$, $N = 9$), Tm2 (G; $n = 16$, $N = 7$), Tm4 (H; $n = 9$, $N = 4$), and Tm9 (I; $n = 9$, $N = 4$) to dark, vertical bars of increasing size (bar widths: 1.5°, 4.5°, 7.5°, 13.5°, 25.5°, 37.5°, 49.5°, 67.5°, and 180°). Error bars indicate ± SEM. See also Figure S7.

to approximately 50% of the maximum response. Tm9 has been shown to receive its main synaptic inputs through a different set of neurons from those for Tm1, Tm2, and Tm4 (L3 for Tm9, compared to L2 for Tm1, Tm2, and Tm4; Takemura et al., 2013). Together with the particular spatial integration property, the anatomical distinctness of Tm9 suggests that lateral inhibition could be implemented by two different mechanisms in the OFF pathway. Taken together, using calcium levels as a proxy for neuronal activity, we established that Tm1, Tm2, Tm4, and Tm9 are small-field columnar neurons that receive isotropic lateral inhibition.

Blocking OFF Pathway Tm Cells Reduces Responses of Lobula Plate Tangential Cells Specifically to OFF Edges

The response properties of *Drosophila* lobula plate tangential cells have been well characterized using various visual stimuli (Joesch et al., 2008, 2010; Schnell et al., 2010; Mauss et al., 2015). Furthermore, these large-field interneurons have been demonstrated to receive excitatory input from T4 and T5 cells (Schnell et al., 2012; Mauss et al., 2014). Hence, responses of lobula plate tangential cells can be used as a readout to assess the contribution of presynaptic elements within the motion detection circuit (Joesch et al., 2010; Schnell et al., 2012; Maisak et al., 2013; Meier et al., 2014). We performed somatic whole-cell patch clamp recordings from tangential cells of the vertical system (VS) and horizontal system (HS) while blocking the output of different Tm cells. We stimulated flies with either multiple ON or OFF edges (Figure S7). Synaptic transmission was silenced by expressing temperature-sensitive *shibire^{ts}* (Pfeiffer et al., 2012) under the control of specific Gal4 driver lines. We confirmed the identities of cell types in the Gal4 lines by expressing GFP

in a small subset of neurons using a flip-out approach (Figures 5A–5D; Nern et al., 2015). To increase block strength without a loss of expression specificity, we used flies with two copies of *UAS-shibire^{ts}* (*shi^{ts}/shi^{ts}*) and one copy of the Gal4 driver. Tangential cells of control flies responded with approximately equal strength to motion of bright or dark edges (Figures 5E–5H). We could thus use these stimuli to probe contrast-polarity-specific effects of Tm cell blocks. Based on the diversity of temporal response properties observed in our calcium imaging experiments reported earlier, we hypothesized that different Tm cell types may play distinct roles depending on motion velocity, as was recently shown for input elements to the ON direction-selective T4 cells (Ammer et al., 2015). We therefore tested flies using edges moving at nine velocities across two orders of magnitude (3.125°/s–800°/s; Figure S2). When Tm1 was removed from the circuit, lobula plate tangential cells responded only with about half of the magnitude of control flies to moving dark edges (Figures 5E and 5I). In agreement with a previous study, responses were strongly reduced when Tm2 was blocked (Meier et al., 2014). Both effects were present over all velocities tested (Figures 5F and 5J). Blocking Tm4 produced the weakest phenotype (Figures 5G and 5K). Interrupting Tm9 signaling resulted in the strongest effect of all cells tested and, as with the other cells, did so consistently across all stimulus velocities (Figures 5H and 5L). To our surprise, here, we did not find differential effects of blocking any of the four Tm cell types when using different edge velocities. To compare the overall effects of silencing single Tm cells, we calculated the average response relative to control flies over the whole range of stimulus velocities (Figures 5M–5P). Critically, in all silencing experiments, responses to ON edges were not significantly altered. Blocking

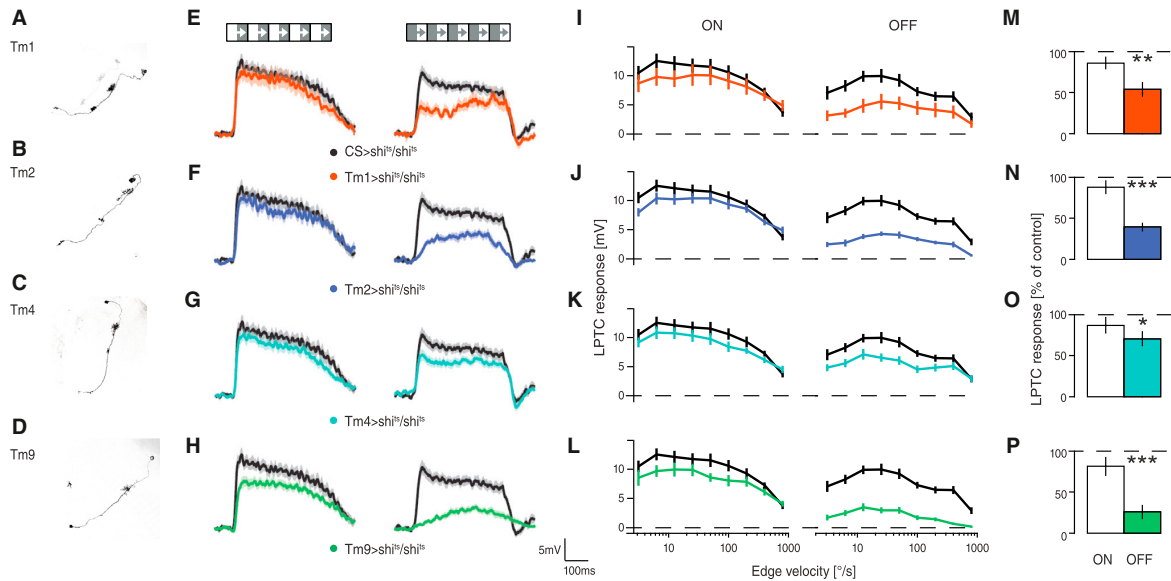


Figure 5. Blocking Tm Cells Impairs OFF Motion Vision

(A–D) Stochastic labeling of single Tm1 (A), Tm2 (B), Tm4 (C), and Tm9 (D) cells, showing the specificity of the Gal4 driver lines. (E–H) Example traces of mean responses to motion along the PD minus the response to motion along the ND of lobula plate tangential cell (LPTC) responses upon stimulation with multiple ON (left) and OFF (right) edges (50°/s) in control CS > *shi^{ts}/shi^{ts}* (black), Tm1 > *shi^{ts}/shi^{ts}* (E), Tm2 > *shi^{ts}/shi^{ts}* (F), Tm4 > *shi^{ts}/shi^{ts}* (G), and Tm9 > *shi^{ts}/shi^{ts}* (H) flies. Stimulus presentation is indicated by the panels on top. (I–L) Mean PD-ND LPTC responses of control (black), Tm1 (I), Tm2 (J), Tm4 (K), and Tm9 (L) block flies upon ON (left panel) and OFF edge (right panel) stimulation for nine velocities (3.125°/s, 6.25°/s, 12.5°/s, 25°/s, 50°/s, 100°/s, 200°/s, 400°/s, and 800°/s). (M–P) Responses averaged over all nine velocities of Tm1 (M), Tm2 (N), Tm4 (O), and Tm9 (P) block flies plotted as percentages of the controls. Responses were obtained from HS and VS cells. Because no difference was detected, data from both cell types were pooled. CS > *shi^{ts}/shi^{ts}* data are from 13 cells (5 HS, 8 VS) in 5 flies, Tm1 block data are from 10 cells (3 HS, 7 VS) in 7 flies, Tm2 block data are from 14 cells (7 HS, 7 VS) in 7 flies, Tm4 block data are from 16 cells (5 HS, 11 VS) in 9 flies, and Tm9 block data are from 15 cells (3 HS, 12 VS) in 8 flies. In all four Tm cell blocks, ON responses are not significantly reduced in comparison to control flies. OFF responses, however, are reduced at different significance levels. * $p < 0.05$, ** $p < 0.01$, *** $p < 0.001$, tested using two-tailed t tests against the controls. Error shades and error bars indicate \pm SEM. See also [Figures S2–S4](#) and [S7](#).

any of the four Tm cell types specifically impaired the responses of lobula plate tangential cells to moving dark edges, irrespective of stimulus velocity. The magnitude of effects, however, covered a wide range, with strong phenotypes for Tm9 (25.69% \pm 6.37% of control, mean \pm SEM, $n = 15$ recordings, $p < 0.001$) and Tm2 (39.22% \pm 4.50%, $n = 14$, $p < 0.001$), intermediate effects for Tm1 block (53.98% \pm 8.33%, $n = 10$, $p < 0.01$), and a weak phenotype for silencing Tm4 (70.59% \pm 8.41%, $n = 16$, $p < 0.05$).

Combinatorial Blocking of Tm Cells Increases OFF Edge Phenotypes

Tm cells could contribute in parallel or modularly to direction selectivity in T5. Combining two cell-specific Gal4 lines, thereby driving the expression of *shibire^{ts}* in two cell populations simultaneously, allowed us to investigate how different Tm cells interact. To detect potential synergistic effects, we decreased individual blocking strength by using flies with only one copy of *shibire^{ts}* (*shi^{ts}/+*). When we repeated the same experiment as described earlier, the tangential cell responses of Tm1 block flies to dark-edge stimulation were only reduced to 76.29% \pm 7.88% (percent of control, $n = 11$, $p = 0.18$; [Figures 6A](#) and [6B](#)) as opposed to 54% for two copies of *shibire^{ts}*. Blocking Tm2 with one copy of

shibire^{ts} resulted in a response reduction to 69.13% \pm 4.25% ($n = 11$, $p = 0.07$; [Figures 6G](#) and [6H](#)), while blocking Tm4 cells did not result in a detectable reduction of tangential cell responses (89.17% \pm 7.95%, $n = 12$, $p = 0.50$; [Figures 6M](#) and [6N](#)). Only responses of Tm9 block flies to dark edges remained significantly different from those of control flies (51.39% \pm 6.02%, $n = 10$, $p < 0.01$; [Figures 6S](#) and [6T](#)), even with only one copy of *shibire^{ts}*. Overall, we found that the effect size was reduced while relative effects remained the same, with blocking Tm9 resulting in the strongest reduction of the OFF response, followed by Tm2, Tm1, and finally Tm4. This offered an opportunity to compare partial single-cell blocks with the combinations of two incompletely blocked classes of neurons. The images in [Figure S3](#) provide an overview of the expression patterns of the six binary combinations of the four Tm cell types. Combining Tm9 with one of the other three cell types resulted in the strongest reductions of tangential cell responses to OFF edges ([Figures 6E](#), [6J](#), and [6O–6R](#)). All three Tm9 combinations decreased responses beyond what we had determined for the single Tm9 block. Furthermore, Tm1/Tm2 and Tm2/Tm4 blocks reduced the responses of lobula plate tangential cells to moving dark stimuli ([Figures 6C](#), [6F](#), [6I](#), and [6L](#)) compared to the isolated

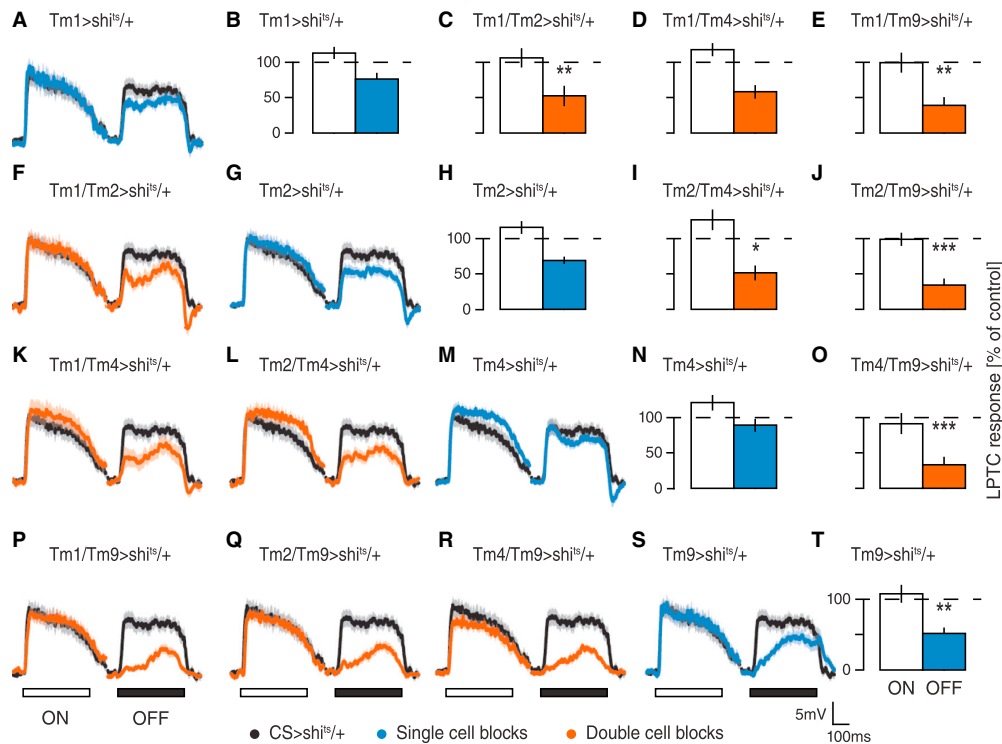


Figure 6. Combinatorial Blocking of Tm Cells

(A, F, G, K-M, and P-S) Mean traces of control (black), single-block (blue), and double-block (orange) flies for ON (left) and OFF (right) edge stimulation at a representative velocity of 50°/s.

(B-E, H-J, N, O, and T) Mean ON and OFF lobula plate tangential cell (LPTC) responses of single (blue) and double (orange) Tm cell block flies compared to control flies over nine velocities. Control CS > shi^{ts}/+ data are from 13 cells (5 HS, 8 VS) in 5 flies, Tm1 > shi^{ts}/+ data are from 11 cells (4 HS, 7 VS) in 6 flies, Tm2 > shi^{ts}/+ data are from 13 cells (6 HS, 7 VS) in 9 flies, Tm4 > shi^{ts}/+ data are from 12 cells (4 HS, 8 VS) in 6 flies, Tm9 > shi^{ts}/+ data are from 10 cells (3 HS, 7 VS) in 7 flies, Tm1/Tm2 > shi^{ts}/+ data are from 11 cells (3 HS, 8 VS) in 7 flies, Tm1/Tm4 > shi^{ts}/+ data are from 11 cells (4 HS, 7 VS) in 7 flies, Tm1/Tm9 > shi^{ts}/+ data are from 10 cells (3 HS, 7 VS) in 7 flies, Tm2/Tm4 > shi^{ts}/+ data are from 13 cells (3 HS, 10 VS) in 7 flies, Tm2/Tm9 > shi^{ts}/+ data are from 12 cells (4 HS, 8 VS) in 8 flies, and Tm4/Tm9 > shi^{ts}/+ data are from 10 cells (3 HS, 7 VS) in 7 flies. In all block flies, ON responses are not significantly reduced in comparison to control flies. OFF responses, however, are reduced at different levels. *p < 0.05, **p < 0.01, ***p < 0.001, tested using two-tailed t tests against the controls. Error shades and error bars indicate ± SEM. See also Figures S3-S5 and S7.

Tm2 block. When the output of Tm1 and Tm4 was blocked simultaneously, we observed an intermediate reduction of tangential cell responses to OFF edges (Figures 6D and 6K). For all single- and double-block experiments with one copy of *shibire^{ts}*, responses to ON edges remained unaltered. Effects were consistent across all velocities tested for PD and ND stimulation (Figure S4). These results corroborate the conclusion drawn from single blocks, namely, that all four Tm cell types are involved in the detection of moving brightness decrements. Moreover, all combinatorial restrictions of two Tm cell outputs decreased OFF responses beyond the level of the respective single-cell blocks. To further investigate the effects of blocking T5 input elements on motion responses in tangential cells, we used square wave gratings (Figure S7) moving at eight temporal frequencies (from 0.07 to 8.89 Hz; Figure S5). In contrast to ON or OFF edges, square wave gratings did not allow for a specific stimulation of ON or OFF pathways. However, in contrast to a

moving edge, they led to ongoing, permanent stimulation of local T5 motion-detecting cells, as well as their input neurons. The responses to square wave gratings were only mildly reduced. The reduction pattern, however, was similar to that for OFF edges (Figures S5A-S5N). Compared to controls (Figures S5O-S5X), it is apparent that responses to gratings in almost all blocking conditions decreased as temporal frequency increased. This effect can be explained through differentially tuned responses of lobula plate tangential cells to ON and OFF edges: tangential cells respond maximally to bright edges moving ~100 deg/s, whereas their responses to dark edges peak ~300 deg/s (Ammer et al., 2015). Hence, the ON channel appears to contribute more strongly to responses at lower frequencies. High frequencies seem to be mostly mediated through the OFF system. This asymmetry could thus account for the increased reductions in high-frequency regimes for the strongest OFF blocks (Figures S5R, S5S, S5U, S5W, and S5X).

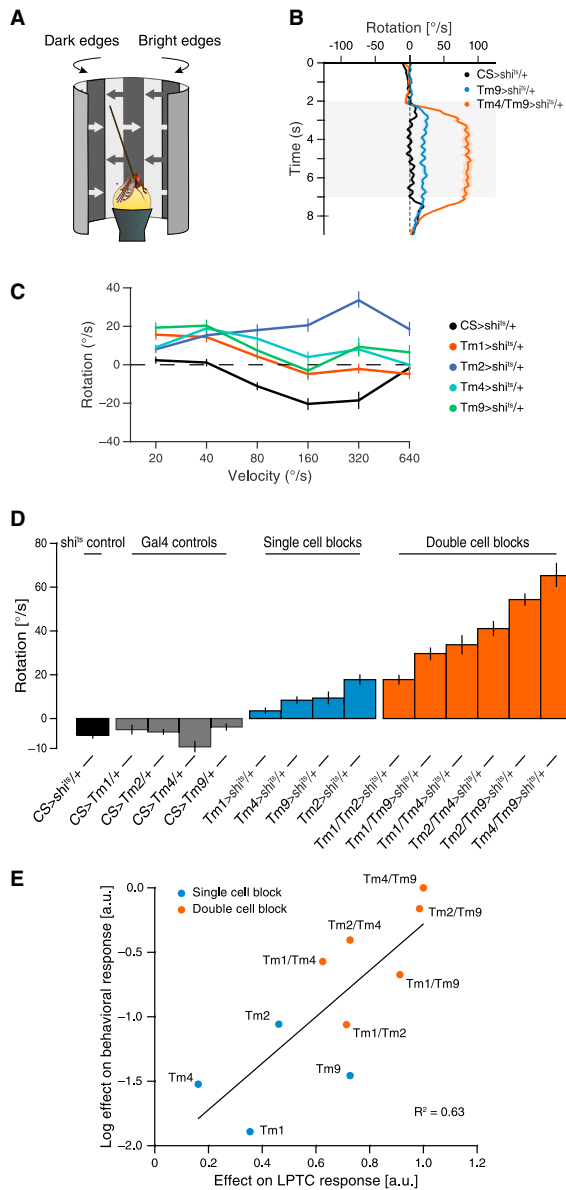


Figure 7. Blocking Tm Cells Affects Turning Behavior in Walking Flies

(A) Schematic illustration of the behavioral setup used in this study. A tethered fruit fly is walking on an air-suspended ball, facing a visual stimulation device. The fly is presented with a balanced motion stimulus (see [Experimental Procedures](#)).

(B) Exemplary optomotor responses of three genotypes to visual stimulation moving at 40°/s. Positive (rightward) rotation follows ON edges; negative (leftward) rotation follows OFF edges. Control flies do not exhibit any turning response for this velocity (black line), Tm9 block flies follow the bright edges with a low turning speed (blue line), and Tm4/Tm9 block flies turn with the direction of ON motion with a high angular velocity (orange line).

Blocking Tm Cells Affects Optomotor Responses in Walking Flies

The detection of visual motion is ultimately used to control behavior. The model proposed by [Hassenstein and Reichardt \(1956\)](#) was derived from quantitative observations of tethered walking beetles. To examine the effects of Tm cell blocks on the flies' turning responses during visual stimulation ([Figure 7A](#)), we monitored tethered *Drosophila* walking on an air-suspended ball and repeated the blocking experiments as described earlier. We used multiple dark and bright edges, simultaneously moving in opposing directions ([Clark et al., 2011](#)). Compared to the direct measurement of optomotor responses to edge motion of a single polarity, this stimulus allows for a differential measurement of the flies' sensitivity to moving ON and OFF edges. Turning responses in walking and flying *Drosophila* are not a direct readout of the membrane potential of lobula plate tangential cells ([Schnell et al., 2014](#)). Instead, signals are subject to leaky integration over a time window of multiple seconds. When examining responses, this may lead to robust behavioral responses despite strongly reduced lobula plate tangential cell signals. The opposing edge assay circumvents this issue by having edges of opposite polarities compete before the integration stage, such that small differences are amplified and become detectable at the level of turning responses. Critically, our electrophysiological experiments demonstrate that ON responses are generally not affected by blocking either of the four cells, suggesting that any imbalance we detect in behavior results from a defect specific to OFF motion processing.

At a stimulus velocity of 40°/s, control flies showed no turning response during presentation of opposing edges ([Figure 7B](#)), indicating that ON and OFF responses are intact and in balance. When we disrupted the output of either Tm9 or Tm4 and Tm9 in combination, block flies constantly followed the direction of moving ON edges (positive turning responses) with different amplitudes. This suggests an impairment of OFF motion detection at the behavioral level. When we used opposing edges moving at multiple velocities, control flies exhibited no turning response for slowly moving stimuli (20°/s and 40°/s) and started following dark edges (negative turning) when stimulated with patterns moving at higher speeds (80°/s–320°/s; [Figures 7C and S6](#)).

(C) Mean turning responses of control (black), Tm1 block (orange), Tm2 block (blue), Tm4 block (cyan), and Tm9 block (green) flies for stimulation with six velocities (20°/s, 40°/s, 80°/s, 160°/s, 320°/s, and 640°/s).

(D) Mean turning response of control (black and gray), single-block (blue), and double-block (orange) flies to stimulation with the balanced motion stimulus over all velocities tested. All blocking experiments were performed using one copy of *shibire^{ts}*. shi-control (N = 14), Tm1-control (N = 13), Tm2-control (N = 17), Tm4-control (N = 15), Tm9-control (N = 13), Tm1 (N = 12), Tm2-block (N = 13), Tm4-block (N = 13), Tm9-block (N = 12), Tm1/Tm2-block (N = 16), Tm1/Tm4-block (N = 12), Tm1/Tm9-block (n = 12), Tm2/Tm4-block (n = 16), Tm2/Tm9-block (n = 17), Tm4/Tm9-block (n = 14).

(E) Comparison of block effect strengths in the turning response of walking flies (y axis, log-transformed data) versus the effect of Tm cell blocks on the responses of lobula plate tangential cell (LPTCs; x axis, data not transformed). Single-cell blocks are colored in blue; double-cell blocks are in orange. The black line indicates a linear fit with $R^2 = 0.63$, indicating an exponential relationship between the behavioral effect and the reduction of the motion response as observed in the tangential cells. For details, see [Experimental Procedures](#). Error shades and error bars indicate \pm SEM. See also [Figures S3, S6, and S7](#).

Turning behavior of Tm1, Tm4, and Tm9 block flies differed from control flies in a roughly constant way across all velocities, showing positive responses (following bright edges) for low velocities and no turning response for higher velocities. To our surprise, and in contrast to our electrophysiological data (Figure 5), we could see a velocity-dependent effect in Tm2 block flies, which followed the motion of bright edges more strongly at high velocities (Figure 7C). These data suggest that removing Tm2 from the circuit has comparatively little effect at low velocities but a pronounced effect at high velocities, suggesting a specialized role of Tm2 for processing of fast input signals.

To compare effects from electrophysiological recordings with the behavioral data, we averaged the turning response over all velocities tested (Figure 7D). On average, all control flies exhibit a small negative turning tendency that can be explained by the high-velocity stimuli where OFF signals dominate (Ammer et al., 2015; Figures 7C and S6). Blocking Tm2 with one copy of *shibire^{TS}* resulted in the strongest turning response, whereas flies with blocked Tm1 cells showed only weak turning responses syndirectional with bright edges. Tm4 and Tm9 block flies exhibited intermediate phenotypes. Hence, suppressing synaptic transmission in single Tm cell types resulted in phenotypes that resembled those of T5 block flies (Maisak et al., 2013) and were qualitatively comparable to the results obtained in electrophysiological experiments. Next, we looked at the turning responses of flies with combinations of two Tm cell types silenced. When we combined Tm9 with Tm4- or Tm2-specific driver lines, we observed the strongest effects, in accordance with our electrophysiological data (Figure 7D). For combinatorial blocks of Tm1/Tm9, Tm1/Tm4, and Tm2/Tm4, the behavioral response was increased compared to single blocks (Figure 7D). Only the combined block of Tm1 and Tm2 cells did not elicit a turning response stronger than that for the Tm2 block alone. To investigate the relation between behavioral and tangential cell responses, we plotted effects of single- and double-cell silencing observed in the tangential cell responses versus those observed in walking flies (Figure 7E). To compare positive measures of effect strength in behavior and electrophysiology, we subtracted the electrophysiological phenotypes (in percent of control) from 100 and normalized them via division by the strongest phenotype. We then normalized the behavioral effect in the same way. We found an interesting relationship between the response reduction at the level of lobula plate tangential cells and the behaviorally measured ON-OFF imbalance. This relation is well explained by an exponential fit (black line in Figure 7E), suggesting that the transformation of tangential cell responses into behavioral output is highly nonlinear. A saturating transfer function, for instance, would explain how small and intermediate block effects at the level of the lobula plate produce comparatively weak effects at the level of walking behavior. Only when lobula plate tangential cell activity is heavily suppressed do walking flies show strong deficiencies for dark-edge motion, as indicated by the opposing edge results. Given that lobula plate networks feed into complex post-synaptic cascades before controlling motor output, this is not surprising. Generally, our electrophysiological findings predicted the behavioral phenotypes well, lending further credence to our results and indicating that the reductions we see at the level of lobula plate tangential cells

have direct impact on course control of behaving flies. Considering the combined dataset of tangential cell responses and behavior of walking flies, we conclude that all four Tm cells investigated here contribute to the computation of motion in the OFF pathway.

Reichardt Detector Simulations Using Tm Cells' Temporal Filters

A classical elementary motion detector (Hassenstein and Reichardt, 1956) consists of two spatially offset input lines that are multiplied after temporal filtering (Figure 1A). This is done in a mirror-symmetric fashion, and the outputs of the multiplication stages are subtracted from each other (insets in Figures 8A–8F). We used the calculated temporal filters of the Tm cells from Figures 3F–3I to simulate the responses of elementary motion detectors that are built from the six binary combinations of two Tm cells to grating stimulation (Figures 8A–8F). To obtain velocity tuning curves, we modeled responses to temporal frequencies ranging from 0.1 to 10 Hz (Figure 8). Except for the combination of Tm2 and Tm4, which have almost identical response dynamics, all Tm cell combinations led to direction-selective responses that varied in relative amplitude and tuning (Figures 8A–8F). Tuning curves of the four pairs Tm1/Tm2, Tm1/Tm4, Tm9/Tm2, and Tm9/Tm4 showed similar shapes and response amplitudes, peaking ~0.5 Hz. The Tm1/Tm9 model produced the strongest responses, peaking ~0.2 Hz. We calculated the mean of all detector outputs and normalized the tuning curve to compare the results with the physiological data (from Figure S5). The frequency tuning curves were largely similar, and both peaked ~0.5 Hz (Figure 8G). The shape of the tangential cell tuning curve, however, was wider than that of the simulation curve, which can be explained by saturation effects in tangential cells. From this, we conclude that the measured temporal response properties of all Tm cells are suitable for correlation-type elementary motion detectors.

DISCUSSION

In this study, we characterized the response properties of the four Tm cell types Tm1, Tm2, Tm4, and Tm9 and analyzed their involvement in *Drosophila* OFF motion detection. We demonstrated that none of these cells are direction selective and thus conclude that the computation of direction selectivity in the OFF pathway takes place on the dendrites of T5 cells.

At multiple levels, this circuit arrangement bears a striking resemblance to a network motif found in the mammalian retina (Kim et al., 2014). First, comparable to T5 cells, direction-selective starburst amacrine cells receive synaptic input from several anatomically similar cell types, i.e., the OFF bipolar cells 1, 2, 3a, 3b, and 4 (Masland, 2012). Second, like the Tm cells presynaptic to T5, these OFF bipolar cells have been shown to respond in a directionally unselective manner (Yonehara et al., 2013; Park et al., 2014). Third, the five OFF bipolar cell types show dynamics similar to those of the four Tm cells described here, ranging from sustained over slow decaying to fast transient (Baden et al., 2013; Borghuis et al., 2013). Depending on their temporal response properties, Tm cells receive input from particular groups of lamina monopolar cells. The two fast and transient

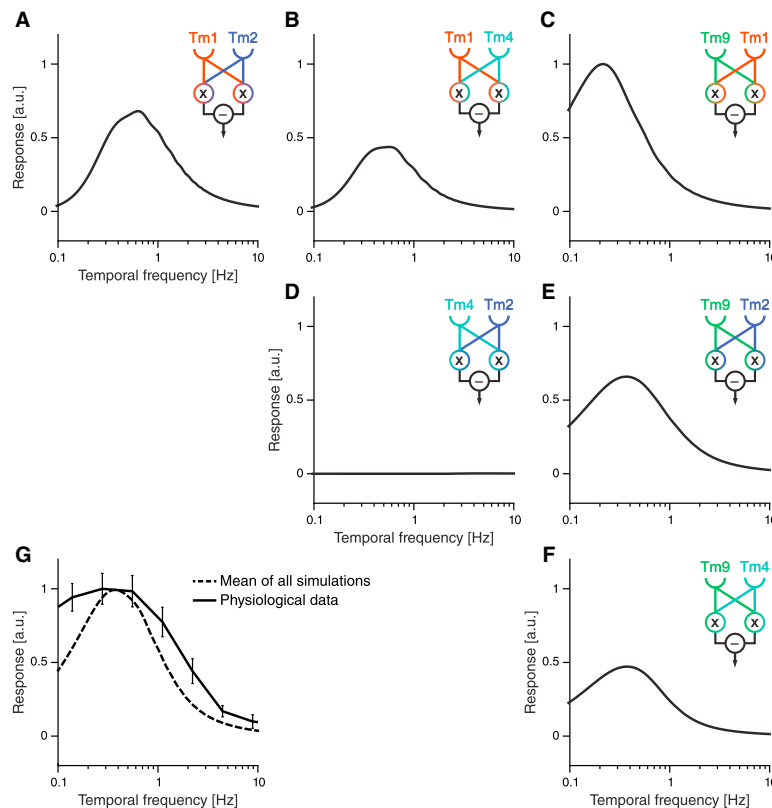


Figure 8. Simulated Frequency Tunings for the Six Combinations of Tm Cells

(A–F) Reichardt detector responses to grating stimulation using the simulated temporal filters (Figure 3) of Tm1/Tm2 (A), Tm1/Tm4 (B), Tm1/Tm9 (C), Tm2/Tm4 (D), Tm2/Tm9 (E), and Tm4/Tm9 (F). The responses were normalized to the maximal response of the Tm1/Tm9 detector (C). (G) Comparison of the normalized mean response of all six simulations with the normalized physiological data of control flies (from Figure S5). Error bars indicate \pm SEM. See also Figure S5.

wave gratings moving at a temporal frequency of about 0.5 Hz (Figures 8G and S5). Except for Tm2/Tm4, whose filter time constants are almost identical, all combinations resulted in frequency optima in a range compatible with tangential cell responses. Furthermore, the mean signal of all simulations matches the tuning curve of electrophysiologically measured responses well. These simulations only represent a simplified view. They do not take into account several important aspects, such as the temporal frequency tuning of the ON channel, the different synaptic weights, or any spatial offsets of Tm cells on the T5 dendrites. Nevertheless, this simple model confirms the functional plausibility of the time constants of the four Tm cells tested.

cells, Tm2 and Tm4, receive their major input from L2 and L4; intermediate Tm1 cells primarily receive input from L2; and tonic Tm9 cells receive input from similarly slow and sustained L3 (Clark et al., 2011; Freifeld et al., 2013; Silies et al., 2013; Takemura et al., 2013; Meier et al., 2014). Finally, the mechanism for the computation of direction selectivity on the dendrites of starburst amacrine cells has been proposed to rely on dendritically offset input from bipolar cells with different temporal filter properties (Kim et al., 2014). For T5, comparable spatial shifts among dendritic target sites of Tm1, Tm2, and Tm9 have been reported (Shinomiya et al., 2014). The aforementioned study, however, was not able to identify the preferred direction of corresponding T5 cells and thus could not correlate it with the particular arrangement of Tm cell input on the dendrite. Nevertheless, the remarkable resemblance of neural circuits between invertebrates and mammals suggests a universality of underlying computational principles (Borst and Helmstaedter, 2015).

Are the measured temporal response properties functionally relevant for the computation of direction-selective signals? We addressed this question by modeling six elementary motion detectors through filtering of the signals in the two neighboring arms with the time constants of all six possible binary combinations of Tm cells (Figure 8). Lobula plate tangential cells exhibit a maximal steady-state response when presented with square

We also demonstrated that the functional importance of each of the four Tm cell types correlates with the number of synaptic contacts to T5 (Shinomiya et al., 2014). Silencing Tm4 cells, which out of the four provide the smallest number of synapses onto T5 cells, resulted in the weakest phenotype, followed by Tm1. Blocking Tm2 and Tm9, numerically the strongest inputs to T5, produced the strongest impairment of the OFF response (Figures 5 and 7). However, silencing L3, which is thought to be the main input to Tm9, does not result in similar, purely OFF-specific effects (Silies et al., 2013; Tuthill et al., 2013). This can be due to two facts. First, L3 also strongly connects to crucial ON pathway element Mi1 (Takemura et al., 2013; Ammer et al., 2015). Second, additional inputs to Tm9 cells may influence their response properties.

Given the increased effects of impairment when blocking pairs of Tm cells, we are able to rule out complete redundancy of individual elements (Figures 6 and 7). How do these four cell types then map onto the elements of correlation-type models? First, the interaction of several Tm cell types may give rise to a nonlinear stage more complex than the simple multiplication in the Hassenstein-Reichardt correlator. It is conceivable that the biophysical implementation of a suitable nonlinearity requires more than two appropriately tuned input lines. Our behavioral data lend some support to this hypothesis, because the

strongest combinatorial blocks display a supra-linear increase in effect strength compared to the sum of the single-cell effects (Figure 7E). Second, standard algorithms generally model the asymmetric processing of direct and delayed lines as single-stage linear filters. For biophysical realizations, this filtering may be more complex. Multiple cells with varying intrinsic membrane properties and different synaptic transmission characteristics could provide many degrees of freedom when implementing filters that are appropriate for motion detection. Thus, temporal processing within one input line of the algorithmic model (Figure 1A) may involve the combination of two or more cells; Tm9 and Tm4, for instance, could both correspond to a module implementing what is the delay line in the Hassenstein-Reichardt model. Third, the four cells may in principle play different roles in different stimulus regimes defined by, for instance, velocity, contrast, luminance, or color. Our results provide some evidence for such a division of labor. In walking flies, the velocity-dependent phenotype of Tm2 block flies, together with the cells' fast response characteristics (Figure 3B), suggests a specific role for Tm2 at high velocities (Figure 7C). Such a design principle may be realized in at least two ways. Functional specialization could be a static property of the system, derived from cell-intrinsic spatiotemporal or chromatic filter properties, or a dynamic property that is subject to regulation depending on stimulus conditions. A recent study showed that changes in the behavior of hawkmoths under dim light conditions can be reproduced by adapting the filter time constants of a Hassenstein-Reichardt correlator (Sponberg et al., 2015). Tm9 could represent a candidate to detect changes in global luminance due to its slow filter properties, which make it sensitive to both brightness increments and decrements at all timescales (Figures 3D and 3I), as well as due to its responsiveness to full-field flicker (Figure 4). Moreover, inputs from the color vision pathway have been demonstrated to improve motion discrimination (Wardill et al., 2012). Histaminergic photoreceptors R7 and R8, known to be involved in color perception (for review, see Behnia and Desplan, 2015), project to the medulla layers where Tm cell dendrites reside. Both Tm2 and Tm9 express a histamine-gated chloride channel (Gao et al., 2008), potentially linking the color and motion detection pathways. Finally, different Tm cells could be of different importance depending on the behavioral state of the animal, e.g., whether it is at rest, walking, or flying. Such behavioral-state dependency has been described at the level of the lobula plate tangential cells (Maimon et al., 2010; Chiappe et al., 2010; Haag et al., 2010; Jung et al., 2011; Schnell et al., 2014) and could be well explained by changes in contribution of synaptic input to T4 and T5 cells. Such a scenario could explain why blocking Tm2, Tm4, and their combinations resulted in stronger phenotypes in walking flies compared to tangential cell responses in a quiescent preparation (Figure 7E).

Taken together, our study sheds light on the circuitry underlying the computation of motion and uncovers striking parallels between vertebrate and invertebrate systems. Unraveling the exact mechanisms awaits further investigation. More naturalistic stimuli and modified algorithmic or biophysically realistic models that reflect the complexity of the neural correlate will play critical roles in this endeavor.

EXPERIMENTAL PROCEDURES

For calcium imaging, we used the genetically encoded indicators GCaMP5 (Akerboom et al., 2012) and GCaMP6f (Chen et al., 2013). Blocking experiments were accomplished using Tm cell-specific Gal4 lines crossed with pJFRC100-20XUAS-TTS-Shibire-ts1 (Pfeiffer et al., 2012) flies. Fly line specificity was tested using stochastic flip-out labeling (Nern et al., 2015) and expression of mCD8-GFP. All genotypes used in this study can be found in Table S1. Flies were prepared as described before: imaging experiments (Reiff et al., 2010), electrophysiology (Joesch et al., 2008), and behavior (Bahl et al., 2013). Two-photon microscopy and visual stimulus presentation was as described in Maisak et al. (2013). The recording protocol for electrophysiological experiments was adapted from Joesch et al. (2008). Under polarized light contrast, the glial sheet was digested locally by applying a stream of 0.5 mg/ml collagenase IV (Gibco) through a cleaning micropipette (~5 μ m opening). Recordings for the blocking electrophysiology experiments were obtained within 2 hr after a 60 min heat-shock application at 37°C. For statistical analysis, we used a two-tailed t test to compare *shibire^{ts}* controls and block flies (* $p < 0.05$, ** $p < 0.01$, *** $p < 0.001$). Behavioral experiments were conducted as previously described (Ammer et al., 2015). For immunostaining procedures, see Schnell et al. (2010). Data were evaluated offline using custom written software (Matlab and Python) and Origin (OriginLab). For modeling the time constants in Figure 3, we fit a three-stage filter model to the mean calcium traces. Within this model, inputs were first high-pass filtered, then rectified by setting negative values to zero, and finally low-pass filtered (Figure 3E). For the modeling results in Figure 8, we simulated grating responses of hypothetical Reichardt detectors whose inputs were band-pass filters as determined in Figure 3E. See Supplemental Experimental Procedures for detailed methods.

SUPPLEMENTAL INFORMATION

Supplemental Information includes Supplemental Experimental Procedures, seven figures, one table, and one movie and can be found with this article online at <http://dx.doi.org/10.1016/j.neuron.2016.01.006>.

AUTHOR CONTRIBUTIONS

E.S. and M.M. jointly performed and evaluated all calcium imaging and electrophysiology experiments. A.L. performed and evaluated the behavioral experiments. A.L. and A.B. performed computer simulations. A.B., E.S., and M.M. designed the study. E.S. and M.M. wrote the manuscript with the help of the other authors.

ACKNOWLEDGMENTS

We thank J. Haag for technical support and help with the two-photon microscope; R. Kutlesa and C. Theile for excellent help with behavior experiments; W. Essbauer, R. Kutlesa, C. Theile, and M. Sauter for fly work and immunostainings; T. Schilling for artwork; and D. Soll for the Dlg antibody. We thank G. Ammer, A. Arenz, J. Pujol-Marti, and A. Mauss for carefully reading the manuscript. All authors are members of the Graduate School for Systemic Neurosciences, Munich. We thank B. Dickson, G. Rubin, and A. Nern for providing us with unpublished fly lines.

Received: June 25, 2015

Revised: November 18, 2015

Accepted: December 18, 2015

Published: February 4, 2016

REFERENCES

Akerboom, J., Chen, T.-W., Wardill, T.J., Tian, L., Marvin, J.S., Mutlu, S., Calderón, N.C., Esposti, F., Borghuis, B.G., Sun, X.R., et al. (2012). Optimization of a GCaMP calcium indicator for neural activity imaging. *J. Neurosci.* 32, 13819–13840.

- Ammer, G., Leonhardt, A., Bahl, A., Dickson, B.J., and Borst, A. (2015). Functional specialization of neural input elements to the *Drosophila* ON motion detector. *Curr. Biol.* *25*, 2247–2253.
- Baden, T., Berens, P., Bethge, M., and Euler, T. (2013). Spikes in mammalian bipolar cells support temporal layering of the inner retina. *Curr. Biol.* *23*, 48–52.
- Bahl, A., Ammer, G., Schilling, T., and Borst, A. (2013). Object tracking in motion-blind flies. *Nat. Neurosci.* *16*, 730–738.
- Behnia, R., and Desplan, C. (2015). Visual circuits in flies: beginning to see the whole picture. *Curr. Opin. Neurobiol.* *34*, 125–132.
- Behnia, R., Clark, D.A., Carter, A.G., Clandinin, T.R., and Desplan, C. (2014). Processing properties of ON and OFF pathways for *Drosophila* motion detection. *Nature* *512*, 427–430.
- Borghuis, B.G., Marvin, J.S., Looger, L.L., and Demb, J.B. (2013). Two-photon imaging of nonlinear glutamate release dynamics at bipolar cell synapses in the mouse retina. *J. Neurosci.* *33*, 10972–10985.
- Borst, A., and Euler, T. (2011). Seeing things in motion: models, circuits, and mechanisms. *Neuron* *71*, 974–994.
- Borst, A., and Helmstaedter, M. (2015). Common circuit design in fly and mammalian motion vision. *Nat. Neurosci.* *18*, 1067–1076.
- Brand, A.H., and Perrimon, N. (1993). Targeted gene expression as a means of altering cell fates and generating dominant phenotypes. *Development* *118*, 401–415.
- Cajal, S.R., and Sánchez, D. (1915). Contribución al conocimiento de los centros nerviosos de los insectos. *Trab. Lab. Inv. Biol.* *13*, 1–168.
- Chen, T.W., Wardill, T.J., Sun, Y., Pulver, S.R., Renninger, S.L., Baohan, A., Schreiter, E.R., Kerr, R.A., Orger, M.B., Jayaraman, V., et al. (2013). Ultrasensitive fluorescent proteins for imaging neuronal activity. *Nature* *499*, 295–300.
- Chiappe, M.E., Seelig, J.D., Reiser, M.B., and Jayaraman, V. (2010). Walking modulates speed sensitivity in *Drosophila* motion vision. *Curr. Biol.* *20*, 1470–1475.
- Clark, D.A., Bursztyn, L., Horowitz, M.A., Schnitzer, M.J., and Clandinin, T.R. (2011). Defining the computational structure of the motion detector in *Drosophila*. *Neuron* *70*, 1165–1177.
- Eichner, H., Joesch, M., Schnell, B., Reiff, D.F., and Borst, A. (2011). Internal structure of the fly elementary motion detector. *Neuron* *70*, 1155–1164.
- Fischbach, K.-F., and Dittrich, A.P.M. (1989). The optic lobe of *Drosophila melanogaster*. I. A Golgi analysis of wild-type structure. *Cell Tissue Res.* *258*, 441–475.
- Fisher, Y.E., Silies, M., and Clandinin, T.R. (2015). Orientation selectivity sharpens motion detection in *Drosophila*. *Neuron* *88*, 390–402.
- Freifeld, L., Clark, D.A., Schnitzer, M.J., Horowitz, M.A., and Clandinin, T.R. (2013). GABAergic lateral interactions tune the early stages of visual processing in *Drosophila*. *Neuron* *78*, 1075–1089.
- Gao, S., Takemura, S.-Y., Ting, C.-Y., Huang, S., Lu, Z., Luan, H., Rister, J., Thum, A.S., Yang, M., Hong, S.-T., et al. (2008). The neural substrate of spectral preference in *Drosophila*. *Neuron* *60*, 328–342.
- Götz, K.G. (1964). Optomotorische Untersuchung des visuellen Systems einiger Augenmutanten der Fruchtfliege *Drosophila*. *Kybernetik* *2*, 77–92.
- Haag, J., Wertz, A., and Borst, A. (2010). Central gating of fly optomotor response. *Proc. Natl. Acad. Sci. USA* *107*, 20104–20109.
- Hassenstein, B., and Reichardt, W. (1956). Systemtheoretische Analyse der Zeit-, Reihenfolgen- und Vorzeichenbewertung bei der Bewegungsperzeption des Rüsselkäfers *Chlorophanus*. *Z. Naturforsch. B* *11*, 513–524.
- Joesch, M., Plett, J., Borst, A., and Reiff, D.F. (2008). Response properties of motion-sensitive visual interneurons in the lobula plate of *Drosophila melanogaster*. *Curr. Biol.* *18*, 368–374.
- Joesch, M., Schnell, B., Raghu, S.V., Reiff, D.F., and Borst, A. (2010). ON and OFF pathways in *Drosophila* motion vision. *Nature* *468*, 300–304.
- Joesch, M., Weber, F., Eichner, H., and Borst, A. (2013). Functional specialization of parallel motion detection circuits in the fly. *J. Neurosci.* *33*, 902–905.
- Jung, S.N., Borst, A., and Haag, J. (2011). Flight activity alters velocity tuning of fly motion-sensitive neurons. *J. Neurosci.* *31*, 9231–9237.
- Kim, J.S., Greene, M.J., Zlateski, A., Lee, K., Richardson, M., Turaga, S.C., Purcaro, M., Balkam, M., Robinson, A., Behabadi, B.F., et al.; EyeWriters (2014). Space-time wiring specificity supports direction selectivity in the retina. *Nature* *509*, 331–336.
- Kitamoto, T. (2001). Conditional modification of behavior in *Drosophila* by targeted expression of a temperature-sensitive *shibire* allele in defined neurons. *J. Neurobiol.* *47*, 81–92.
- Land, M.F. (1997). Visual acuity in insects. *Annu. Rev. Entomol.* *42*, 147–177.
- Maimon, G., Straw, A.D., and Dickinson, M.H. (2010). Active flight increases the gain of visual motion processing in *Drosophila*. *Nat. Neurosci.* *13*, 393–399.
- Maisak, M.S., Haag, J., Ammer, G., Serbe, E., Meier, M., Leonhardt, A., Schilling, T., Bahl, A., Rubin, G.M., Nern, A., et al. (2013). A directional tuning map of *Drosophila* elementary motion detectors. *Nature* *500*, 212–216.
- Masland, R.H. (2012). The neuronal organization of the retina. *Neuron* *76*, 266–280.
- Mauss, A.S., Meier, M., Serbe, E., and Borst, A. (2014). Optogenetic and pharmacologic dissection of feedforward inhibition in *Drosophila* motion vision. *J. Neurosci.* *34*, 2254–2263.
- Mauss, A.S., Pankova, K., Arenz, A., Nern, A., Rubin, G.M., and Borst, A. (2015). Neural circuit to integrate opposing motions in the visual field. *Cell* *162*, 351–362.
- Meier, M., Serbe, E., Maisak, M.S., Haag, J., Dickson, B.J., and Borst, A. (2014). Neural circuit components of the *Drosophila* OFF motion vision pathway. *Curr. Biol.* *24*, 385–392.
- Nern, A., Pfeiffer, B.D., and Rubin, G.M. (2015). Optimized tools for multicolor stochastic labeling reveal diverse stereotyped cell arrangements in the fly visual system. *Proc. Natl. Acad. Sci. USA* *112*, E2967–E2976.
- Park, S.J.H., Kim, I.-J., Looger, L.L., Demb, J.B., and Borghuis, B.G. (2014). Excitatory synaptic inputs to mouse on-off direction-selective retinal ganglion cells lack direction tuning. *J. Neurosci.* *34*, 3976–3981.
- Pfeiffer, B.D., Truman, J.W., and Rubin, G.M. (2012). Using translational enhancers to increase transgene expression in *Drosophila*. *Proc. Natl. Acad. Sci. USA* *109*, 6626–6631.
- Reiff, D.F., Plett, J., Mank, M., Griesbeck, O., and Borst, A. (2010). Visualizing retinotopic half-wave rectified input to the motion detection circuitry of *Drosophila*. *Nat. Neurosci.* *13*, 973–978.
- Rivera-Alba, M., Vitaladevuni, S.N., Mishchenko, Y., Lu, Z., Takemura, S.Y., Scheffer, L., Meinertzhagen, I.A., Chklovskii, D.B., and de Polavieja, G.G. (2011). Wiring economy and volume exclusion determine neuronal placement in the *Drosophila* brain. *Curr. Biol.* *21*, 2000–2005.
- Schnell, B., Joesch, M., Forstner, F., Raghu, S.V., Otsuna, H., Ito, K., Borst, A., and Reiff, D.F. (2010). Processing of horizontal optic flow in three visual interneurons of the *Drosophila* brain. *J. Neurophysiol.* *103*, 1646–1657.
- Schnell, B., Raghu, S.V., Nern, A., and Borst, A. (2012). Columnar cells necessary for motion responses of wide-field visual interneurons in *Drosophila*. *J. Comp. Physiol. A Neuroethol. Sens. Neural Behav. Physiol.* *198*, 389–395.
- Schnell, B., Weir, P.T., Roth, E., Fairhall, A.L., and Dickinson, M.H. (2014). Cellular mechanisms for integral feedback in visually guided behavior. *Proc. Natl. Acad. Sci. USA* *111*, 5700–5705.
- Shinomiya, K., Karupudurai, T., Lin, T.Y., Lu, Z., Lee, C.H., and Meinertzhagen, I.A. (2014). Candidate neural substrates for off-edge motion detection in *Drosophila*. *Curr. Biol.* *24*, 1062–1070.
- Silies, M., Gohl, D.M., Fisher, Y.E., Freifeld, L., Clark, D.A., and Clandinin, T.R. (2013). Modular use of peripheral input channels tunes motion-detecting circuitry. *Neuron* *79*, 111–127.
- Sponberg, S., Dyrh, J.P., Hall, R.W., and Daniel, T.L. (2015). Insect Flight: luminance-dependent visual processing enables moth flight in low light. *Science* *348*, 1245–1248.
- Strother, J.A., Nern, A., and Reiser, M.B. (2014). Direct observation of ON and OFF pathways in the *Drosophila* visual system. *Curr. Biol.* *24*, 976–983.

Takemura, S.Y., Karuppudurai, T., Ting, C.-Y., Lu, Z., Lee, C.-H., and Meinertzhagen, I.A. (2011). Cholinergic circuits integrate neighboring visual signals in a *Drosophila* motion detection pathway. *Curr. Biol.* 21, 2077–2084.

Takemura, S.Y., Bharioke, A., Lu, Z., Nern, A., Vitaladevuni, S., Rivlin, P.K., Katz, W.T., Olbris, D.J., Plaza, S.M., Winston, P., et al. (2013). A visual motion detection circuit suggested by *Drosophila* connectomics. *Nature* 500, 175–181.

Tuthill, J.C., Nern, A., Holtz, S.L., Rubin, G.M., and Reiser, M.B. (2013). Contributions of the 12 neuron classes in the fly lamina to motion vision. *Neuron* 79, 128–140.

Wardill, T.J., List, O., Li, X., Dongre, S., McCulloch, M., Ting, C.-Y., O’Kane, C.J., Tang, S., Lee, C.-H., Hardie, R.C., and Juusola, M. (2012). Multiple spectral inputs improve motion discrimination in the *Drosophila* visual system. *Science* 336, 925–931.

Werblin, F.S., and Dowling, J.E. (1969). Organization of the retina of the mudpuppy, *Necturus maculosus*. II. Intracellular recording. *J. Neurophysiol.* 32, 339–355.

Yonehara, K., Farrow, K., Ghanem, A., Hillier, D., Balint, K., Teixeira, M., Jüttner, J., Noda, M., Neve, R.L., Conzelmann, K.-K., and Roska, B. (2013). The first stage of cardinal direction selectivity is localized to the dendrites of retinal ganglion cells. *Neuron* 79, 1078–1085.

Neuron

Supplemental Information

**Comprehensive Characterization
of the Major Presynaptic Elements
to the *Drosophila* OFF Motion Detector**

Etienne Serbe, Matthias Meier, Aljoscha Leonhardt, and Alexander Borst

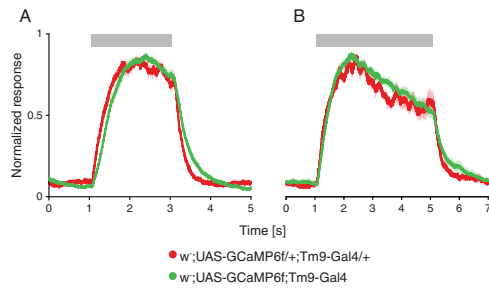


Figure S1. Related to Figure 3. Different expression levels of GCaMP do not affect the response kinetics of Tm9

(A and B) Normalized line scan calcium responses in Tm9 axonal arbors upon stimulation with a 4.5° wide, dark bar appearing for 2s (A) and 4s (B) to investigate long term temporal dynamics of Tm9 responses. To exclude effects of GCaMP6f expression level on the dynamics of the response, two traces were obtained using flies with homozygous (green) and heterozygous (red) expression of the Gal4 and the UAS construct. Error shades indicate \pm SEM.

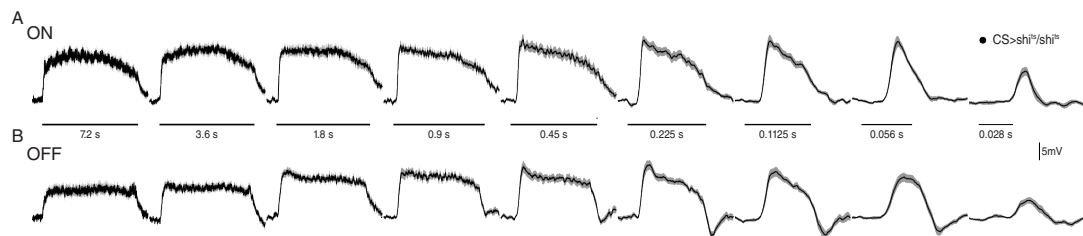


Figure S2. Related to Figure 5. LPTC responses to multiple edges moving at different velocities

Average voltage traces of lobula plate tangential cells in control flies ($N=5$, $n=13$), stimulated with multiple moving ON (A) and OFF (B) edges at 9 different velocities ($3.125^\circ/s$, $6.25^\circ/s$, $12.5^\circ/s$, $25^\circ/s$, $50^\circ/s$, $100^\circ/s$, $200^\circ/s$, $400^\circ/s$, and $800^\circ/s$). Black bars indicate duration of stimulus presentation. Error shades indicate \pm SEM.

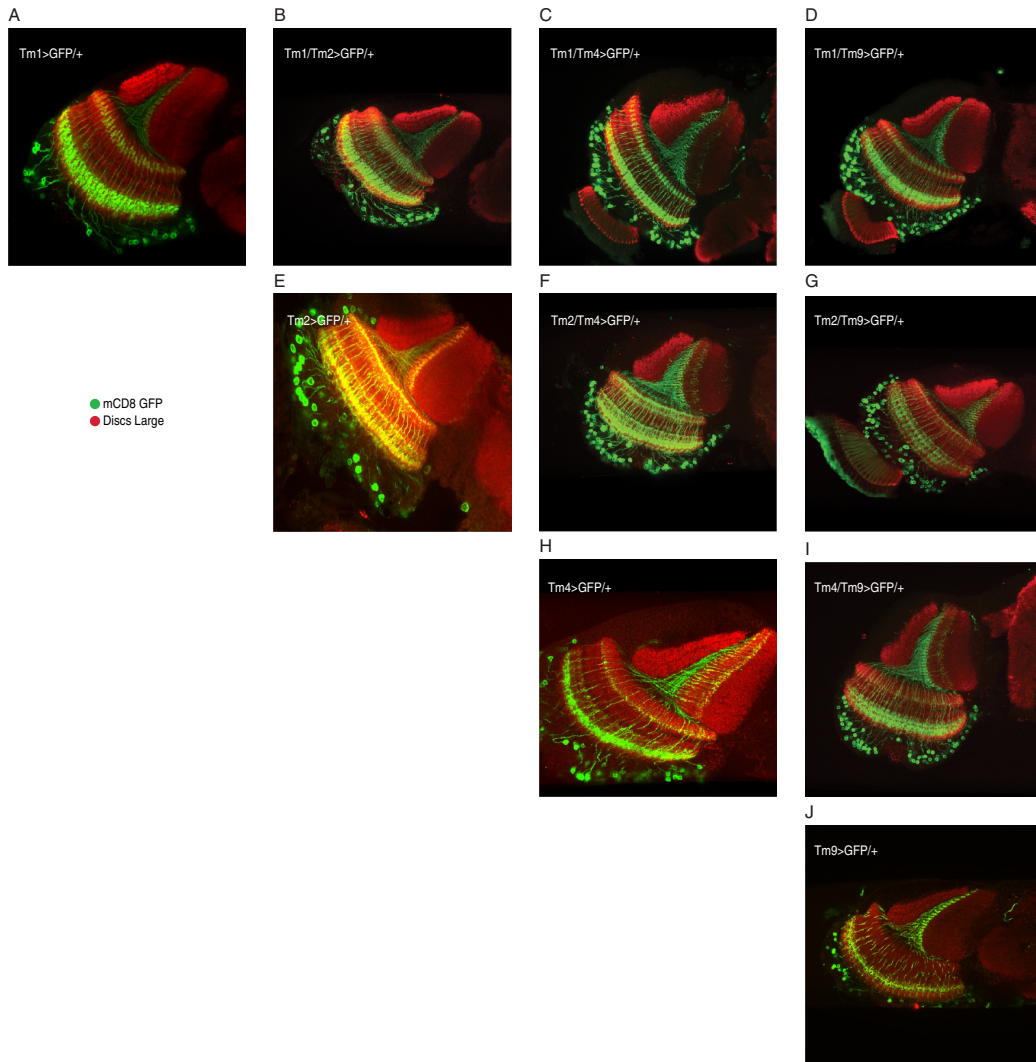


Figure S3. Related to Figures 5-7. Tm cell expression patterns

(A-J) Confocal images of the Gal4 driver cell lines used in the silencing experiments, shown in horizontal cross sections. Tm1 (A), Tm2 (E), Tm4 (H), and Tm9 (J) neurons are labeled in green (mCD8-GFP expression) and neuropils in red (antibody against Discs Large). The six possible binary combinations (B-D, F, G, I) of the Gal4 driver lines exhibit clear expression of two neuron types.

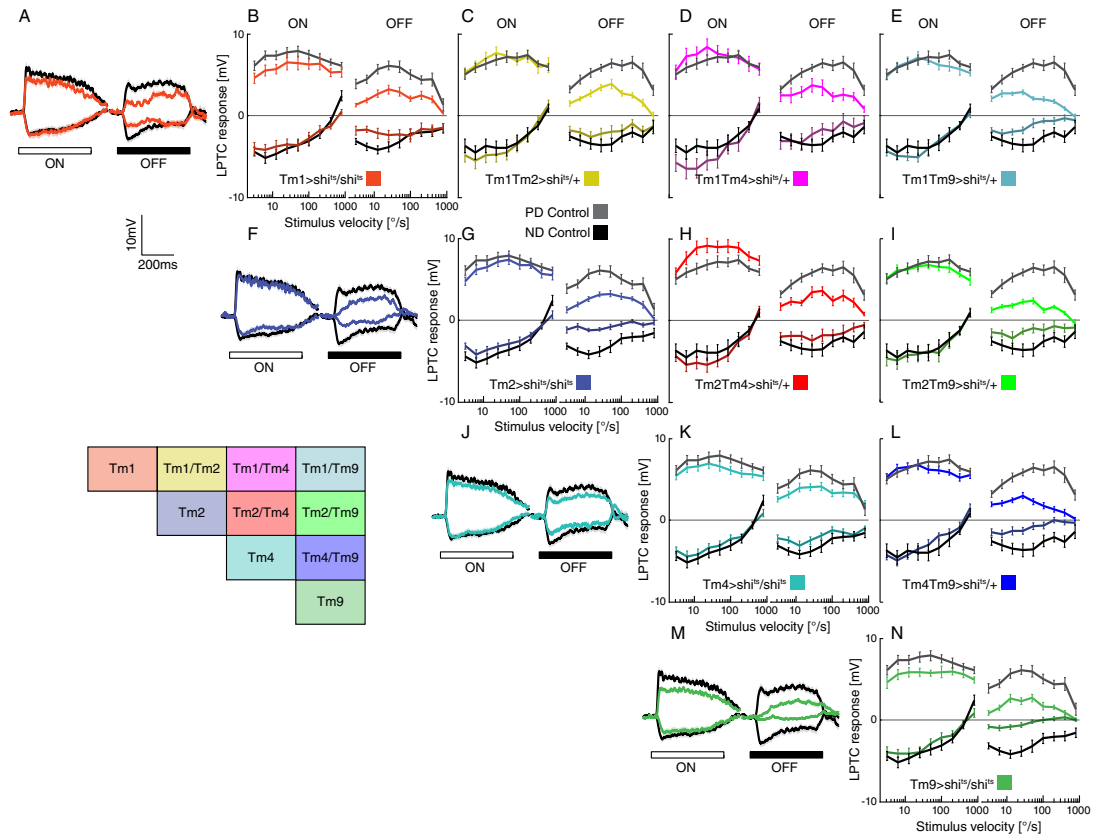


Figure S4. Related to Figures 5 and 6. Preferred and null direction responses of LPTCs to multiple ON and OFF edges (A, F, J, M) Mean voltage traces of lobula plate tangential cells stimulated with multiple ON and OFF edges moving at $50^\circ/\text{s}$ in preferred (PD) and null direction (ND). Black traces depict recordings from control flies. Red traces in (A) represent LPTC responses in Tm1 block flies, blue traces in (F) Tm2 block flies, cyan traces in (J) Tm4 block flies, and green traces in (M) Tm9 block flies. Error shades indicate \pm SEM. (B-E, G-I, K, L, and N) Average responses (errorbars indicate \pm SEM) of all four single block (with two copies of *shibire^{ts}*) and six possible combinations with corresponding controls (black) to multiple ON and OFF edges moving with nine different velocities ($3.125^\circ/\text{s}$, $6.25^\circ/\text{s}$, $12.5^\circ/\text{s}$, $25^\circ/\text{s}$, $50^\circ/\text{s}$, $100^\circ/\text{s}$, $200^\circ/\text{s}$, $400^\circ/\text{s}$, $800^\circ/\text{s}$) in PD (light colors) and ND (dark colors). Colored boxes on the bottom left indicate locations of corresponding panels in the matrix.

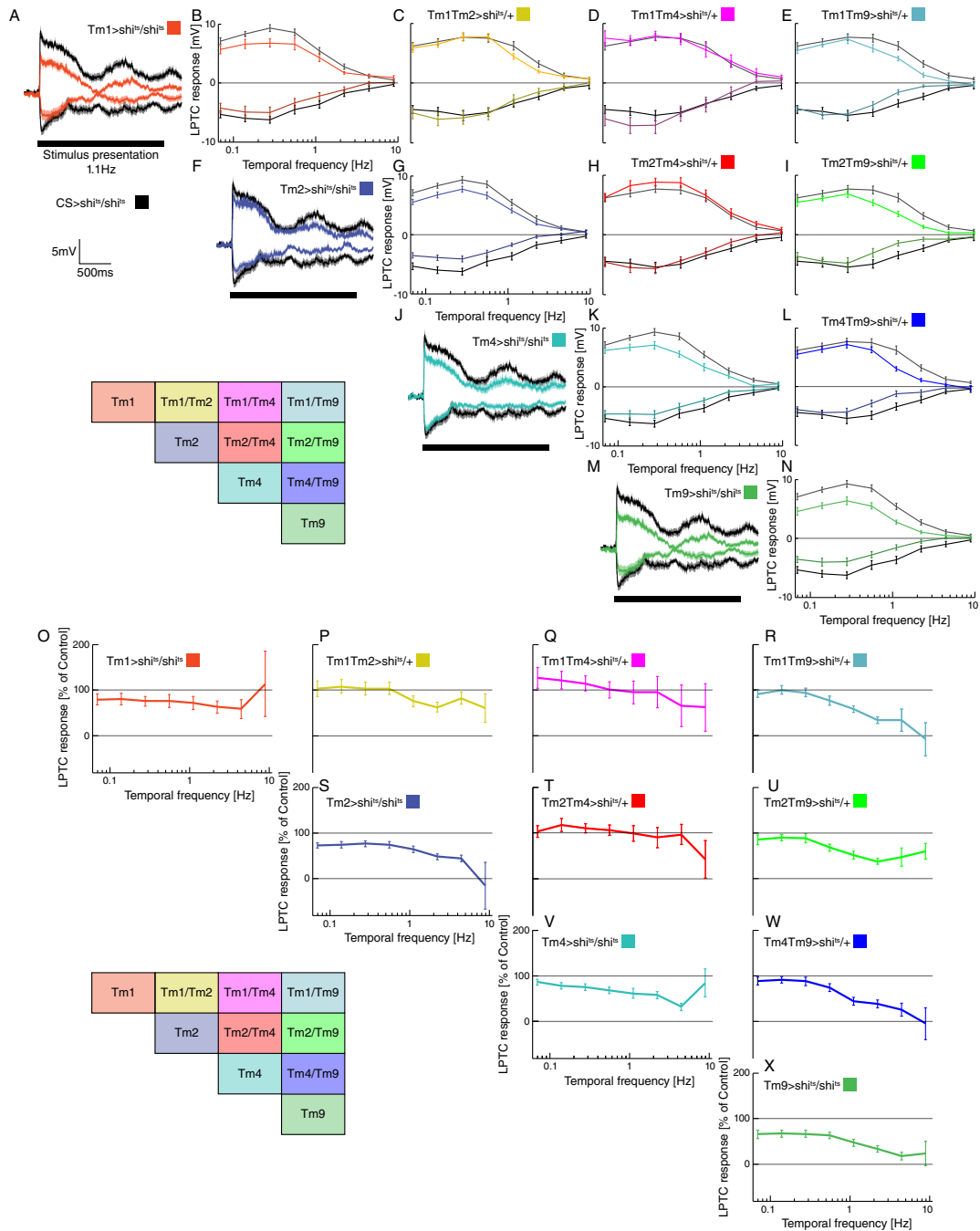


Figure S5. Related to Figures 6 and 8. Detailed analysis of LPTC responses to square wave gratings

(A,F,J,M) Mean voltage traces of lobula plate tangential cells stimulated with square wave gratings (45° spatial wavelength) moving at a temporal frequency of 1.11 Hz in preferred (PD) and null-direction (ND). Black traces depict recordings from control flies. Red traces in (A) represent LPTC responses in Tm1 block flies, blue traces in (F) Tm2 block flies, cyan traces in (J) Tm4 block flies, and green traces in (M) Tm9 block flies. Errorshades indicate \pm SEM. (B-E, G-I, K-L, and N) Average responses (errorbars indicate \pm SEM) of all four single cell block (with two copies of *shibire^{ts}*) and six possible combinations with corresponding controls (black) to gratings moving with eight different temporal frequencies (0.07Hz, 0.14Hz, 0.28Hz, 0.56Hz, 1.11Hz, 2.22Hz, 4.44Hz, 8.89Hz) in PD (light colors) and ND (dark colors). Colored boxes on the bottom left indicate locations of corresponding panels in the matrix. (O-X) Average voltage responses of LPTCs as above represented as the percentage of the corresponding response in control flies.

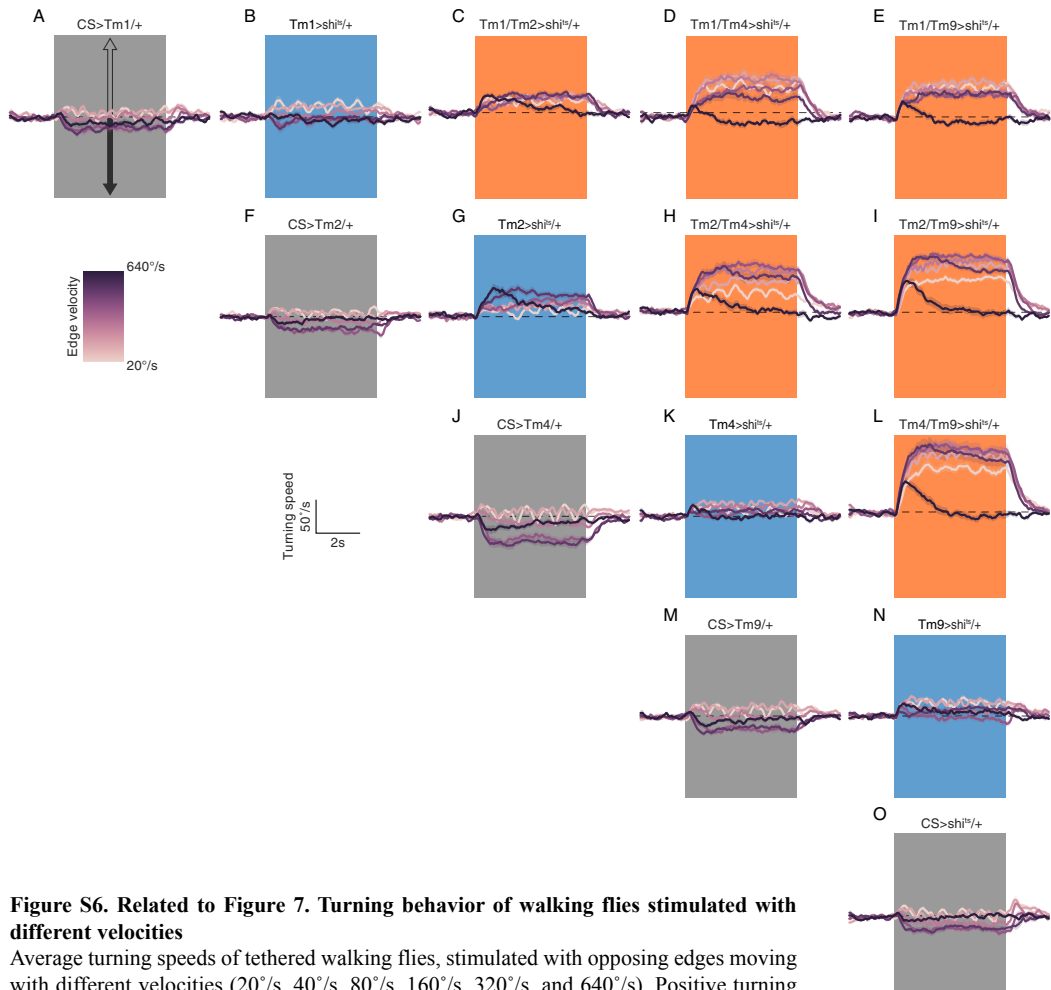


Figure S6. Related to Figure 7. Turning behavior of walking flies stimulated with different velocities

Average turning speeds of tethered walking flies, stimulated with opposing edges moving with different velocities (20°/s, 40°/s, 80°/s, 160°/s, 320°/s, and 640°/s). Positive turning responses correspond to flies turning with ON-edges, negative turning responses indicate turning with OFF-edges (see arrows in A). Stimulus presentation is indicated by shaded boxes. Errorshades indicate \pm SEM. (A, F, J, M, and O) Four Gal4 controls and the *shibire^{ts}* control. (B, G, K, and N) Single cell blocks with one copy of *shibire^{ts}*. (C-E, H, I and L) Double cell blocks with one copy of *shibire^{ts}*.

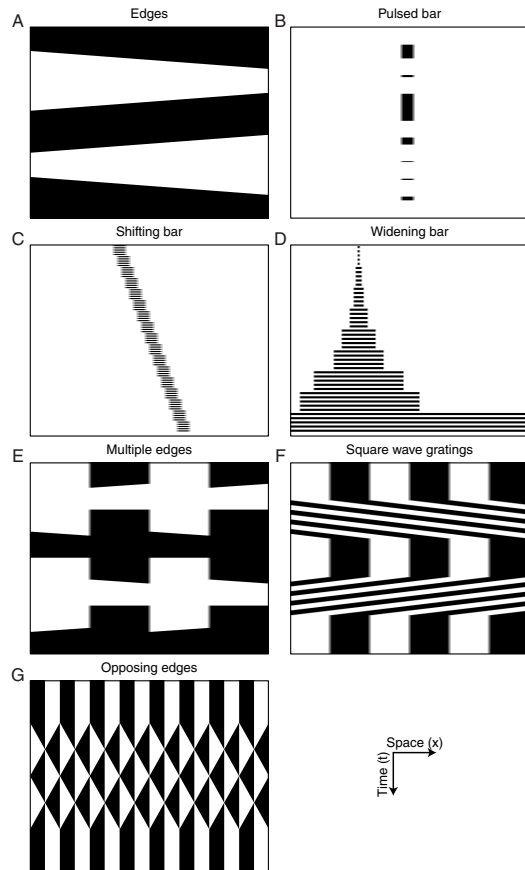


Figure S7. Related to Figures 2-7. Space-time (xt) plots of all visual stimuli used in the study

(A) Single ON and OFF Edges were used for stimulation in Figure 2. (B) Flickering bars with randomly ordered durations were used to test temporal properties in Figure 3. (C and D) Shifting and widening bars were used to test spatial properties in Figure 4. (E) Multiple edges were used in electrophysiological experiments in Figures 5 and 6. (F) Square wave gratings were used in electrophysiological experiments in Figure S5. (G) Opposing edges were used for behavioral experiments in Figure 7.

Movie S1. Related to Figure 4. Retinotopic organization of Tm9 cells

Representative raw two-photon microscope time course of Tm9 cells expressing GCaMP5 (smoothed in ImageJ). The fly is stimulated with a 4.5° wide vertical dark bar that is flickering five times at one position and is subsequently shifted by 1.5° (see Figure3, Supplemental Experimental Procedures). The movie has been accelerated 8 times (15fps compared to 1.87Hz acquisition). The insert at the top right indicates the stimulus. Tm9 cell activity follows the stimulus in a retinotopic fashion.

Table S1. Related to Figures 1-7. Genotypes used throughout the study.

Supplemental Experimental Procedures

Flies

Flies were raised on standard cornmeal-agar medium with 12hr light/12hr dark cycles, 25°C, and 60% humidity. Female flies were used for all experiments. For calcium imaging, we used the genetically encoded indicators GCaMP5 (Akerboom et al., 2012) and GCaMP6f (Chen et al., 2013). Blocking experiments were accomplished using Tm cell-specific Gal4 lines crossed with pJFRC100-20XUAS-TTS-Shibire-ts1 (Pfeiffer et al., 2012) flies. Fly line specificity was tested using stochastic flip-out labeling (Nern et al., 2015) and expression of mCD8-GFP. We used different driver lines because of different expression strengths and specificities. All genotypes used in this study can be found in Table S1. Flies were prepared as described previously: imaging experiments, Reiff et al., 2010; electrophysiology, Joesch et al., 2008; and behavior, Bahl et al., 2013.

Immunohistochemistry and confocal imaging

For immuno-staining procedures see Schnell et al., 2010. Primary antibodies used were mouse anti-Discs Large (DLG, RRID:MGI_4354991, Developmental Studies Hybridoma Bank) and anti-GFP-Alexa488 conjugate (RRID:AB_221477, Molecular Probes). For visualization we used (1:200 in PBT): goat anti-mouse Alexa 568 (RRID:AB_10562737). Brains were mounted (Vectashield) and optically sectioned in the horizontal plane with a Leica SP5 confocal microscope. For documentation, single sections were processed in ImageJ 1.46r (NIH, Bethesda, Maryland, USA).

Behavioral experiments

Flies were placed on an air-suspended polyurethane ball in a virtual environment projected onto three monitors spanning approximately 270° (horizontal) and 114° (vertical) of the fly's visual field. This stimulation system offered less than 0.1° of angular pixel size, a value well below *Drosophila's* optical resolution capability. We used six such setups for recording fly locomotion as described previously (Bahl et al., 2013). On two setups, stimuli were presented at a screen refresh frequency of 120Hz; on four setups, the refresh frequency was 144Hz. We never observed qualitative or quantitative differences between these setups in any of the experiments. All monitors were equilibrated in brightness and contrast. Temperature within the immediate surround of the fly was controlled using a custom-built closed-loop thermoregulation system. We employed the following temperature protocol for all experiments and genotypes: Temperature was kept at 25°C for the first 5 minutes and then, within 10 minutes, raised to a restrictive 34°C.

Two-photon microscopy and visual stimulation

Two-photon microscopy and visual stimulus presentation was as described in Maisak et al., 2013. Edges had a contrast of 88%, moving at 30°/s. Each edge motion was shown twice within a single sweep, resulting in a total of eight stimulation periods, each lasting 4s. Subsequent stimuli were preceded by a 3s pause. To map the receptive fields, we flickered 4.5° wide vertical and horizontal dark bars on a bright background with 0.5 Hz at 20 different positions shifted by 1.5°. The position with the maximum response was set to 0°. The responses of the surrounding locations were normalized and plotted dependent on their distance to the peak response. The spatial integration experiments were conducted using vertical dark bars, increasing in size. We measured the responses of flickering bars with 9 different widths (1.5°, 4.5°, 7.5°, 13.5°, 25.5°, 37.5°, 49.5°, 67.5°, 180°) at the peak response position. The responses were normalized to their peak response. For the line scan experiments, a 4.5° vertical dark bar was presented on a bright background for 7 different periods: 50ms, 75ms, 125ms, 225ms, 425ms, 825ms, and 1625ms. The duration of bar presentation was varied in a randomized fashion and each stimulus was presented three times. For the electrophysiology experiments, multiple edges were used as stimuli moving simultaneously at nine different velocities (3.125°/s, 6.25°/s, 12.5°/s, 25°/s, 50°/s, 100°/s, 200°/s, 400°/s, 800°/s). To stimulate HS cells, a vertical, stationary square wave grating with 45° spatial wavelength was presented. For ON edge motion, the right (PD) or the left edge (ND) of each light bar started moving until it merged with the neighboring bar. For OFF edge motion, the right or the left edge of each dark bar was moving. To stimulate VS cells, the pattern was rotated by 90°. Consequently, we used the 36 different stimuli for every recording in a randomized fashion for one to three trials. For behavioral experiments, the balanced motion stimulus resembled previous iterations (Clark et al., 2011). Briefly, we presented flies with a stationary square wave grating that had an initial spatial wavelength of 45° visual angle and a constant Michelson contrast of 50%. Each individual trial lasted 9s. Between 2s and 7s, bright edges moved in one

direction at a fixed velocity while dark edges moved in the other direction at the same velocity. In contrast to previous versions, we reset the stimulus to the initial state after edges had traversed 20° of visual angle. This allowed us to keep the stimulus duration fixed for varying edge velocities. Additionally, we applied a random phase shift after each reset in order to rule out symmetry effects. This was done for 6 velocities (20°/s, 40°/s, 80°/s, 160°/s, 320°/s, and 640°/s) and 2 possible edge directions (dark edge leftwards/bright edge rightwards and vice versa), resulting in 12 conditions that were repeated 50 times per fly. The stimulus was rendered in real-time using Panda3D, an open source game engine, and Python 2.7. x-t plots of all stimuli used are illustrated in Figure S7.

Data analysis and simulations

Data were evaluated off-line using custom written software (Matlab and Python) and Origin (OriginLab Corporation, Massachusetts, USA). To evaluate the calcium imaging data, the raw image series were first converted into a relative fluorescence change ($\Delta F/F$) series by using the first five images as reference. Then, a region was defined within a raw image, and average $\Delta F/F$ values were determined within that region for each image, resulting in a $\Delta F/F$ signal over time. Example calcium signal traces to edge stimulation were obtained by calculating the average $\Delta F/F$ signal over trials. For Figures 2E-2H we normalized the derivative of the mean response trace of every cell. Then, we calculated the mean of the extrema over cells. The evaluation time was the stimulation period with additional four frames.

We fit a three-stage filter model to the mean calcium traces. Within this model, inputs were first high-pass filtered, then rectified by setting negative values to zero, and finally low-pass filtered (Figure 3E). The filters were linear RC filters and of first order. We simulated the visual stimuli as one-dimensional time series whose baseline was zero; for the duration of bar presentation, the values were set to one. The fitting procedure minimized the mean squared error between model output and the calcium traces by exhaustively scanning the two-dimensional parameter space spanned by the time constants of the filters. Errors were summed across presentation lengths of the dark bar, yielding a single optimum per cell type across all seven stimuli. We mapped time constants up to 2000ms in steps of 10ms and additionally allowed filtering to be switched off, equivalent to the time constant being either zero (for a low-pass) or infinite (for a high-pass). The time step for the simulations was 1ms.

To obtain the graphs in Figures 4A-4D and 4F-4I we calculated the mean of the $\Delta F/F$ signal of a single axonal arbor of a Tm cell during the time when dark vertical bars were flickering at a certain position for five times and divided that response by the mean of the $\Delta F/F$ signal when no stimulation was present. For electrophysiological experiments we calculated the mean over the stimulation time shifted by 25ms. For behavioral experiments we analyzed the data as described previously (Maisak et al., 2013). Briefly, optical tracking sensors were equipped with lens and aperture systems to focus on the sphere behind the fly. The tracking data were processed at 4 kHz internally, read out via a USB interface and processed by a computer at <200 Hz. This allowed real-time calculation of the instantaneous rotation axis of the sphere. We resampled the rotation traces to 20Hz for further processing and applied a first-order low pass filter with a time constant of 100ms to each trace. For all flies, we manually selected 20 consecutive trials out of the 50 available that fulfilled the following criteria: First, the temperature was at a stable 34°C. Second, the average turning tendency of the fly was approximately 0°/s. Third, the average forward velocity of the fly was at least 5mm/s, indicating a visually responsive state. Flies were selected without blinding. Application of the criteria excluded, on average, 20% of all flies. For further processing, we subtracted responses for the two symmetrical edge directions in order to reduce the impact of walking asymmetries. Trials were then averaged. For statistical purposes, we calculated the turning tendency of each fly for each velocity condition as the mean of the turning response between 3s (walking onset) and 7s (stimulus offset). Other evaluation time frames produced qualitatively equivalent results. The scatter plot in Figure 7E was generated by linearly normalizing values to the average of the respective genotype that showed the largest effect and plotting electrophysiology block effects against the natural logarithm of behavioral block effects. We then fit a linear regression model to the transformed data using the least-squares method. All data analysis was performed using Python 2.7 and the NumPy library.

For the modelling results in Figure 8, we simulated grating responses of hypothetical Reichardt detectors whose inputs were bandpass filters as determined in Figure 8. Sinusoidal grating stimuli moved for 3s, preceded and followed by 1s of stationary presentation. The gratings had a spatial wavelength of 10 degrees; no further spatial filtering was applied. An array of 10 detectors viewed the grating. For each possible combination of cells, we then applied the corresponding filters to the two input signals, multiplied the output, and summed over all detectors. This was done twice with spatially mirrored input lines, and results were subtracted and rectified in order to generate an approximation of lobula plate tangential cell signals. Finally, we averaged across the stimulation period. For each cell type combination, we chose the spatial order of input filters such that the mean grating responses were positive. This simulation was performed for 150 temporal frequencies located on a logarithmic scale. Each output was normalized to the maximum response across all cell type combinations.

2.4 OPTOGENETIC AND PHARMACOLOGIC DISSECTION OF FEEDFORWARD INHIBITION IN *drosophila* MOTION VISION

This study ([Mauss et al., 2014](#)) investigated the synaptic mechanisms underlying the biphasic responses of lobula plate tangential cells. It appeared in *Journal of Neuroscience* in February 2014.

Summary

Optogenetic experiments provided evidence for a direct excitatory connection between T₄/T₅ cells and lobula plate tangential cells. Recording postsynaptic potentials in lobula plate tangential cells under light-induced stimulation of upstream T₄ and T₅ cells resulted in a biphasic response profile, consisting of a fast excitatory and a slower inhibitory component. Acetylcholine application reproduced solely the excitatory response, while injections of GABA and glutamate resulted only in hyperpolarizations. When we investigated the transmitter system of T₄/T₅ cells via immunohistochemistry we observed specificity only for choline acetyltransferase and not for the vesicular GABA transporter. From this we concluded that the fast excitation is likely to be mediated directly via acetylcholine released from T₄/T₅ cells onto tangential cell dendrites, while the delayed hyperpolarization must originate from inhibitory signaling via unidentified interneurons.

The following authors contributed to this work:

Author contribution

Alex S. Mauss, **Matthias Meier**, Etienne Serbe, and Alexander Borst
Alex Mauss and Alexander Borst designed research; Alex S. Mauss, **Matthias Meier**, and Etienne Serbe performed research; Alexander Borst contributed unpublished reagents/analytic tools; Alex S. Mauss, **Matthias Meier**, Etienne Serbe, and Alexander Borst analyzed data; Alex S. Mauss and Alexander Borst wrote the paper.

Optogenetic and Pharmacologic Dissection of Feedforward Inhibition in *Drosophila* Motion Vision

Alex S. Mauss, Matthias Meier, Etienne Serbe, and Alexander Borst

Max-Planck-Institute of Neurobiology, 82152 Martinsried, Germany

Visual systems extract directional motion information from spatiotemporal luminance changes on the retina. An algorithmic model, the Reichardt detector, accounts for this by multiplying adjacent inputs after asymmetric temporal filtering. The outputs of two mirror-symmetrical units tuned to opposite directions are thought to be subtracted on the dendrites of wide-field motion-sensitive lobula plate tangential cells by antagonistic transmitter systems. In *Drosophila*, small-field T4/T5 cells carry visual motion information to the tangential cells that are depolarized during preferred and hyperpolarized during null direction motion. While preferred direction input is likely provided by excitation from T4/T5 terminals, the origin of null direction inhibition is unclear. Probing the connectivity between T4/T5 and tangential cells in *Drosophila* using a combination of optogenetics, electrophysiology, and pharmacology, we found a direct excitatory as well as an indirect inhibitory component. This suggests that the null direction response is caused by feedforward inhibition via yet unidentified neurons.

Key words: *Drosophila*; feedforward inhibition; motion vision; optogenetics; pharmacology; synaptic connectivity

Introduction

The perception of dynamically changing visual images derives from time-varying brightness changes projected onto a 2D array of photoreceptors. To extract higher order features that are not explicitly encoded at the level of individual inputs, signals from each point in space need to be processed by downstream parallel circuits. An important question is how the direction of local image motion is detected, a process that requires the comparison of signals from at least two neighboring photoreceptors in time. An algorithmic model, the Reichardt detector, accounts for this by multiplying adjacent inputs after asymmetric temporal filtering (Hassenstein and Reichardt, 1956; Borst and Euler, 2011). A functional unit comprises two mirror-symmetrical half detectors tuned to opposite directions. Their outputs are thought to be subtracted on the dendrites of motion-sensitive cells by antagonistic neurotransmitter systems.

Much of our knowledge about the functional organization of such a neural circuit has emerged from studies in flies (Borst et al.,

2010), where large tangential cells in the lobula plate (LPTCs) display direction-selective responses: depolarization during motion along their preferred direction and hyperpolarization during motion along the opposite/null direction. Two pathways, corresponding to separate ON and OFF channels, convey signals from photoreceptors to the LPTCs (Joesch et al., 2010, 2013; Eichner et al., 2011; Maisak et al., 2013), and their behavioral relevance has been investigated in great detail (Rister et al., 2007; Clark et al., 2011; Bahl et al., 2013; Maisak et al., 2013; Silies et al., 2013; Tuthill et al., 2013). The presumed outputs of these pathways are arrays of columnar T4 and T5 cells that are therefore prime candidates to represent the last processing stage of the antagonistic half detectors. In support of this notion, genetically silencing T4/T5 eliminates all motion sensitivity in LPTCs (Schnell et al., 2012). Moreover, both cell types carry direction-selective Ca^{2+} signals but differ in their preference for edge polarity (Maisak et al., 2013). In the lobula plate, individual T4/T5 axons segregate into four layers according to their tuning: cells selective for front-to-back motion target layer 1, those selective for back-to-front layer 2, cells tuned to upward motion terminate in layer 3, and those tuned to downward motion in layer 4 (Maisak et al., 2013). The planar dendrites of LPTCs are generally, though not exclusively, restricted to individual layers that match the T4/T5 cells' preferred direction (Hausen, 1982, 1984; Hengstenberg et al., 1982). Therefore, LPTCs likely obtain their preferred direction input by integrating excitation from T4/T5 terminals over large receptive fields. However, the synaptic origin of null direction inhibition in LPTCs is unknown.

We studied the functional connectivity of the lobula plate in *Drosophila* by optogenetically stimulating T4/T5 cells while recording the synaptic responses in LPTCs electrophysiologically. Combining this approach with intersectional genetics and pharmacology we found that LPTCs receive excitatory cholinergic

Received Sept. 13, 2013; revised Dec. 13, 2013; accepted Dec. 31, 2013.

Author contributions: A.S.M. and A.B. designed research; A.S.M., M.M., and E.S. performed research; A.B. contributed unpublished reagents/analytic tools; A.S.M., M.M., E.S., and A.B. analyzed data; A.S.M. and A.B. wrote the paper.

The authors declare no competing financial interests.

This work was supported by the Max-Planck-Society and the CRC 870 of the Deutsche Forschungsgemeinschaft. Preparatory experiments were carried out at the Marine Biological Laboratory (Woods Hole, MA), funded by a Grass Fellowship (A.S.M.). We are greatly indebted to Gerald Rubin, Aljoscha Nern, and Barry Dickson for generously sending us driver lines before publishing. We would also like to thank Bettina Schnell for teaching A.S.M. lobula plate tangential cell recordings; Chi-Hon Lee, Stefan Pulver, and Andreas Prokop for kindly providing fly strains; Johannes Plett for advice on the LED arena; and Wolfgang Essbauer, Christian Theille, Renate Gleich, Dieter Mauss, and the MPI workshop for excellent technical support. We are grateful to Alexander Arenz, Armin Bahl, and Jürgen Haag for critically reading this manuscript.

Correspondence should be addressed to Alex S. Mauss, Max-Planck-Institute of Neurobiology, 82152 Martinsried, Germany. E-mail: amauss@neuro.mpg.de.

DOI:10.1523/JNEUROSCI.3938-13.2014

Copyright © 2014 the authors 0270-6474/14/342254-10\$15.00/0

input from both T4 and T5. Importantly, optogenetic activation of T4/T5 cells also elicits delayed indirect synaptic inhibition. We propose that LPTC dendrites indeed receive their preferred direction input from correspondingly tuned T4/T5 cell terminals in the same lobula plate layer. Their null direction input, however, likely arises from T4/T5 cells with opposite direction tuning terminating in the adjacent layer by feedforward inhibition via yet unidentified local interneurons.

Materials and Methods

Fly stocks. Flies were raised at 25°C and 60% humidity on standard cornmeal agar medium at a 12 h light/dark cycle. The following fly strains were used: T4/T5-specific driver lines from the Howard Hughes Medical Institute Janelia Farm (Pfeiffer et al., 2008) and IMP Vienna stock collections (generously provided by Gerald Rubin and Barry Dickson) *R42F06-Gal4* on third chromosome (T4+T5), *R42F06-p65-AD* on second (T4+T5), and *VT37588-Gal4* on third (T4; Maisak et al., 2013); *Cha-DBD* on third (courtesy of Chi-Hon Lee; Gao et al., 2008); *UAS-Channelrhodopsin2-H134R-mCherry* on second (*UAS-ChR2-H134R*, courtesy of Stefan Pulver; Nagel et al., 2005; Pulver et al., 2009; Mattis et al., 2012); *norpA⁷* on X (dysfunctional phototransduction mutant; Hotta and Benzer, 1970); *UAS-mCD8-GFP* on second (courtesy of Barry Dickson); *UAS-synaptotagmin-HA* on second (*UAS-syt-HA*, courtesy of Andreas Prokop; Löhr et al., 2002; Robinson et al., 2002); and *UAS-stinger-GFP* on second. The genotypes of flies used in our experiments are as follows, in order of appearance in the Results section: (1) *w⁻*; *UAS-stinger-GFP/+*; *R42F06-Gal4/+*, (2) *w⁻*; *UAS-syt-HA*, *UAS-mCD8-GFP/+*; *R42F06-Gal4/+*, (3) *w⁻*; *UAS-ChR2-H134R*; *R42F06-Gal4*, (4) *w⁻*; *UAS-ChR2-H134R*; *VT37588-Gal4*, (5) *w⁻*; *R42F06-p65-AD*, *UAS-ChR2-H134R/R42F06-p65-AD*; *Cha-DBD*, (6) *w⁻*; +; *R42F06-Gal4* (control without ChR2 expression), (7) *norpA⁷*; *UAS-ChR2-H134R*; *R42F06-Gal4*, (8) *norpA⁷*; *UAS-ChR2-H134R*; *VT37588-Gal4*, and (9) wild-type Canton-S.

Immunohistochemistry and confocal imaging. For immunostainings brains of 1- to 2-d-old female flies were dissected in PBS, fixed for 30–40 min in PBS/4% paraformaldehyde (PFA) at room temperature, and washed in PBS/0.5% Triton X-100 (PBT). Preparations were blocked for 2 h in PBT/5% NGS, incubated for 1–2 d at 4°C with primary antibodies and 2–3 d with secondary antibodies (5% normal goat serum added to antibody solutions). Primary and secondary antibodies used for T4/T5 > GFP, *sytHA* flies (genotype 2) were as follows: rabbit anti-GFP (1:1000; Torrey Pines Biolabs) + Alexa Fluor 488 goat anti-rabbit (1:500), rat anti-HA (1:50; Roche) + Alexa Fluor 568 goat anti-rat (1:500), and mouse anti-bruchpilot (1:25; NC82, Developmental Studies Hybridoma Bank) + Alexa Fluor 633 goat anti-mouse (1:500). Primary and secondary antibodies used for T4/T5 > *stinger-GFP* flies (genotype 1) were as follows: mouse anti-ChAT (1:1000; courtesy of P. Salvaterra; Takagawa and Salvaterra, 1996) + Alexa Fluor 568 goat anti-mouse (1:200), and rabbit anti-vGAT (1:200; courtesy of D. Kranz; Fei et al., 2010) + Alexa Fluor 568 goat anti-rabbit (1:200). All secondary antibodies were from Invitrogen. Brains were mounted (IMM; ibidi) and optically sectioned with a Leica SP5 confocal laser scanning microscope. To quantify anti-ChAT-positive and anti-vGAT-positive T4/T5 cells, respectively, two nonoverlapping optical sections from two brains for each staining were used for analysis. A total number of 2717 somata for anti-ChAT and 2503 somata for anti-vGAT were evaluated.

To verify ChR2-H134R-mCherry expression specificity and strength with the different driver lines we dissected brains from female flies (1 d after eclosion, genotypes as used in physiological experiments) in PBS (pH 7.4, 280 mOsmol/kg). Brains were fixed at room temperature for 30 min in PBS/4% PFA and an additional 10 min in PBS/4% PFA/0.1% Triton X-100. After three and two washing steps in PBT and PBS, respectively, brains were mounted (IMM; ibidi) and optically sectioned in the horizontal plane with a Leica SP5 confocal laser scanning microscope using 568 nm excitation and a step size of 1 μ m. Identical procedures and confocal settings were applied throughout to compare relative signal intensities between different driver lines. For documentation, single sections were processed in ImageJ 1.46r (National Institutes of Health,

Bethesda, Maryland), pseudocolored using the “Fire” lookup table, and images assembled in Adobe Photoshop CS5.

Cell counts. A software-aided manual counting strategy was used to estimate T4/T5 cell numbers in confocal stacks (step size 1 μ m) generated from brains expressing nuclear-targeted stinger-GFP with a T4/T5-specific driver line (*UAS-stinger-GFP/+*; *R42F06-Gal4/+*). While scrolling through a stack at two orthogonal views distinctly colored spheres were incrementally anchored to centers of individual nuclei. Thus, cells were only counted once and omitted nuclei could easily be detected.

Electrophysiology. For all experiments 20- to 30-h-old female flies kept at 25°C were used, except for neurotransmitter injections where flies were 7–30 h old. For optogenetic experiments, yeast paste containing 1 mM all-*trans*-retinal (ATR, R2500; Sigma Aldrich) was fed to freshly eclosed flies. Preparation and recording conditions were modified from Joesch et al. (2008) and Maimon et al. (2010). Flies were anesthetized on ice and attached to a Plexiglas holder with the head bent down using melted beeswax. The holder was placed underneath a recording chamber with a magnet so that the back of the fly’s head was accessible through a 1 mm slit in the bottom of the chamber consisting of thin foil. The head was gently attached to the slit edges on one side with melted beeswax. Under external solution, a window was cut into the head capsule on the other side with a hypodermic needle. Further dissection and recordings were performed under a Zeiss Axiotech vario microscope equipped with polarized light contrast and epifluorescence. Under polarized light contrast, the glial sheath was digested locally by applying a stream of 0.5 mg/ml Collagenase IV (Gibco) through a cleaning micropipette (~5 μ m opening). Whole-cell recordings were established with patch electrodes of 5–8 M Ω resistance. We used a BA-1S bridge amplifier (npi Electronics) to record in current-clamp, low-pass filtered at 3 kHz, and digitized signals at 10 kHz via an analog/digital converter (PCI-DAS6025; Measurement Computing). All physiological data were acquired in MATLAB (R2010b; Mathworks) using the data acquisition toolbox. Normal external solution contained the following (in mM): 103 NaCl, 3 KCl, 5 TES, 10 trehalose, 10 glucose, 3–7 sucrose, 26 NaHCO₃, 1 NaH₂PO₄, 1.5 CaCl₂, and 4 MgCl₂, pH 7.3–7.35, 280–290 mOsmol/kg. Zero Ca²⁺/high Mg²⁺ external solution contained the following (in mM): 66 NaCl, 22 Na-glucuronate, 3 KCl, 5 TES, 10 trehalose, 5 glucose, 25 NaHCO₃, 1 NaH₂PO₄, and 20 MgCl₂, pH 7.3–7.35, 280 mOsmol/kg. External solution was carboxygenated (95% O₂/5% CO₂) and, except for α -bungarotoxin (α -BTX) experiments, constantly perfused over the preparation at 2 ml/min. Internal solution, adjusted to pH 7.26 with 1N KOH, contained the following: 140 K-aspartate, 10 HEPES, 4 Mg-ATP, 0.5 Na-GTP, 1 EGTA, 1 KCl, and 0.1 Alexa Fluor 488 hydrazide salt (265 mOsmol/kg). Dye-filled cells included for analyses were VS and HS cells, identified by visual response profile (not possible in blind *norpA⁷* mutant flies) and morphology. Apart from visual direction tuning, no discernible differences were observed for VS and HS cells in all assays.

Optogenetic stimulation. During electrophysiological recordings, wide-field light pulses for optogenetic stimulation were delivered via the epifluorescence light path of the microscope through a 40 \times /0.8 NA water-immersion objective (LUMPlan FI; Olympus). As a light source, a Lambda DG-4 Plus wavelength switcher (Sutter) with a 300 mW Xenon Arc lamp was connected to the illumination port of the microscope via a liquid light guide. Attenuating the output of the DG-4 was achieved by offsetting the output galvanometer. The output for each setting was measured with a power meter (Thorlabs PM100D) under the 40 \times objective in air. Taking into account the field of illumination under water immersion, the light intensity per area on the specimen was estimated, as given in the Results section and figures. Light stimuli were triggered via the data acquisition software with voltage steps (~500 μ s delay to light onset according to the manufacturer and own measurements using a photodiode). A stimulus trial consisted of eight 2 ms light pulses interleaved by 5 s. For analysis, responses to the eight light pulses were averaged for each experimental condition and time point. All values in the text are given as mean \pm SEM.

Pharmacology. Aqueous stock solutions were prepared from the following antagonists at the following concentrations: 10 mM methyllyca-

conitine (MLA; Sigma M168), 100 μ M mecamylamine (MEC; Sigma M9020) and 1 μ M α -BTX (Tocris Bioscience 2133). Picrotoxinin (PTX; Sigma P8390) was dissolved in dimethylsulfoxide at 50 μ M. For experiments, α -BTX was added directly to the bath with perfusion switched off. All other compounds were diluted in external solution to concentrations given in the results section and perfused over the preparation at 2 ml/min.

Neurotransmitter pressure injection. All neurotransmitters were dissolved in dH₂O at 50 μ M (glutamate) or 100 μ M (acetylcholine, GABA; all from Sigma; stocks kept aliquoted at -20°C), diluted at day of experiment in external solution to 1 μ M with additional 10 μ M Alexa Fluor 488 hydrazide (Invitrogen), and back-loaded into patch pipettes (~ 1 μ m tip diameter). The Alexa 488/neurotransmitter-filled pipettes were connected via a holder and rubber tube to a pressure-injection system (FemtoJet; Eppendorf) that was triggered via the MATLAB data acquisition software. During recordings of LPTCs, the neurotransmitter-filled pipettes were carefully positioned by a micro-manipulator toward Alexa 488-filled LPTC dendrites in the lobula plate under epifluorescence illumination and electrophysiological responses to brief puffs of neurotransmitters (generally 100 ms) were monitored. Once robust responses remained stable for 5–10 min, a protocol was started during which responses to visual motion stimulation and transmitter puffs were probed continuously every 1–2.5 min while antagonists were washed in and out via the perfusion system. Ejection of Alexa 488/neurotransmitter solution from pipettes was controlled in regular intervals under epifluorescence. For each cell and time point, the average responses to five consecutive pressure pulses at intervals of 5 s were analyzed. Responses were quantified by subtracting the integrated voltage deviations during 1 s before stimulus trigger from 1 s following stimulus trigger. This was done separately for positive and negative values. For each cell and experiment, all positive and negative integrals were normalized either to positive baseline values for acetylcholine injections or negative baseline values for GABA and glutamate injections. All values in the text are given as mean \pm SEM.

Results

T4/T5 cell numbers suggest eight distinct functional subtypes

T4/T5 cells represent the major small-field motion-sensitive input elements to the lobula plate and are required for both preferred direction excitation and null direction inhibition of LPTCs (Schnell et al., 2012). Golgi impregnations have identified eight anatomical types (Fischbach and Dittrich, 1989) and Ca²⁺ imaging data have categorized T4/T5 cells into eight functional subgroups: T4 and T5 cells are selective for moving positive and negative contrast changes, respectively, but are otherwise individually tuned to the same four cardinal directions of motion (Maisak et al., 2013). This provides evidence that T4 and T5 cells convey equivalent motion information to the lobula plate. We aimed to determine whether apart from their anatomy and visual response properties the T4/T5 cells could be further functionally subdivided, for instance, into two antagonistic sets implementing different transmitter systems. We reasoned that the total number of T4 and T5 cells divided by approximately 750 ommatidia of a *Drosophila* eye would yield the number of T4/T5 cells per column and therefore the maximum number of different functional subtypes repeated across the retinotopic array. To analyze T4/T5 cell

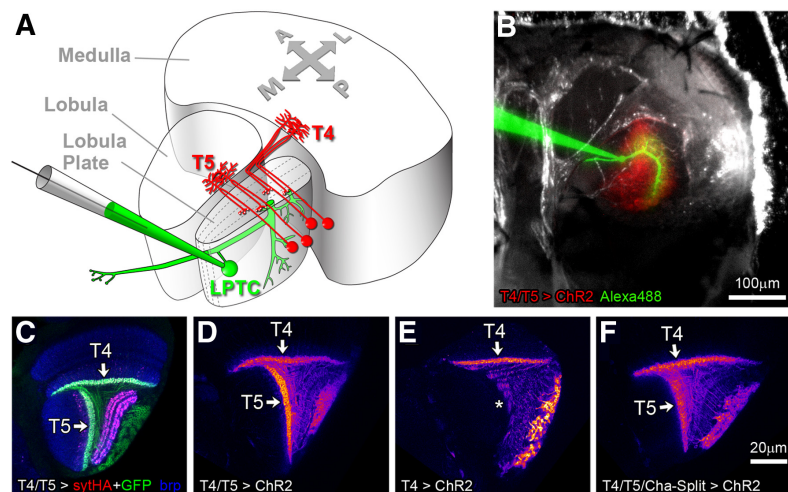


Figure 1. Probing synaptic connectivity between T4/T5 and LPTCs. **A**, Schematic to illustrate anatomical layout of fly visual neuropils medulla, lobula, and lobula plate. One LPTC of the vertical system (VS) is shown in green with recording electrode; the dendrites arborize in layer 4 of the lobula plate. Examples of two T4 and two T5 cells are depicted in red that receive input onto their dendrites in the medulla and lobula, respectively. Individual terminals providing synaptic input to the lobula plate are located either in layer 3 or 4. Equivalent cells innervating layers 1 and 2 are omitted. **A**, anterior; **P**, posterior; **M**, medial; **L**, lateral. **B**, View on a preparation from posterior onto the back of the head (right hemisphere). T4/T5 cells express mCherry-tagged ChR2–H134R (red). A VS cell is filled via a patch electrode with a fluorescent dye (green). **C–F**, Single confocal images of horizontally sectioned *Drosophila* brains. **C**, Immunostaining of GFP (green) and the presynaptic marker synaptotagmin-HA (sythA, red) expressed in T4 and T5 cells, bruchpilot (brp) is labeled in blue for neuropil reference. sythA clearly demarcates the four synaptic layers in the lobula plate. **D–F**, ChR2–H134R-mCherry expression using three driver lines as used for optogenetic experiments. **D**, T4 and T5 cells; **E**, T4 cells only; **F**, cholinergic T4 and T5 cells.

numbers we expressed a nuclear GFP marker using a T4/T5-specific Gal4 line, generated confocal stacks of optic lobes, and counted nuclei manually with the aid of a custom-made tracking software. Our analyses yielded a total number of 5264 ± 433 (SD) T4 and T5 cells ($N = 4$). If a set of T4/T5 cells were represented by every retinotopic unit this would indicate a number of approximately seven cells per column, approximating eight. Taking into account that a small fraction of cells might have escaped from analysis or that numbers might be reduced toward the edges of the visual field, this result is well in agreement with an electron microscopy study that has identified four T4 cells per medulla column each projecting to one of the four different lobula plate layers (Takemura et al., 2013). In the light of these findings we interpret our result such that in general for each ommatidium each of the four lobula plate layers is innervated by one T4 and one T5 terminal only, both tuned to the same direction of visual motion but individually specialized for moving contrast increments and decrements, respectively.

Probing synaptic connectivity between T4/T5 and LPTCs

T4 and T5 cells receive synaptic input on their dendrites located in the medulla and lobula, respectively, and convey signals to the lobula plate where they are thought to connect to LPTC dendrites via chemical synapses (Fig. 1A,C; Strausfeld and Lee, 1991). Making use of specific T4/T5 driver lines (Fig. 1B–F) we set out to probe the underlying connectivity by optically stimulating T4/T5-expressing Channelrhodopsin2–H134R-mCherry while recording the synaptic responses in LPTCs by whole-cell patch clamp (Fig. 1A,B). Applying 2 ms blue light pulses at ~ 3 mW mm^{-2} (472 nm center wavelength, 30 nm bandwidth) to T4/T5 > ChR2 brains resulted in a fast excitatory peak (latency 5.4 ± 0.4 ms after onset of stimulus trigger) followed by an

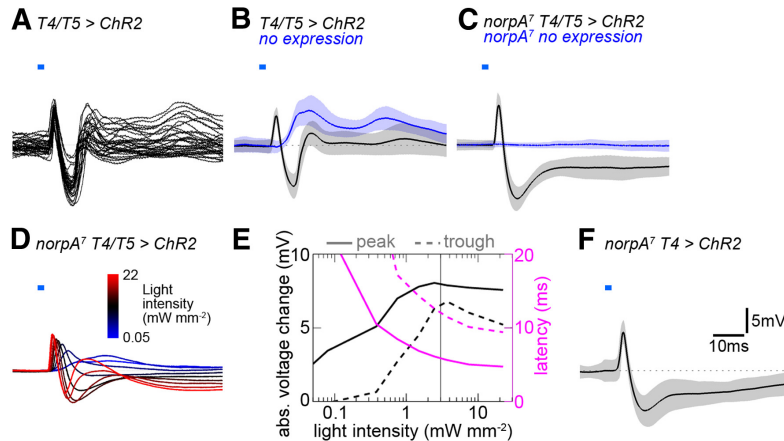


Figure 2. Synaptic LPTC responses to optogenetic T4/T5 cell stimulation. **A**, Individual voltage traces of LPTCs ($N = 4$) responding to optogenetic stimulation of T4 and T5 cells ($T4/T5 > ChR2$; $n = 32$ stimuli total). Optic stimuli consisted of 2 ms wide-field light flashes delivered through the microscope objective onto the preparation with a center wavelength and bandwidth of 472/30 nm and an intensity of ~ 3 $mW\ mm^{-2}$. LPTCs respond with initial biphasic voltage deflections consisting of a fast depolarization and a subsequent hyperpolarization. **B**, Average of the same traces as in **A** in black, with SD as shaded area. The blue trace is the response of LPTCs in control flies (*Gal4* only) to the same stimulus ($N = 4$), showing the retina input only. **C**, Same as **B**, but with blind flies homozygously carrying the *norpA7* mutation (black, $N = 7$; blue, $N = 4$). **D**, Same condition as for black trace in **C**, but light intensity varied between 0.05 and 22 $mW\ mm^{-2}$ ($N = 8$, SD omitted for clarity). **E**, Responses were quantified and plotted as absolute (abs.) amplitudes (black) and latencies (magenta) of peak maxima (solid lines) and trough minima (dashed lines). The vertical gray line at 3 $mW\ mm^{-2}$ denotes the approximate light intensity for all other optogenetic experiments except for *T4/T5/Cha-Split* flies. **F**, Optogenetic stimulation of T4 cells only (*norpA7 T4 > ChR2*; 3 $mW\ mm^{-2}$, $N = 5$) evokes a biphasic voltage response in LPTCs that is comparable to the joint T4/T5 cell stimulation.

inhibitory trough ($\Delta 11.2 \pm 0.2$ ms) and a second smaller excitatory peak ($\Delta 16.3 \pm 1.2$ ms). The time course of the response was highly reproducible as shown for four cells and a total number of 32 stimuli (Fig. 2A). Figure 2B (black trace) depicts the average of the same trials with the shaded area indicating the SD. A concern was the unintended stimulation of photoreceptors by the optogenetic light stimulus. To characterize visual artifacts we applied blue light pulses to control flies without expression (*T4/T5-Gal4* only) and observed an excitatory response in all preparations starting with a latency of 8 ms and peaking at $\Delta 15.5 \pm 1.7$ ms (Fig. 2B, blue trace). The relatively slow time course and long latency of the retina artifact suggests that the initial biphasic depolarizing and hyperpolarizing potential changes in *T4/T5 > ChR2*-expressing flies are caused by synaptic input from optogenetically stimulated T4/T5 cells to LPTCs with the second excitatory peak being evoked by visual input. To further isolate the optogenetic from the retina components we performed experiments in flies without functional phototransduction (*norpA7*: phospholipase C mutated; Hotta and Benzer, 1970). As expected, *norpA7*-mutant flies without ChR2 expression did not show a response to blue light pulses at the level of LPTCs (Fig. 2C, blue trace). Repeating the same stimulation in the mutant background with additional ChR2 expression in T4/T5 lead to an initial biphasic response as in visually intact flies (Fig. 2C, black trace; latency excitatory peak: $\Delta 5.4 \pm 0.4$ ms, inhibitory trough: $\Delta 11.7 \pm 0.9$ ms). This result demonstrates that the biphasic response is generated exclusively by optogenetic T4/T5 stimulation. It also supports the notion that the formation of visual circuits in flies is largely independent of sensory experience (Karmeier et al., 2001; Hiesinger et al., 2006). Differences between visually intact and blind flies were only discernible >8 ms after stimulus onset in that LPTCs in *norpA* mutants presumably due to the lack of visual input showed a sustained modest hyperpolarization with a time constant of 0.1 s (Fig. 2, compare B and C, black traces).

We next investigated the dependence of the optogenetic response on varying stimulus intensities to obtain a quantitative description of the underlying input–output relationship (Fig. 2D,E). Several features became apparent: (1) inhibition had a higher threshold than excitation; (2) the amplitudes increased approximately proportional to the logarithm of the stimulus intensity over a wide range; (3) the latency of the excitatory peak was approximately half of that for the inhibitory trough, a ratio that remained fairly stable across a wide range of intensities; and (4) at high light intensities the voltage progression became triphasic (not quantified).

Since we measured the LPTC responses to stimulation of both T4 and T5 cells at the same time the question arises in how far the two cell types might be differentially connected to LPTCs. We made use of a specific *Gal4* line to optogenetically stimulate exclusively T4 cells (Figs. 1E, 2F). LPTC recordings show a biphasic response to 2 ms blue light flashes that is very similar to the joint T4/T5 stimulation at comparable light intensities (Fig. 2, compare C, black trace and F; latency excitatory peak: $\Delta 5.9 \pm 0.4$ ms, inhibitory trough: $\Delta 13.3 \pm 1.3$ ms). Due to the lack of a sufficiently selective driver line we were not able to perform corresponding experiments with T5 cells. However, the identical effects of our optogenetic T4 and T4/T5 stimulation argue that both cell types are synaptically connected to LPTCs in similar ways and that the initial sharp EPSP arises by direct excitation of LPTCs by both T4 and T5 terminals. This is to be expected because T4 and T5 cells are individually tuned to moving ON and OFF edges, respectively (Maisak et al., 2013), while LPTCs reliably depolarize in response to both visual stimuli.

The delayed hyperpolarization in LPTCs is less straightforward to explain and might be caused by one of the following mechanisms, which we will further address below: (1) direct synaptic inhibition by T4/T5 cells (slower than direct excitation); (2) feedforward inhibition via an additional cell type between T4/T5 and LPTCs; (3) LPTC intrinsic mechanisms, for instance, depolarization-triggered opening of hyperpolarizing conductances; or (4) feedback inhibition postsynaptic of LPTCs.

The delayed hyperpolarization in LPTCs is less straightforward to explain and might be caused by one of the following mechanisms, which we will further address below: (1) direct synaptic inhibition by T4/T5 cells (slower than direct excitation); (2) feedforward inhibition via an additional cell type between T4/T5 and LPTCs; (3) LPTC intrinsic mechanisms, for instance, depolarization-triggered opening of hyperpolarizing conductances; or (4) feedback inhibition postsynaptic of LPTCs.

T4/T5 cells are primarily cholinergic

Acetylcholine is the primary excitatory neurotransmitter in insect CNS. It is reasonable to assume that at least a substantial fraction of T4/T5 releases acetylcholine onto LPTCs since those express nicotinic cholinergic receptors (nAChRs), depolarize in response to acetylcholine and its agonist carbachol (Brotz and Borst, 1996; Raghu et al., 2009), and receive excitatory preferred direction input, which is eliminated when T4 and T5 cells are genetically silenced (Schnell et al., 2012). However, LPTCs also receive inhibitory null direction input, which is presumably GABAergic (Brotz and Borst, 1996; Single et al., 1997; Raghu et al., 2007). Moreover, genetic expression data and histochemistry have indicated that T4 and T5 cells might also secrete GABA, glutamate, and/or aspartate as neurotransmitters (Strausfeld et

al., 1995; Sinakevitch and Strausfeld, 2004; Raghu and Borst, 2011). We therefore asked whether T4/T5 cells employ neurotransmitters other than acetylcholine. First, we took an intersectional genetic approach (“Split Gal4”; Luan et al., 2006) to exclude potential noncholinergic T4/T5 cells from ChR2 expression. We targeted two functional domains (AD and DBD) both required for UAS activation independently to T4/T5 (*R42F06-p65-AD*) and cholinergic cells (*Cha-DBD*; Gao et al., 2008), respectively, by two different regulatory elements. Thus, functional transcription factor to activate *UAS-ChR2*

is reconstituted only in the intersection of the two expression patterns, i.e., in cholinergic T4 and T5 cells. It should be noted that in contrast to the other experimental backgrounds only a single copy of ChR2 was included because homozygous animals were not viable. Confocal images reveal that the resulting expression (*T4/T5-p65-AD + Cha-DBD = T4/T5/Cha-Split > ChR2-H134R-mCherry*) is generally weaker but otherwise not obviously different compared with *T4/T5 > ChR2* (Fig. 1*D,F*). Notably, optic stimulation of *T4/T5/Cha-Split > ChR2* brains (with higher intensities to compensate for weak expression: $\sim 30 \text{ mW mm}^{-2}$) resulted in initial biphasic synaptic responses in LPTCs that were quite similar to the responses seen when driving ChR2 with *T4/T5-Gal4* (compare Figs. 3*A*, 2*B*, black trace). Second, we expressed a nuclear reporter (stinger-GFP) using the T4/T5-specific driver line and stained brains with an antibody against choline acetyltransferase (ChAT). Confocal imaging of optic lobes revealed that 99.2% cells labeled with stinger-GFP colocalized with anti-ChAT (Fig. 3*B,B'*). We also labeled GABAergic neurons in brains of the same genotype with an antibody against vesicular GABA transporter (vGAT). The vast majority (97.6%) of stinger-GFP-labeled cells was clearly vGAT negative (Fig. 3*C,C'*). Therefore, assuming that T4/T5 cells transmit a single fast neurotransmitter, we conclude that T4/T5 cells are not GABAergic but instead primarily cholinergic.

Pharmacologic profile of lobula plate tangential cells

The data so far strongly suggest that T4/T5 cells represent a homogenous group with respect to their cholinergic transmitter phenotype. Therefore, the biphasic effect observed in the LPTC membrane potential upon T4/T5 stimulation must arise by mechanisms postsynaptic of T4/T5 terminals. One possibility might be the existence of antagonistic cholinergic receptors expressed in LPTC dendrites, since both excitatory and inhibitory acetylcholine-gated channels have been documented in invertebrates (Pfeiffer-Linn and Glantz, 1989; Dent, 2010). However, this scenario seems unlikely because acetylcholine and its agonist carbachol elicit strong depolarizations but no hyperpolarizations in LPTCs in *Calliphora* and *Drosophila* (Brotz and Borst, 1996; Raghu et al., 2009). We aimed to confirm and extend these findings by dissecting the direct and indirect effects of neurotransmitters pharmacologically. To this end, we pressure injected neurotransmitters via micropipettes into the lobula plate while simultaneously recording from LPTCs. In agreement with the previous studies, injection of 1 mM acetylcholine generated strong excitatory peaks in LPTCs (Fig. 4*A–C*, white arrows; $+10.9 \pm 0.7 \text{ mV}$, $N = 18$). In 17/18 cases, the excitation was followed by a clear hyperpolarizing response smaller in amplitude ($-1.9 \pm 0.27 \text{ mV}$, $N = 18$) but with a prolonged time course

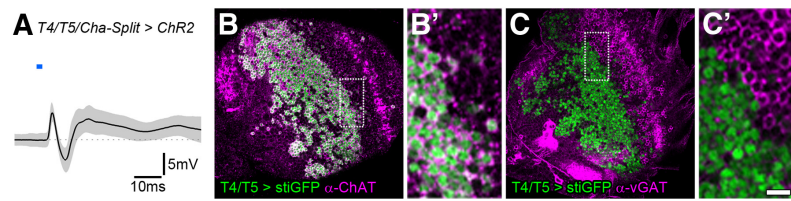


Figure 3. T4 and T5 cells are primarily cholinergic. **A**, Optogenetic stimulation of exclusively cholinergic T4/T5 cells leads to initial depolarization and subsequent hyperpolarization in LPTCs (Split-Gal4 approach: *T4/T5-p65-AD + Cha-DBD > ChR2*; 30 mW mm^{-2} , $N = 8$), comparable to T4 and T4/T5 cell stimulation as in Figure 2. The following second excitatory peak is likely caused by retina input. **B–C'**, Confocal images of immunostained *T4/T5-Gal4 > UAS-stiGFP*-expressing brains reveal that the vast majority of T4/T5 cells are (**B, B'**; 2696/2717: 99.2%) positive for ChAT and (**C, C'**; 2444/2503: 97.6%) negative for vGAT. Scale bars: **B, C**, 20 μm ; for enlarged insets (**B', C'**) 5 μm .

(Fig. 4*A–C*, black arrows), reminiscent of the T4/T5 optogenetic stimulation effect albeit on a longer timescale due to the slower stimulus delivery. To quantify these effects relative to each other we divided the negative by the positive stimulus-evoked response integral (see Material and Methods) and obtained a relationship of -0.84 ± 0.16 . We then performed acetylcholine injection experiments under conditions where synaptic transmission is silenced (Fig. 4*D*; $N = 7$, external solution without Ca^{2+} and with high Mg^{2+} concentration). We found excitatory responses comparable to the condition with intact synaptic transmission ($+13.5 \pm 1.1 \text{ mV}$). However, hyperpolarization was almost absent ($-0.3 \pm 0.08 \text{ mV}$) and averaged integrated responses relative to excitation amounted to a significantly smaller value (-0.1 ± 0.02) compared with the normal condition (Wilcoxon rank sum test, -0.84 ± 0.16 vs -0.1 ± 0.02 ; $p = 0.001$). These results demonstrate that acetylcholine injection evokes a direct depolarizing and an indirect hyperpolarizing response in LPTCs. Moreover, this outcome corroborates the notion that alone acetylcholine release from optogenetically stimulated T4/T5 might underlie the biphasic response in LPTCs. We went on to explore the sensitivity of LPTCs to two other prevalent neurotransmitters. Both pressure-applied GABA and glutamate elicited pronounced inhibitory potential changes (Fig. 4*E–H*) suggesting that both GABA- and glutamate-gated chloride channels (Cleland, 1996; Hosie et al., 1997) are expressed in LPTCs.

Next, we used the pressure-injection assay to establish specificity and effectiveness of available cholinergic and GABAergic antagonists. We consider this strategy essential because neurotoxins can display a considerable degree of cross-reactivity particularly for the functionally diverse group of phylogenetically related pentameric ionotropic receptors in insects (Bai et al., 1992; Barbara et al., 2005; Dent, 2010). We thus combined acetylcholine pressure injection into the lobula plate with patch-clamp recordings from LPTCs and bath perfusion of the nicotinic antagonists MLA, α -BTX (both competitive), and MEC (non-competitive). We found that 1 μM MLA was most effective and irreversibly eliminated all acetylcholine responses within 10–15 min after administering the drug (Fig. 4*A–A''*). MEC was less potent and reduced both depolarizing and hyperpolarizing responses at a concentration of 100 μM to 9 and 5%, respectively, with a similar time course (Fig. 4*B–B''*). This effect, however, was reversible (110% for depolarization and 80% for hyperpolarization) after washing for ~ 40 min ($N = 7$; Fig. 4*B'*, dashed trace). Depolarization in response to acetylcholine was also blocked by 10 μM α -BTX (30%) within 40 min (Fig. 4*C–C''*). The longer time course is presumably due to the much larger molecular weight of the α -BTX peptide compared with the other compounds or the different delivery (see Material and Methods). Notably, in con-

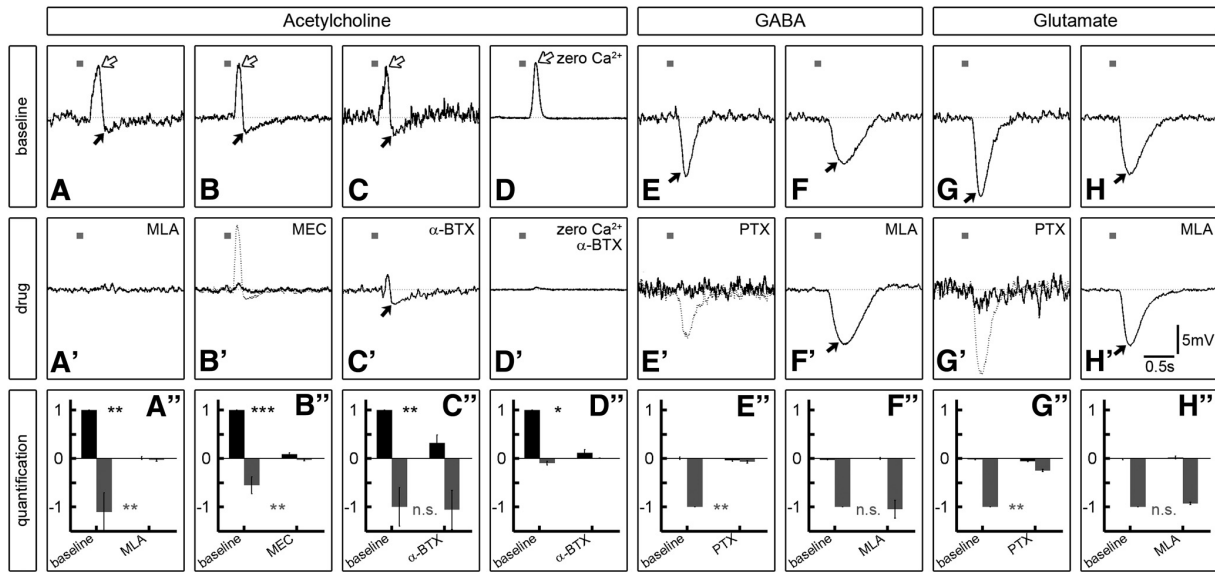


Figure 4. Responses to neurotransmitter injections and pharmacologic profile of LPTCs. **A–H**, Representative average voltage traces from single LPTCs in response to five neurotransmitter pressure injections onto the dendrites in the lobula plate are shown (100 ms pulses indicated by small gray bars, neurotransmitters at 1 mM concentration indicated at the top). **A–C**, Acetylcholine injection evokes an initial depolarizing peak (white arrow) and a subsequent hyperpolarization (black arrow) in LPTCs. **D**, In conditions where synaptic transmission is silenced (zero Ca^{2+} , high Mg^{2+} concentration in external solution) depolarization is still present while hyperpolarization is almost completely absent. **E–H**, Both GABA and glutamate injection leads to strong hyperpolarization in all cells recorded. **A'–H'**, Responses from the same cells after application of the indicated antagonists: (**A'**) 15 min 1 μM MLA, (**B'**) 15 min 100 μM MEC, (**C' + D'**) 40 min 10 μM α -BTX, (**E' + G'**) 10–15 min 25 μM PTX, (**F' + H'**) 25 min 1 μM MLA. The dashed traces in **B'**, **E'**, and **G'** denote responses after 30–60 min wash following MEC or PTX treatment. MLA and α -BTX effects could not be washed out effectively. **A''–H''**, Responses of individual cells were quantified as positive (black bars) and negative integrals (gray bars; the period 1 s before the stimulus was used as a baseline and subtracted away from the response 1 s after the stimulus; error bars denote SEM) normalized to the baseline depolarization for acetylcholine and baseline hyperpolarization for GABA and glutamate. **A''**, $N = 5$, **B''**, $N = 8$, **C''**, $N = 5$, **D''**, $N = 4$, **E''**, $N = 5$, **F''**, $N = 2$, **G''**, $N = 5$, **H''**, $N = 2$. Two-tailed Wilcoxon rank-sum test: n.s., Not significant; $p > 0.3$; $*p < 0.05$; $**p \leq 0.01$; $***p < 0.001$.

trast to MLA and MEC, α -BTX did not significantly change the indirect inhibitory effect of acetylcholine, which remained at 106% of baseline level. Because insect nAChR subunits are known to substantially differ in their sensitivity to α -BTX (Thany et al., 2007, 2010) this result indicates that α -BTX-sensitive receptors might be expressed on LPTCs while α -BTX-insensitive receptors are located on another cell type also activated by acetylcholine and providing inhibitory input to LPTCs. We confirmed that the hyperpolarizing component in LPTCs in response to acetylcholine in presence of α -BTX is indeed indirect, since, as for the baseline, it is absent in conditions where synaptic release is prevented (Fig. 4D–D').

We then tested the noncompetitive GABA receptor antagonist PTX in combination with GABA injection onto LPTC dendrites. As expected, 25 μM PTX effectively reduced the hyperpolarizing GABA response to 7% (Fig. 4E–E'; recovery 90% after 50–60 min wash; Fig. 4E', dashed trace). As a control, we confirmed that the cholinergic antagonist MLA did not have any effect on GABA-evoked hyperpolarization, which remained reliably at baseline levels throughout drug treatment (Fig. 4F–F'). Since glutamate also produces hyperpolarizing conductances in LPTCs in our assay, we wanted to test a potential blocking action of PTX on those. Indeed, PTX reduced glutamate responses to 25% (Fig. 4G–G'; recovery 86% after 30–60 min wash; Fig. 4G', dashed trace) indicating that PTX does not selectively block GABA-gated receptors but also other ligand-gated chloride channels in insects, in line with previous accounts (Rohrbough and Broadie, 2002; Barbara et al., 2005; Liu and Wilson, 2013). As in combination with GABA, MLA had no discernible effect on the LPTC responses to glutamate (Fig. 4H–H').

Feedforward inhibition from T4/T5 to LPTCs

The experiments above established that T4/T5 cells are cholinergic and that pressure-applied acetylcholine elicits monosynaptic depolarizing responses in LPTCs. Hence, acetylcholine release from T4/T5 cells most likely directly excites tangential cells. In contrast, the inhibitory component of the biphasic synaptic response in LPTCs upon optogenetic T4/T5 stimulation is probably indirectly elicited by yet unidentified inhibitory neurons. To further demonstrate this point, we compared LPTC responses to optogenetic stimulation of T4/T5 cells before and after the application of the cholinergic antagonists characterized above. Since the action of pharmacologic substances build up rather slowly *in vivo* we wanted to control for unspecific changes of the synaptic response in LPTCs over time, for instance, caused by synaptic depletion. However, we observed that the biphasic LPTC response did not substantially change at least over 50 individual stimulations and 40 min recording time (Fig. 5A, the black trace represents average baseline responses, the red trace recordings from the same cells 40 min later). Next, we combined T4/T5 stimulation with bath application of the potent and specific cholinergic antagonist MLA. Indeed, in full agreement with indirect synaptic inhibition, both the excitatory and the inhibitory responses were almost completely eliminated within 15 min after applying the drug (Fig. 5B, red trace). We then combined T4/T5 stimulation with the less potent cholinergic antagonist MEC (Fig. 5C). Now, the inhibitory component was abolished but a slowed excitatory component remained. Like in the acetylcholine pressure application assay, effects of MEC were largely reversible (data not shown). The residual excitation in presence of MEC with absent inhibition could mean that cholinergic receptors on

LPTCs are less affected by MEC than receptors on the putative inhibitory neuron type. The existence of nAChRs that differ in their sensitivity to MEC has, for instance, been suggested in cockroach DUM neurons (Courjaret and Lapied, 2001). Alternatively, regardless of nicotinic receptor properties, the putative inhibitory interneurons might have a higher threshold to become activated by T4/T5 cells than the LPTCs. The latter explanation is supported by experiments in which reduced light intensities were applied to optogenetically stimulate T4/T5 cells ($<0.5 \text{ mW mm}^{-2}$). Similar to MEC treatment, low light intensities resulted in slow and predominantly depolarizing responses in LPTCs (Fig. 2*D,E*). We wondered how the biphasic response would be affected by the more selective drug α -BTX. As expected, the excitatory peak was effectively reduced (Fig. 5*D*, red trace). However, the IPSP was virtually unchanged similar to the result obtained by acetylcholine injection into the lobula plate (Fig. 4*C–C'*). This finding demonstrates that T4/T5-mediated inhibition in LPTCs does not require a preceding depolarization in those and thus rules out LPTC-intrinsic depolarization-triggered processes and feedback inhibition downstream of LPTCs. This conclusion is also supported by direct stimulation of ChR2-expressing tangential cells, which produced strong depolarizations without following hyperpolarizing troughs ($N = 3$, data not shown). Given that at least 10 nAChR subunits are encoded by the *Drosophila* genome (Jones and Sattelle, 2010), and expressed in various combinations in the optic lobe (Takemura et al., 2011), our experiments point toward a more complex connectivity between T4/T5 and LPTCs than just a direct cholinergic synapse. Rather, T4 and T5 cells additionally activate a yet unidentified cell type potentially expressing α -BTX-insensitive receptors, which in turn supplies inhibition to LPTCs.

Furthermore, we also combined optogenetic T4/T5 stimulation with bath perfusion of PTX (Fig. 5*E*). LPTCs responded with depolarizations of rise time kinetics similar to the baseline but with enhanced peak amplitude. Importantly, fully in agreement with an indirect inhibitory synaptic connection from T4/T5 to the LPTCs, PTX strongly delayed and reduced hyperpolarizing effects of T4/T5 optogenetic stimulation. Since hyperpolarizing responses of LPTCs to both GABA and glutamate injection could be blocked by PTX (Fig. 4*E',G'*) this indicates that the postulated inhibitory cell type could be either GABAergic or glutamatergic.

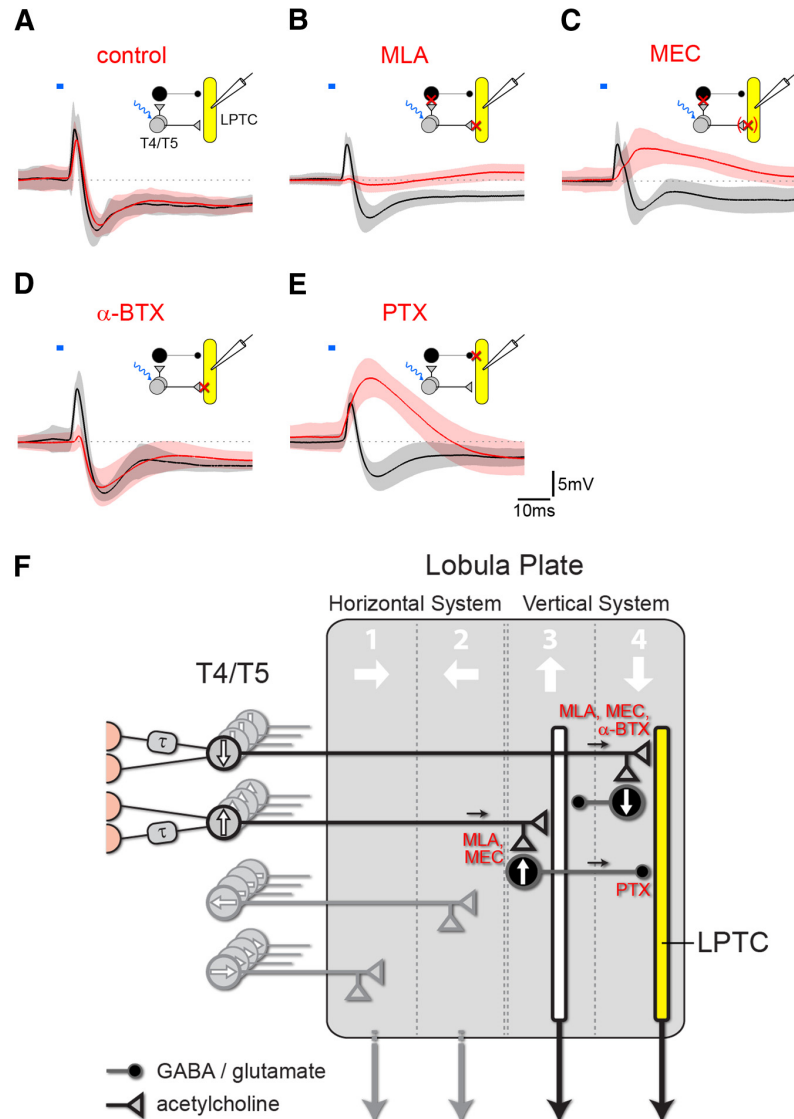


Figure 5. Effects of neurotransmitter antagonists on T4/T5-mediated synaptic potentials in LPTCs. *A*, Biphasic LPTC voltage response to optogenetic T4/T5 cell stimulation ($T4/T5 > ChR2$; 2 ms 472/30 nm at $\sim 3 \text{ mW mm}^{-2}$) over at least 50 individual stimulations and 40 min recording time ($N = 5$; black, baseline; red, the same cells 40 min later). Amplitude and dynamics have not obviously changed over time. *B–E*, Responses of LPTCs (same genotype and stimulation) before (black trace) and after (red trace) indicated drug application ($1 \mu\text{M}$ MLA: $N = 5$, 15 min; $100–200 \mu\text{M}$ MEC: $N = 4$, 15 min; $10 \mu\text{M}$ α -BTX: $N = 6$, 40 min; $25 \mu\text{M}$ PTX: $N = 7$, 15 min). The schematic insets illustrate the connectivity supported by the data between T4/T5 and LPTCs with a direct excitatory connection and an inhibitory indirect arm. Synaptic targets of the individual antagonists are indicated with red crosses. The bracketed cross for MEC treatment indicates a potentially incomplete block. *F*, Connectivity model of the lobula plate that incorporates results from this study as well as previously published data (see Discussion). T4 and T5 cells terminate in one of four lobula plate layers according to their direction tuning where they directly connect to LPTC dendrites (yellow) in the same layer via cholinergic synapses and thus provide preferred direction excitation. T4 and T5 cells with opposite tuning terminate in the adjacent layer and provide feedforward null direction input to the same LPTC via putative GABAergic or glutamatergic inhibitory neurons. The inferred synaptic blocking sites of the antagonists (red) are indicated.

Discussion

The visual ganglia of insects have been powerful model systems to address questions related to visual processing and circuit function largely because of experimental accessibility and the existence of individually identifiable neurons (Borst, 2009; Borst et al., 2010; Fotowat and Gabbiani, 2011; Homberg et al., 2011). However, due to the intricate connectivity and small sizes of most

visual interneurons detailed circuit information has been difficult to establish. Here, we present a strategy to probe functional synaptic connectivity between identified neurons in *Drosophila* by combining optogenetic stimulation, electrophysiology, and pharmacology. The outcome of this work reveals a new synaptic processing stage in the fly motion vision circuitry.

Our experiments have established that wide-field visual motion-sensitive lobula plate tangential cells receive fast excitation when T4/T5 cells are optogenetically stimulated. We have shown that the excitatory input is cholinergic because it can be effectively blocked by selective nicotinic antagonists. The short latency of the optogenetic response (<3 ms after light onset; not taking into account the delay caused by ChR2-H134R opening kinetics) suggests that this excitatory cholinergic connection of T4/T5 cells onto LPTCs is most likely direct, well in agreement with functional, light microscopy and ultrastructure data (Fischbach and Dittrich, 1989; Strausfeld and Lee, 1991; Schnell et al., 2012; Maisak et al., 2013). Moreover, all T4/T5 somata are labeled by a choline acetyltransferase-specific antibody and acetylcholine pressure injection onto LPTC dendrites also elicits strong excitatory peaks in conditions where synaptic release is blocked (zero Ca^{2+} /high Mg^{2+}). These optogenetic and pressure injection paradigms provide opportunities to explore synaptic ligand-gated receptors and their pharmacologic profiles on the level of individually identifiable neurons. In *Drosophila*, 10 nAChR subunits have been identified but their individual properties are not well understood largely because heterologous expression of functional insect nAChRs has been exceedingly difficult (Sattelle et al., 2005; Thany et al., 2007; Jones and Sattelle, 2010; Millar and Lansdell, 2010). LPTCs have been proposed to express $\text{D}\alpha 7$ nAChR subunits (Raghu et al., 2009) that are candidates to form channels of an α -BTX-sensitive type (Thany et al., 2007). In line with this view, depolarizing responses to acetylcholine and carbachol can be largely eliminated by α -BTX (Fig. 4D–D’; Brotz and Borst, 1996). Somewhat surprisingly, however, in $\text{D}\alpha 7$ -mutant flies visual responses in LPTCs are largely unaltered and a fluorophore-conjugated α -BTX probe still binds to LPTC dendrites (Raghu et al., 2009) suggesting that other α -BTX-sensitive subunits can substitute for $\text{D}\alpha 7$ absence. It remains to be seen whether the cholinergic receptors are of heteromeric or homomeric types. Transcript profiling of individual LPTCs could help to assign nicotinic subunit composition to identified neurons (Takemura et al., 2011) and perhaps also reveal post-transcriptional modifications that might further functionally diversify receptors in a cell-specific manner (Sattelle et al., 2005). This approach in combination with whole-cell recordings, optogenetic stimulation, neurotransmitter injection, and genetic manipulation would open up this system for detailed analyses of the pharmacologic properties of nicotinic and other channels at the level of individual subunits and functional domains.

In addition to direct excitation, both optogenetic stimulation of T4/T5 cells and acetylcholine pressure injection onto LPTC dendrites elicit delayed hyperpolarization. This inhibitory component is indirect because it can be eliminated by the cholinergic antagonists MLA and MEC (Figs. 4A–A’, B–B’, 5B, C) and because it is absent for acetylcholine injection when synaptic transmission is blocked (Fig. 4D). We therefore propose that cholinergic T4/T5 cells excite yet unidentified local interneurons, which supply inhibition to LPTCs. Such putative local interneurons might express acetylcholine receptors of an α -BTX-insensitive type because this neurotoxin had no effect on inhibition evoked by optogenetic T4/T5 cell stimulation and acetylcholine injection (Figs. 4C–C’, 5D). What is the functional

significance of the T4/T5 cell-mediated direct excitation and indirect inhibition onto LPTCs? During visual stimulation, LPTCs receive two kinds of inputs: excitation tuned to their preferred direction and inhibition tuned to the opposite/null direction. Since T4/T5 cells have been identified to represent the motion-sensitive input elements to the lobula plate (Schnell et al., 2012; Maisak et al., 2013; Takemura et al., 2013) three scenarios seemed conceivable to underlie preferred and null direction responses in LPTCs. (1) T4/T5 cells convey signals to LPTCs via a single neurotransmitter with graded positive and negative release modulations from a spontaneous level, similar to photoreceptor terminals. (2) Synaptic connections between T4/T5 and LPTCs comprise two antagonistic types, for instance, implementing different transmitter systems mediating oppositely tuned excitation and inhibition. In line with this model T4 and T5 cells have been suggested to release acetylcholine, GABA, glutamate, and aspartate as neurotransmitters (Strausfeld et al., 1995; Sinakevitch and Strausfeld, 2004; Raghu and Borst, 2011; Raghu et al., 2011). (3) Excitatory output from T4/T5 cells is partly sign inverted and fed forward to LPTCs by inhibitory cells in a direction-specific manner. Possibility 1 appears highly unlikely on the basis of current injections in LPTCs during visual motion stimulation (Borst et al., 1995, 2010; Joesch et al., 2008). These experiments reveal that the synaptic currents underlying preferred and null direction responses are mediated by different synaptic receptors because the responses have markedly different reversal potentials. As for the remaining possibilities, previous data (Fischbach and Dittrich, 1989; Maisak et al., 2013; Takemura et al., 2013) and our cell counts indicate eight functional types of T4/T5 per retinotopic column: each tuned to one of two contrast polarities and one of the four cardinal directions of motion. This number is difficult to reconcile with the second model, because it would require a further subdivision of T4/T5 cells according to transmitter profile. Moreover, individual LPTC dendrites generally do not anatomically overlap with T4/T5 terminals tuned to the LPTC’s null direction. Rather, our results clearly support the third possibility because, as we have shown, all T4/T5 cells are in fact cholinergic and supply direct excitation and indirect inhibition to LPTCs.

We thus favor a model where LPTC dendrites receive cholinergic input during preferred direction motion from T4/T5 terminals in one layer of the lobula plate where they overlap, and input from the neighboring layer conveyed by yet unidentified inhibitory cells during null direction motion (Fig. 5F). Furthermore, the postulated inhibitory neurons might additionally inhibit presynaptic T4/T5 terminals in the adjacent layer and thereby antagonize excitatory inputs to tangential cells both presynaptically and postsynaptically at the same time. Such a wiring would constitute a recurrent inhibitory motive and potentially explain why optogenetic stimulation of all T4/T5 cells with high intensities generates a triphasic voltage progression in tangential cells (Fig. 2D, red trace). In line with this idea, prolonged optogenetic T4/T5 cell stimulation evokes membrane potential oscillations in tangential cells (data not shown). The transmitter used by neurons responsible for null direction inhibition has been suggested to be GABA. This conclusion is primarily based on experiments in which PTX has been used to block inhibition (Schmid and Bülthoff, 1988; Egelhaaf et al., 1990; Brotz and Borst, 1996; Single et al., 1997). However, we have found that LPTCs respond with hyperpolarization both to GABA and to glutamate injection, and that both responses can be blocked by PTX. These results challenge the notion that GABA underlies the null direction responses in LPTCs and suggest glutamate as another candidate neurotransmitter that should be taken into consideration.

The identification of the neurons underlying null direction inhibition will be required for the verification of the underlying neurotransmitter system and to complete the suggested wiring model of the lobula plate. Previous anatomical studies might provide an entry point. Fischbach and Dittrich (1989), Raghu et al. (2011, 2013), and Raghu and Borst (2011) describe cells such as Tlp, Lpi, and Y neurons, which arborize in more than one lobula plate layer but also in other neuropils and are therefore not immediately persuasive to fulfill the postulated role. Additional anatomical analyses and identification of novel cell types might therefore be necessary. Genetic control over the postulated inhibitory neurons would facilitate the study of the integration and functional implications of antagonistic preferred and null direction inputs on tangential cells. Depending on the anatomical and physiological properties of the postulated inhibitory cells some null direction-specific processing might occur. For instance, while ON and OFF motion vision pathways likely converge first at the level of the tangential cells during preferred direction motion (Maisak et al., 2013), it remains to be determined whether null direction ON and OFF motion signals are perhaps integrated in the inhibitory neurons presynaptic to tangential cells.

References

- Bahl A, Ammer G, Schilling T, Borst A (2013) Object tracking in motion-blind flies. *Nat Neurosci* 16:730–738. [CrossRef Medline](#)
- Bai D, Erdbrugger H, Breer H, Sattelle DB (1992) Acetylcholine receptors of thoracic dorsal midline neurones in the cockroach, *Periplaneta americana*. *Arch Insect Biochem Physiol* 21:289–301. [CrossRef Medline](#)
- Barbara GS, Zube C, Rybak J, Gauthier M, Grünewald B (2005) Acetylcholine, GABA and glutamate induce ionic currents in cultured antennal lobe neurons of the honeybee, *Apis mellifera*. *J Comp Physiol A Neuroethol Sens Neural Behav Physiol* 191:823–836. [CrossRef Medline](#)
- Borst A (2009) *Drosophila's* view on insect vision. *Curr Biol* 19:R36–R47. [CrossRef Medline](#)
- Borst A, Euler T (2011) Seeing things in motion: models, circuits, and mechanisms. *Neuron* 71:974–994. [CrossRef Medline](#)
- Borst A, Egelhaaf M, Haag J (1995) Mechanisms of dendritic integration underlying gain control in fly motion-sensitive interneurons. *J Comput Neurosci* 2:5–18. [CrossRef Medline](#)
- Borst A, Haag J, Reiff DF (2010) Fly motion vision. *Annu Rev Neurosci* 33:49–70. [CrossRef Medline](#)
- Brotz TM, Borst A (1996) Cholinergic and GABAergic receptors on fly tangential cells and their role in visual motion detection. *J Neurophysiol* 76:1786–1799. [Medline](#)
- Clark DA, Bursztyn L, Horowitz MA, Schnitzer MJ, Clandinin TR (2011) Defining the computational structure of the motion detector in *Drosophila*. *Neuron* 70:1165–1177. [CrossRef Medline](#)
- Cleland TA (1996) Inhibitory glutamate receptor channels. *Mol Neurobiol* 13:97–136. [CrossRef Medline](#)
- Courjaret R, Lapied B (2001) Complex intracellular messenger pathways regulate one type of neuronal alpha-bungarotoxin-resistant nicotinic acetylcholine receptors expressed in insect neurosecretory cells (dorsal unpaired median neurons). *Mol Pharmacol* 60:80–91. [Medline](#)
- Dent JA (2010) The evolution of pentameric ligand-gated ion channels. *Adv Exp Med Biol* 683:11–23. [CrossRef Medline](#)
- Egelhaaf M, Borst A, Pils B (1990) The role of GABA in detecting visual motion. *Brain Res* 509:156–160. [CrossRef Medline](#)
- Eichner H, Joesch M, Schnell B, Reiff DF, Borst A (2011) Internal structure of the fly elementary motion detector. *Neuron* 70:1155–1164. [CrossRef Medline](#)
- Fei H, Chow DM, Chen A, Romero-Calderón R, Ong WS, Ackerson LC, Maidment NT, Simpson JH, Frye MA, Krantz DE (2010) Mutation of the *Drosophila* vesicular GABA transporter disrupts visual figure detection. *J Exp Biol* 213:1717–1730. [CrossRef Medline](#)
- Fischbach KF, Dittrich A (1989) The optic lobe of *Drosophila melanogaster*. I. A Golgi analysis of wild-type structure. *Cell Tissue Res* 258:441–475.
- Fotowat H, Gabbiani F (2011) Collision detection as a model for sensory-motor integration. *Annu Rev Neurosci* 34:1–19. [CrossRef Medline](#)
- Gao S, Takemura SY, Ting CY, Huang S, Lu Z, Luan H, Rister J, Thum AS, Yang M, Hong ST, Wang JW, Odenwald WF, White BH, Meinertzhagen IA, Lee CH (2008) The neural substrate of spectral preference in *Drosophila*. *Neuron* 60:328–342. [CrossRef Medline](#)
- Hassenstein B, Reichardt W (1956) Systemtheoretische Analyse der Zeit-, Reihenfolgen- und Vorzeichenbewertung bei der Bewegungsperzeption des Rüsselkäfers *Chlorophanus*. *Z Naturforsch* 11b:513–524.
- Hausen K (1982) Motion sensitive interneurons in the optomotor system of the fly I. The horizontal cells: structure and signals. *Biol Cybernet* 45:143–156. [CrossRef](#)
- Hausen K (1984) The lobula-complex of the fly: structure, function and significance in visual behaviour. In: *Photoreception vision invertebrates*, NATO ASI Series, Vol 74, pp 523–559. New York: Springer.
- Hengstenberg R, Hausen K, Hengstenberg B (1982) The number and structure of giant vertical cells (VS) in the lobula plate of the blowfly *Calliphora erythrocephala*. *J Comp Physiol A Neuroethol Sens Neural Behav Physiol* 149.
- Hiesinger PR, Zhai RG, Zhou Y, Koh TW, Mehta SQ, Schulze KL, Cao Y, Verstreken P, Clandinin TR, Fischbach KF, Meinertzhagen IA, Bellen HJ (2006) Activity-independent prespecification of synaptic partners in the visual map of *Drosophila*. *Curr Biol* 16:1835–1843. [CrossRef Medline](#)
- Homberg U, Heinze S, Pfeiffer K, Kinoshita M, el Jundi B (2011) Central neural coding of sky polarization in insects. *Philos Trans R Soc Lond B Biol Sci* 366:680–687. [CrossRef Medline](#)
- Hosie AM, Aronstein K, Sattelle DB, French-Constant RH (1997) Molecular biology of insect neuronal GABA receptors. *Trends Neurosci* 20:578–583. [CrossRef Medline](#)
- Hotta Y, Benzer S (1970) Genetic dissection of the *Drosophila* nervous system by means of mosaics. *Proc Natl Acad Sci U S A* 67:1156–1163. [CrossRef Medline](#)
- Joesch M, Plett J, Borst A, Reiff DF (2008) Response properties of motion-sensitive visual interneurons in the lobula plate of *Drosophila melanogaster*. *Curr Biol* 18:368–374. [CrossRef Medline](#)
- Joesch M, Schnell B, Raghu SV, Reiff DF, Borst A (2010) ON and OFF pathways in *Drosophila* motion vision. *Nature* 468:300–304. [CrossRef Medline](#)
- Joesch M, Weber F, Eichner H, Borst A (2013) Functional specialization of parallel motion detection circuits in the fly. *J Neurosci* 33:902–905. [CrossRef Medline](#)
- Jones AK, Sattelle DB (2010) Diversity of insect nicotinic acetylcholine receptor subunits. *Adv Exp Med Biol* 683:25–43. [CrossRef Medline](#)
- Karmer K, Tabor R, Egelhaaf M, Krapp HG (2001) Early visual experience and the receptive-field organization of optic flow processing interneurons in the fly motion pathway. *Vis Neurosci* 18:1–8. [CrossRef Medline](#)
- Liu WW, Wilson RI (2013) Glutamate is an inhibitory neurotransmitter in the *Drosophila* olfactory system. *Proc Natl Acad Sci U S A* 110:10294–10299. [CrossRef Medline](#)
- Löhr R, Godenschwege T, Buchner E, Prokop A (2002) Compartmentalization of central neurons in *Drosophila*: a new strategy of mosaic analysis reveals localization of presynaptic sites to specific segments of neurites. *J Neurosci* 22:10357–10367. [Medline](#)
- Luan H, Peabody NC, Vinson CR, White BH (2006) Refined spatial manipulation of neuronal function by combinatorial restriction of transgene expression. *Neuron* 52:425–436. [CrossRef Medline](#)
- Maimon G, Straw AD, Dickinson MH (2010) Active flight increases the gain of visual motion processing in *Drosophila*. *Nat Neurosci* 13:393–399. [CrossRef Medline](#)
- Maisak MS, Haag J, Ammer G, Serbe E, Meier M, Leonhardt A, Schilling T, Bahl A, Rubin GM, Nern A, Dickson BJ, Reiff DF, Hopp E, Borst A (2013) A directional tuning map of *Drosophila* elementary motion detectors. *Nature* 500:212–216. [CrossRef Medline](#)
- Mattis J, Tye KM, Ferenczi EA, Ramakrishnan C, O'Shea DJ, Prakash R, Gunaydin LA, Hyun M, Fenno LE, Gradinaru V, Yizhar O, Deisseroth K (2012) Principles for applying optogenetic tools derived from direct comparative analysis of microbial opsins. *Nat Methods* 9:159–172. [Medline](#)
- Millar NS, Lansdell SJ (2010) Characterisation of insect nicotinic acetylcholine receptors by heterologous expression. *Adv Exp Med Biol* 683:65–73. [CrossRef Medline](#)
- Nagel G, Brauner M, Liewald JF, Adeishvili N, Bamberg E, Gottschalk A (2005) Light activation of channelrhodopsin-2 in excitable cells of *Caenorhabditis elegans* triggers rapid behavioral responses. *Curr Biol* 15:2279–2284. [CrossRef Medline](#)

- Pfeiffer BD, Jenett A, Hammonds AS, Ngo TT, Misra S, Murphy C, Scully A, Carlson JW, Wan KH, Laverty TR, Mungall C, Svirskas R, Kadonaga JT, Doe CQ, Eisen MB, Celniker SE, Rubin GM (2008) Tools for neuroanatomy and neurogenetics in *Drosophila*. *Proc Natl Acad Sci U S A* 105:9715–9720. [CrossRef Medline](#)
- Pfeiffer-Linn C, Glantz RM (1989) Acetylcholine and GABA mediate opposing actions on neuronal chloride channels in crayfish. *Science* 245:1249–1251. [CrossRef Medline](#)
- Pulver SR, Pashkovski SL, Hornstein NJ, Garrity PA, Griffith LC (2009) Temporal dynamics of neuronal activation by Channelrhodopsin-2 and TRPA1 determine behavioral output in *Drosophila* larvae. *J Neurophysiol* 101:3075–3088. [CrossRef Medline](#)
- Raghu SV, Borst A (2011) Candidate glutamatergic neurons in the visual system of *Drosophila*. *PLoS One* 6:e19472. [CrossRef Medline](#)
- Raghu SV, Joesch M, Borst A, Reiff DF (2007) Synaptic organization of lobula plate tangential cells in *Drosophila*: gamma-aminobutyric acid receptors and chemical release sites. *J Comp Neurol* 502:598–610. [CrossRef Medline](#)
- Raghu SV, Joesch M, Sigris SJ, Borst A, Reiff DF (2009) Synaptic organization of lobula plate tangential cells in *Drosophila*: D α 7 cholinergic receptors. *J Neurogenet* 23:200–209. [CrossRef Medline](#)
- Raghu SV, Reiff DF, Borst A (2011) Neurons with cholinergic phenotype in the visual system of *Drosophila*. *J Comp Neurol* 519:162–176. [CrossRef Medline](#)
- Raghu SV, Claussen J, Borst A (2013) Neurons with GABAergic phenotype in the visual system of *Drosophila*. *J Comp Neurol* 521:252–265. [CrossRef Medline](#)
- Rister J, Pauls D, Schnell B, Ting CY, Lee CH, Sinakevitch I, Morante J, Strausfeld NJ, Ito K, Heisenberg M (2007) Dissection of the peripheral motion channel in the visual system of *Drosophila melanogaster*. *Neuron* 56:155–170. [CrossRef Medline](#)
- Robinson IM, Ranjan R, Schwarz TL (2002) Synaptotagmins I and IV promote transmitter release independently of Ca(2+) binding in the C(2)A domain. *Nature* 418:336–340. [CrossRef Medline](#)
- Rohrbough J, Broadie K (2002) Electrophysiological analysis of synaptic transmission in central neurons of *Drosophila* larvae. *J Neurophysiol* 88:847–860. [Medline](#)
- Sattelle DB, Jones AK, Sattelle BM, Matsuda K, Reenan R, Biggin PC (2005) Edit, cut and paste in the nicotinic acetylcholine receptor gene family of *Drosophila melanogaster*. *Bioessays* 27:366–376. [CrossRef Medline](#)
- Schmid A, Bülthoff H (1988) Using neuropharmacology to distinguish between excitatory and inhibitory movement detection mechanisms in the fly *Calliphora erythrocephala*. *Biol Cybernet* 59:71–80. [CrossRef](#)
- Schnell B, Raghu SV, Nern A, Borst A (2012) Columnar cells necessary for motion responses of wide-field visual interneurons in *Drosophila*. *J Comp Physiol A* 198:389–395. [CrossRef Medline](#)
- Silies M, Gohl DM, Fisher YE, Freifeld L, Clark DA, Clandinin TR (2013) Modular use of peripheral input channels tunes motion-detecting circuitry. *Neuron* 79:111–127. [CrossRef Medline](#)
- Sinakevitch I, Strausfeld NJ (2004) Chemical neuroanatomy of the fly's movement detection pathway. *J Comp Neurol* 468:6–23. [CrossRef Medline](#)
- Single S, Haag J, Borst A (1997) Dendritic computation of direction selectivity and gain control in visual interneurons. *J Neurosci* 17:6023–6030. [Medline](#)
- Strausfeld NJ, Lee JK (1991) Neuronal basis for parallel visual processing in the fly. *Vis Neurosci* 7:13–33. [CrossRef Medline](#)
- Strausfeld NJ, Kong A, Milde JJ, Gilbert C, Ramaiah L (1995) Oculomotor control in calliphorid flies: GABAergic organization in heterolateral inhibitory pathways. *J Comp Neurol* 361:298–320. [CrossRef Medline](#)
- Takagawa K, Salvaterra P (1996) Analysis of choline acetyltransferase protein in temperature sensitive mutant flies using newly generated monoclonal antibody. *Neurosci Res* 24:237–243. [CrossRef Medline](#)
- Takemura SY, Bharioke A, Lu Z, Nern A, Vitaladevuni S, Rivlin PK, Katz WT, Olbris DJ, Plaza SM, Winston P, Zhao T, Horne JA, Fetter RD, Takemura S, Blazek K, Chang LA, Ogundeyi O, Saunders MA, Shapiro V, Sigmund C, et al. (2013) A visual motion detection circuit suggested by *Drosophila* connectomics. *Nature* 500:175–181. [CrossRef Medline](#)
- Takemura SY, Karuppudurai T, Ting CY, Lu Z, Lee CH, Meinertzhagen IA (2011) Cholinergic circuits integrate neighboring visual signals in a *Drosophila* motion detection pathway. *Curr Biol* 21:2077–2084. [CrossRef Medline](#)
- Thany SH (2010) Electrophysiological studies and pharmacological properties of insect native nicotinic acetylcholine receptors. *Adv Exp Med Biol* 683:53–63. [CrossRef Medline](#)
- Thany SH, Lenaers G, Raymond-Delpech V, Sattelle DB, Lapied B (2007) Exploring the pharmacological properties of insect nicotinic acetylcholine receptors. *Trends Pharmacol Sci* 28:14–22. [CrossRef Medline](#)
- Tuthill JC, Nern A, Holtz SL, Rubin GM, Reiser MB (2013) Contributions of the 12 neuron classes in the fly lamina to motion vision. *Neuron* 79:128–140. [CrossRef Medline](#)

2.5 NEURAL MECHANISMS FOR *drosophila* CONTRAST VISION

This paper (Bahl et al., 2015) investigates the cellular mechanisms underlying contrast vision in *Drosophila*. It was published in *Neuron* in December 2015.

Summary

Similar to humans, flies are susceptible to some visual illusions, like contrast motion illusions. With a combination of transgenic manipulations and behavioral readout we discovered a processing stream responsible for the computation of local contrast differences. A first experiment revealed that flies lacking local motion detectors T₄ and T₅ were still susceptible to contrast motion illusions while they failed to detect visual motion. An extensive genetic screen identified two neurons, Mi₁ and Tm₃, to be involved in the computation of contrast. Blocking their synaptic output rendered both, walking flies as well as lobula plate tangential cells insensitive to contrast stimuli. Hence, we provided evidence a visual processing stream, working in parallel to the motion vision pathway. We further showed that the two systems share some elements and both converge onto lobula plate tangential cells.

The following authors contributed to this work:

Armin Bahl, Etienn Serbe, **Matthias Meier**, Georg Ammer, and Alexander Borst

Author contribution

Armin Bahl and Alexander Borst designed the study. Etienne Serbe and **Matthias Meier** performed electrophysiological recordings. Georg Ammer provided the Mi₁, Tm₃, and Mi₁/Tm₃-Gal₄ lines and did the immunostainings. Armin Bahl built the behavioral setup, programmed the visual stimuli, performed the behavioral experiments, and analyzed the data. Armin Bahl wrote the paper with help from the other authors.

Neural Mechanisms for *Drosophila* Contrast Vision

Highlights

- Flies are susceptible to contrast illusions in the same way as human observers
- Contrast and motion computations are carried out in parallel pathways
- Medulla cells Mi1 and Tm3 form a center-surround antagonism for contrast computation
- Signals from the motion and contrast pathways converge again in the lobula plate

Authors

Armin Bahl, Etienne Serbe, Matthias Meier, Georg Ammer, Alexander Borst

Correspondence

arminbahl@fas.harvard.edu

In Brief

Bahl et al. employ optical illusions in behavioral experiments in *Drosophila* to investigate mechanisms and neuronal correlates of spatial contrast computation. They find that spatial contrast and motion cues are computed largely in parallel and that both pathways eventually converge.

Neural Mechanisms for *Drosophila* Contrast Vision

Armin Bahl,^{1,2,*} Etienne Serbe,¹ Matthias Meier,¹ Georg Ammer,¹ and Alexander Borst¹

¹Max Planck Institute of Neurobiology, Am Klopferspitz 18, 82152 Martinsried, Germany

²Present address: Department of Molecular and Cell Biology, Harvard University, 16 Divinity Avenue, Cambridge, MA 02138, USA

*Correspondence: arminbahl@fas.harvard.edu

<http://dx.doi.org/10.1016/j.neuron.2015.11.004>

SUMMARY

Spatial contrast, the difference in adjacent luminance values, provides information about objects, textures, and motion and supports diverse visual behaviors. Contrast computation is therefore an essential element of visual processing. The underlying mechanisms, however, are poorly understood. In human psychophysics, contrast illusions are means to explore such computations, but humans offer limited experimental access. Via behavioral experiments in *Drosophila*, we find that flies are also susceptible to contrast illusions. Using genetic silencing techniques, electrophysiology, and modeling, we systematically dissect the mechanisms and neuronal correlates underlying the behavior. Our results indicate that spatial contrast computation involves lateral inhibition within the same pathway that computes motion of luminance increments (ON pathway). Yet motion-blind flies, in which we silenced downstream motion-sensitive neurons needed for optomotor behavior, have fully intact contrast responses. In conclusion, spatial contrast and motion cues are first computed by overlapping neuronal circuits which subsequently feed into parallel visual processing streams.

INTRODUCTION

Computation of spatial contrast, the local difference in adjacent luminance values, allows animals to distinguish between figure and ground, to detect edges, and to visually adapt to the dynamic range of the current visual scene. Despite the importance of such computations for a wide range of visual behaviors, the mechanisms underlying spatial contrast computation are not well-understood in any organism. Optical illusions elicit visual perceptions that differ from physical reality and can serve as a tool in psychophysical experiments to explore how the brain computes. For example, when a gray bar of uniform luminance is embedded in a gradient background, humans perceive a brightness gradient within the bar, which indicates that human brightness estimation is based on relative rather than absolute luminance (Adelson, 2000). Such illusions are static and require the experimental subject to report its perception. Hence, they are difficult to use in other species. Motion illusions, however,

often elicit behavioral responses and can be transferred to simple model organisms (Bülthoff and Götz, 1979; Eichner et al., 2011; Tuthill et al., 2011). A motion illusion based on spatial contrast computation, the contrast motion illusion, has recently been described in human psychophysics (Shapiro and Hamburger, 2007). Here, several dark stripes are embedded in a gradient background which is dark on the left and bright on the right end. When all stripes brighten simultaneously, humans report illusory motion to the right (see [Movie S1](#) available online). The contrast motion illusion is thought to rest on similar principles as another type of contrast illusion known as the single-field contrast asynchrony illusion (Shapiro et al., 2004): A single stripe is embedded in a dark or in a bright background. When an identical sinusoidal luminance change is applied to the stripe, humans report that the modulations are out of phase for the different background conditions ([Movie S2](#)). This indicates that humans perceive temporal variations of spatial contrast rather than luminance. Responses to such contrast stimuli cannot be explained by classical models of motion vision based on spatio-temporal correlation of luminance (Shapiro et al., 2005). Alternatively, it was hypothesized that rectified center-surround filters compute spatial contrast and further integrate such cues in higher visual centers. However, detailed systematic dissections of the computational mechanisms are missing, and very little is known about potential neuronal circuits involved.

In order to investigate visual processing at the cellular level, humans offer limited experimental access. In contrast, other species, such as the fruit fly *Drosophila melanogaster*, provide various tools for such a purpose. *Drosophila* has a set of innate and robust visual behaviors and can be genetically modified. The anatomy and connectivity of the visual system is well-known (Fischbach and Dittrich, 1989; Takemura et al., 2013) and is accessible via electrophysiology (Behnia et al., 2014; Joesch et al., 2008). The visual system is arranged in a retinotopic manner and forms several neuropils for visual processing ([Figure 1A](#)). Photoreceptor input from R1–R6 provides direct or indirect signals to lamina neurons L1–L5 ([Figures 1B and S1A](#)). Subsequently, L1/L5 and L2/L3/L4 form separate visual pathways specialized for motion computation of luminance increments (ON pathway) and decrements (OFF pathway), respectively (Clark et al., 2011; Eichner et al., 2011; Joesch et al., 2010; 2013; Maisak et al., 2013; Meier et al., 2014; Strother et al., 2014). Connectomics has revealed potential components of both pathways, namely Mi1 and Tm3 within the ON pathway and Tm1, Tm2, Tm4, and Tm9 within the OFF pathway (Shinomiya et al., 2014; Takemura et al., 2013). Neurons in the two pathways converge onto T4 and T5 neurons (Bausenwein et al., 1992), which are the first direction-selective elements in

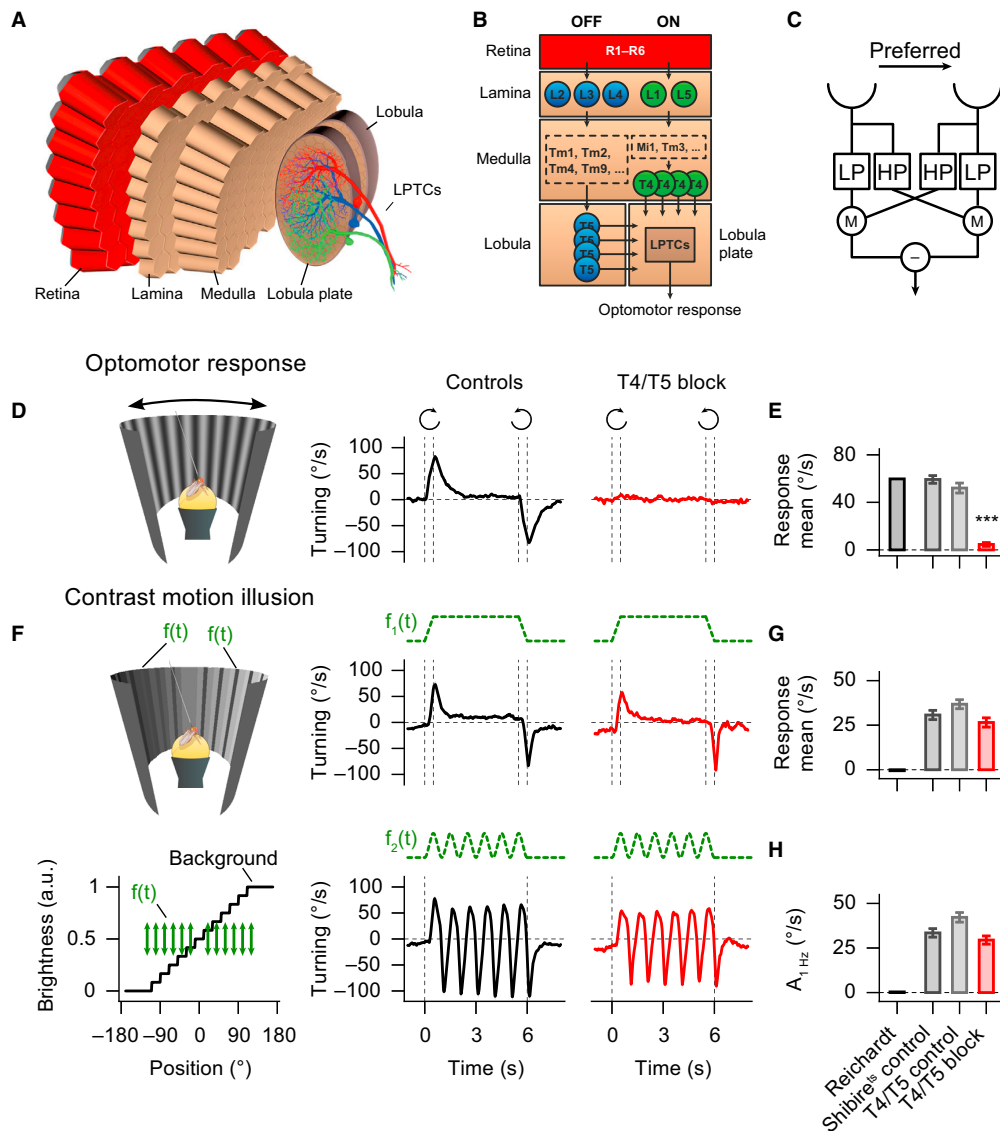


Figure 1. Control and Motion-blind Flies Respond to Contrast Motion Illusions

(A and B) Schematic of the fly's optic lobe and its cellular composition within the ON (green) and OFF (blue) pathways.

(C) Hassenstein-Reichardt detector with preferred direction to the right.

(D) Experiment with full-field moving sine-grating. Motion direction and stimulus on- and offset are illustrated by circular arrows and vertical dashed lines.

(E) Quantification of the optomotor response (response to clockwise motion minus that to counterclockwise motion divided by two; averaged between 0.1 and 1.1 s after stimulus onset) of the Hassenstein-Reichardt detector simulation and of the experimental groups.

(F) Contrast motion illusion. Several vertical stripes are embedded in a stepped luminance gradient background (black trace in bottom part) and simultaneously change luminance according to $f_1(t)$ or $f_2(t)$ (green arrows and green dashed time traces).

(G) Quantification of the response to the contrast motion illusion with stripe luminance dynamics according to $f_1(t)$ (response to luminance increment minus that to luminance decrement divided by two; averaged between 0.1–1.1 s after stimulus onset) of the Hassenstein-Reichardt detector simulation and of the experimental groups.

(H) Quantification of the response for luminance dynamics according to $f_2(t)$ (1 Hz amplitude of the Fourier-transformed response during stimulation) of the Hassenstein-Reichardt detector simulation and of the experimental groups.

(legend continued on next page)

the fly visual system and which are selective for motion of brightness increments and decrements, respectively (Maisak et al., 2013). Mi1 and Tm3 have been proposed to provide temporally different and spatially offset inputs to the T4 dendrite, giving rise to its direction selectivity (Behnia et al., 2014; Takemura et al., 2013). Furthermore, Mi1 and Tm3 were recently shown to also be functionally necessary for motion computation of brightness increments (Ammer et al., 2015). Eventually, T4 and T5 neurons converge onto lobula plate tangential cells (Figures S1B and S1C) and render vertical system cells and horizontal system cells direction-selective for motion along the vertical and horizontal axis, respectively. Genetic silencing of T4 and T5 neurons abolishes direction-selective responses in lobula plate tangential cells (Schnell et al., 2012). Moreover, in behavioral experiments, flies are motion-blind and no longer show an optomotor response (Bahl et al., 2013). Various aspects of fly motion vision can be modeled by the Hassenstein-Reichardt detector (Hassenstein and Reichardt, 1956). In this model, luminance signals from two neighboring ommatidia are differently filtered in time and subsequently multiplied. Subtracting the output of a mirror-symmetric detector subunit leads to fully opponent direction-selective responses (Figure 1C). Computation of visual cues other than motion, such as color (Morante and Desplan, 2008) or spatial contrast, are less explored in flies.

In this paper, we employ contrast illusions as a tool to study spatial contrast computation in *Drosophila*. We use tethered flies walking on an air-suspended ball in a virtual environment. Throughout the paper, we measure fly turning speed in response to various kinds of visual stimuli, which allows quantitative comparisons of the behavior and systematic dissections of the underlying computational mechanisms. In order to identify neuronal correlates, we use the GAL4-UAS system (Brand and Perrimon, 1993) to genetically target specific subsets of neurons for silencing synaptic transmission via temperature-sensitive shibire (shibire^{ts}) (Kitamoto, 2001; Pfeiffer et al., 2012).

RESULTS

Flies Respond to Contrast Motion Illusions

In a first set of control experiments, we tested behavioral performance to full-field sine-grating motion (Figure 1D). As expected, control flies responded with a robust optomotor response, a behavior predicted by the Hassenstein-Reichardt detector (Figures 1D and 1E). Next, we tested the contrast motion illusion as used in human psychophysics (Shapiro and Hamburger, 2007) (Figure 1F): several stripes are embedded in a stepped luminance gradient. We applied identical luminance dynamics to the stripes. The stimulus is designed such that luminance change is symmetric around the fly and, therefore, potential directed turning responses toward luminance change average out. Moreover, the local stripe environment is symmetric in luminance, and hence pairwise local comparisons, as performed by the Hassenstein-Reichardt detector, cancel out as well. We

tested two luminance dynamics for the stripes: first, stripe luminance increased, remained bright for a few seconds, and then decreased again. Second, stripe luminance oscillated sinusoidally at 1 Hz. As expected, the Hassenstein-Reichardt detector predicted no turning response for both stimuli (Figures 1G and 1H). However, control flies robustly responded to the contrast motion illusion: when the background was dark on the left and bright on the right end, a luminance increase elicited turning to the right and a luminance decrease turning to the left. For the 1 Hz luminance oscillations, control flies responded with a robust 1 Hz oscillatory turning response. Notably, response strengths were similar to those observed for the optomotor response, and turning directions matched the direction of illusory motion reported by human observers (Shapiro and Hamburger, 2007).

Since the observed responses to the contrast motion illusion cannot be explained by the Hassenstein-Reichardt detector, we developed two alternative hypotheses which could explain the result. First, the behavior might be a side effect of potentially unexplored interactions within the motion pathway. Second, it might be controlled by an independent visual pathway dedicated to the computation of spatial contrast. In order to test both hypotheses, we used a driver line which selectively labels T4 and T5 neurons, allowing us to silence synaptic transmission from these cells via shibire^{ts}. T4/T5 block flies are completely motion-blind and lack an optomotor response (Bahl et al., 2013) (Figures 1D and 1E). Yet, when we tested the contrast motion illusion, such flies responded with exactly the same magnitude and direction as control flies (Figures 1F–1H). In conclusion, spatial contrast and motion computations seem to be carried out in parallel visual pathways.

Flies Respond to Single-Field Contrast Asynchronies

In order to gain a better understanding of the computational mechanisms underlying spatial contrast computation in the fly brain, we further investigated behavioral responses to another type of contrast illusion known as the single-field contrast asynchrony illusion (Shapiro et al., 2004). In particular, this stimulus allows us to investigate whether flies respond to signed or unsigned (absolute) spatial contrast, which is not possible with the global contrast motion illusion. We presented flies with a single vertical stripe in the right visual field and modulated the stripe luminance sinusoidally at 1 Hz (Figure 2A). Such a stimulus contains two components, flicker of luminance and flicker of relative spatial luminance (spatial contrast flicker). The luminance flicker dynamics remain independent of background light levels but the spatial contrast flicker is background-dependent. To explore responses to spatial contrast flicker, we varied background light levels. When the stripe was presented against a dark background, control and T4/T5 block flies responded with 1 Hz turning speed oscillations of large amplitude with the same phase as the stimulus (Figures 2B and 2C). In contrast, when the stripe was presented against a bright background, control and T4/T5 block flies still responded with 1 Hz turning speed

Data represent mean \pm SEM with $n = 12$ – 13 flies per group. p values based on a two-sided Welch's t test, comparing T4/T5 block flies with both control groups (** $p < 0.001$; $p = 0.26$ in G; $p = 0.25$ in H). Detailed statistics in Table S1A. Hassenstein-Reichardt detector simulation result in black, shibire^{ts} flies in dark gray, T4/T5 control flies in light gray and T4/T5 block flies. Raw time traces for control flies (black) in (D) and (F) are pooled from both control groups.

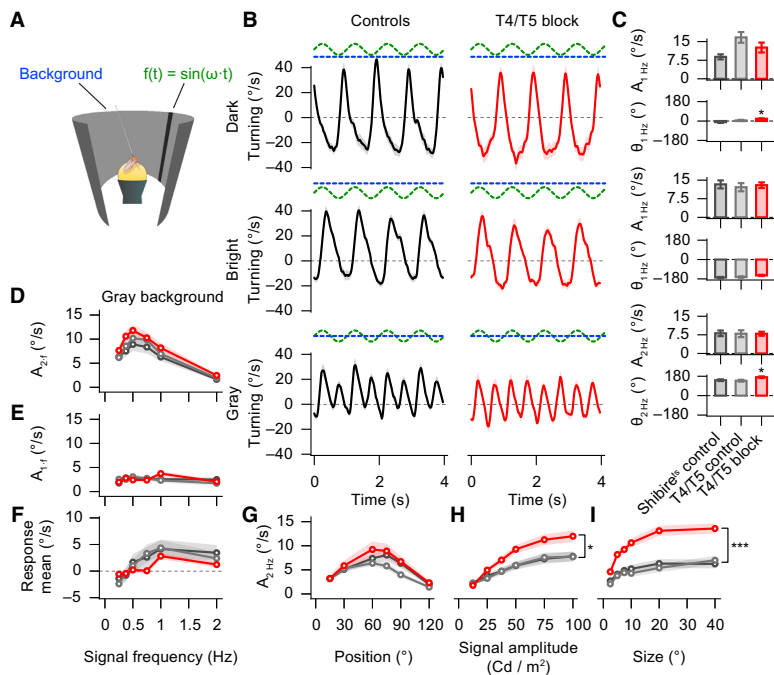


Figure 2. Control and Motion-Blind Flies Respond to Single-Field Contrast Asynchrony Illusions

(A) A single nonmoving vertical stripe on the right side of the fly flickers sinusoidally in luminance with frequency ω on a uniform background.

(B) Responses for 1 Hz stripe flicker (identical in all conditions; green dashed lines) on three different backgrounds (dark, bright, and gray; blue dashed lines).

(C) Quantification of amplitude A and phase Θ of the 1 Hz or 2 Hz response components.

(D–F) Quantification of the response amplitudes ($2 \cdot f$ and $1 \cdot f$ components) and the response mean to stripes flickering at different frequencies on a gray background.

(G–I) Quantification of 2 Hz amplitude response components to a 1 Hz flickering stripe on a gray background when varying stripe position, signal amplitude, or size. All stimuli lasted for 10 s, the last 9 s were analyzed. Only the last 4 s are illustrated in (B).

Data represent mean \pm SEM with $n = 12$ –14 flies per group. p values based on a two-sided Welch's t test, comparing T4/T5 block flies with both control groups ($*p < 0.05$; $***p < 0.001$; $p = 0.18, 0.69, \text{ and } 0.99$ for response amplitudes for the different background conditions, respectively, and $p = 0.10$ for response phase for the bright background in C). Detailed statistics in Table S1B. Shibire^{ts} flies in dark gray, T4/T5 control flies in light gray, T4/T5 block flies in red. Raw time traces for control flies (black) in (B) are pooled from both control groups.

oscillations but responses were shifted in phase by 180° . Interestingly, an intermediate gray background led to 2 Hz turning speed oscillations, following the 2 Hz absolute spatial contrast dynamics of the flickering stripe. In summary, the observed behaviors rely on the computation of unsigned spatial contrast and are largely independent of T4 and T5 neurons, both in terms of amplitude and phase. These findings provide further evidence that spatial contrast computations are carried out in a T4/T5-independent visual circuit.

We further characterized the response oscillation amplitude to different parameters of a flickering stripe on a gray background (Figures 2D–2I). We first varied stimulus frequency. For all tested frequencies, control and T4/T5 block flies responded with turning speed oscillations of the frequency of the spatial contrast flicker ($2 \cdot f$ component of the response), with the strongest response for 0.5 Hz signals (Figure 2D). The $1 \cdot f$ response component, corresponding to the luminance dynamics, however was small (Figure 2E) and response averages over time were close to zero (Figure 2F). The latter result is in contrast to previous findings which suggested that flickering stripes elicit strong directed turning toward the stimulus (Bahl et al., 2013; Pick, 1974). We further characterized responses as function of azimuthal position, signal amplitude, and size. For both control and T4/T5 block flies, responses were strongest for stripes located at $\sim 70^\circ$ (Figure 2G), became stronger with increasing signal amplitude (Figure 2H), and increased for stripe sizes up to 20° , after which the response saturated (Figure 2I).

The amount of luminance flicker increases with stripe size. Spatial contrast flicker however only occurs at the boundary of the flickering stripe and remains independent of size once the stripe exceeds the receptive field of the underlying neuronal elements. Interestingly, T4/T5 block flies responded stronger than control flies for large signal amplitudes and for large stripe sizes (Figures 2H and 2I). This suggests that luminance flicker, analyzed via T4/T5 cells, can reduce the responsiveness of the circuit performing spatial contrast computation.

Receptive Field Properties of Spatial Contrast Computation

In further experiments, we wanted to better characterize the spatial receptive field properties of the contrast response. To this end, we used counterphase flicker (Movie S3) which provide contrast flicker covering a large extent of the visual field. Such stimuli do not contain any net-motion and the average luminance in the area of stimulation remains constant. Hence, counterphase flicker allow characterization of the contrast system in isolation. We presented stimuli within a unilateral circular window on the right side of the fly and varied spatial frequency and orientation (Figure 3A).

As a control experiment, we first characterized responses to moving sine-gratings. As expected, control flies turned right and left for front-to-back and back-to-front motion, respectively, with comparable absolute amplitudes (Figure 3B). When we tested different spatial frequencies, motion responses in control flies decreased for high spatial frequencies and even inverted for

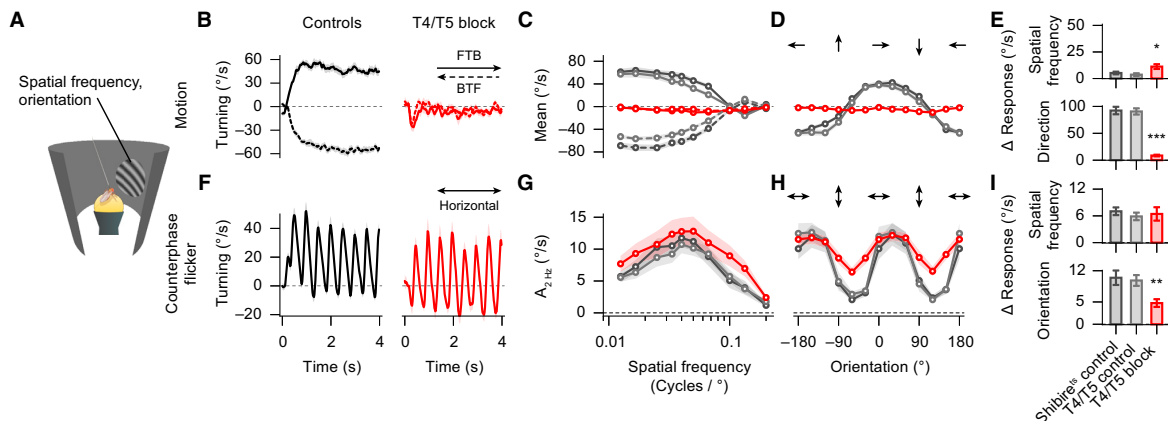


Figure 3. Characterization of Receptive Field Properties of Motion and Contrast Systems

(A) A circular window is shown on the right side of the fly in which a sine-grating moves or flickers in counterphase with different spatial frequencies or orientations. (B) Example traces for horizontal front-to-back motion (FTB; solid lines) and back-to-front motion (BTF; dashed lines). (C and D) Spatial frequency and orientation tuning for motion. (E) Quantification of spatial frequency tuning (difference between maximal absolute response and that for the smallest spatial frequency) and direction-selectivity (difference between maximal absolute response and that of motion in the opposite direction). (F) Example traces for the counterphase flicker stimulus. (G and H) Spatial frequency and orientation tuning curves of the 2 Hz response component. (I) Quantification of spatial frequency tuning (difference between maximal absolute response and that for the smallest spatial frequency) and orientation tuning (difference between maximal absolute response and that for counterphase flicker in perpendicular orientation). All stimuli lasted for 10 s, the last 9 s were analyzed, and the first 4 s are illustrated in (B) and (FF). Data represent mean \pm SEM with $n = 12$ –14 flies per group. p values based on a two-sided Welch's t test, comparing T4/T5 block flies with both control groups (* $p < 0.05$; ** $p < 0.01$; *** $p < 0.001$; $p = 0.75$ for the spatial frequency tuning in I). Detailed statistics in [Table S1C](#). Shibre^{ts} flies in dark gray, T4/T5 control flies in light gray, T4/T5 block flies in red. Raw time traces for control flies (black) in (B) and (F) are pooled from both control groups.

spatial frequencies larger than 0.1 cycles per degree ($\lambda = 10^\circ$) but no tuning was apparent for low spatial frequencies (Figures 3C and 3E). The response reduction and inversion for high spatial frequencies is due to the resolution of the *Drosophila* eye ($\sim 5^\circ$) (Götz, 1964). Next, we presented grating motion along different axes and quantified direction-selectivity (Figures 3D and 3E). As expected, control flies were able to discriminate motion direction well and did not respond with horizontal turning to motion along the vertical axis. Irrespective of spatial frequency or direction, T4/T5 block flies did not respond to any of the motion stimuli (Figures 3B–3E).

We next tested counterphase flicker. The luminance at each point was modulated at 1 Hz, resulting in a 2 Hz modulation of the absolute spatial contrast (Movie S3). If flies follow changes in absolute spatial contrast, they should respond with a 2 Hz oscillation in turning speed. Indeed, this was the case for both control and T4/T5 block flies (Figure 3F). Quantification of the response to different spatial frequencies revealed a clear tuning peak at a spatial frequency of 0.5 cycles per degree ($\lambda = 20^\circ$) (Figures 3G and 3I). Such band-pass properties are reminiscent of a spatial antagonism involving center-surround receptive fields, which indicates that lateral inhibition is involved in the computation of spatial contrast. In order to characterize the receptive field isotropy of the contrast system, we quantified turning responses to differently oriented counterphase flicker (Figures 3H and 3I). We found that responses of control and T4/T5 block flies were strongly orientation-tuned. Interestingly, counterphase flicker

along the vertical axis also elicited small responses and the orientation tuning curves were shifted by $\sim 30^\circ$. This shift corresponds to a 30° backward-tilted pattern and is probably due to the position of the flies which walk slightly upward on the ball.

Responses to orientations perpendicular to the preferred orientation were almost zero for control flies but still present in T4/T5 block flies. It is known that counterphase flicker elicits depolarization in T4/T5 neurons (Maisak et al., 2013). T4 and T5 cells then target lobula plate tangential cells as well as lobula plate intrinsic inhibitory interneurons (Mauss et al., 2015). If the contrast and motion pathways converge in later processing stages, the latter cells might then actively suppress contrast responses along the vertical axis, improving counterphase flicker orientation tuning in control flies.

In summary, the observed spatial frequency and orientation tuning properties suggest a mechanism for contrast computation which involves lateral inhibition. T4 and T5 neurons are not required for such computations.

Identification of Neuronal Elements of Contrast Computation

Having found that unilateral counterphase flicker elicit robust contrast responses, we next used this stimulus to screen for neuronal elements underlying contrast computation. To maximize stimulus strength, we presented a vertically oriented sine-grating in a rectangular window on the right side of the fly. The sine-grating either moved front-to-back or back-to-front along

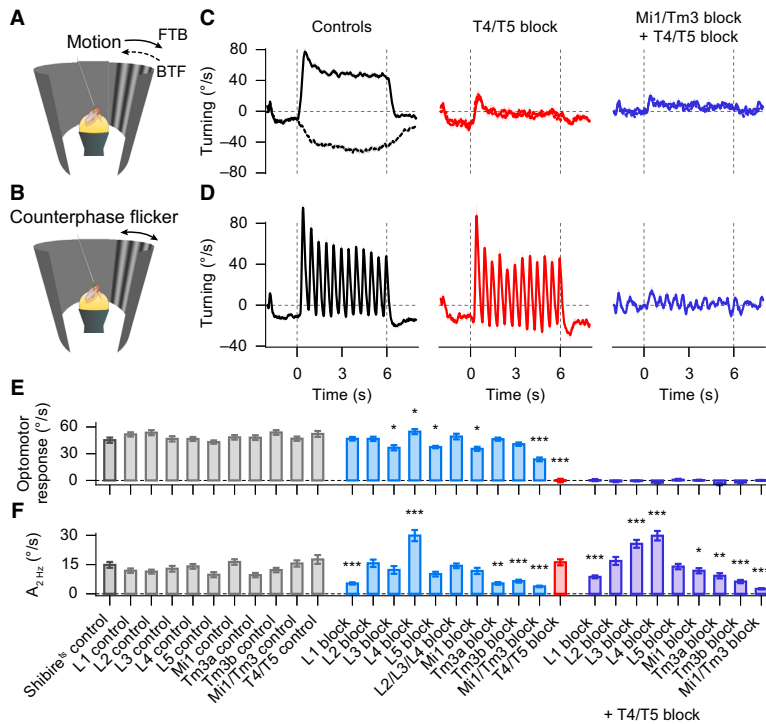


Figure 4. Mi1 and Tm3 Neurons Are Key Neuronal Elements of Contrast Computation

(A and B) A vertical oriented sine-grating either moves front-to-back (FTB), back-to-front (BTF; dashed lines), or flickers in counterphase in a rectangular window on the right side of the fly.

(C and D) Example traces of control, T4/T5 block, and combined Mi1/Tm3 block + T4/T5 block flies. Vertical gray dashed lines indicate onset and offset of the stimulus.

(E) Quantification of the optomotor response (response to front-to-back motion minus response to back-to-front motion divided by two; averaged from 2 to 6 s).

(F) Quantification of the response to counterphase flicker (2 Hz response amplitude component of the Fourier-transformed signal from 2 to 6 s).

Data represent mean \pm SEM with $n = 14$ –19 flies per group. p values based on a two-sided Welch's t test, comparing the group of block flies with respective control groups (for example, L1 block with L1 control and shibire^{ts} control; groups with combined lamina or medulla block + T4/T5 block (right side) were compared only to the T4/T5 block group; * $p < 0.05$; ** $p < 0.01$; *** $p < 0.001$). Detailed statistics in [Tables S4](#) and [S5](#). Expression patterns and list of genotypes in [Figures S2A](#)–[S2C](#). Shibire^{ts} control flies in dark gray, Gal4 control flies in light gray, lamina and medulla block flies in blue, T4/T5 block flies in red, and combined lamina or medulla block + T4/T5 block flies in violet. Raw time traces for control flies (black) in (C) and (D) are pooled from shibire^{ts} control, T4/T5 control, and Mi1/Tm3 control flies. See [Figures 1A](#), [1B](#), and [S1A](#) for schematics of cell types and locations.

the horizontal axis with a temporal frequency of 1 Hz or it flickered in counterphase, providing a 2 Hz spatial contrast flicker ([Figures 4A](#) and [4B](#)). As expected, control flies followed the direction of stimulus motion ([Figure 4C](#)) and responded robustly to counterphase flicker with strong 2 Hz oscillatory turning responses ([Figure 4D](#)), as previously described ([Figures 3B](#) and [3F](#)). We tested ten different Gal4 driver lines, labeling cells in the lamina, medulla, and lobula ([Figures S2A](#) and [S2B](#)), and quantified optomotor behavior ([Figure 4E](#)) and responses to counterphase flicker ([Figure 4F](#)) for control and block flies. All flies had a comparable walking speed of around 1 cm/s ([Figure S2D](#)).

First, we tested the optomotor response in flies with silenced lamina neurons L1–L5. Surprisingly, we did not find response reductions when blocking L1 or L2. This can be attributed to the fact that the ON or OFF motion pathways receive redundant signals when stimulated with sine-grating motion ([Joesch et al., 2010](#); [Silies et al., 2013](#); [Tuthill et al., 2013](#)). Nevertheless, we found small but significant decreases when blocking L3 or L5 and an unexpected mild increase in the response when silencing L4. Next, we quantified responses to the counterphase flicker: Blocking output of L1 led to a strong reduction of the contrast response. Blocking L2, L3, or L5 however showed no significant phenotypes. Notably, silencing L4 almost doubled the response strength, suggesting that L4 not only modulates elements for motion computation ([Meier et al., 2014](#)), but also affects the contrast computation circuit.

These experiments indicated that the ON pathway seems to be the key player for contrast computation. In order to test for its sufficiency, we next silenced the output of L2, L3, and L4 at the same time, abolishing all input channels into the OFF pathway. We did not find a reduction of the contrast response even though further analysis indicated that the triple lamina block is functional ([Figure S3](#)). This finding provides evidence that the ON pathway alone can compute spatial contrast.

We next tested medulla interneurons Mi1 and Tm3 which are known to be the major postsynaptic elements to L1 ([Takemura et al., 2013](#)). We first tested motion responses: Mi1 block flies showed a mild, but significant, optomotor response reduction. In contrast, using two different driver lines for Tm3, we found that silencing Tm3 output did not alter the response. Blocking the output of Mi1 and Tm3 together, using a driver line which labels both neuron types (revealed by stochastic GFP-labeling; [Figures S2A](#) and [S2C](#)), led to a strong response reduction of $\sim 50\%$ compared to controls. Because L1-silenced flies did not show such a phenotype, this finding suggests that further lamina input to Mi1 or Tm3 play a role in motion computation, such as L3 ([Silies et al., 2013](#); [Takemura et al., 2013](#)). As expected, silencing T4 and T5 neurons abolished optomotor behavior completely ([Figures 4C](#) and [4E](#)).

When testing counterphase flicker, Mi1-silenced flies showed a response reduction tendency, and blocking Tm3 output led to a strong response reduction comparable to that found in L1-silenced flies. Since blocking Tm3 left some residual response

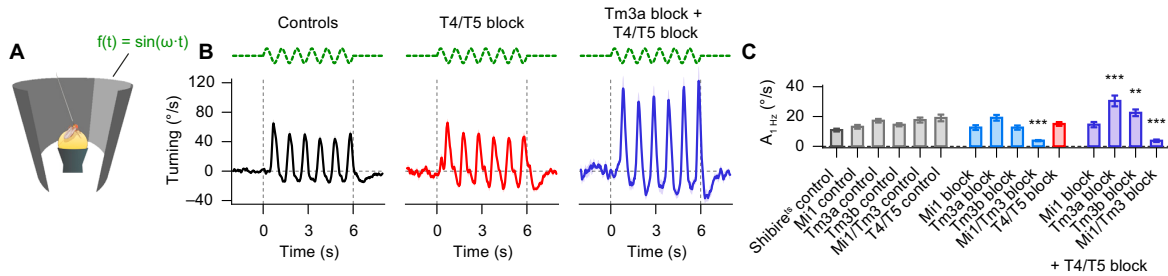


Figure 5. Tm3 Cells Provide Lateral Inhibition

(A) A large field sinusoidal 1 Hz luminance flicker (green dashed lines) on a gray background is presented on the right side. (B) Example response traces for control, T4/T5 block and combined Tm3a block + T4/T5 block flies. (C) Response quantification (1 Hz response amplitude component of the Fourier-transformed signal from 2 to 6 s). Data represent mean \pm SEM with $n = 14$ – 19 flies per group. p values based on a two-sided Welch's t test, comparing the group of block flies with respective control groups (groups with combined lamina or medulla block + T4/T5 block were compared only to the T4/T5 block group; ** $p < 0.01$; *** $p < 0.001$). Detailed statistics in Table S1D. Shibire^{ts} control flies in dark gray, Gal4 control flies in light gray, lamina and medulla block flies in blue, T4/T5 block flies in red, and combined lamina or medulla block + T4/T5 block flies in violet. Raw time traces for control flies (black) in (B) are pooled from shibire^{ts} control, T4/T5 control, and Tm3a control flies. See Figures 1A, 1B, and S1A for schematics of cell types and locations.

intact, we tested the combined Mi1/Tm3 block flies and found that responses to counterphase flicker were almost completely abolished in these flies. Yet, when blocking T4/T5, contrast responses remained fully intact (Figures 4D and 4F), as found previously (Figures 3F–3I).

L1, Mi1, and Tm3 are part of the ON pathway for motion vision which converges onto T4 cells (Takemura et al., 2013). In order to determine whether these cells act directly on the contrast response or indirectly through T4, we repeated the screen in a T4/T5 block background. Moreover, working in such a simplified visual circuit makes it easier to interpret a particular phenotype when silencing neurons upstream to T4 and T5. As expected, the optomotor response remained abolished for flies in which lamina or medulla neurons were blocked in addition to T4 and T5 (Figure 4E). When analyzing responses to counterphase flicker, we found that blocking L1 led to a strong response reduction while silencing L3 or L4 increased the response strength, and blocking L2 or L5 did not have a significant effect (Figure 4F). Blocking Mi1 led to a small, but significant, response reduction and blocking Tm3 strongly reduced the response. We also combined the Mi1/Tm3 block with the T4/T5 block and found that such flies no longer responded at all to the counterphase flicker (Figures 4D and 4F). We conclude that medulla interneurons Mi1 and Tm3 act directly on the contrast response, and not via T4/T5, and that the response is modulated by L3 and L4.

Mi1 and Tm3 neurons are thought to provide temporally different and spatially offset signals to the dendrites of T4 neurons for computing motion direction of luminance increments (Behnia et al., 2014; Takemura et al., 2013). The optomotor response reduction we observed when Mi1 and Tm3 were jointly silenced is in agreement with previous findings (Ammer et al., 2015) which indicated an important role of these neurons in fly motion vision. Our data further suggest that Mi1 and Tm3 are also key elements for spatial contrast computation. In addition to targeting T4 neurons, Mi1 and Tm3 project onto yet unidentified neurons which function in parallel to T4 cells. In summary, thus, motion and contrast computations are carried out by

shared neuronal circuit elements within the ON pathway and, subsequently, visual processing streams diverge.

Mi1 and Tm3 Neurons Form a Center-Surround Antagonism

We found that responses to counterphase flicker were spatial frequency-tuned, which suggested that the underlying neuronal system uses lateral inhibition for contrast computation (Figures 3G and 3I). Taking away lateral inhibition should decrease responses to intermediate spatial frequency but should increase the response strength to large spatial frequencies, in particular to homogeneous field flicker. Such a differential effect allows distinguishing lateral inhibition from localized inhibition as silencing a cell involved in localized inhibition should affect responses to all spatial frequencies equally. Our experiments show that silencing Mi1 or Tm3 leads to a reduced responsiveness to counterphase flicker of intermediate spatial frequency ($\lambda = 20^\circ$; Figure 4F). To test for responses to large spatial frequency flicker, we presented flies with a wide 1 Hz homogeneous flickering region on the right side (Figure 5A). We observed that the turning speed of control and T4/T5 block flies followed the luminance dynamics of the stimulus: Flies turned right for luminance decrease and left for luminance increase (Figures 5B and 5C). Blocking Mi1 or Tm3, with intact T4 and T5, had no effect on the behavior, and silencing Mi1 in a T4/T5-blocked background did not change the behavior either. However, silencing Tm3 together with T4 and T5 cells almost doubled the response amplitude. In contrast, blocking Mi1 and Tm3 at the same time abolished responses to field flicker completely (Figure 5C). These findings, together with our previous silencing experiments (Figure 4F), suggest that Mi1 and Tm3 neurons form a center-surround antagonism for the computation of spatial contrast. In this arrangement, Tm3 cells provide lateral inhibition, not localized inhibition.

The fact that the Tm3 block phenotype was only visible when T4 and T5 neurons were additionally silenced suggests an interesting interplay between the motion and contrast circuit: Since

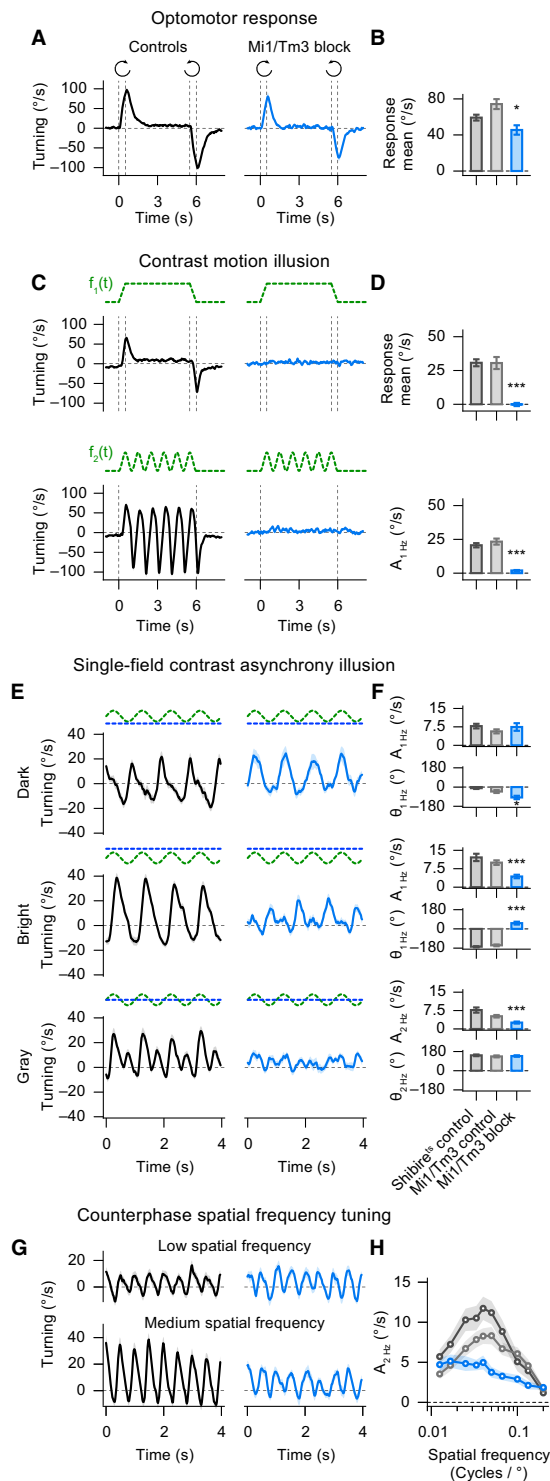


Figure 6. Mi1/Tm3-Silenced Flies Lack Responses to Contrast Illusions

(A and B) Responses of control and Mi1/Tm3 block flies to full-field sine-grating motion (= optomotor response) and quantification (see Figures 1D and 1E for comparison).

(C and D) Responses to contrast motion illusions with stripe luminance profiles $f_1(t)$ and $f_2(t)$ (green dashed lines) and quantification (see Figures 1F–1H for comparison).

(E and F) Responses to the single-field contrast asynchrony illusion and quantification (see Figures 2A–2C for comparison; green dashed lines represent the sinusoidal luminance modulation of the single vertical stripe, blue dashed lines represent background luminances dark, bright, and gray).

(G and H) Example traces for the counterphase flicker stimulus with low ($\lambda = 80^\circ$) and intermediate ($\lambda = 25^\circ$) spatial frequency and quantification of the 2 Hz response components.

Data represent mean \pm SEM with $n = 12$ –13 flies per group. p values based on a two-sided Welch's t test, comparing Mi1/Tm3 block flies with both control groups ($*p < 0.001$; $***p < 0.001$; $p = 0.85$ for the amplitude of the 1 Hz response component for the dark background condition, and $p = 0.78$ for the phase of the 2 Hz response component for the gray background condition in F). Detailed statistics in Table S2A. Shibire^{ts} flies in dark gray, Mi1/Tm3 control flies in light gray, Mi1/Tm3 block flies in blue. Raw time traces for control flies (black) in (A), (C), (E), and (G) are pooled from both control groups.

Tm3 is connected to T4 (Takemura et al., 2013), Tm3 output likely modulates T4 responses to field flicker. In turn, T4 and T5 output can reduce the responsiveness of the contrast system using mechanisms discussed previously (Figures 2H, 2I, 3H, and 3I). Hence, silencing only Tm3 might show no phenotype in the response to field flicker because an increased flicker sensitivity in the contrast system is compensated by an increased flicker sensitivity in the motion system.

Contrast Illusions in Mi1/Tm3-Silenced Flies

Having identified Mi1 and Tm3 as the key players shaping response dynamics to counterphase and homogeneous field flicker (Figures 4 and 5), we wondered whether such flies also show deficits when presented with contrast illusions (Figures 1F–1H and 2). We first stimulated Mi1/Tm3-silenced flies with full-field sine-grating motion and found a reduction of the optomotor response (Figures 6A and 6B). The effect was smaller compared to our previous findings (Figure 4E), since we used bilateral motion stimuli here, likely leading to a response saturation. When presenting the contrast motion illusion (Figure 1F) to Mi1/Tm3 block flies, turning responses were completely abolished (Figures 6C and 6D). This finding suggests that the contrast motion illusion is mediated by spatial contrast computations within the ON pathway. Subsequently, neurons postsynaptic to Mi1/Tm3 globally integrate these contrast cues and control behavior.

We also tested Mi1/Tm3 block flies with the single-field contrast asynchrony illusion (compare Figures 2A–2C, 6E, and 6F). The response amplitude to a flickering stripe on a dark background was not different to that of control flies. Yet, when the background was bright or gray, response amplitudes were strongly reduced (Figures 6E and 6F). Moreover, we compared response phases for the dark and bright background condition and found that responses were still in antiphase to one another. However, turning speed oscillations for the two background conditions were shifted in phase by $\sim 90^\circ$ compared to controls. The

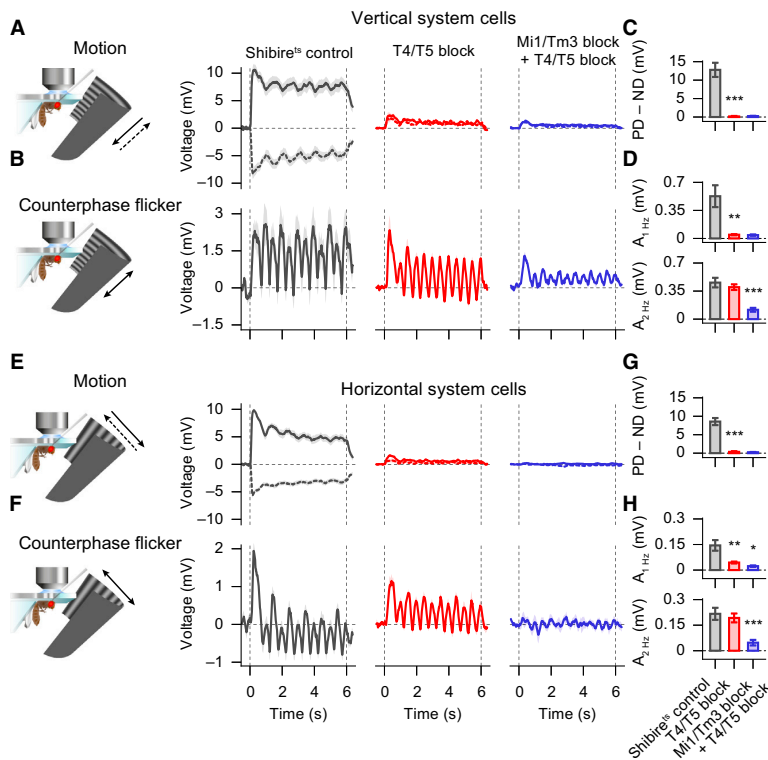


Figure 7. Lobula Plate Tangential Cell Membrane Voltage Reflects Spatial Contrast Dynamics of Counterphase Flicker

(A and B) Vertical system cell responses to a horizontally oriented sine-grating moving downward (PD, solid lines), upward (ND, dashed lines), or flickering in counterphase (2 Hz spatial contrast flicker).

(C and D) Quantification of the motion responses (mean of PD-ND) and of the 1 Hz and 2 Hz amplitude components of the Fourier-transformed responses to the counterphase flicker.

(E-H) Same as in (A)-(D), but for a vertically oriented sine-grating which moves along the horizontal axis or flickers in counterphase. Data represent mean \pm SEM with $n = 4-11$ cells per group (of two to eight flies per group), analyzed from 1-6 s after stimulus onset. p values based on a two-sided Welch's t test, comparing *shibire^{ts}* control flies with T4/T5 block flies and T4/T5 block flies with combined Mi1/Tm3 block + T4/T5 block flies ($*p < 0.05$; $**p < 0.01$; $***p < 0.001$; $p = 0.42$ and $p = 0.59$ for the amplitudes of the 2 Hz response component of the T4/T5 block in D and H, respectively). Detailed statistics in Table S2C. *Shibire^{ts}* flies in dark gray, T4/T5 block flies in red, combined Mi1/Tm3 block + T4/T5 block flies in violet. See Figures 1A, 1B, and S1 for schematics of cell types and locations.

same was true for Mi1/Tm3 block flies in a T4/T5 block background (Figure S4).

We also performed spatial frequency tuning experiments in Mi1/Tm3 block flies (Figures 6G and 6H). To our surprise, we found that for low spatial frequencies, control and Mi1/Tm3 block flies showed weak but identical responses to counterphase flicker. Only for intermediate spatial frequencies, control flies had a much stronger contrast response.

These experiments indicated that beside the Mi1/Tm3-dependent local spatial contrast system, another Mi1/Tm3-independent contrast system exists which operates on larger spatial scales, perhaps globally. To directly test this hypothesis, we slightly modified the single-field contrast asynchrony stimulus and now only varied the background luminance locally around the 1 Hz flickering stripe (Figure S5A). The rest of the arena was gray. Hence, the global light levels remain approximately gray for any local background luminance. If a Mi1/Tm3-independent global contrast system exists, Mi1/Tm3 block flies should respond, independently of local background light levels, with a 2 Hz contrast response as the flickering stripe is compared to global gray background light levels. When we tested the new stimulus, control flies behaved as before (compare Figures 2B, 2C, S5B, and S5C), indicating that the local contrast system is the dominating one. Mi1/Tm3 block flies however responded with a weak 2 Hz response that was independent of local background luminance (Figure S5B-S5D), providing evidence for the existence of a global contrast system.

In summary, the observed residual turning responses in Mi1/Tm3-silenced flies (Figures 6E-6H) are likely mediated by another, weaker, subsystem which analyzes spatial contrast on a global scale.

Output Elements of the Circuit for Spatial Contrast Computation

Next, we wanted to identify the output elements of the contrast computation circuit. As neurons with major input from both Mi1 and Tm3, other than T4, have not yet been identified (Takemura et al., 2013), we could not proceed further with our strategy of characterizing circuit elements based on their behavioral phenotype when silenced. Since membrane depolarization in lobula plate tangential cells elicits an optomotor response (Haikala et al., 2013), we wondered whether the membrane voltage of these cells might also reflect the contrast responses we observed in the behavioral experiments. In order to test this hypothesis, we performed electrophysiological whole-cell patch clamp recordings from these neurons, stimulated flies with motion and counterphase flicker, and silenced synaptic output of either T4 and T5, or Mi1, Tm3, T4, and T5, as in the behavioral experiments.

When stimulated with motion along the vertical axis of a horizontally oriented sine-grating, lobula plate vertical system cells responded in a direction-selective manner (Figures 7A and 7B). As expected from previous studies (Schnell et al., 2012), motion responses were completely abolished when blocking T4 and T5.

Blocking Mi1 and Tm3 in addition did not change responses further. Next, we stimulated flies with counterphase flicker of the same orientation, providing 1 Hz local luminance flicker and 2 Hz spatial contrast flicker. We observed complex oscillatory voltage dynamics in control flies (Figure 7C) which contained both a 1 Hz and a 2 Hz component (Figure 7D). Hence, vertical system cells integrate both the 1 Hz luminance dynamics of counterphase flicker as well as its 2 Hz spatial contrast dynamics. When we tested T4/T5 block flies, the neurons' voltage dynamics were much simpler: While the 1 Hz component was completely abolished, the 2 Hz response component remained unchanged and when silencing Mi1/Tm3 together with T4/T5, the 2 Hz response component was strongly decreased as well. In further experiments, we also recorded from lobula plate horizontal system cells and presented sine-gratings with vertical orientation (Figure 7E). We obtained essentially the same results as we did in vertical system cells (Figures 7E–7H). Because no motion and contrast responses were detectable in flies with silenced Mi1, Tm3, T4, and T5, we also tested full-field flicker (Figure S6). In these flies, we still found robust voltage responses to such stimuli, indicating that even more visual processing pathways arrive at the lobula plate (Schnell et al., 2012) and that the recorded neurons were functionally intact.

From these experiments, we conclude that lobula plate tangential cells not only collect direction-selective input from T4 and T5; they also receive signals from another, unidentified, visual pathway which computes spatial contrast. This pathway requires Mi1 and Tm3 to be functional and bypasses T4 and T5. Hence, spatial contrast and motion cues converge in the lobula plate where they shape visuomotor behavior together. Such interactions could also explain the smaller contrast responses in control flies compared to that of T4/T5 block flies which we observed in some of the behavioral experiments (Figures 2H, 2I, 3H, 3I, and 5C).

Modeling

Our experiments revealed that contrast responses rely on the change of absolute spatial contrast. In particular, when spatial contrast decreases on the right side, flies turn right, when it increases, flies turn left (Figures 2 and 3). Based on these experimental findings, we developed a minimal computational model which could reproduce our results.

Spatial contrast can be computed by taking the difference between adjacent luminance values, i.e., by lateral inhibition,

$$S_{i,rel} = S_i - 0.5 \cdot (S_{i-1} + S_{i+1}),$$

where S_i describes signals of an ommatidium at location i . The change in absolute spatial contrast can then be described by a full-wave rectification followed by a high-pass filter:

$$R_i = -\text{HP}(\text{abs}(S_{i,rel})).$$

This equation can be translated into a simple detector model diagram (Figure 8A). We modeled motion detectors as classical Hassenstein-Reichardt detectors (Hassenstein and Reichardt, 1956). The output of an array of both types of detectors was locally weighted and summated according to the position-dependent function found in our experiments (Figure 2G). A final

low-pass filter mimicked the inertia of the motor system. We presented the model with exactly the same visual stimuli as used in the behavioral experiments. We then tested the model under two conditions, the complete model (both systems = simulating control flies) and the model without Hassenstein-Reichardt detectors (only contrast system = simulating T4/T5 block flies).

The model reproduced the antiphase turning response oscillations for the flickering stripe under the dark and bright background conditions, respectively, as well as the frequency doubling when the background was gray (Figures 8B–8D). Moreover, we observed a small 1 Hz component in the response in the complete model (Figures 8B and 8E). The phase and the mean of the response oscillation were only slightly different compared to those measured experimentally (compare Figures 8C and 2C). Next, we varied the position, the signal amplitude, and the size of the flickering stripe on a gray background. As expected, the model reproduced the position dependency because positional weighting was an intrinsic component of the model construction. Moreover, the model showed a linear dependency on the signal amplitude (Figure 8H), which is expected from the model structure. Our model also reproduced the other experimental findings which were not used for its design. The model reproduced the shape of the size dependency and even predicted a small reduction for larger sizes under control conditions (compare Figures 8I and 2I). We also probed the spatial receptive field properties of the model (Figure 8J) and obtained very similar results as observed in our experiments (Figure 3). Finally, we presented the contrast motion illusion to our model (Figure 8K): The model faithfully reproduced both the direction and the amplitude of the response for both stripe luminance profiles as seen in our experiments (Figures 1F–1H). The negative arm of the Hassenstein-Reichardt detector was minimally weighted less than the positive arm (Eichner et al., 2011), which is the reason why simulated control flies have slightly different contrast responses to stripe flicker and counterphase flicker than simulated block flies.

In summary, using a single set of parameters, the simple model reproduced our experimental results astonishingly well, both qualitatively and quantitatively. We conclude that spatial contrast computation in the fly visual system is based on lateral inhibition followed by full-wave rectification and high-pass filtering. The resulting spatial contrast signals are then globally integrated in a similar fashion as local motion cues.

As our experimental findings indicate that Mi1 and Tm3 neurons are required for both spatial contrast computation and for motion vision (Figures 4 and 6), we also wanted to know to what extent a more detailed model, incorporating such a circuit overlap, can account for our results (Figure S7). The detailed model is based on separate pathways for brightness increments (ON pathway) and for brightness decrements (OFF pathway). Within each pathway, motion is computed by independent polarity-specific Hassenstein-Reichardt detectors (Eichner et al., 2011). We extended the ON pathway by a stage for the computation of absolute spatial contrast, as done in the less complex model (Figure 8). Simulation of the model under different conditions (control condition = full model; T4/T5 block = only the contrast system; Mi1/Tm3 block = only the OFF pathway) revealed a qualitative and quantitative match to most of our experimental data. This shows that overlapping circuitry in the ON

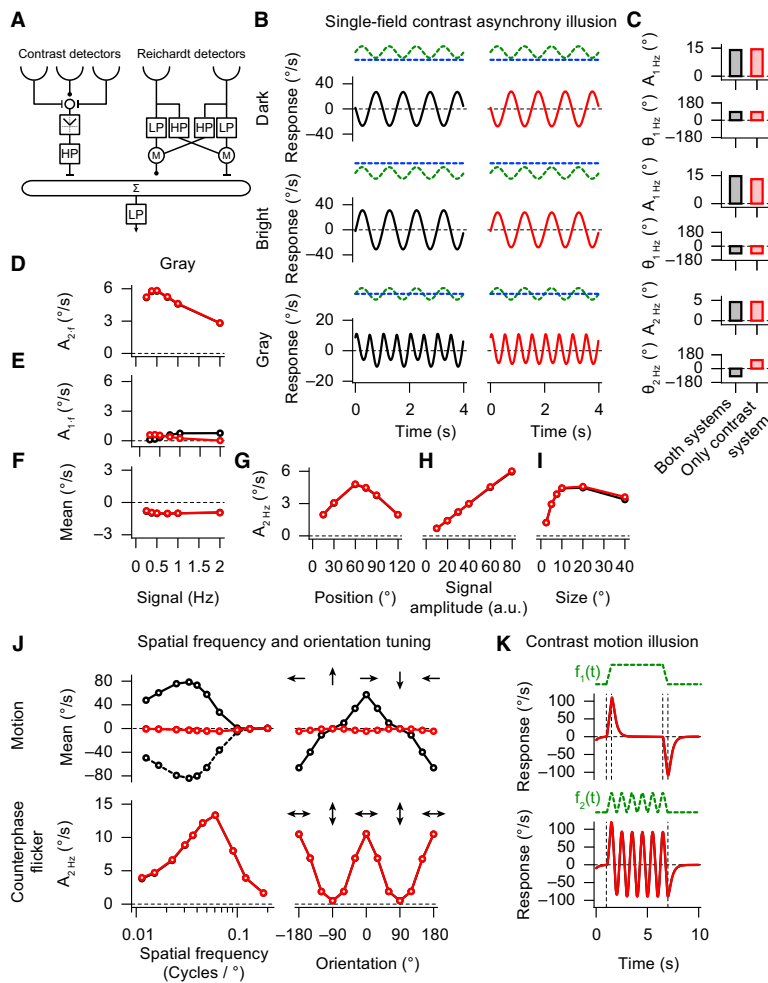


Figure 8. A Simple Computational Model Reproduces Contrast Responses Observed in the Behavioral Experiments

(A) Model structure of contrast detectors combined with Hassenstein-Reichardt detectors. We use an array of these detectors, weighted according to the function in Figure 2G.

(B and C) Responses to the single-field contrast asynchrony illusion for different backgrounds (blue dashed lines) and quantification of amplitude A and phase θ of the 1 Hz and 2 Hz response components (green dashed lines illustrate sinusoidal 1 Hz flicker of the vertical stripe). See Figures 2A–2C for comparison.

(D–I) Responses as a function of stripe flicker frequency, position, signal amplitude, and size (Figure 2D–2I for comparison).

(J) Variation of spatial frequency and orientation of a sine-grating which moves (upper part) or flickers in counterphase (bottom part) in a circular window on the right side. See Figure 3 for comparison.

(K) Responses to the contrast motion illusion for vertical stripe luminance profiles $f_1(t)$ and $f_2(t)$, as in Figures 1F–1H. Black and red traces are simulation results from the complete model (contrast + Hassenstein-Reichardt detectors; corresponds to control flies) and from a model in which motion responses were blocked (only contrast detector; corresponds to T4/T5 block flies), respectively.

contrast system operating on a larger spatial scale can account for the residual responses seen in Mi1/Tm3 block flies (Figure 6).

DISCUSSION

In this paper, we studied contrast computation in *Drosophila*. We employed two types of contrast illusions, the contrast motion illusion and the single-field contrast asynchrony illusion, as a tool to

pathway can account for spatial contrast computation as well as for motion computation.

As suggested by our experiments, apart from computing local spatial contrast, flies also have a system for the computation of spatial contrast on a global scale (Figures 6C–6H and S5). We incorporated such a system in our detailed model by taking signals from photoreceptors minus the global average luminance level followed by full-wave rectification and high-pass filtering (Figure S8). Interestingly, the model now reproduced the residual responses to the single-field contrast asynchrony illusion (compare Figures 6E and 6F with Figures S8B and S8C), the counterphase spatial frequency tuning experiment (compare Figures 6G, 6H, and S8J) and the lack of responses to the contrast motion illusion (compare Figures 6C, 6D, and S8K) under Mi1/Tm3 block conditions (only the OFF pathway and the system for global contrast computation intact). This close agreement between modeling and experiments provides further evidence that a Mi1/Tm3-independent

explore the underlying circuit mechanisms. Testing the first type of illusion, we found that flies responded with a turning response along the direction of illusory motion as perceived by humans (Shapiro and Hamburger, 2007) (Figures 1F–1H). Moreover, when testing the second type of illusion, flies responded to the flickering spatial contrast rather than to its flickering luminance (Figure 2), a phenomenon which is also observed in human psychophysics (Shapiro et al., 2004). Genetic silencing of the essential elements of motion computation, T4 and T5, left responses to contrast stimuli largely unaffected. This suggested that spatial contrast and motion computations are implemented in different visual pathways. Further behavioral analysis revealed that lateral inhibition is involved in the computation, resulting in spatial frequency and orientation tuning of contrast responses (Figure 3). Using counterphase flicker as a stimulus which elicits robust responses to spatial contrast change, we identified the lamina neuron L1 and its postsynaptic partners Mi1 and Tm3 to be essential for contrast computation (Figure 4D). Moreover,

silencing the output of both Mi1 and Tm3 at the same time, completely abolished responses to the contrast motion illusion and reduced, or even inverted, responses to the single-field contrast asynchrony illusion (Figures 6C–6F). These results held also true when blocking T4 and T5 in combination with Mi1 and Tm3 (Figures 4D and S2).

Notably, connectomics (Takemura et al., 2013) and electrophysiological recordings (Behnia et al., 2014) revealed small receptive fields for Mi1 and larger receptive fields for Tm3. Both neuron types provide spatially offset and temporally different input to the T4 dendrite in order to shape its direction-selectivity (Behnia et al., 2014; Takemura et al., 2013). In agreement with previous silencing experiments (Ammer et al., 2015), our experiments provide further behavioral evidence for an important role of Mi1 and Tm3 in motion vision because Mi1/Tm3-silenced flies show a reduced optomotor response (Figures 4C, 6A, and 6B). We identified Tm3 to be important for lateral inhibition during contrast computation (Figure 5), but lateral inhibition is not apparent in electrophysiological recordings from Tm3 (Behnia et al., 2014). Hence, lateral inhibition ought to be further downstream. Taking these findings and our modeling results (Figure 8) into account, we suggest that Mi1 provides fast excitatory input and Tm3 delayed surround inhibition to neurons other than T4 in order to compute spatial contrast. We speculate that a similar circuit motif might also be found on the T4 dendrite (Behnia et al., 2014; Takemura et al., 2013), forming the basis for orientation-selective responses described for these cells (Fisher et al., 2015; Maisak et al., 2013).

Using electrophysiological recordings, we found voltage oscillations in lobula plate tangential cells that correlate with the contrast dynamics of counterphase flicker (Figure 7). Blocking T4 and T5 cells left the response intact, but silencing additionally Mi1 and Tm3 neurons abolished the response. Hence, contrast cues converge on the level of the lobula plate, bypassing T4 and T5. Tm3 is known to synapse also in the lobula (Fischbach and Dittrich, 1989) (Figures S1A, S2A, and S2C), which could be the area where spatial contrast cues are integrated and then transmitted into the lobula plate.

Nevertheless, the identification of a membrane voltage representation of contrast computation does not necessarily imply that lobula plate tangential cells control the behavioral responses we observed. The responses to counterphase flicker might simply be a reflection of other, unidentified, neurons within the highly interconnected network of lobula plate tangential cells (Haag and Borst, 2001, 2002, 2004; Schnell et al., 2010). Moreover, the contrast system might provide signals to neurons in the lobula as well. In order to identify such elements, it will be required to explore further postsynaptic partners of Mi1 and Tm3, and probe the response properties of lobula plate neurons, after silencing such cells.

In conclusion, spatial contrast and motion computation in the fly brain share some of the neuronal circuit elements, pre- and postsynaptic to T4 cells. Such a circuit design suggests that computation of contrast provides important auxiliary signals which assist or further shape direction-selective responses in lobula plate tangential cells. Such cues could, for example, equilibrate motion responses to local variations of contrast, shape motion response to edges or bars (Bahl et al., 2013), improve

orientation or spatial frequency tuning, or realize figure-ground discrimination (Egelhaaf, 1985). Our identification of the mechanisms and neuronal elements of spatial contrast computation opens the door for further behavioral, genetic, anatomical, and physiological dissections of these interactions and might help to elucidate the functional relevance of spatial contrast computation, and the associated contrast illusions, in flies and, perhaps, even humans.

EXPERIMENTAL PROCEDURES

Behavioral experiments were performed as described previously (Bahl et al., 2013). Briefly, tethered flies were walking on an air-suspended ball in a monitor-based virtual environment. Temperature was precisely controlled. In the electrophysiological experiments, control and block flies were heat-shocked for one hour before the experiments. The recording protocol was as described previously (Joesch et al., 2008). Immunostainings and stochastic flip-outs (Figures S2A and S2C) were performed as previously described (Nern et al., 2015; Yu et al., 2010). For statistical analysis, we use a two-sided Welch's t test throughout the paper. In order to average circular phase angles and to determine their variance, we applied circular operators. Statistical tests were performed between both genetic controls and block flies (shibire^{ts} and Gal4 control versus block) and the larger p value determined significance: $p < 0.05$, $p^{**} < 0.01$, and $p^{***} < 0.001$. For the simulations, we used movies of 360×180 pixels at 60 Hz as model stimuli which were rendered from cylindrical projections of the same stimuli used in the experiments. Simulations were carried out according to the models shown in Figures 8A, S7A, and S8A. See Supplemental Experimental Procedures for detailed methods.

SUPPLEMENTAL INFORMATION

Supplemental Information includes eight figures, six tables, two movies, and Supplemental Experimental Procedures and can be found with this article at <http://dx.doi.org/10.1016/j.neuron.2015.11.004>.

AUTHOR CONTRIBUTIONS

A.Ba. and A.Bo. designed the study. E.S. and M.M. performed electrophysiological recordings. G.A. provided the Mi1, Tm3, and Mi1/Tm3-Gal4 lines and did the immunostainings. A.Ba. built the behavioral setup, programmed the visual stimuli, performed the behavioral experiments, and analyzed the data. A.Ba. wrote the paper with help from the other authors.

ACKNOWLEDGMENTS

We are grateful to Romina Kutlesa and Christian Theile for superb technical assistance with the behavioral experiments and fly work, and to Aljoscha Leonhardt for many valuable discussions. We also wish to thank Aljoscha Nern und Gerald M. Rubin for providing the T4/T5 split-Gal4 line and stochastic flippase, and Aljoscha Leonhardt, Alison Barker, Alexander Arenz, and Anna Schützenberger for critically reading the manuscript.

Received: April 13, 2015

Revised: September 24, 2015

Accepted: October 28, 2015

Published: December 3, 2015

REFERENCES

- Adelson, E.H. (2000). Lightness perception and lightness illusions. In *The New Cognitive Neurosciences*, Second Edition, M. Gazzaniga, ed. (Cambridge, MA: MIT Press), pp. 339–351.
- Ammer, G., Leonhardt, A., Bahl, A., Dickson, B.J., and Borst, A. (2015). Functional specialization of neural input elements to the *Drosophila* ON motion detector. *Curr. Biol.* 25, 2247–2253.

- Bahl, A., Ammer, G., Schilling, T., and Borst, A. (2013). Object tracking in motion-blind flies. *Nat. Neurosci.* *16*, 730–738.
- Bausenwein, B., Dittrich, A.P., and Fischbach, K.F. (1992). The optic lobe of *Drosophila melanogaster*. II. Sorting of retinotopic pathways in the medulla. *Cell Tissue Res.* *267*, 17–28.
- Behnia, R., Clark, D.A., Carter, A.G., Clandinin, T.R., and Desplan, C. (2014). Processing properties of ON and OFF pathways for *Drosophila* motion detection. *Nature* *512*, 427–430.
- Brand, A.H., and Perrimon, N. (1993). Targeted gene expression as a means of altering cell fates and generating dominant phenotypes. *Development* *118*, 401–415.
- Bülthoff, H., and Götz, K.G. (1979). Analogous motion illusion in man and fly. *Nature* *278*, 636–638.
- Clark, D.A., Bursztyn, L., Horowitz, M.A., Schnitzer, M.J., and Clandinin, T.R. (2011). Defining the computational structure of the motion detector in *Drosophila*. *Neuron* *70*, 1165–1177.
- Egelhaaf, M. (1985). On the neuronal basis of figure-ground discrimination by relative motion in the visual system of the fly. I. Behavioural constraints imposed on the neuronal network and the role of the optomotor system. *Biol. Cybern.* *52*, 123–140.
- Eichner, H., Joesch, M., Schnell, B., Reiff, D.F., and Borst, A. (2011). Internal structure of the fly elementary motion detector. *Neuron* *70*, 1155–1164.
- Fischbach, K.F., and Dittrich, A. (1989). The optic lobe of *Drosophila melanogaster*. I. A Golgi analysis of wild-type structure. *Cell Tissue Res.* *258*, 441–475.
- Fisher, Y.E., Silies, M., and Clandinin, T.R. (2015). Orientation selectivity sharpens motion detection in *Drosophila*. *Neuron* *88*, 390–402.
- Götz, K.G. (1964). Optomotorische Untersuchung des visuellen Systems einiger Augenmutanten der Fruchtfliege *Drosophila*. *Kybernetik* *2*, 77–92.
- Haag, J., and Borst, A. (2001). Recurrent network interactions underlying flow-field selectivity of visual interneurons. *J. Neurosci.* *21*, 5685–5692.
- Haag, J., and Borst, A. (2002). Dendro-dendritic interactions between motion-sensitive large-field neurons in the fly. *J. Neurosci.* *22*, 3227–3233.
- Haag, J., and Borst, A. (2004). Neural mechanism underlying complex receptive field properties of motion-sensitive interneurons. *Nat. Neurosci.* *7*, 628–634.
- Haikala, V., Joesch, M., Borst, A., and Mauss, A.S. (2013). Optogenetic control of fly optomotor responses. *J. Neurosci.* *33*, 13927–13934.
- Hassenstein, B., and Reichardt, W. (1956). Systemtheoretische Analyse der Zeit, Reihenfolgen und Vorzeichenauswertung bei der Bewegungsperzeption des Rüsselkäfers *Chlorophanus*. *Z. Naturforsch. B* *11*, 513–524.
- Joesch, M., Plett, J., Borst, A., and Reiff, D.F. (2008). Response properties of motion-sensitive visual interneurons in the lobula plate of *Drosophila melanogaster*. *Curr. Biol.* *18*, 368–374.
- Joesch, M., Schnell, B., Raghu, S.V., Reiff, D.F., and Borst, A. (2010). ON and OFF pathways in *Drosophila* motion vision. *Nature* *468*, 300–304.
- Joesch, M., Weber, F., Eichner, H., and Borst, A. (2013). Functional specialization of parallel motion detection circuits in the fly. *J. Neurosci.* *33*, 902–905.
- Kitamoto, T. (2001). Conditional modification of behavior in *Drosophila* by targeted expression of a temperature-sensitive *shibire* allele in defined neurons. *J. Neurobiol.* *47*, 81–92.
- Maisak, M.S., Haag, J., Ammer, G., Serbe, E., Meier, M., Leonhardt, A., Schilling, T., Bahl, A., Rubin, G.M., Nern, A., et al. (2013). A directional tuning map of *Drosophila* elementary motion detectors. *Nature* *500*, 212–216.
- Mauss, A.S., Pankova, K., Arenz, A., Nern, A., Rubin, G.M., and Borst, A. (2015). Neural circuit to integrate opposing motions in the visual field. *Cell* *162*, 351–362.
- Meier, M., Serbe, E., Maisak, M.S., Haag, J., Dickson, B.J., and Borst, A. (2014). Neural circuit components of the *Drosophila* OFF motion vision pathway. *Curr. Biol.* *24*, 385–392.
- Morante, J., and Desplan, C. (2008). The color-vision circuit in the medulla of *Drosophila*. *Curr. Biol.* *18*, 553–565.
- Nern, A., Pfeiffer, B.D., and Rubin, G.M. (2015). Optimized tools for multicolor stochastic labeling reveal diverse stereotyped cell arrangements in the fly visual system. *Proc. Natl. Acad. Sci. USA* *112*, E2967–E2976.
- Pfeiffer, B.D., Truman, J.W., and Rubin, G.M. (2012). Using translational enhancers to increase transgene expression in *Drosophila*. *Proc. Natl. Acad. Sci. USA* *109*, 6626–6631.
- Pick, B. (1974). Visual flicker induces orientation behaviour in the fly *Musca*. *Z. Naturforsch. C* *29*, 310–312.
- Schnell, B., Joesch, M., Forstner, F., Raghu, S.V., Otsuna, H., Ito, K., Borst, A., and Reiff, D.F. (2010). Processing of horizontal optic flow in three visual interneurons of the *Drosophila* brain. *J. Neurophysiol.* *103*, 1646–1657.
- Schnell, B., Raghu, S.V., Nern, A., and Borst, A. (2012). Columnar cells necessary for motion responses of wide-field visual interneurons in *Drosophila*. *J. Comp. Physiol. A Neuroethol. Sens. Neural Behav. Physiol.* *198*, 389–395.
- Shapiro, A.G., and Hamburger, K. (2007). Last but not least. *Perception* *36*, 1104–1107.
- Shapiro, A.G., D'Antona, A.D., Charles, J.P., Belano, L.A., Smith, J.B., and Shear-Heyman, M. (2004). Induced contrast asynchronies. *J. Vis.* *4*, 459–468.
- Shapiro, A.G., Charles, J.P., and Shear-Heyman, M. (2005). Visual illusions based on single-field contrast asynchronies. *J. Vis.* *5*, 764–782.
- Shinomiya, K., Karuppudurai, T., Lin, T.-Y., Lu, Z., Lee, C.-H., and Meinertzhagen, I.A. (2014). Candidate neural substrates for off-edge motion detection in *Drosophila*. *Curr. Biol.* *24*, 1062–1070.
- Silies, M., Gohl, D.M., Fisher, Y.E., Freifeld, L., Clark, D.A., and Clandinin, T.R. (2013). Modular use of peripheral input channels tunes motion-detecting circuitry. *Neuron* *79*, 111–127.
- Strother, J.A., Nern, A., and Reiser, M.B. (2014). Direct observation of ON and OFF pathways in the *Drosophila* visual system. *Curr. Biol.* *24*, 976–983.
- Takemura, S.-Y., Bharioke, A., Lu, Z., Nern, A., Vitaladevuni, S., Rivlin, P.K., Katz, W.T., Olbris, D.J., Plaza, S.M., Winston, P., et al. (2013). A visual motion detection circuit suggested by *Drosophila* connectomics. *Nature* *500*, 175–181.
- Tuthill, J.C., Chiappe, M.E., and Reiser, M.B. (2011). Neural correlates of illusory motion perception in *Drosophila*. *Proc. Natl. Acad. Sci. USA* *108*, 9685–9690.
- Tuthill, J.C., Nern, A., Holtz, S.L., Rubin, G.M., and Reiser, M.B. (2013). Contributions of the 12 neuron classes in the fly lamina to motion vision. *Neuron* *79*, 128–140.
- Yu, J.Y., Kanai, M.I., Demir, E., Jefferis, G.S.X.E., and Dickson, B.J. (2010). Cellular organization of the neural circuit that drives *Drosophila* courtship behavior. *Curr. Biol.* *20*, 1602–1614.

Neuron, Volume 88

Supplemental Information

Neural Mechanisms for Drosophila Contrast Vision

Armin Bahl, Etienne Serbe, Matthias Meier, Georg Ammer, and Alexander Borst

SUPPLEMENTAL EXPERIMENTAL PROCEDURES

FLIES

Flies were raised on standard cornmeal-agar medium on a 12h light/12h dark cycle and 60% humidity for the entire period of development. For the first seven days of development, flies were kept at 25 °C and then transferred to 18 °C. In experiments, we only used female flies aged ~1 day. We used the following driver lines: L1-splitGal4 (OK371-AD, ort-C1-3-DBD), L2-Gal4 (21D), L3-Gal4 (VT40568), L4-Gal4 (VT40547), L5-splitGal4 (R21A05-AD; R31H09-DBD), Mi1-Gal4 (VT7747), Tm3a-Gal4 (R12C11), Tm3b-Gal4 (R13E12), Mi1/Tm3-Gal4 (VT0465), T4/T5-splitGal4 (R59E08-AD; R42F06-DBD), T4/T5-Gal4 (R42F06). These lines were either crossed to wild type Canton S flies or to 20xUAS-shibire^{ts} flies (Pfeiffer et al., 2012), resulting in the genotypes presented in Figure S2B.

ELECTROPHYSIOLOGY

The glial sheet was digested locally by application of a stream of 0.5 mg/ml collagenase IV (GIBCO) through a cleaning micropipette (5 µm opening) under polarized light contrast. Then, somata of lobula plate tangential cells were whole-cell patched. We identified vertical and horizontal system cells based on their directional tuning properties (control flies), cell body location and resting membrane potential (block flies). For visual stimulation, we used a LED arena covering ±90° in azimuth and ±48° in elevation. Patterns had a spatial wavelength of $\lambda = 22.5^\circ$ and 100% contrast (maximal luminance 75 cd/m²). Recordings were performed at 2 kHz, the signal was then downsampled to 50 Hz and 2–4 trials were averaged per cell. Further analysis was performed as in the behavioral experiments.

IMMUNOHISTOCHEMISTRY

Primary antibodies used were rabbit polyclonal anti-GFP (1:2000, Torri Pines) and mouse anti-nc82 (1:25, Developmental Studies Hybridoma Bank). We used the following secondary antibodies: goat anti-rabbit Alexa-488 and goat anti-mouse Alexa-633 (both 1:500, Invitrogen). Brains were mounted in Vectashield (Vectalabs) and optically sectioned in the horizontal plane with a Leica SP5 confocal microscope. For documentation, single sections were processed in ImageJ 1.46r (NIH). For stochastic labeling of cells in the VT0465-Gal4 line, we used a weak flippase which sparsely removes an FRT-flanked stop cassette and thereby allows Gal4-driven expression of a GFP reporter (Nem et al., 2015).

BEHAVIORAL EXPERIMENTS

We used six independent setups (almost identical to those presented in Bahl et al. 2013) for visual stimulation and to record fly locomotion. All monitors were equilibrated in brightness and contrast. We applied the same temperature protocol in all behavioral experiments: Temperature was kept at 25 °C for the first 5 min and then, within 10 min, raised to 34 °C. The sine-grating in Figure 1D had a spatial wavelength of $\lambda = 20^\circ$, 60% contrast and moved at a velocity of 20 °/s. In the contrast motion illusion, we used a stepped gradient background (20° wide steps) ranging from luminance 0–100 cd/m². Twelve 5° wide vertical stripes were superimposed within the centers of the background steps. The luminance of these stripes varied from 9–45 cd/m² according to the functions illustrated in Figure 1F. In Figures 2A–F and 6E–F, we used a single 10° wide vertical stripe located at 70° in azimuth. The luminance of the stripe varied sinusoidally (1 Hz) from 4–57 cd/m². In Figure 2G–I, only the illustrated parameters were varied, the other parameters were as in Figure 2B (gray background) but in Figure 2I, the stripe was centered at 80° in azimuth. The uniformly dark, bright, and gray backgrounds had luminances of 1.3, 27, and 86 cd/m², respectively. The sine pattern in Figures 3 and 6G,H had a contrast of 60%. Stimuli were shown in a circular window (radius = 40°) positioned at 90° in azimuth and 0° in elevation. Stimuli in Figure 4 were shown within a 70° wide rectangular window located at 90° in azimuth and full elevation. The sine-grating had a spatial wavelength of $\lambda = 20^\circ$ and 60% contrast. Field flicker (Figure 5) was shown within the same window and varied from 4–57 cd/m² in luminance. The rest of the visual field for stimuli in Figures 3, 4 and 5 was gray (27 cd/m²). The size of the local background around the flickering stripe in Figure S5 was 30°, the rest of the arena was gray (27 cd/m²). Otherwise the stimulus was as in Figure 2A. The spatial phase of all sine-gratings (Figures 1A, 3, 4,

6A) was chosen randomly before each trial. In all behavioral experiments, we additionally presented exact mirror-symmetrical versions of the stimuli.

For each experiment, fly locomotion was sampled for ~90 min at 4 kHz and data was subsequently downsampled to 50 Hz. We then picked a trial range during which the average walking speed in each trial was above 0.5 cm/s. Trials were then averaged. Experiments not having at least 9 of such trials were discarded. Further, responses to all stimuli and to their mirror-symmetrical versions were subtracted from another and divided by two, which removed potential turning biases and improved data quality. Finally, we applied a first order low-pass filter ($\tau = 40$ ms). The resulting data was then analyzed by averaging or via Fourier transform within a specific time range. In the Fourier-transformed signal, we picked the frequency of interest and calculated its amplitude and phase. For each stimulus, we then averaged these values and calculated the standard error of the mean (s.e.m.) over flies.

STATISTICS

The Welch's t-test is a variant of Student's t-test and does not require equal variances (https://en.wikipedia.org/wiki/Welch%27s_t_test). T-values were calculated as

$$t = \frac{\bar{X}_1 - \bar{X}_2}{\sqrt{\frac{s_1^2}{N_1} + \frac{s_2^2}{N_2}}},$$

where \bar{X}_i , s_i^2 and N_i are population mean, variance, and size of group i , respectively. We used the Welch-Satterthwaite equation to calculate degrees of freedom:

$$df = \frac{\left(\frac{s_1^2}{N_1} + \frac{s_2^2}{N_2}\right)^2}{\frac{s_1^4}{N_1^2 \cdot (N_1 - 1)} + \frac{s_2^4}{N_2^2 \cdot (N_2 - 1)}}.$$

In order to work with circular variables (response phases), we used the following circular operators to calculate mean ($\bar{\alpha}$) and variance (s_α^2) of the values:

$$\bar{\alpha} = \arg \left(\sum_{j=1}^N \exp(i \cdot \alpha_j) \right),$$

$$s_\alpha^2 = -2 \cdot \log \left(\frac{1}{N} \cdot \left| \sum_{j=1}^N \exp(i \cdot \alpha_j) \right| \right).$$

To obtain the enumerator in the Welch's t test, we determined the smallest difference of angular means:

$$(\bar{\alpha}_1 - \bar{\alpha}_2 + \pi) \text{ modulo } 2\pi - \pi.$$

MODELING

In the first step, frames were spatially convolved with a 2D Gaussian kernel of isotropic $\sigma = 1.75^\circ$ and then fed into an array of 90×45 4° -spaced input elements. For input elements on the left visual hemisphere, the Hassenstein-Reichardt detector had a mirror-symmetrical structure. All filters in the input stage had the same time constants of $\tau = 100$ ms. Lateral inhibition in the contrast detector along the horizontal axis was calculated as

$$R_i = S_i - 0.5 \cdot (S_{i-1} + S_{i+1}),$$

where S_i is the central input element. Output weighting of the contrast detector was 20, of the positive arm of the Hassenstein-Reichardt detector 0.15 and of the negative arm 0.147. Output of all detectors was then summated according to the weighting function

$$w(x) = \exp\left(-\frac{x^2}{2 \cdot 60^2}\right) - 0.9 \cdot \exp\left(-\frac{x^2}{2 \cdot 40^2}\right),$$

approximating the function in [Figure 2G](#), and values along the y-axis were summated. For simplicity, all motion and contrast detectors were weighted with the same function, as done in previous modeling studies ([Bahl et al., 2013](#)). In the left visual hemisphere, output signals were multiplied by -1 . The resulting signal was then low-pass filtered ($\tau = 300$ ms). All filters were of first-order and implemented according to https://en.wikipedia.org/wiki/Low-pass_filter and https://en.wikipedia.org/wiki/High-pass_filter, respectively. The high-pass filter in the input stage take away signal means completely and, for example, reduce a sinusoidal 1 Hz input signal to 50 % in amplitude and produce a phase shift of around $0.3 \cdot \pi$.

In the detailed models ([Figures S7](#) and [S8](#)), the DC component was 40% of the photoreceptor signal and the half-wave rectification in the OFF pathway was shifted by +80. The weight for the spatial contrast detector in the ON pathway was 30, for the positive and negative arms of the Hassenstein-Reichardt detectors 0.1 and 0.098, respectively. The output weight of the global contrast system was either 0 ([Figure S7](#)) or 2 ([Figure S8](#)). All other parameter were as in the less complex model.

The output weights, the DC component and the shift in the OFF rectification (only in the detailed models) were the only free model parameters and were adjusted by hand. Time constants were approximately the same as in previous modeling studies ([Eichner et al., 2011](#)) and were not optimized.

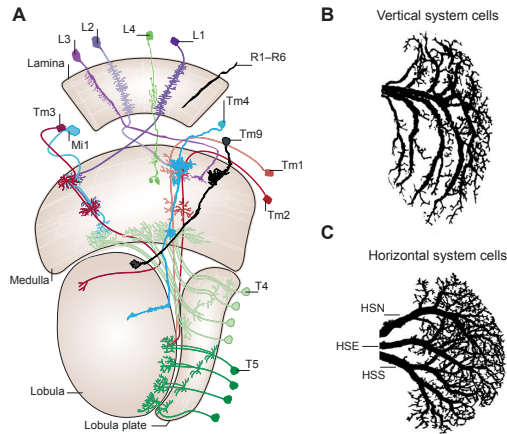


Figure S1, related to Figure 1. Cellular Schematic of the Fly Optic Lobe and Morphology of Lobula Plate Tangential Cells

(A) Cellular schematic of the fly optic lobe. See corresponding abstract schematic in Figure 1A,B for comparison. (B,C) Anatomy of five of the six vertical system cells and of the three horizontal system cells in *Drosophila*. Both cell types reside in the lobula plate and receive input from T4 and T5 neurons. The scheme in (A) was modified from Borst, 2014. The images of lobula plate tangential cells in (B,C) are taken from Rajashekhar and Shamprasad, 2004. Cell sizes not to scale.

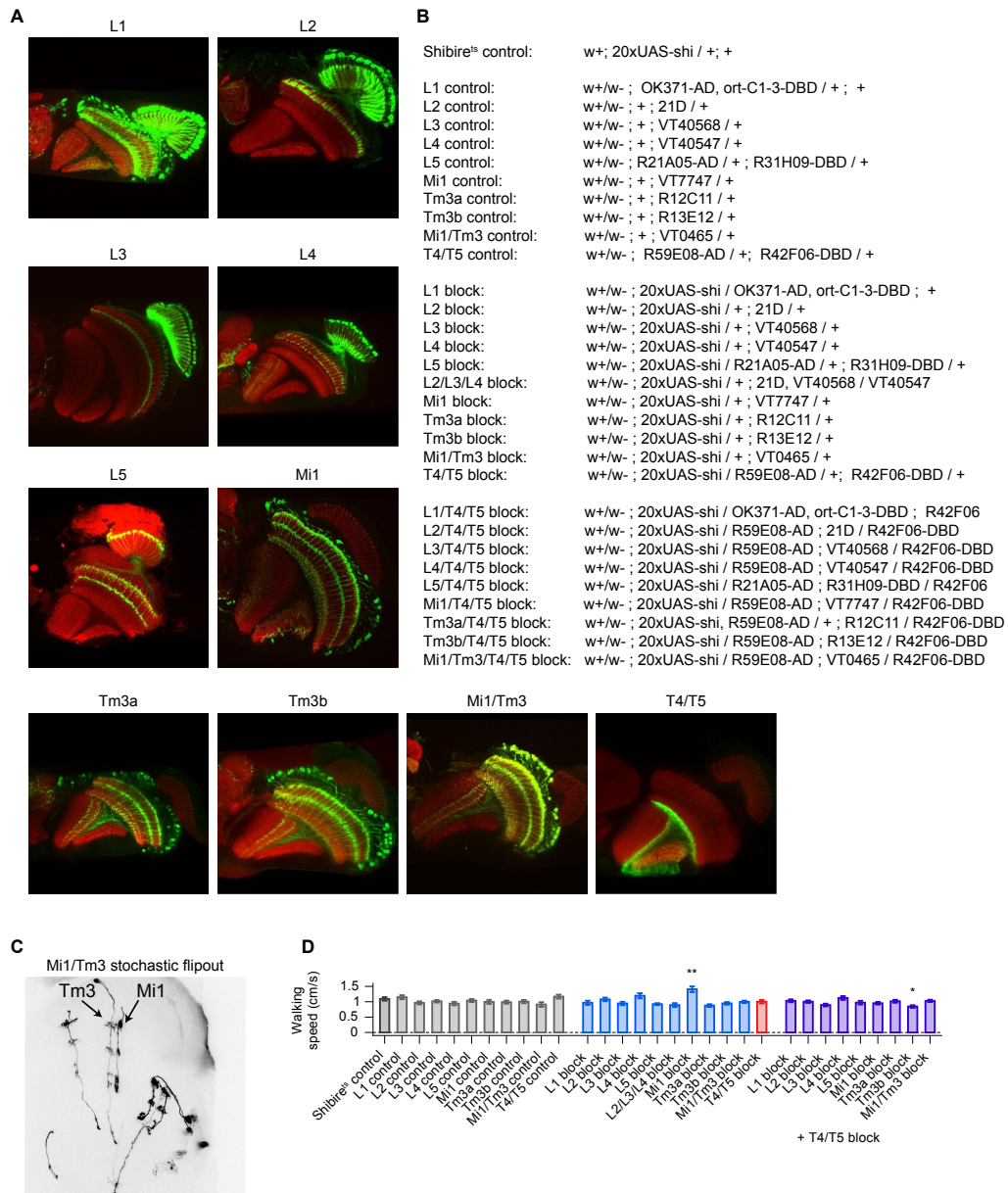


Figure S2, related to Figures 4, 5, S3, and S4. Expression Patterns, Genotypes, and Walking Speed

(A) GFP expression pattern of GAL4 driver lines. Horizontal sections of the optic lobe. (B) Genotypes used in the experiments. (C) Stochastic GFP labeling of neurons in the VT0465 Gal4 line. Flipouts of several Mi1 and Tm3 cells are distinguishable. In addition to these cells, we occasionally found weak expression in unidentified Mi and Dm cells. (D) Walking speed (averaged over same trial range as used for quantification of turning speeds and over all stimuli). Data represent mean \pm s.e.m with $n = 14-19$ flies per group. P-values based on a two-sided Welch's t test, comparing the group of block flies with respective control groups (for example, L1 block with L1 control and shibire^{ts} control; groups with combined lamina or medulla block + T4/T5 block (right side) were compared only to the T4/T5 block group; $P^* < 0.05$; $P^{**} < 0.01$). Detailed statistics in Table S6. Shibire^{ts} control flies in dark gray, Gal4 control flies in light gray, lamina and medulla block flies in blue, T4/T5 block flies in red, and combined lamina or medulla block + T4/T5 block flies in violet.

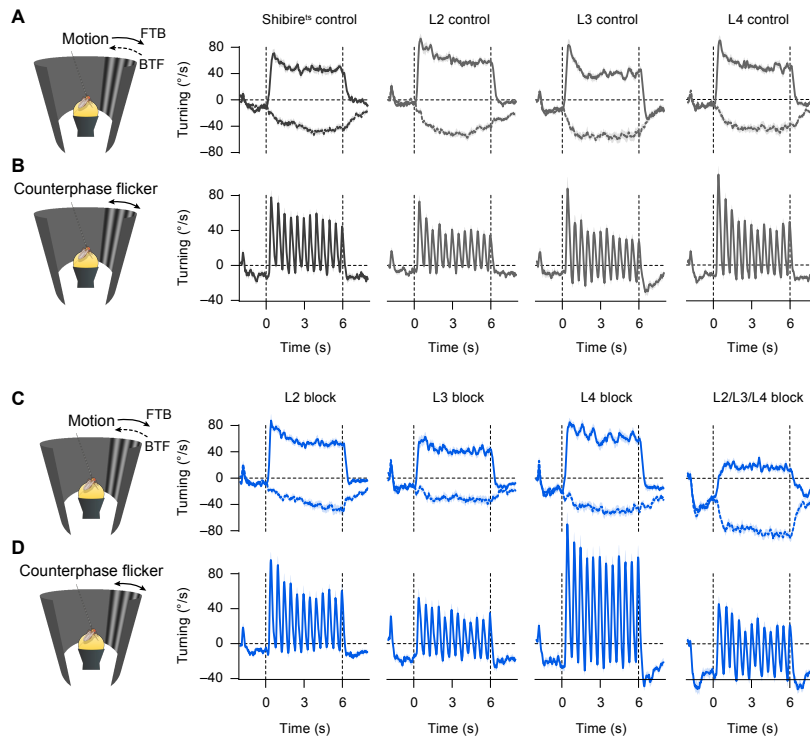


Figure S3, related to Figure 4. Raw Time Traces for OFF Pathway Lamina Blocks

(A,B) Responses of control flies to motion and counterphase flicker. (C,D) Responses of L2, L3, L4 and combined L2/L3/L4 block flies to motion and counterphase flicker. L2/L3/L4 block flies strongly turn away from stationary patterns ($\approx 40^\circ/s$). For motion and counterphase flicker, all responses were shifted to negative values. This effect was not found in any of the controls or in any of the flies where L2, L3, or L4 cells were blocked independently. Even though we do not understand these dynamics, it shows that the triple lamina block works. For quantification, we calculated the optomotor response by subtracting front-to-back and back-to-front motion responses and by determining the 2 Hz response amplitude to counterphase flicker. Hence, a shift of the traces to negative values is not seen in the quantification in Figure 4E,F. Vertical gray dashed lines indicate on- and offset of the stimulus. *Shibire^{ts}* control flies in dark gray, Gal4 control flies in light gray, lamina block flies in blue. Data represent mean \pm s.e.m with $n = 14-19$ flies per group. Same flies as in Figure 4.

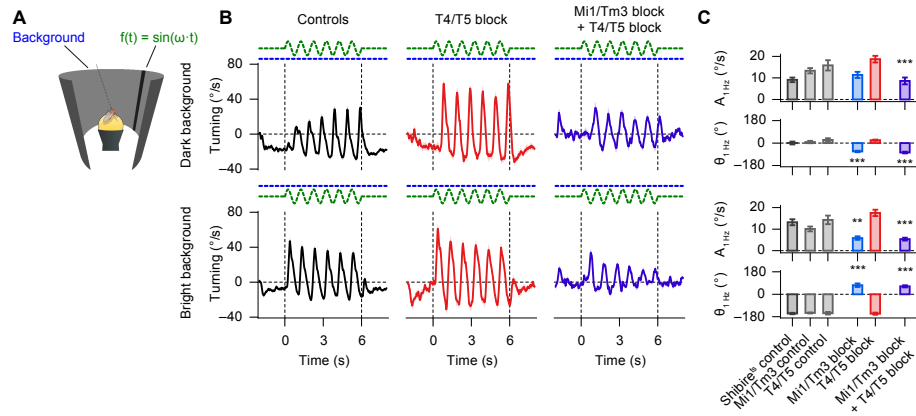


Figure S4, related to Figure 6. Single-field Contrast Illusion in Mi1/Tm3 Block Flies

(A) Same as in Figure 2A. (B) Fly turning responses for 1 Hz stripe flicker (identical in the two conditions; green dashed line) on two different backgrounds (dark and bright; blue dashed line). (C) Quantification of response amplitude A and phase Θ . Data represent mean \pm s.e.m with $n = 14$ – 19 flies per group. Same flies as in Figures 4 and 5. P-values based on a two-sided Welch's t test, comparing the group of block flies with respective control groups (Mi1/Tm3 block with Mi1/Tm3 control and shibire^{ts} control; The combined Mi1/Tm3 block + T4/T5 block (right side) was compared only to the T4/T5 block group; $P^{**} < 0.01$; $P^{***} < 0.001$). Detailed statistics in Table S2B. Expression patterns and list of genotypes in Figure S2A–C. Shibire^{ts} control flies in dark gray, Gal4 control flies in light gray, Mi1/Tm3 block flies in blue, T4/T5 block flies in red, and combined Mi1/Tm3 block + T4/T5 block flies in violet. Raw time traces for control flies (black) in (C,D) are pooled from shibire^{ts} control, T4/T5 control and Mi1/Tm3 control flies.

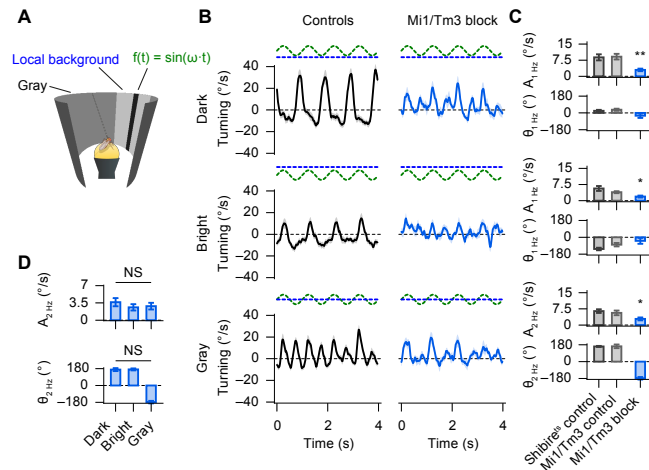


Figure S5, related to Figure 6. Single-Field Contrast Asynchrony Illusion with Local Background Variation in Mi1/Tm3 Block Flies

(A) The global background is gray for all conditions. Varied is the local background (dark, bright, and gray; blue dashed line) surrounding the $\omega = 1$ Hz flickering stripe (identical in all conditions; green dashed line). Compare with stimuli in Figures 2A and 6E where global background luminance is varied. (B,C) Fly turning responses for the three local background conditions and quantification of response amplitude A and phase Θ . (D) Quantification of the 2 Hz response component for the three local background conditions for Mi1/Tm3 block flies. Data represent mean \pm s.e.m with $n = 8-12$ flies per group. P-values based on a two-sided Welch's t test, comparing Mi1/Tm3 block flies with both control groups ($P^* < 0.05$; $P^{**} < 0.01$). Statistics in (D) was done by pairwise comparing responses between the different conditions. None of these combinations was statistically different. Detailed statistics in Table S3. Shibire^{es} control flies in dark gray, Mi1/Tm3 control flies in light gray, Mi1/Tm3 block flies in blue. Raw time traces for control flies (black) in (B) are pooled from shibire^{es} control and Mi1/Tm3 control flies.

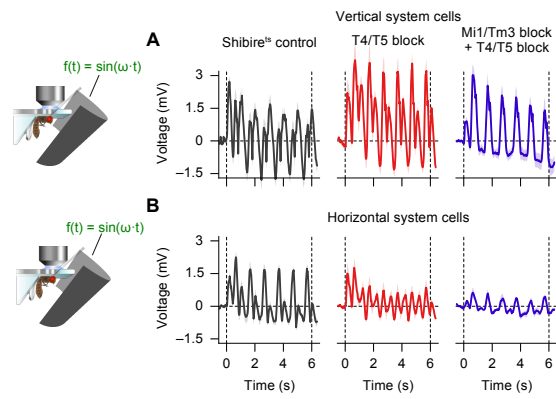


Figure S6, related to Figure 7. Responses of Lobula Plate Tangential Cells to Full Field Flicker

(A,B) Responses of vertical system and horizontal system cells to 1 Hz full field flicker. Data represent mean \pm s.e.m with $n = 4-11$ cells per group (of 2-8 flies per group). Same flies and cells as in Figure 7. Shibire^{ts} flies in dark gray, T4/T5 block flies in red, combined Mi1/Tm3 block + T4/T5 block flies in violet. See Figure S1B,C for illustration of the recorded neurons.

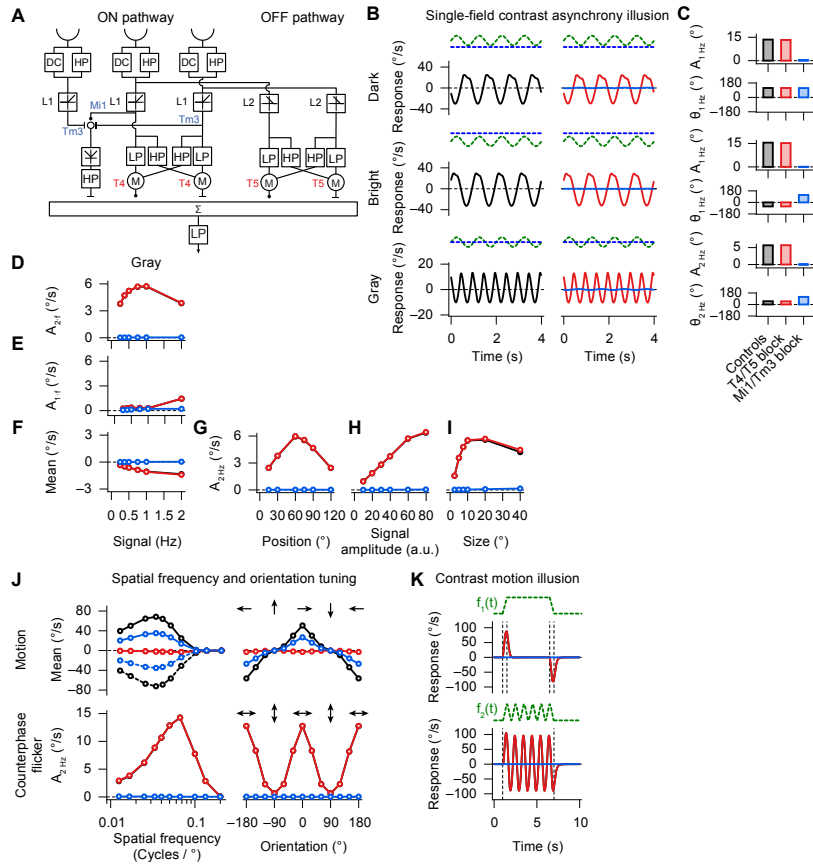


Figure S7, related to Figure 8. Detailed Model with Contrast Computation within the ON Pathway

(A) Detailed model with two pathways computing motion from brightness increments (ON pathway) and brightness decrements (OFF pathway). See Eichner et al., 2011. Within the ON pathway, lateral inhibition by Tm3 neurons and central excitation by Mi1 neurons are used to compute local spatial contrast (compare with Figure 8A). T4 and T5 neurons represent the output of the Hassenstein-Reichardt detectors in the two motion pathways. (B,C) Model responses for the single-field contrast asynchrony illusion (same stimulus as in Figures 2A–C and 6E–F) and quantification of amplitude A and phase Θ . (D–I) Quantification of responses to varying signal frequency, position, amplitude, and stripe size. (J) Model responses for motion and counterphase flicker spatial frequency and orientation tuning (same stimulus as in Figure 3). (K) Model responses for the contrast motion illusion (same stimulus as in Figures 1F–H and 6C,D). Control conditions (full model) in black. T4/T5 block (model without Hassenstein-Reichardt detectors) in red. Mi1/Tm3 block (only OFF motion pathway intact) in blue.

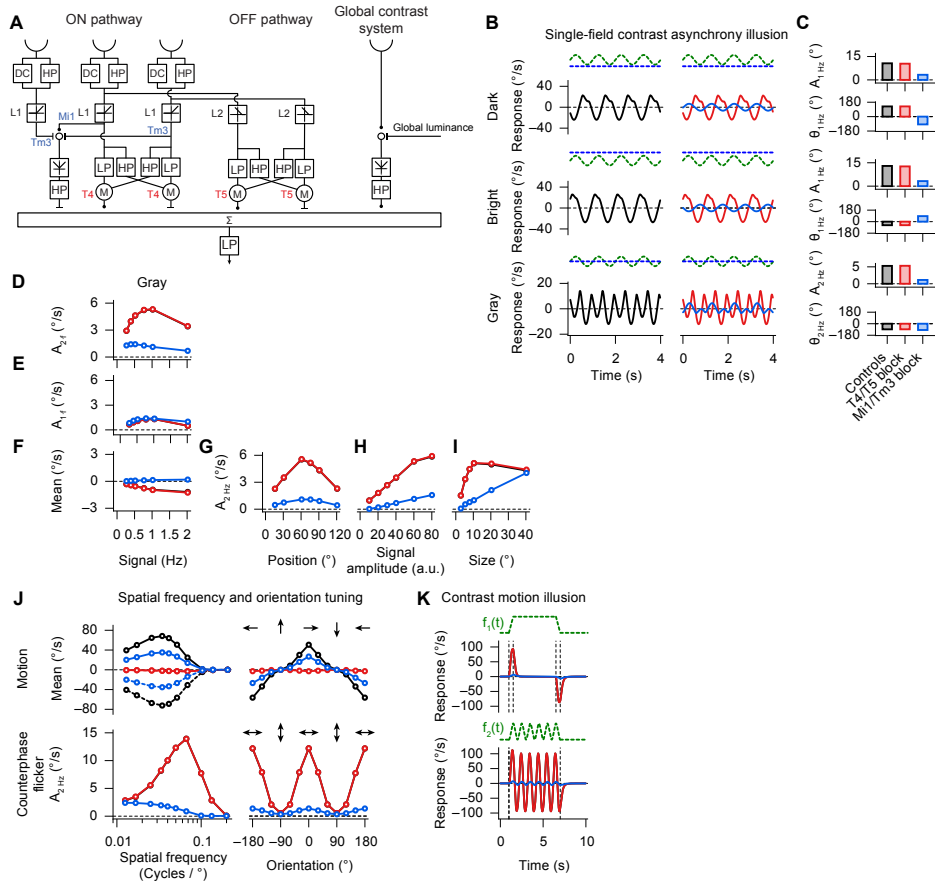


Figure S8, related to Figure 8. Detailed Model with Local Contrast Computation within the ON Pathway and an Additional Pathway for Global Contrast Computation
 (A–K) Same as in Figure S7 but with an additional pathway for global contrast computation. Control conditions (full model) in black. T4/T5 block (model without Hassenstein-Reichardt detectors) in red. Mi1/Tm3 block (only OFF motion pathway and global contrast pathway intact) in blue.

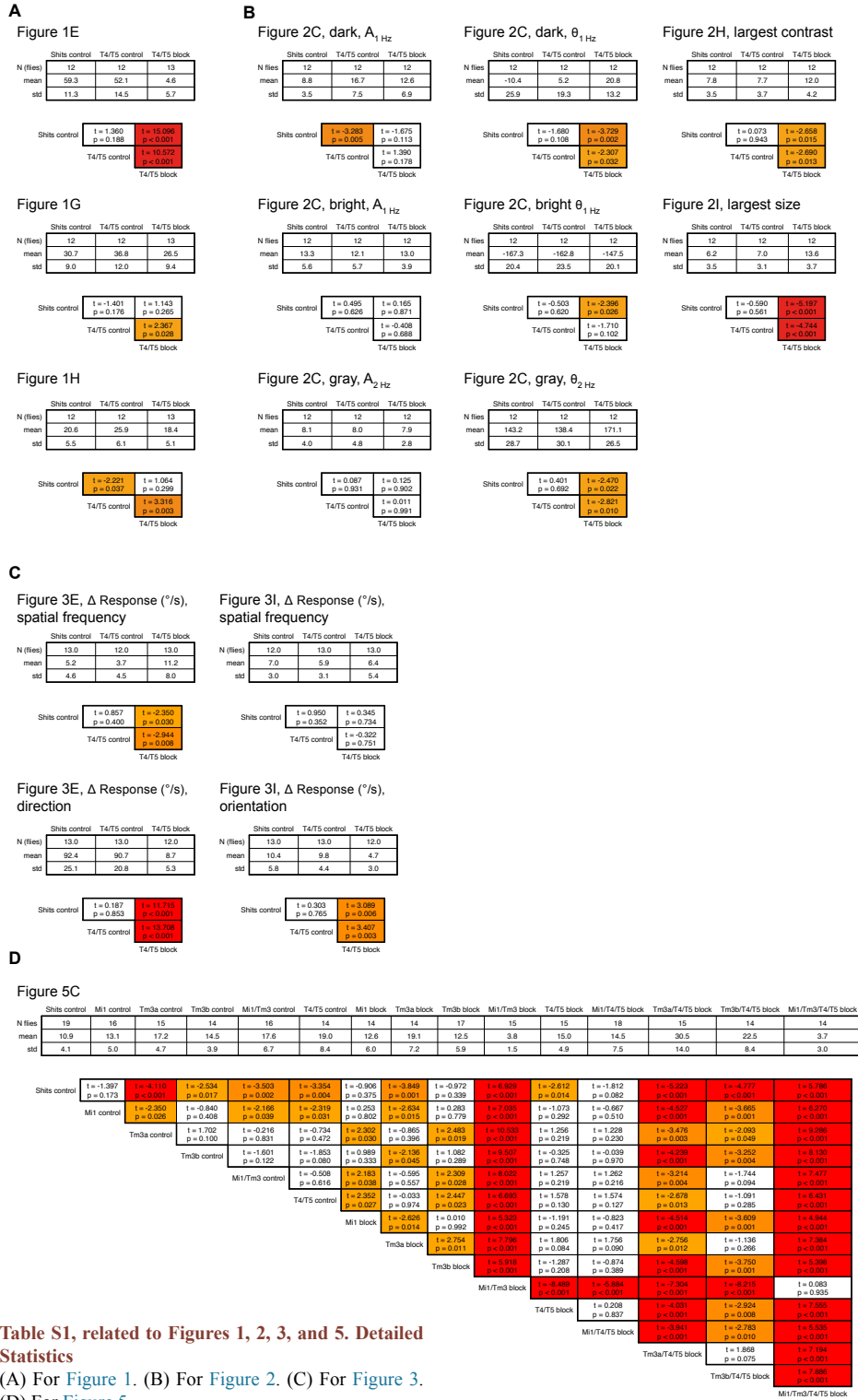


Table S1, related to Figures 1, 2, 3, and 5. Detailed Statistics
 (A) For Figure 1. (B) For Figure 2. (C) For Figure 3. (D) For Figure 5.

A Figure 6B

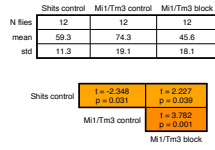


Figure 6F, A_{1Hz}^2 dark

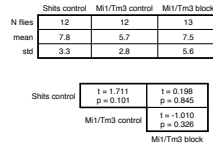


Figure 6F, θ_{1Hz}^2 dark

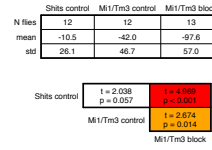


Figure 6D, response mean

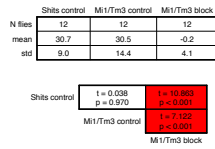


Figure 6F, A_{1Hz}^2 bright

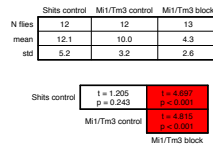


Figure 6F, θ_{1Hz}^2 bright

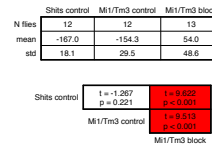


Figure 6D, A_{1Hz}

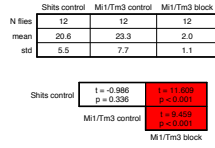


Figure 6F, A_{2Hz}^2 gray

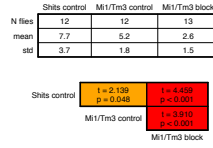
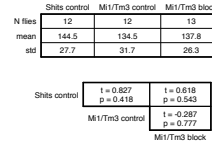


Figure 6F, θ_{2Hz}^2 gray



B

Figure S4C, A_{1Hz}^2 dark

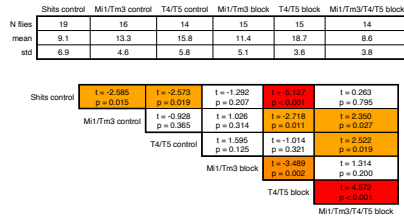


Figure S4C, A_{1Hz}^2 bright

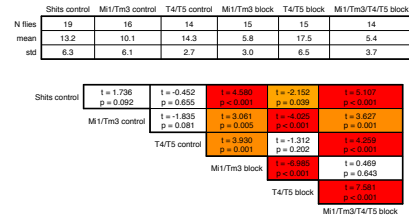


Figure S4C, θ_{1Hz}^2 dark

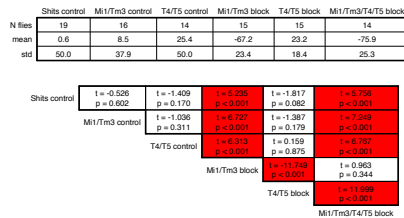
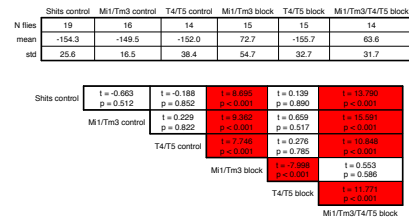


Figure S4C, θ_{1Hz}^2 bright



C

Figure 7C

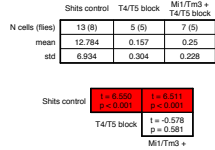


Figure 7D, A_{1Hz}

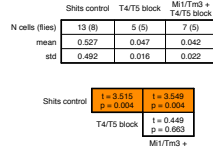


Figure 7D, A_{2Hz}

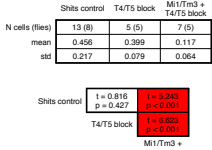


Figure 7G

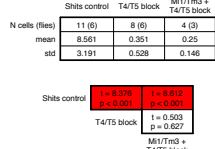


Figure 7H, A_{1Hz}

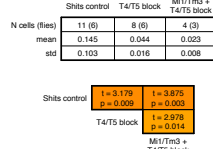


Figure 7H, A_{2Hz}

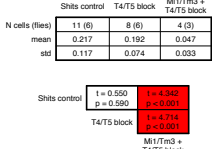


Table S2, related to Figures 6, S4, and 7. Detailed Statistics (A) For Figure 6. (B) For Figure S4. (C) For Figure 7.

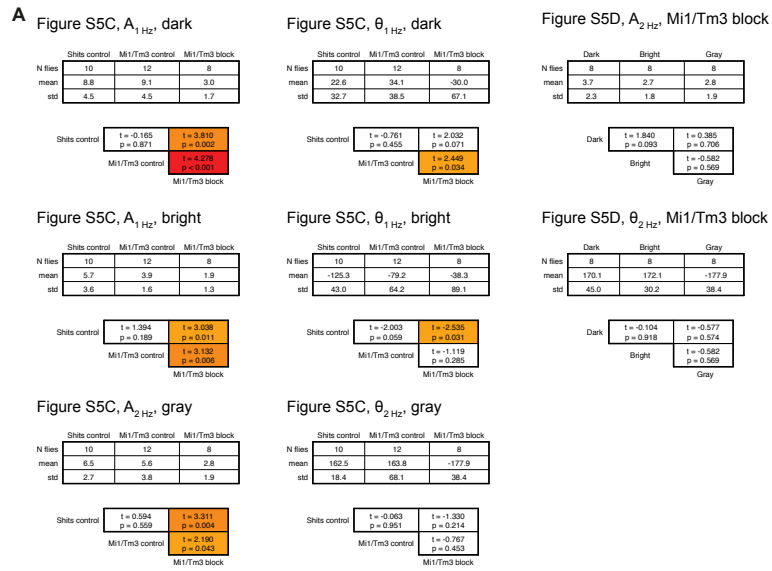


Table S3, related to Figure S5. Detailed Statistics
(A) For Figure S5.

A

Figure 4F

Shweta.comsol	L1.comsol	L2.comsol	L3.comsol	LS.comsol	MI.comsol	TI.comsol	MS.comsol	MT.comsol	LSI.comsol	LSII.comsol	LSIII.comsol	LSIV.comsol	LSV.comsol	LSVI.comsol	LSVII.comsol	LSVIII.comsol	LSIX.comsol	LSX.comsol	LSXI.comsol	LSXII.comsol	LSXIII.comsol	LSXIV.comsol	LSXV.comsol	LSXVI.comsol	LSXVII.comsol	LSXVIII.comsol	LSXIX.comsol	LSXX.comsol	LSXXI.comsol	LSXXII.comsol	LSXXIII.comsol	LSXXIV.comsol	LSXXV.comsol	LSXXVI.comsol	LSXXVII.comsol	LSXXVIII.comsol	LSXXIX.comsol	LSXXX.comsol
1.0000 p=0.0000	1.0000 p=0.0000	1.0000 p=0.0000	1.0000 p=0.0000	1.0000 p=0.0000	1.0000 p=0.0000	1.0000 p=0.0000	1.0000 p=0.0000	1.0000 p=0.0000	1.0000 p=0.0000	1.0000 p=0.0000	1.0000 p=0.0000	1.0000 p=0.0000	1.0000 p=0.0000	1.0000 p=0.0000	1.0000 p=0.0000	1.0000 p=0.0000	1.0000 p=0.0000	1.0000 p=0.0000	1.0000 p=0.0000	1.0000 p=0.0000	1.0000 p=0.0000	1.0000 p=0.0000	1.0000 p=0.0000	1.0000 p=0.0000	1.0000 p=0.0000	1.0000 p=0.0000	1.0000 p=0.0000	1.0000 p=0.0000	1.0000 p=0.0000	1.0000 p=0.0000	1.0000 p=0.0000	1.0000 p=0.0000	1.0000 p=0.0000	1.0000 p=0.0000	1.0000 p=0.0000	1.0000 p=0.0000	1.0000 p=0.0000	

Table S5, related to Figure 4. Detailed Statistics

(A) For Figure 4F.

A Figure S2D

	Shires.correct			L1.correct			L2.correct			L3.correct			L4.correct			L5.correct			L6.correct			L7.correct			L8.correct			L9.correct			L10.correct			L11.correct			L12.correct			L13.correct			L14.correct			L15.correct			L16.correct			L17.correct			L18.correct			L19.correct			L20.correct			L21.correct			L22.correct			L23.correct			L24.correct			L25.correct			L26.correct			L27.correct			L28.correct			L29.correct			L30.correct			L31.correct			L32.correct			L33.correct			L34.correct			L35.correct			L36.correct			L37.correct			L38.correct			L39.correct			L40.correct			L41.correct			L42.correct			L43.correct			L44.correct			L45.correct			L46.correct			L47.correct			L48.correct			L49.correct			L50.correct			L51.correct			L52.correct			L53.correct			L54.correct			L55.correct			L56.correct			L57.correct			L58.correct			L59.correct			L60.correct			L61.correct			L62.correct			L63.correct			L64.correct			L65.correct			L66.correct			L67.correct			L68.correct			L69.correct			L70.correct			L71.correct			L72.correct			L73.correct			L74.correct			L75.correct			L76.correct			L77.correct			L78.correct			L79.correct			L80.correct			L81.correct			L82.correct			L83.correct			L84.correct			L85.correct			L86.correct			L87.correct			L88.correct			L89.correct			L90.correct			L91.correct			L92.correct			L93.correct			L94.correct			L95.correct			L96.correct			L97.correct			L98.correct			L99.correct			L100.correct			L101.correct			L102.correct			L103.correct			L104.correct			L105.correct			L106.correct			L107.correct			L108.correct			L109.correct			L110.correct			L111.correct			L112.correct			L113.correct			L114.correct			L115.correct			L116.correct			L117.correct			L118.correct			L119.correct			L120.correct			L121.correct			L122.correct			L123.correct			L124.correct			L125.correct			L126.correct			L127.correct			L128.correct			L129.correct			L130.correct			L131.correct			L132.correct			L133.correct			L134.correct			L135.correct			L136.correct			L137.correct			L138.correct			L139.correct			L140.correct			L141.correct			L142.correct			L143.correct			L144.correct			L145.correct			L146.correct			L147.correct			L148.correct			L149.correct			L150.correct			L151.correct			L152.correct			L153.correct			L154.correct			L155.correct			L156.correct			L157.correct			L158.correct			L159.correct			L160.correct			L161.correct			L162.correct			L163.correct			L164.correct			L165.correct			L166.correct			L167.correct			L168.correct			L169.correct			L170.correct			L171.correct			L172.correct			L173.correct			L174.correct			L175.correct			L176.correct			L177.correct			L178.correct			L179.correct			L180.correct			L181.correct			L182.correct			L183.correct			L184.correct			L185.correct			L186.correct			L187.correct			L188.correct			L189.correct			L190.correct			L191.correct			L192.correct			L193.correct			L194.correct			L195.correct			L196.correct			L197.correct			L198.correct			L199.correct			L200.correct		
--	----------------	--	--	------------	--	--	------------	--	--	------------	--	--	------------	--	--	------------	--	--	------------	--	--	------------	--	--	------------	--	--	------------	--	--	-------------	--	--	-------------	--	--	-------------	--	--	-------------	--	--	-------------	--	--	-------------	--	--	-------------	--	--	-------------	--	--	-------------	--	--	-------------	--	--	-------------	--	--	-------------	--	--	-------------	--	--	-------------	--	--	-------------	--	--	-------------	--	--	-------------	--	--	-------------	--	--	-------------	--	--	-------------	--	--	-------------	--	--	-------------	--	--	-------------	--	--	-------------	--	--	-------------	--	--	-------------	--	--	-------------	--	--	-------------	--	--	-------------	--	--	-------------	--	--	-------------	--	--	-------------	--	--	-------------	--	--	-------------	--	--	-------------	--	--	-------------	--	--	-------------	--	--	-------------	--	--	-------------	--	--	-------------	--	--	-------------	--	--	-------------	--	--	-------------	--	--	-------------	--	--	-------------	--	--	-------------	--	--	-------------	--	--	-------------	--	--	-------------	--	--	-------------	--	--	-------------	--	--	-------------	--	--	-------------	--	--	-------------	--	--	-------------	--	--	-------------	--	--	-------------	--	--	-------------	--	--	-------------	--	--	-------------	--	--	-------------	--	--	-------------	--	--	-------------	--	--	-------------	--	--	-------------	--	--	-------------	--	--	-------------	--	--	-------------	--	--	-------------	--	--	-------------	--	--	-------------	--	--	-------------	--	--	-------------	--	--	-------------	--	--	-------------	--	--	-------------	--	--	-------------	--	--	-------------	--	--	-------------	--	--	-------------	--	--	-------------	--	--	-------------	--	--	-------------	--	--	-------------	--	--	-------------	--	--	-------------	--	--	-------------	--	--	-------------	--	--	-------------	--	--	-------------	--	--	--------------	--	--	--------------	--	--	--------------	--	--	--------------	--	--	--------------	--	--	--------------	--	--	--------------	--	--	--------------	--	--	--------------	--	--	--------------	--	--	--------------	--	--	--------------	--	--	--------------	--	--	--------------	--	--	--------------	--	--	--------------	--	--	--------------	--	--	--------------	--	--	--------------	--	--	--------------	--	--	--------------	--	--	--------------	--	--	--------------	--	--	--------------	--	--	--------------	--	--	--------------	--	--	--------------	--	--	--------------	--	--	--------------	--	--	--------------	--	--	--------------	--	--	--------------	--	--	--------------	--	--	--------------	--	--	--------------	--	--	--------------	--	--	--------------	--	--	--------------	--	--	--------------	--	--	--------------	--	--	--------------	--	--	--------------	--	--	--------------	--	--	--------------	--	--	--------------	--	--	--------------	--	--	--------------	--	--	--------------	--	--	--------------	--	--	--------------	--	--	--------------	--	--	--------------	--	--	--------------	--	--	--------------	--	--	--------------	--	--	--------------	--	--	--------------	--	--	--------------	--	--	--------------	--	--	--------------	--	--	--------------	--	--	--------------	--	--	--------------	--	--	--------------	--	--	--------------	--	--	--------------	--	--	--------------	--	--	--------------	--	--	--------------	--	--	--------------	--	--	--------------	--	--	--------------	--	--	--------------	--	--	--------------	--	--	--------------	--	--	--------------	--	--	--------------	--	--	--------------	--	--	--------------	--	--	--------------	--	--	--------------	--	--	--------------	--	--	--------------	--	--	--------------	--	--	--------------	--	--	--------------	--	--	--------------	--	--	--------------	--	--	--------------	--	--	--------------	--	--	--------------	--	--	--------------	--	--	--------------	--	--	--------------	--	--	--------------	--	--	--------------	--	--	--------------	--	--	--------------	--	--	--------------	--	--	--------------	--	--	--------------	--	--

Table S6, related to Figure S2. Detailed Statistics

(A) For Figure S2D.

SUPPLEMENTAL REFERENCES

Borst, A. (2014). Fly visual course control: behaviour, algorithms and circuits. *Nat. Rev. Neurosci.* 15, 590–599.

Rajashekhar, K.P., and Shamprasad, V.R. (2004). Golgi analysis of tangential neurons in the lobula plate of *Drosophila melanogaster*. *J. Biosci.* 29, 93–104.

2.6 ASYMMETRY OF *drosophila* ON AND OFF MOTION DETECTORS ENHANCES REAL-WORLD VELOCITY ESTIMATION

This study (Leonhardt et al., 2016) examined the temporal tuning of the parallel ON and OFF motion vision streams to natural images. It appeared in *Nature Neuroscience* in February 2016.

Similar to the vertebrate retina, in the fly visual system brightness increments and decrements are processed separately. Here, we investigated functional differences between the ON and the OFF channel of *Drosophila* motion vision. Lobula plate tangential cells respond more strongly to higher velocities when probed with moving dark edges while the tuning to bright edges peaks at comparatively low stimulus speeds. Behavioral experiments with an opposing-edge stimulus confirmed this notion. In low velocity regimes, flies follow bright edge motion, at intermediate velocities ON and OFF are in balance, while at higher speeds flies turn with the movement of dark edges. Optimizing ON-OFF detector models to natural images resulted in similar asymmetric tuning. Interestingly, the asymmetric tuning of ON and OFF channels explains the responses of tangential cells and walking flies to higher order motion stimuli that are not detected by classical, symmetric motion detectors. Hence, this study provided evidence that asymmetric tuning of ON and OFF channels visual processing can increase the performance of motion detectors in naturalistic scenarios.

Summary

The following authors contributed to this work:

Aljoscha Leonhardt¹, Georg Ammer¹, **Matthias Meier**, Etienne Serbe, Armin Bahl, and Alexander Borst

Aljoscha Leonhardt, Georg Ammer, and Alexander Borst designed the study. Aljoscha Leonhardt performed behavioral experiments, associated data analysis and all modeling work. Georg Ammer, **Matthias Meier**, and Etienne Serbe performed electrophysiological experiments. Georg Ammer performed calcium imaging. Aljoscha Leonhardt and Georg Ammer analyzed physiological data. Armin Bahl designed the behavioral apparatuses and performed behavioral experiments. Aljoscha Leonhardt wrote the manuscript with help from all of the authors.

Author contribution

¹ equal contribution

Asymmetry of *Drosophila* ON and OFF motion detectors enhances real-world velocity estimation

Aljoscha Leonhardt^{1,3}, Georg Ammer^{1,3}, Matthias Meier¹, Etienne Serbe¹, Armin Bahl^{1,2} & Alexander Borst¹

The reliable estimation of motion across varied surroundings represents a survival-critical task for sighted animals. How neural circuits have adapted to the particular demands of natural environments, however, is not well understood. We explored this question in the visual system of *Drosophila melanogaster*. Here, as in many mammalian retinas, motion is computed in parallel streams for brightness increments (ON) and decrements (OFF). When genetically isolated, ON and OFF pathways proved equally capable of accurately matching walking responses to realistic motion. To our surprise, detailed characterization of their functional tuning properties through *in vivo* calcium imaging and electrophysiology revealed stark differences in temporal tuning between ON and OFF channels. We trained an *in silico* motion estimation model on natural scenes and discovered that our optimized detector exhibited differences similar to those of the biological system. Thus, functional ON-OFF asymmetries in fly visual circuitry may reflect ON-OFF asymmetries in natural environments.

Motion cues resulting from movement through space constitute an important source of information about the external world, supporting course stabilization, navigation or tracking of landmarks¹. Biological motion detectors have evolved in environments of astounding complexity. Visual landscapes from which animals derive such cues are cluttered and produce rapidly fluctuating signals. Exploiting a priori knowledge about scene features is therefore critical for organisms to reliably extract the spatiotemporal correlations that indicate motion. Basic statistical properties such as the shape of power spectra are known to be conserved between natural scenes^{2–4}. Higher order features such as textures, edges or contrast distributions yield additional cues and exhibit consistent statistics across visual environments. Examples of neural adaptation to natural scene statistics abound, operating at various levels of visual processing hierarchies^{5–7}.

Segregated processing of positive (ON) and negative (OFF) changes in sensory magnitude is a common trait among modalities ranging from olfaction to motion detection in the insect and mammalian visual systems^{1,8,9}. Splitting time-varying signals into two streams, covering opposite directions of change, is thought to confer various advantages to sensory circuits. For instance, ON-OFF systems maximize information transfer when resources are constrained⁸. In the case of motion detection, the ON-OFF split may drastically simplify the biophysical implementation of operations such as sign-correct multiplication^{10,11}.

Luminance distributions in real-world environments are heavily asymmetric with regard to positive and negative contrast^{2,12}. Visual systems take this into account: in the mammalian retina, for example, more ganglion cells are dedicated to processing negative than positive spatial contrast, consistent with naturally encountered skewness¹³. Theoretical studies on motion detection have proposed that, in ON-OFF asymmetric environments, higher order correlations carry valuable

information about scene motion¹⁴. Indeed, flies and humans alike appear to be capable of extracting higher order cues^{12,15}, suggesting that both apply this strategy for motion estimation. However, little is known about the neural mechanism by which either visual system gains access to higher order correlations.

As a result of the availability of powerful genetic tools and extensive connectomic^{16,17} as well as functional^{18–24} characterizations, knowledge about the neural substrate of *Drosophila* motion detectors has grown exponentially in recent years⁹. Briefly, signals impinging on the photoreceptors are split into two polarity-specific channels, with one processing brightness increases (from L1 to T4 via at least Mi1 and Tm3) and the other processing brightness decreases (from L2, L3 and L4 to T5 via Tm1, Tm2, Tm4 and Tm9). Local ON and OFF motion signals are then extracted on the dendrites of T4 and T5, respectively, in a manner that is well explained by the Hassenstein-Reichardt correlation model^{9,11,21}. Large tangential cells in the lobula plate pool these signals and influence behavioral output^{1,9,25,26}.

Given the ON-OFF asymmetries encountered in natural environments, we set out to determine how the specific features of natural scenes have shaped ON and OFF motion detectors in the fly visual system. In contradistinction to previous studies, we were able to directly assess the behavioral performance of neural pathways by isolating them genetically. We found that asymmetries of natural environments had direct correspondence in tuning asymmetries of the fly motion detection system.

RESULTS

ON and OFF motion detectors reliably estimate velocity

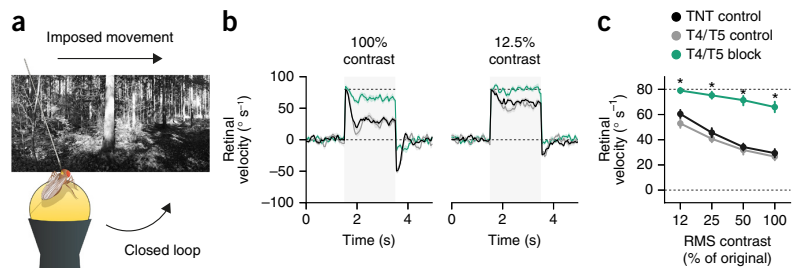
Flies react to visual wide-field motion by turning with the environment^{1,19,27}. During navigation, this optomotor response stabilizes the animal's course in the face of external perturbations or internal noise.

¹Max Planck Institute of Neurobiology, Martinsried, Germany. ²Present address: Department of Molecular and Cell Biology, Harvard University, Cambridge, Massachusetts, USA. ³These authors contributed equally to this work. Correspondence should be addressed to A.L. (leonhardt@neuro.mpg.de).

Received 19 November 2015; accepted 29 January 2016; published online 29 February 2016; corrected online 7 March 2016 (details online); doi:10.1038/nn.4262

Figure 1 Flies stabilize their path in naturalistic environments using a combination of ON and OFF motion detectors. **(a)** Illustration of behavioral setup. Tethered flies walk in a virtual closed-loop environment. During certain time periods, their trajectories are perturbed externally. **(b)** Path stabilization under different contrast conditions. Retinal velocity describes environment rotation relative to the fly's eye. During epochs shaded in gray, a constant rotation bias of 80° s^{-1} was added. Upper dashed line indicates imposed velocity. Control flies (TNT control in black, $N = 19$;

T4/T5 control in gray, $N = 12$) reduced the imposed retinal velocity effectively whereas T4/T5 block flies (in green, $N = 13$) did not. Left, unmodified image contrast. Right, artificial reduction of root-mean-square (RMS) contrast to 12.5% of initial value. Exact genotypes are listed in **Supplementary Table 1**. **(c)** Quantification of stabilization performance across contrasts. Retinal velocity was averaged between 2 and 3 s. Dashed lines correspond to zero and full correction of the perturbation. Shaded areas around traces and vertical bars signify bootstrapped 68% confidence intervals around the mean. Asterisks indicate significant differences of block flies from both genotype controls after Bonferroni-corrected two-tailed t tests ($*P < 0.05$); exact test statistics are reported in **Supplementary Table 2**.



Any deviation from a straight path results in retinal flow that is counteracted by matching direction and, ideally, velocity of perceived drift through locomotion. Responses of behaving fruit flies and wide-field motion-sensitive neurons to simplified motion stimuli such as sinusoidal gratings have been studied extensively^{27,28}. Tethered flying flies placed in such artificial environments do indeed correct for externally applied biases²⁹. However, flies generally solve this problem in vastly more complex environments. So far, nothing is known about the quantitative extent of their ability to perform path stabilization in naturalistic contexts.

We addressed this question by allowing tethered flies to stabilize their walking trajectories in virtual environments. To cover many possible surroundings, we generated a library of panoramic images spanning the entire visual field of the fly. Randomly selected images were projected onto a virtual cylinder whose orientation was controlled in closed loop through the angular trajectory of flies walking on an air-suspended ball (**Fig. 1a**). In addition, we superimposed fixed-velocity rotations and recorded the relative motion between the fly and its environment. Our approach therefore simulated translation-free walking through a distant visual scene in the presence of external course perturbations. As expected, control flies actively reduced retinal slip speed by rotating in the direction of and with similar velocity as their visual environment (**Fig. 1b**). A combination of neural, motor and setup-intrinsic delays resulted in characteristic over- and undershoots on the order of hundreds of milliseconds, trailing both onset and offset of the motion bias. Notably, control flies rarely achieved a retinal velocity of zero, which would indicate full compensation of the involuntary rotation.

Although combined synaptic silencing of cell types T4 and T5 abolishes behavioral and electrophysiological sensitivity to grating motion^{27,30}, it is unclear whether naturalistic stimuli can provide additional cues exploited by secondary circuits. When we used Gal4-controlled³¹ expression of the light chain of tetanus toxin³² (TNT) to genetically disrupt synaptic output of all T4 and T5 cells, which are known to implement local motion detection^{21,27,30}, we discovered a marked impairment of stabilization performance. This was the case across the full range of artificially reduced image contrasts tested (**Fig. 1b,c**). The effect did not stem from gross motor defects; the flies' walking speed was at control level (**Supplementary Fig. 1**). Contrast reductions also negatively affected the stabilization ability of control flies. This replicated a previously described property of motion-sensitive lobula plate tangential cells in a behavioral setting: response gain of these cells is diminished for natural images artificially reduced in contrast³³. In summary, we found that flies actively

stabilized their path in complex visual scenes and that T4 and T5 cells were necessary neural elements for this feedback behavior.

Previous work confirmed that T4 and T5 cells are predominantly sensitive to motion defined by luminance increases and decreases, respectively²¹. Full-field motion of naturalistic scenes, especially at large viewing distances and in cluttered environments, creates a rich gamut of both ON and OFF motion. Arrays of ON or OFF detectors may therefore be equally capable of reporting the direction and velocity of realistic global motion. However, nothing is known about the individual contributions of ON and OFF detectors to velocity estimation in such contexts. Moreover, the transformation from stimulus velocity to response strength for all read-outs of the fly motion system is highly sensitive to geometrical features of the stimulus: the fly motion detector is generally not a pure speedometer^{1,9}. Even though most gain regimes would eventually lead to stabilization, the optomotor response should ideally match true retinal velocity to correct the fly's course quickly and efficiently²⁹. Indeed, tangential cells exhibit a linearized and reliable velocity-response curve when stimulated with natural images as opposed to periodic stimuli such as gratings³³. We sought to test whether this is reflected by optomotor behavior.

To this end, we assessed *Drosophila's* behavioral ability to track scene velocity in open loop (**Fig. 2a**). Velocity-response curves were stochastically probed by presenting randomly chosen images moving at constant velocities drawn from a Gaussian distribution on each individual trial. Estimation performance was then defined as the linear correlation between environment rotation and average turning response of the fly. A correlation coefficient of $r = 1.0$ indicates a perfectly reliable linear mapping of global motion onto behavioral response across all scenes, as would be required of a functional speedometer. Following visual stimulation, flies responded with robust turning responses that increased until stimulus offset and decayed right after (**Supplementary Fig. 2**). To our surprise, control flies performed the velocity estimation task exceedingly well (**Fig. 2b**). For our image set, individual flies reached correlation coefficients above 0.8 across hundreds of trials. Not all behavioral complexity was captured by the linear model: trials with turning responses close to 0° s^{-1} , for instance, were rare (**Fig. 2b**). However, several effects suggested that our simplified measure was indeed valid. First, as anticipated, flies with disrupted T4 and T5 activity exhibited correlation coefficients and response gain close to zero (**Fig. 2c–e**). Second, the correlation coefficients of control flies were heavily decreased by the reduction of image contrast (**Fig. 2d**). This reflected increasing task difficulty at the lower end of the contrast spectrum. Third,

Figure 2 ON and OFF channels are equally capable of estimating the velocity of natural scenes. **(a)** Sketch of experimental approach. Flies were subjected to a set of natural images rotating at random velocities drawn from a Gaussian distribution (s.d. = 50° s^{-1}) in open loop. **(b)** Velocity estimation performance of control flies. Each dot represents the average rotational response for one trial at full contrast. Trials were pooled across flies of all control groups ($n = 1,936$ trials from $N = 13$ TNT control flies, $n = 1,879/N = 12$ for T4/T5 control, $n = 2,070/N = 13$ for T4 control, $n = 1,331/N = 12$ for T5 control); the linear fit is for illustrative purposes only. The shaded curve to the right shows a kernel density estimate of rotational responses. **(c)** Velocity estimation performance of block flies, displayed as in **b** ($n = 1,755/N = 11$ for T4/T5 block, $n = 1,976/N = 12$ for T4 block, $n = 1,778/N = 12$ for T5 block). **(d)** Quantification of velocity estimation performance across artificially modified image contrasts. Performance was measured as the Pearson correlation between environment rotation and integrated response. Although T4/T5 block flies were strongly impaired at all contrasts, silencing T4 or T5 individually had no measurable effect on estimation performance. **(e)** Quantification of response gain across contrast range. Gain was measured as the slope of a linear regression model mapping environmental rotation onto rotational response. Vertical bars signify bootstrapped 68% confidence intervals around the mean. Asterisks indicate significant differences for block flies from both Gal4 and UAS controls after Bonferroni-corrected two-tailed t tests ($*P < 0.05$); exact test statistics are reported in **Supplementary Table 3**.

we once again found a contrast-dependent decrease of response gain as determined by the slope of a linear fit (**Fig. 2e**). It should be noted that these gain values depend on the choice of averaging window. For this reason, and because control systems tend to overcompensate in the absence of feedback, large gain values in open loop do not necessarily entail full compensation in closed loop (**Fig. 1c**).

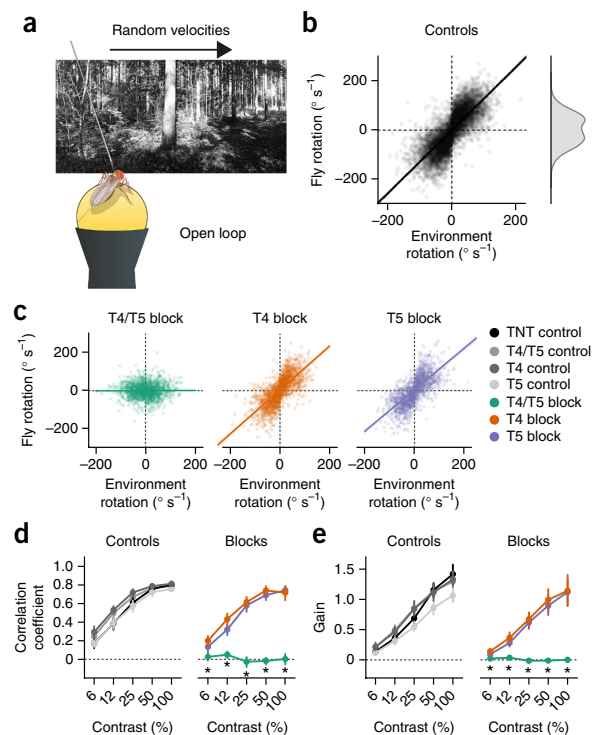
To determine potentially differential contributions of ON and OFF detectors to velocity estimation in naturalistic contexts, we then silenced only T4 or T5 using TNT. In a previous study using the same lines²¹, we found that blocking T4 or T5 led to a strongly reduced ability to detect bright or dark edges, respectively, at both the electrophysiological and behavioral level. In stark contrast to these effects, we found no impairment of velocity estimation for our naturalistic image set. Correlation coefficients for both T4 block and T5 block flies were not substantially different from control groups, even at low contrast levels (**Fig. 2c,d** and **Supplementary Fig. 2**). Finally, we alternatively quantified estimation performance as the root-mean-square error of a Bayesian estimator trained on the behavioral data, the results of which supported similar conclusions (**Supplementary Fig. 3**).

Taken together, we found that combined silencing of T4 and T5 completely abolished flies' ability to track the velocity of global motion in naturalistic scenes. Notably, ON and OFF channels appeared to be redundant for this task. Either was sufficient to recapitulate naturalistic behavior.

Tuning properties of ON and OFF channels are asymmetric

Given that ON and OFF channels seemed equally capable of performing reliable velocity estimation across various visual scenes, it is plausible to assume that they share temporal tuning properties. Previous studies reported comparable temporal frequency optima for sinusoidal gratings²¹. Calcium imaging, however, lacks the temporal resolution required for a precise characterization of pathway kinetics. Moreover, considering the polarity specialization of T4 and T5, we sought to characterize the channels using pure ON or OFF stimuli as opposed to sinusoidal gratings defined equally by brightness increments and decrements.

First, we confirmed that T4 and T5 respond exclusively to bright and dark edges, respectively. The T4 driver line used for imaging

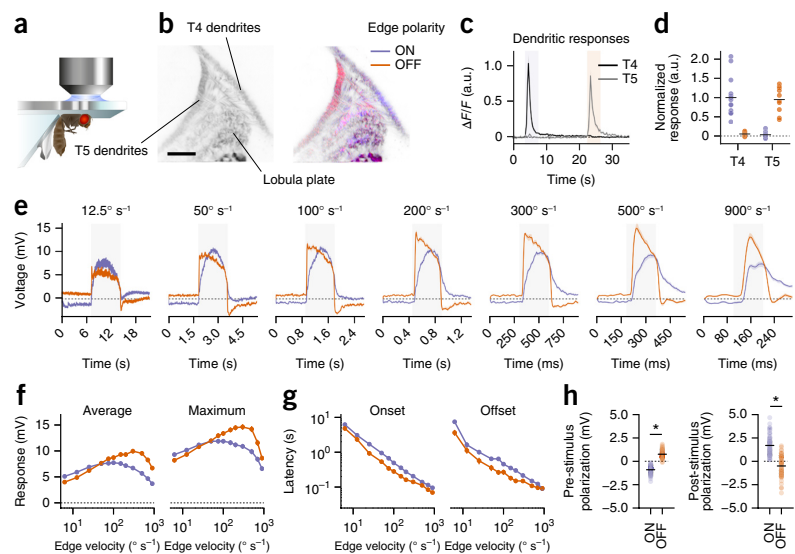


in a previous study²¹ showed marginal coexpression in T5 cells; the converse applied to the T5 driver line. Our earlier work had revealed minor sensitivity for OFF edges in T4 cells as well as small responses for ON edges in T5 cells, measured in the confines of the lobula plate, where both cell types intermingle. We speculated that this was a result of either Gal4 coexpression or actual physiological crosstalk between ON and OFF circuitry. Moreover, a physiological characterization of T4 input elements suggests that T4 should only be mildly selective for ON motion²⁴. To conclusively decide between the alternatives, we performed two-photon calcium imaging using a combined T4 and T5 line in conjunction with the calcium reporter GCaMP6f³⁴ (**Fig. 3a**). Separation of T4 and T5 signals was then achieved by restricting the region of interest to the cells' dendrites in the medulla or lobula, respectively (**Fig. 3b**). Dendrites showed strong calcium increases following visual edge stimulation that were perfectly polarity specific (**Fig. 3c,d**). This allowed us to characterize the temporal tuning properties of T4 and T5 by means of highly time-resolved electrophysiological recordings from downstream cells.

We determined velocity tuning curves for ON and OFF edges moving at speeds spanning two orders of magnitude by recording from the large-field motion-sensitive cells of the horizontal and vertical systems^{9,28} in the lobula plate. These cells are the primary recipients of feedforward ON and OFF signals, receiving direct input from T4 and T5 for stimuli moving in preferred direction and indirect inhibitory input via lobula plate interneurons for null direction motion^{30,35}. Cells depolarized when stimulated with ON or OFF edge motion along their preferred direction. Unexpectedly, tuning curves as well as general kinetics differed substantially between ON and OFF (**Fig. 3e**). Both channels showed increasing response strength up to a certain velocity, after which responses fell off (**Fig. 3f**). For ON edges, however, this peak was located at approximately 100° s^{-1} , whereas OFF responses reached their maximum at edge velocities of $\sim 300^\circ \text{ s}^{-1}$. This held true

Figure 3 Physiological characterization of ON and OFF channels reveals tuning asymmetries.

(a) Schematic of preparation used for two-photon calcium imaging and patch-clamp recordings from lobula plate tangential cells (LPTCs). (b) Left, two-photon image of GCaMP6f expression in T4 and T5 cells. Scale bar represents 10 μm . Right, representative T4 and T5 activity during ON (blue) or OFF (red) edge stimulation overlaid onto left-hand image. Activity was confined to T4 or T5 dendrites, depending on edge polarity. (c) Relative fluorescence ($\Delta F/F$) across time for regions of interest centered on either T4 (black, $N = 14$) or T5 (gray, $N = 10$) dendrites. (d) Quantification of responses as averages over edge presentation period indicated by shaded areas in c. (e) Average responses of LPTCs for ON and OFF edges moving at a range of velocities in preferred direction. Time axes are scaled differently. Shaded area indicates edge presentation and covers visual field traversal (90°) at the specified velocity. Vertical and horizontal system cells from wild-type flies were pooled ($n = 70$ from $N = 43$ flies). (f) Velocity tuning curves for ON and OFF edges based on either average or maximum response during full stimulation period. (g) Response kinetics for ON and OFF edges on logarithmic scale. (h) Static properties averaged across velocities. Dots represent individual observations and black bars indicate group averages. Vertical bars and shaded areas signify bootstrapped 68% confidence intervals around the mean. Asterisks indicate significant differences between ON and OFF after two-tailed t tests ($*P < 0.05$). Exact test statistics are reported in **Supplementary Table 4**.



regardless of whether we quantified average or maximum voltage. Moreover, both onset and offset latencies were larger for ON edges than for OFF edges across the full range of velocities tested (**Fig. 3g**). We also observed a constant polarization that closely reflected surround luminance (**Fig. 3h**); for instance, the field illumination preceding the onset of an OFF edge led to steady-state depolarization of the cell, which gave way to hyperpolarization after the dark edge had traveled through the fly's visual field (**Fig. 3e**). In a second set of experiments, we examined whether such differential pre-stimulus polarization could explain the observed ON-OFF asymmetries. Flies were presented with edges starting from an intermediate background luminance that was equal for both polarities (**Supplementary Fig. 4a**). Notably, edge velocity tuning curves were not affected by this alteration, whereas differences in onset kinetics vanished (**Supplementary Fig. 4b,c**). This suggests that luminance adaptation has a strong effect on the dynamics of tangential cell responses, but does not influence temporal tuning.

In summary, we observed strongly differential velocity tuning for ON and OFF pathways, with the former responding maximally to slower velocities than the latter. To determine whether the observed tuning differences are behaviorally relevant, we performed balanced motion experiments on walking flies. Multiple resetting ON and OFF edges distributed across the visual field moved simultaneously in opposite directions over several seconds^{19,21,23} (**Fig. 4a**). This was done for a large velocity range and offered a behavioral read-out of the weighting between ON and OFF pathways. Here, a turning tendency of zero implies equal ON and OFF responses. Consistent with electrophysiological results, we found that the balance between ON and OFF responses was clearly modulated by edge velocity (**Fig. 4b**). At low speeds, ON responses dominated the overall turning behavior and control flies continuously rotated in the direction of bright edges (**Fig. 4c**). At higher velocities, this turning tendency was reversed, indicating dominant OFF responses. ON and OFF were only completely in balance at an edge velocity of around 80° s^{-1} . To test whether these imbalances also occur at the transient time scales dominating walking behavior,

we then shortened the stimulus duration to 500, 250 or 100 ms. These opposing edge pulses produced robust responses whose amplitude diminished with decreasing stimulus length. Notably, all tuning curves had shapes that were comparable to the steady-state condition (**Supplementary Fig. 5**).

We also performed blocking experiments using this assay (**Fig. 4c**). Removing T4 and T5 from the circuit resulted in abolished turning tendencies across all velocities. For individual blocks, we recovered effects whose general direction had been described before²¹: T4 block flies always rotated in the direction of OFF edges and T5 block flies consistently followed motion of ON edges (**Fig. 4b**). Notably, these block effects were most pronounced at different velocities. For T4 block flies, the curve peaked at 160° s^{-1} . For T5 block flies, the maximum was found at 80° s^{-1} . This roughly confirmed the edge tuning curves from tangential cell recordings (**Fig. 3f**) under the assumption that each individual block was reasonably complete, leaving only one pathway intact. From this, we generated linear predictions for wild-type behavior. *Post hoc* tuning curves were calculated by either subtracting edge tuning curves measured as average voltage or summing the behavioral curves of T4 block and T5 block flies (**Fig. 4d**). Both models successfully predicted response signs and approximate zero crossing of control flies, corroborating the notion that tangential cells combine T4 and T5 signals in an approximately linear regime and then control turning behavior directly.

Despite their comparable performance during naturalistic velocity estimation, the ON and OFF pathways represented by T4 and T5 are tuned to different velocity regimes at both the electrophysiological and behavioral level. We next explored whether this tuning asymmetry is critical for their estimation fidelity.

Optimized detectors are ON-OFF asymmetric

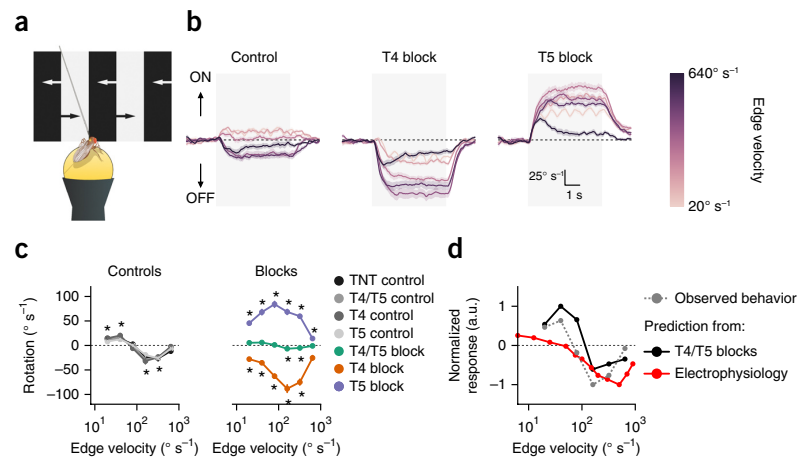
The *Drosophila* motion detection system is well described by a two-quadrant ON-OFF detector: the combination of two motion detectors, one processing only ON signals akin to the physiological T4 channel and one processing only OFF signals akin to the physiological

Figure 4 Asymmetry between ON and OFF channels persists at the behavioral level.

(a) Schematic drawing of balanced motion stimulus with ON and OFF edges simultaneously moving into opposite directions at various velocities. (b) Rotational responses for TNT control flies as well as T4 and T5 block flies. Trace color indicates velocity of edges. Positive responses are syndirectional with ON edge motion; negative responses follow OFF edge motion. Gray-shaded area denotes epoch during which edges were moving. T4 and T5 block flies are consistently biased away from the disrupted polarity. For control flies, the dominant polarity changes with velocity.

(c) Quantification of turning responses averaged over stimulation period (3 to 7 s; $N = 12$ for TNT control, $N = 12$ for T4/T5 control, $N = 12$ for T4 control, $N = 13$ for T5 control, $N = 12$ for T4/T5 block, $N = 15$ for T4 block, $N = 14$ for T5 block). For controls, asterisks indicate responses that are significantly different from zero ($*P < 0.05$).

For block genotypes, asterisks indicate significant differences from both corresponding Gal4 and UAS controls (Bonferroni-corrected t tests, $*P < 0.05$). (d) Comparison of observed control tuning curves (gray) with tuning curves linearly predicted from either the sum of behavioral T4 block and T5 block tuning curves (black) or the difference between electrophysiologically determined ON and OFF tuning curves (red; Fig. 3). Vertical bars and shaded areas surrounding traces signify bootstrapped 68% confidence intervals around the mean. Exact test statistics are reported in **Supplementary Table 5**.



T5 channel¹⁰. Each subunit then computes motion according to the well-established Hassenstein-Reichardt correlation model based on the multiplication of differentially filtered, spatially separated signals¹¹. Counter-intuitively, such models are capable of explaining complex phenomena such as the reverse-phi effect observed for motion accompanied by contrast reversals^{10,19,36}. Critical for this is the inclusion of a weighted tonic signal (DC component) in addition to the high-pass signal modeling processing in lamina monopolar cells. Parameters for the model are generally chosen such that the ON and OFF subunits of the detector remain symmetric^{10,19}. Our results concerning edge velocity tuning, however, speak in favor of asymmetric tuning. Moreover, work on natural scenes has repeatedly shown that realistic environments are strongly asymmetric with regard to ON and OFF^{2,12,13}. What does an ON-OFF detector look like that is tuned to naturalistic environments?

Various estimation objectives may be prioritized, depending on the given task^{29,37}. For this study, we operationalized detector fitness analogously to previous studies¹² and equivalently to our own behavioral experiments as the linear correlation between the velocity of a rigidly translating natural image and time-averaged detector output. Given that Hassenstein-Reichardt detectors directly explain many aspects of fly optomotor behavior^{1,9}, and considering that flies achieve extremely high correlation values in the corresponding experimental setting (Fig. 2), this seemed to be a sensible target for the model. We optimized by exhaustively scanning the parameter space spanned by low-pass filter time constant and DC component of simplified ON and OFF detectors (Fig. 5a). This was done in a cross-validated manner. We chose a small set of parameters for optimization in which ON-OFF asymmetries had been observed previously. Our own results on edge tuning (Fig. 3e,f) indicated that there were large temporal tuning differences between ON and OFF pathways. Physiological characterization of medulla interneurons Mi1 and Tm3 for T4 as well as Tm1 and Tm2 for T5 has revealed distinct differences with regard to the strength of DC signals present at the input of motion detectors²⁴. Thus, we looked for combinations of low-pass filter time constants and DC weightings that would maximize velocity estimation performance of isolated ON and OFF detectors for a large

set of natural scenes from the van Hateren image database⁶. Velocities were drawn from a Gaussian distribution whose width was based on turning speed distributions determined in our closed-loop experiments. Optimized parameters were modulated in physiologically plausible ranges; all other settings were chosen based on previous modeling work¹⁰ and not tuned for any particular result.

The resulting fitness landscape as a function of low-pass time constant and DC component was smooth and strongly asymmetric with respect to ON and OFF (Fig. 5b). Indeed, when we extracted the parameter sets that maximized fitness for independent ON and OFF detectors, we found that optimal settings were ON-OFF asymmetric with respect to both parameters (Fig. 5c). Specifically, the best time constants for ON detectors were larger than those achieving maximum correlation for OFF detectors. The best DC weights had higher values for ON detectors than for OFF detectors and opposite signs (Fig. 5c).

To ascertain whether parameter asymmetry improved velocity estimation over that achieved by symmetric models, we compared equally weighted combinations of independently optimized ON and OFF detectors to optimized detectors that were constrained to be symmetric. The cross-validated performance improvement was small but significant ($t(98) = 4.08$, $P < 0.001$), suggesting that detector asymmetry is an advantageous strategy (Fig. 5d). The differences between ON and OFF parameters of optimal asymmetric models were substantial (Fig. 5e). We therefore looked for functional disparities between the average optimized models. Simulated temporal frequency tuning curves for sinusoidal gratings were highly similar, with slightly shifted response optima (Fig. 5f). The asymmetric and the symmetric model also produced comparable output for a dynamically moving grating (Fig. 5g). When we simulated edge velocity tuning curves as we had measured experimentally (Figs. 3 and 4), the symmetric model exhibited identical tuning for ON and OFF edges, as was expected from identical temporal parameters. Our asymmetric model, however, correctly replicated the shift between optima for ON and OFF edges with the detector being tuned to higher OFF than ON edge velocities (Fig. 5h). In addition, the asymmetric model predicted a difference in overall strength between ON and

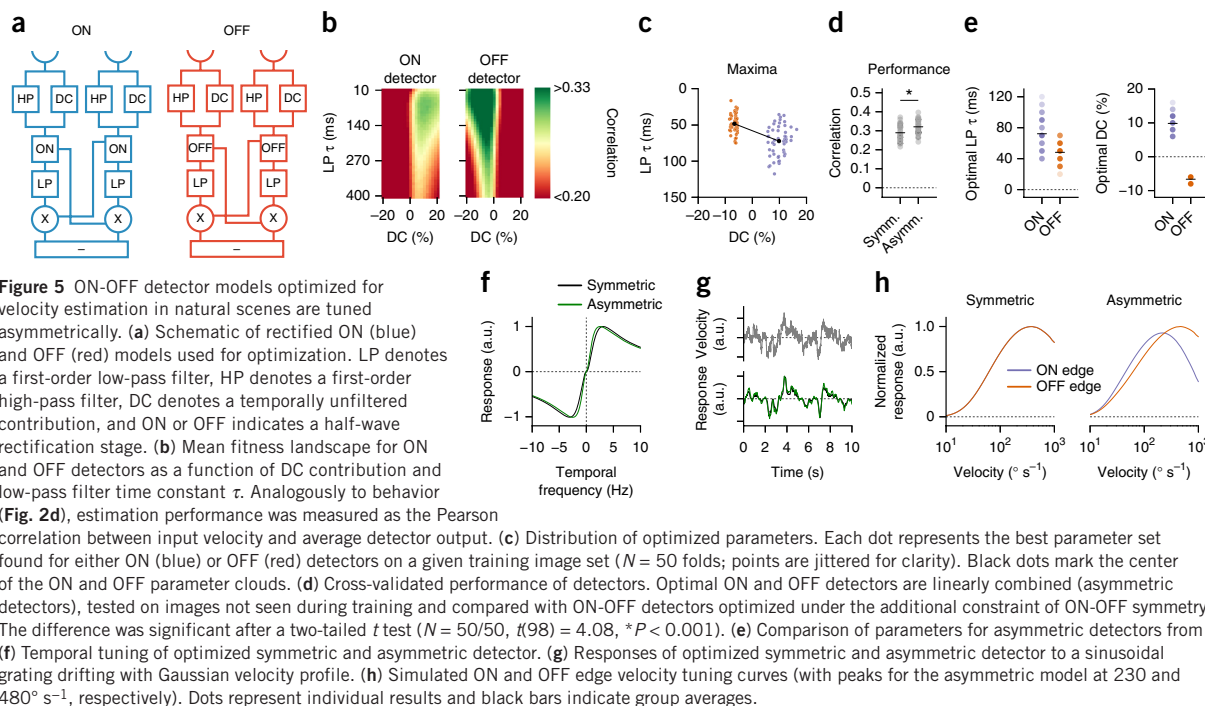


Figure 5 ON-OFF detector models optimized for velocity estimation in natural scenes are tuned asymmetrically. **(a)** Schematic of rectified ON (blue) and OFF (red) models used for optimization. LP denotes a first-order low-pass filter, HP denotes a first-order high-pass filter, DC denotes a temporally unfiltered contribution, and ON or OFF indicates a half-wave rectification stage. **(b)** Mean fitness landscape for ON and OFF detectors as a function of DC contribution and low-pass filter time constant τ . Analogously to behavior (**Fig. 2d**), estimation performance was measured as the Pearson correlation between input velocity and average detector output. **(c)** Distribution of optimized parameters. Each dot represents the best parameter set found for either ON (blue) or OFF (red) detectors on a given training image set ($N = 50$ folds; points are jittered for clarity). Black dots mark the center of the ON and OFF parameter clouds. **(d)** Cross-validated performance of detectors. Optimal ON and OFF detectors are linearly combined (asymmetric detectors), tested on images not seen during training and compared with ON-OFF detectors optimized under the additional constraint of ON-OFF symmetry. The difference was significant after a two-tailed t test ($N = 50/50$, $t(98) = 4.08$, $*P < 0.001$). **(e)** Comparison of parameters for asymmetric detectors from **c**. **(f)** Temporal tuning of optimized symmetric and asymmetric detector. **(g)** Responses of optimized symmetric and asymmetric detector to a sinusoidal grating drifting with Gaussian velocity profile. **(h)** Simulated ON and OFF edge velocity tuning curves (with peaks for the asymmetric model at 230 and 480° s^{-1} , respectively). Dots represent individual results and black bars indicate group averages.

OFF edge responses (**Fig. 3f**) even though subunits were summed at equal gain. The modeled edge optima occurred at higher velocities than those we had determined experimentally. As optimized parameters for the detectors depended on the s.d. of the distribution from which test velocities were drawn, their absolute scale was

somewhat arbitrary; conditional on behavioral state, turning speed distributions may differ substantially. The direction of the asymmetry, however, was consistent with experimental findings.

We then determined natural image features necessary for asymmetries to appear in tuned ON-OFF detectors. To this end, we repeated the optimization procedure for image sets in which we had manipulated specific statistical properties. First, for the unaltered set, the best asymmetric ON and OFF detectors showed large differences for both low-pass time constant, as well as absolute DC level (**Fig. 6a**). Second, we randomized the phase structure of every image, thereby removing all higher level features such as textures or edges, as well as making scenes largely ON-OFF symmetric¹³, while retaining the typical power spectrum of natural scenes. Here, the asymmetry of time constants disappeared (**Fig. 6b**). Third, we artificially reinstated the natural luminance distribution in phase-randomized images (**Fig. 6c**). This manipulation rescued the time constant asymmetry, suggesting that a skewed luminance distribution is the critical constraint forcing filter

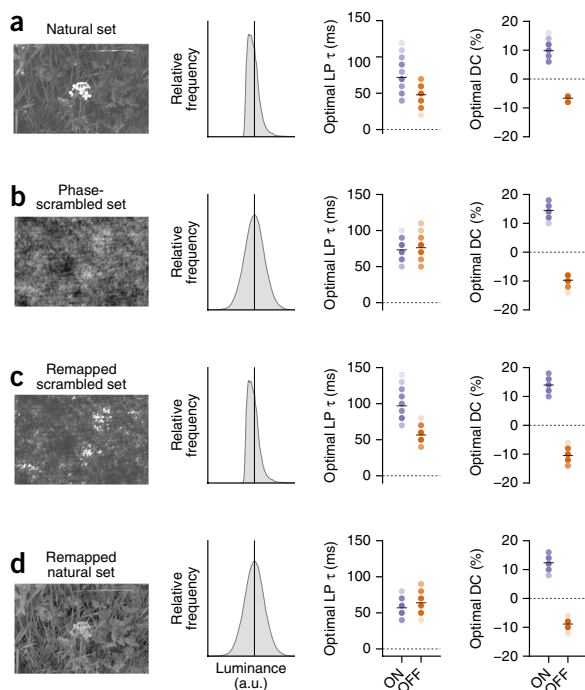


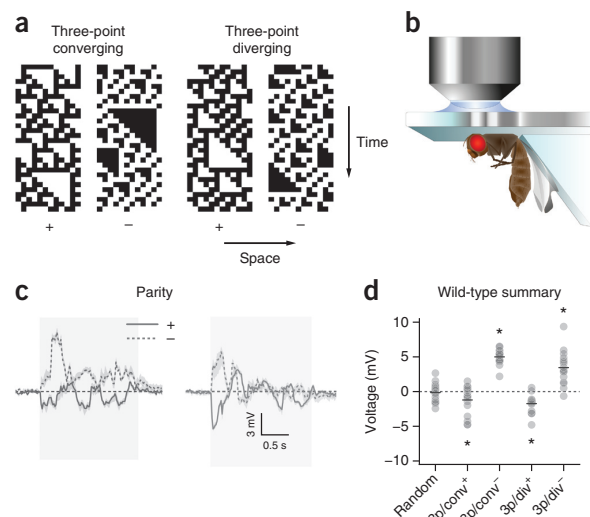
Figure 6 Luminance asymmetry in natural scenes is critically responsible for asymmetry of ON-OFF parameters in optimized motion detector. **(a-d)** Left, example picture from image set used for optimization. Middle, kernel density estimate of pixel luminance distribution for example picture. The vertical line indicates average image luminance. Right-hand panels, optimized parameters for ON (blue) and OFF (red) detector trained on corresponding image set. **(a)** Unmodified image set used for earlier optimizations (**Fig. 5**). **(b)** Phase-scrambled image set in which the phase structure of each image was replaced by that of a random image, effectively rendering the luminance distribution symmetric. **(c)** Luminance-remapped image set in which the luminance distribution of natural images was remapped onto phase-scrambled images. **(d)** Luminance-remapped image set in which the luminance distribution of phase-scrambled images was remapped onto natural images. Dots represent individual observations and black bars indicate group averages ($N = 50$ cross-validations for all image sets). No significance tests were performed in this figure.

Figure 7 LPTCs are sensitive to higher order correlation stimuli.

(a) Space-time plots of glider stimuli used to probe LPTC sensitivity to triple correlations. (b) Schematic drawing of *in vivo* electrophysiology preparation and setup. (c) Average responses to full-field three-point glider stimulation of pooled vertical and horizontal system cells ($n = 16$ cells from $N = 12$ flies). Gray shaded area shows duration of stimulus presentation. Shaded areas surrounding traces signify bootstrapped 68% confidence intervals around the mean. (d) Quantification of integrated responses (averaged over the first second of stimulus presentation); “3p/conv” or “3p/div” indicate three-point converging or diverging glider orientation, respectively, and superscript the stimulus parity. All recordings were done in wild-type Canton S flies. Depicted responses are the difference between glider presentation in preferred and null direction. Dots represent individual observations and black bars show group averages. Asterisks indicate significant differences from zero after two-tailed t tests ($*P < 0.05$); exact test statistics are reported in **Supplementary Table 6**.

properties to diverge between ON and OFF channels. Finally, replacing the skewed luminance distribution of natural images with a symmetric one again abolished the temporal tuning differences (**Fig. 6d**). Notably, the DC asymmetry did not depend on higher order statistics of the stimulus. This particular tuning difference may be advantageous for ON-OFF detectors regardless of image statistics.

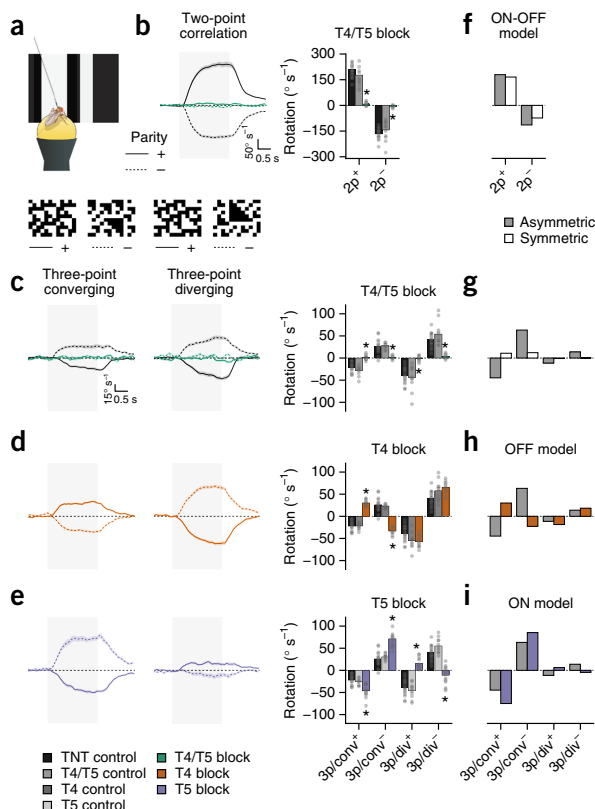
Taken together, our optimization findings demonstrate that, in realistic environments, the ON and OFF channels of motion detectors that were optimal under our criterion were tuned asymmetrically. The specific parameters that best estimated motion in natural scenes reproduced tuning properties of the biological fly motion detector we determined experimentally. At no point did we use our previous experimental findings as a constraint during optimization; the procedure arrived at this specific asymmetry independently.



Higher-order motion sensitivity derives from ON-OFF asymmetry

Theoretical considerations indicate that spatiotemporal correlations of orders higher than two become informative indicators of visual motion in environments that are ON-OFF asymmetric¹⁴. Hassenstein-Reichardt detectors exclusively capture two-point correlations. Experimental work, however, confirmed that *Drosophila* responds to triple correlations¹². This suggests that such correlations are either computed explicitly by secondary circuits or implicitly extracted by detectors that treat ON and OFF motion differentially. We assessed whether an asymmetric detector can account for *Drosophila*'s sensitivity to higher order motion.

First, we tested whether tangential cells respond to higher order motion cues given that these neurons receive their primary direction-selective input from T4 and T5 (ref. 30). We made use of previously characterized three-point glider stimuli^{12,15} (**Fig. 7a**), which enforce the mean sign of correlations across three spatiotemporal points. They have four possible forms: converging or diverging, depending on their spatiotemporal orientation, and either positive or negative parity. Notably, they are guaranteed to contain on average zero

**Figure 8** Behavioral sensitivity to higher order correlations depends on T4 and T5 and is predicted by an asymmetric ON-OFF model.

(a) Illustration of behavioral experiment. (b) Two-point glider responses. Left, average response traces for two-point glider stimuli. Here, as in all following panels, the gray shaded area indicates stimulus presentation. Right, rotational responses for two-point gliders representing phi and reverse-phi motion are abolished in T4/T5 block flies. (c) Control flies respond to three-point gliders in a specific pattern. Blocking T4 and T5 in conjunction eliminates these responses completely. (d,e) Silencing T4 or T5 modulates responses by reversing rotation for converging or diverging gliders, respectively. (f) Asymmetric and symmetric models account for two-point glider responses. (g) Only the asymmetric model correctly predicts three-point glider responses of control flies. (h,i) Simulating individual T4 and T5 blocks in the asymmetric ON-OFF model by setting the gain for either ON (red) or OFF (blue) channel to zero replicates the behavioral effects. Shaded areas surrounding traces signify bootstrapped 68% confidence intervals around the mean. Dots represent individual flies and bars show group averages. Asterisks indicate significant differences of block flies from both Gal4 and UAS controls after Bonferroni-corrected two-tailed t tests ($N = 18$ for TNT control, $N = 12$ for T4/T5 control, $N = 12$ for T4 control, $N = 12$ for T5 control, $N = 14$ for T4/T5 block, $N = 13$ for T4 block, $N = 17$ for T5 block; $*P < 0.05$). Exact test statistics are reported in **Supplementary Table 7**.

directed two-point correlations, allowing the isolated characterization of responses to higher order motion. When we recorded from tangential cells of both the horizontal and vertical system (Fig. 7b), they responded to single instantiations of three-point gliders with complex dynamics (Fig. 7c). Their time-averaged voltage signals replicated the response pattern observed for behaving flies¹² (Fig. 7d). Given that fly locomotion is thought to reflect integrated tangential cell responses²⁶, the combination of T4 and T5 thus appeared to be sufficient for higher order motion sensitivity.

We then examined the necessity of T4 and T5 for three-point glider responses. Tethered walking flies were presented with a complete set of two-point and three-point gliders (Fig. 8a). Next, we silenced T4 and T5 in isolation as well as simultaneously. For control flies, turning responses to two-point correlations were as expected for standard phi and reverse-phi stimuli: flies turned strongly in the direction of positive correlations (positive glider parity) and reversed this tendency for negative correlations (negative glider parity; Fig. 8b). Blocking T4 and T5 in conjunction completely abolished sensitivity to all two-point gliders. This is, to the best of our knowledge, the first demonstration that reverse-phi motion, defined by spatiotemporal anti-correlations, depends on the combined activity of ON and OFF motion detectors^{10,19,36}. We then replicated the previously reported behavioral response pattern for three-point gliders¹². Flies in which both T4 and T5 were silenced failed to respond to any of the higher order motion stimuli, indicating that T4 and T5 are also necessary for motion detection beyond two-point correlations (Fig. 8c). Blocking T4 or T5 in isolation had no effect on two-point responses (Supplementary Fig. 6a–c). We were, however, surprised to find that isolated T4 or T5 blocks resulted in particular three-point glider phenotypes. Silencing the ON pathway specifically reversed the flies' turning tendency for converging gliders while slightly boosting diverging glider responses (Fig. 8d). For OFF block flies, the opposite pattern emerged (Fig. 8e).

Finally, we probed our symmetric and asymmetric detector models for higher order motion sensitivity. Both produced comparable two-point glider responses (Fig. 8f). For three-point gliders, both detectors generated nonzero output, but only the asymmetric model qualitatively matched the pattern we observed in our electrophysiological experiments as well as in walking flies (Fig. 8g). Notably, when evaluating detector responses to individual glider instantiations, we found complex and strongly fluctuating responses that resembled tangential cell responses (Supplementary Fig. 6d,g). Responses became smooth and regular only after integration of many repetitions (Fig. 7 and Supplementary Fig. 6e,f,h,i). We then simulated T4 or T5 silencing by setting ON or OFF gain to zero. These models reliably predicted the specific response reversals (Fig. 8h,i) observed in behavior (Fig. 8d,e). We therefore posit that T4 and T5 are capable of extracting triple correlations on their own. ON and OFF edges have been found to contain a particular combination of triple correlations¹². The reverse also held: three-point gliders elicited strong signals of opposite sign in pure ON or OFF detectors (Fig. 8d,e,h,i). Only if the pathways were perfectly symmetric did these responses cancel out. If they were asymmetric, as in our optimized detector or the *Drosophila* visual system, then residual responses remained. Our optimized models correctly predicted the sign and relative magnitude of these effects, suggesting that the asymmetries we found *in silico* track the asymmetries of the biological system.

DISCUSSION

We studied the roles of ON and OFF motion pathways for velocity estimation in natural scenes. *Drosophila* stabilized their walking trajectories in a closed-loop virtual environment whose statistics

resembled those of natural scenes. Genetically silencing cells T4 and T5 rendered flies unable to perform this path correction. In an open-loop setting, flies reliably tracked whole-field motion of naturalistic images. Interrupting the activity of ON or OFF pathways did not affect this capability, suggesting that the two channels subserved redundant functions in information-rich natural scenes. In physiological and behavioral experiments, we found that ON and OFF motion estimators exhibit diverging temporal tuning. When we optimized the estimation performance of an ON-OFF motion detector, we obtained asymmetric models whose temporal tuning properties resembled those found for the biological system. This suggests that *Drosophila* motion detectors are tailored to an ON-OFF asymmetric visual world, with each channel covering the most informative temporal range. In a final set of experiments and without specific tuning of the model, we found that *Drosophila's* sensitivity to certain types of higher order motion has a straightforward explanation in this framework of differentially tuned pathways.

One could interpret the shifted tuning ranges of T4 and T5 as a solution for maximizing information transfer by avoiding coding redundancy. However, for the asymmetric detector, pathways were optimized independently, forcing both to adequately encode the input velocity distribution. We therefore favor the interpretation that features reliably indicating scene velocity operate on time scales that differ between ON and OFF signals. The skewed luminance distribution of real images (Fig. 6a) offers an intuition for this notion: ON signals are dominated by infrequent and large positive deflections, whereas OFF signals are generally smaller and more regular. As neither RC filters nor lamina cells act as perfect differentiators, these differences plausibly persist at later levels of motion detection, where they may be exploited by appropriately tuned mechanisms¹³. Notably, detector performance was generally better for OFF detectors than for ON detectors (Fig. 5b), possibly reflecting the sparseness of informative ON signals.

During conditioning of detector parameters on natural images, we also optimized the weight of the tonic DC signal. We found nonzero optima for both pathways, as postulated in previous studies on reverse-phi responses¹⁰. Electrophysiologically, ON pathway interneurons Mi1 and Tm3 did indeed show static responses to absolute brightness levels with the amplitude ratio between high-pass and DC signal qualitatively matching our findings²⁴. In contrast to our prediction, OFF intermediaries Tm1 and Tm2 did not exhibit inverted tonic signals. However, other cells presynaptic to T5 still await characterization¹⁷. How DC signals can be reconciled with our demonstration that T4 and T5 responses are fully polarity specific remains unclear. In particular, theoretical considerations on the basis of the response properties of Mi1 and Tm3 predict sensitivity to OFF edges for T4 (ref. 24). This is not borne out by our experiments (Fig. 3).

Theoretical studies have proposed that responding to higher order correlations allows motion detectors to exploit natural ON-OFF asymmetries^{12,14}. The asymmetry between ON and OFF pathways reported here does indeed confer sensitivity to triple correlations. Only under the assumption that ON and OFF steps are processed equally do spurious two-point correlations vanish. However, whether *Drosophila's* higher order motion responses are an epiphenomenon of detector asymmetries or whether detector asymmetry represents a way of accessing higher order correlations is up for debate. Moreover, it remains to be seen whether the findings at hand generalize to other forms of higher order motion perceived by *Drosophila*³⁸.

Our previous characterization of cell types T4 and T5 revealed only minor differences in temporal frequency tuning for gratings²¹. It is currently not well understood how physiological tuning curves for edges and gratings relate to each other. Given the drastically different

kinetics of the two stimuli, large ON-OFF differences for one may lead to only small ON-OFF differences for the other. In addition, we suggest that edges provide a better approximation of visual kinetics in the real world than artificial gratings that are periodic as well as constant in mean luminance, contrast and geometry. Moreover, measurements from tangential cells in behaving flies have indicated grating response optima that are shifted toward higher frequencies compared with quiescence^{26,39,40}. How this state dependency translates to the tuning for edge velocity is unclear. Indeed, our linear prediction of opposing edge responses from physiological edge tuning underestimates the true crossing point between ON and OFF dominance (Fig. 4d). A shift toward higher preferred velocities, as observed for grating optima, could account for this discrepancy. Notably, our behavioral data demonstrate that basic characteristics of temporal ON-OFF asymmetries are preserved in active flies.

The ON-OFF asymmetry we describe represents one of many examples for the adaptation of sensory systems to the environment in which they evolved^{5,6,13,41}. Contrast asymmetries between ON and OFF are a widespread feature shared by most visual niches. It therefore seems probable that the sensory asymmetries found in *Drosophila* are conserved across species. ON-OFF divergence has previously been described for several computations in vertebrate visual systems^{42–44}. It will be interesting to examine the effects on optimal tuning exerted by features of the mammalian retina, such as contrast normalization⁴⁵. Finally, motion energy models have been successfully used to explain the psychophysics of motion perception in higher organisms⁴⁶. Given that Hassenstein-Reichardt detectors and motion energy models are generally mathematically equivalent⁴⁷, our optimization results could also emerge for an appropriately rectified ON-OFF motion energy detector.

T4 and T5 are critically involved in behaviors other than the optomotor response. Recently, studies have implicated motion detectors in object fixation²⁷, depth perception⁴⁸ or looming responses⁴⁹. Given the variety of tasks and resulting visual statistics, optimal tuning needs to be examined under various constraints. Finally, we believe this ecological perspective on biological motion detection could have a decisive role in the continued mapping of the fly visual system. The abundance of information-bearing features in natural visual scenes may necessitate complex filter banks and multi-cell processing stages^{17,20,23,50}. Real-world demands will then be critical constraints when assigning function to cells in the *Drosophila* optic lobe.

METHODS

Methods and any associated references are available in the [online version of the paper](#).

Note: Any Supplementary Information and Source Data files are available in the online version of the paper.

ACKNOWLEDGMENTS

A. Nern and G.M. Rubin (Janelia Research Campus) generated and kindly provided the splitGal4 line targeting T4 and T5. We are grateful for fly work and behavioral experiments performed by R. Kutlesa, C. Theile and W. Essbauer. We thank A. Arenz and A. Mauss for carefully reading the manuscript, T. Schilling for fly illustrations, and all of the members of the Borst laboratory for extensive discussions. The Bernstein Center for Computational Neuroscience Munich supplied computing resources for our simulations. A.L., G.A., M.M., E.S., A. Bahl and A. Borst are members of the Graduate School for Systemic Neurosciences, Munich.

AUTHOR CONTRIBUTIONS

A.L., G.A. and A. Borst designed the study. A.L. performed behavioral experiments, associated data analysis and all modeling work. G.A., M.M. and E.S. performed electrophysiological experiments. G.A. performed calcium imaging. A.L. and

G.A. analyzed physiological data. A. Bahl designed the behavioral apparatuses and performed behavioral experiments. A.L. wrote the manuscript with help from all of the authors.

COMPETING FINANCIAL INTERESTS

The authors declare no competing financial interests.

Reprints and permissions information is available online at <http://www.nature.com/reprints/index.html>.

- Borst, A. Fly visual course control: behavior, algorithms and circuits. *Nat. Rev. Neurosci.* **15**, 590–599 (2014).
- Ruderman, D.L. & Bialek, W. Statistics of natural images: Scaling in the woods. *Phys. Rev. Lett.* **73**, 814–817 (1994).
- Simoncelli, E.P. & Olshausen, B.A. Natural image statistics and neural representation. *Annu. Rev. Neurosci.* **24**, 1193–1216 (2001).
- Field, D.J. Relations between the statistics of natural images and the response properties of cortical cells. *J. Opt. Soc. Am. A* **4**, 2379–2394 (1987).
- Laughlin, S. A simple coding procedure enhances a neuron's information capacity. *Z. Naturforsch. C* **36**, 910–912 (1981).
- van Hateren, J.H. & van der Schaaf, A. Independent component filters of natural images compared with simple cells in primary visual cortex. *Proc. Biol. Sci.* **265**, 359–366 (1998).
- Yu, Y., Schmid, A.M. & Victor, J.D. Visual processing of informative multipoint correlations arises primarily in V2. *eLife* **4**, e06604 (2015).
- Gjorgjieva, J., Sompolinsky, H. & Meister, M. Benefits of pathway splitting in sensory coding. *J. Neurosci.* **34**, 12127–12144 (2014).
- Borst, A. & Helmstaedter, M. Common circuit design in fly and mammalian motion vision. *Nat. Neurosci.* **18**, 1067–1076 (2015).
- Eichner, H., Joesch, M., Schnell, B., Reiff, D.F. & Borst, A. Internal structure of the fly elementary motion detector. *Neuron* **70**, 1155–1164 (2011).
- Hassenstein, B. & Reichardt, W. Systemtheoretische Analyse der Zeit-, Reihenfolgen- und Vorzeichenbewertung bei der Bewegungsperzeption des Rüsselkäfers *Chlorophanus*. *Z. Naturforsch. B* **11**, 513–524 (1956).
- Clark, D.A. *et al.* Flies and humans share a motion estimation strategy that exploits natural scene statistics. *Nat. Neurosci.* **17**, 296–303 (2014).
- Ratliff, C.P., Borghuis, B.G., Kao, Y.-H., Sterling, P. & Balasubramanian, V. Retina is structured to process an excess of darkness in natural scenes. *Proc. Natl. Acad. Sci. USA* **107**, 17368–17373 (2010).
- Fitzgerald, J.E., Katsov, A.Y., Clandinin, T.R. & Schnitzer, M.J. Symmetries in stimulus statistics shape the form of visual motion estimators. *Proc. Natl. Acad. Sci. USA* **108**, 12909–12914 (2011).
- Hu, Q. & Victor, J.D. A set of high-order spatiotemporal stimuli that elicit motion and reverse-phi percepts. *J. Vis.* **10**, 9.1–9.16 (2010).
- Takemura, S.-Y. *et al.* A visual motion detection circuit suggested by *Drosophila* connectomics. *Nature* **500**, 175–181 (2013).
- Shinomiya, K. *et al.* Candidate neural substrates for off-edge motion detection in *Drosophila*. *Curr. Biol.* **24**, 1062–1070 (2014).
- Joesch, M., Schnell, B., Raghu, S.V., Reiff, D.F. & Borst, A. ON and OFF pathways in *Drosophila* motion vision. *Nature* **468**, 300–304 (2010).
- Clark, D.A., Bursztyn, L., Horowitz, M.A., Schnitzer, M.J. & Clandinin, T.R. Defining the computational structure of the motion detector in *Drosophila*. *Neuron* **70**, 1165–1177 (2011).
- Silies, M. *et al.* Modular use of peripheral input channels tunes motion-detecting circuitry. *Neuron* **79**, 111–127 (2013).
- Maisak, M.S. *et al.* A directional tuning map of *Drosophila* elementary motion detectors. *Nature* **500**, 212–216 (2013).
- Meier, M. *et al.* Neural circuit components of the *Drosophila* OFF motion vision pathway. *Curr. Biol.* **24**, 385–392 (2014).
- Ammer, G., Leonhardt, A., Bahl, A., Dickson, B.J. & Borst, A. Functional specialization of neural input elements to the *Drosophila* ON motion detector. *Curr. Biol.* **25**, 2247–2253 (2015).
- Behnia, R., Clark, D.A., Carter, A.G., Clandinin, T.R. & Desplan, C. Processing properties of ON and OFF pathways for *Drosophila* motion detection. *Nature* **512**, 427–430 (2014).
- Haikala, V., Joesch, M., Borst, A. & Mauss, A.S. Optogenetic control of fly optomotor responses. *J. Neurosci.* **33**, 13927–13934 (2013).
- Schnell, B., Weir, P.T., Roth, E., Fairhall, A.L. & Dickinson, M.H. Cellular mechanisms for integral feedback in visually guided behavior. *Proc. Natl. Acad. Sci. USA* **111**, 5700–5705 (2014).
- Bahl, A., Ammer, G., Schilling, T. & Borst, A. Object tracking in motion-blind flies. *Nat. Neurosci.* **16**, 730–738 (2013).
- Joesch, M., Plett, J., Borst, A. & Reiff, D.F. Response properties of motion-sensitive visual interneurons in the lobula plate of *Drosophila melanogaster*. *Curr. Biol.* **18**, 368–374 (2008).
- Warzecha, A.-K. & Egelhaaf, M. Intrinsic properties of biological motion detectors prevent the optomotor control system from getting unstable. *Phil. Trans. R. Soc. Lond. B* **351**, 1579–1591 (1996).
- Schnell, B., Raghu, S.V., Nern, A. & Borst, A. Columnar cells necessary for motion responses of wide-field visual interneurons in *Drosophila*. *J. Comp. Physiol. A Neuroethol. Sens. Neural Behav. Physiol.* **198**, 389–395 (2012).

ARTICLES

31. Brand, A.H. & Perrimon, N. Targeted gene expression as a means of altering cell fates and generating dominant phenotypes. *Development* **118**, 401–415 (1993).
32. Sweeney, S.T., Broadie, K., Keane, J., Niemann, H. & O’Kane, C.J. Targeted expression of tetanus toxin light chain in *Drosophila* specifically eliminates synaptic transmission and causes behavioral defects. *Neuron* **14**, 341–351 (1995).
33. Straw, A.D., Rainsford, T. & O’Carroll, D.C. Contrast sensitivity of insect motion detectors to natural images. *J. Vis.* **8**, 32.1–32.9 (2008).
34. Chen, T.-W. *et al.* Ultrasensitive fluorescent proteins for imaging neuronal activity. *Nature* **499**, 295–300 (2013).
35. Mauss, A.S. *et al.* Neural circuit to integrate opposing motions in the visual field. *Cell* **162**, 351–362 (2015).
36. Tuthill, J.C., Chiappe, M.E. & Reiser, M.B. Neural correlates of illusory motion perception in *Drosophila*. *Proc. Natl. Acad. Sci. USA* **108**, 9685–9690 (2011).
37. Dror, R.O., O’Carroll, D.C. & Laughlin, S.B. Accuracy of velocity estimation by Reichardt correlators. *J. Opt. Soc. Am. A Opt. Image Sci. Vis.* **18**, 241–252 (2001).
38. Theobald, J.C., Duistermars, B.J., Ringach, D.L. & Frye, M.A. Flies see second-order motion. *Curr. Biol.* **18**, R464–R465 (2008).
39. Jung, S.N., Borst, A. & Haag, J. Flight activity alters velocity tuning of fly motion-sensitive neurons. *J. Neurosci.* **31**, 9231–9237 (2011).
40. Chiappe, M.E., Seelig, J.D., Reiser, M.B. & Jayaraman, V. Walking modulates speed sensitivity in *Drosophila* motion vision. *Curr. Biol.* **20**, 1470–1475 (2010).
41. Dyakova, O., Lee, Y.-J., Longden, K.D., Kiselev, V.G. & Nordström, K. A higher order visual neuron tuned to the spatial amplitude spectra of natural scenes. *Nat. Commun.* **6**, 8522 (2015).
42. Komban, S.J. *et al.* Neuronal and perceptual differences in the temporal processing of darks and lights. *Neuron* **82**, 224–234 (2014).
43. Chichilnisky, E.J. & Kalmar, R.S. Functional asymmetries in ON and OFF ganglion cells of primate retina. *J. Neurosci.* **22**, 2737–2747 (2002).
44. Pandarinath, C., Victor, J.D. & Nirenberg, S. Symmetry breakdown in the ON and OFF pathways of the retina at night: functional implications. *J. Neurosci.* **30**, 10006–10014 (2010).
45. Carandini, M. & Heeger, D.J. Normalization as a canonical neural computation. *Nat. Rev. Neurosci.* **13**, 51–62 (2012).
46. Adelson, E.H. & Bergen, J.R. Spatiotemporal energy models for the perception of motion. *J. Opt. Soc. Am. A* **2**, 284–299 (1985).
47. van Santen, J.P. & Sperling, G. Elaborated Reichardt detectors. *J. Opt. Soc. Am. A* **2**, 300–321 (1985).
48. Schwegmann, A., Lindemann, J.P. & Egelhaaf, M. Depth information in natural environments derived from optic flow by insect motion detection system: a model analysis. *Front. Comput. Neurosci.* **8**, 83 (2014).
49. Schilling, T. & Borst, A. Local motion detectors are required for the computation of expansion flow-fields. *Biol. Open* **4**, 1105–1108 (2015).
50. Burge, J. & Geisler, W.S. Optimal speed estimation in natural image movies predicts human performance. *Nat. Commun.* **6**, 7900 (2015).



ONLINE METHODS

Fly strains and genetics. We raised *Drosophila melanogaster* on cornmeal-agar medium under standard conditions (60% humidity, 18 °C for behavioral and 25 °C for physiology experiments, 12-h light/12-h dark schedule) for the full duration of their developmental cycle. Female flies were used in all experiments. For physiological experiments, we selected flies 5–20 h post-eclosion. Flies in behavioral experiments were 1–3 d old. Behavioral experiments targeting T4 or T5 used the following driver lines, as described previously²¹: T4-Gal4 (VT37588) and T5-Gal4 (R42H07). When targeting T4 and T5 simultaneously, we employed a new, highly specific driver line: T4/T5-splitGal4 (R59E08-AD; R42F06-DBD), kindly provided to us by A. Nern and G.M. Rubin at Janelia Research Campus. For visualization of expression patterns (Supplementary Fig. 1), we crossed driver lines to UAS-mCD8GFP reporter flies. For experiments, Gal4 flies were then crossed to either wild type Canton S flies or UAS-TNT-E flies resulting in Gal4 control or block flies, respectively. Crossing UAS-TNT-E flies to Canton S flies generated UAS control flies. For calcium imaging, we combined two different Gal4 lines (VT25965 and VT37588) that in conjunction expressed at comparable levels in T4 and T5. These were crossed to UAS-GCaMP6³⁴ flies. Genotypes derived from these crossings and their aliases as used throughout the text are listed in the supplementary material (Supplementary Table 1).

Immunohistochemistry. Antibody stainings (Supplementary Fig. 1) were performed as described previously⁵¹. We used the following antibodies and dilutions. Primary antibodies: rabbit anti-GFP (Torri Pines, TP401, 1:2,000), mouse anti-nc82 (DSHB, AB_2314866, 1:25); secondary antibodies: goat anti-rabbit 488 (Invitrogen, A-11008, 1:500), goat anti-mouse 633 (Invitrogen, A-21053, 1:500). Imaging was performed on a SP5 confocal microscope (Leica) at a resolution of $1,024 \times 1,024$. Images were processed in ImageJ 1.46f (US National Institutes of Health). Single z-slices are shown for horizontal views.

Behavioral experiments. We performed behavioral experiments as described previously^{21,23,27}. Briefly, tethered flies were placed on an air-suspended polyurethane ball in a virtual environment consisting of three computer screens covering a substantial part of the animal's visual field (approximately 270° in azimuth and 120° in elevation). Experiments were run on six set-ups in parallel; two of them displayed visual stimuli at 120 Hz and the remaining four at 144 Hz with all screens calibrated to display at comparable contrast and brightness. We never observed any differences in behavior between refresh rates. All stimuli were rendered in real-time using the graphics engine Panda3D, allowing visual feedback based on flies' instantaneous walking behavior. Due to high pixel density on all computer screens, stimulus pixel size was well below the resolution limit of *Drosophila*. The immediate surround of the ball was temperature-controlled by means of a closed-loop thermoregulation system. Each experiment used the same temperature protocol: Temperature was kept at 25 °C for the first 5 min and then linearly raised to 34 °C within 10 min.

All behavioral experiments ran for 60–90 min and comprised 50–60 repeated trials, except for open-loop velocity estimation experiments (Fig. 2) that lasted 280 trials. In each trial, we randomized stimulus presentation order. Movement of the ball was tracked at 4 kHz and down-sampled to 20 Hz for offline analysis. For each fly, we manually selected a continuous range of 100–200 (Fig. 2) or 25 trials (other experiments) based on the following criteria: First, the temperature was at a constant 34 °C. Second, the average forward walking speed of the fly was above 0.3 cm s^{-1} , indicating healthy locomotion and visual responsiveness. Third, the average turning tendency of the fly was stable and close to 0° s^{-1} . These criteria excluded approximately 20% of all flies we measured. During analysis, we averaged traces across trials, resulting in a single walking trace per fly per experimental condition. Where applicable (Figs. 1, 4 and 8, and Supplementary Fig. 5), we then subtracted responses to mirror-symmetric stimulus presentations to minimize the impact of small rotational biases in turning behavior. Traces were filtered using a first-order low-pass filter ($\tau = 100 \text{ ms}$). In open-loop experiments (Fig. 2), we generated a regression model for each fly that mapped rotation of the environment to the turning response of the fly (averaged over 1 s after stimulus onset) using least-squares fitting. Response gain was then defined as the slope of this model. The intercepts clustered around 0° s^{-1} , indicating trajectories that were on average straight. For additional analysis (Supplementary Fig. 3), we constructed Bayesian decoders that minimize the squared error of their estimates. This was done on a fly-by-fly basis. We first split the data set consisting of pairs of image

velocity and turning response as for the correlation analysis (Fig. 2) into training and test sets at a ratio of 3:1, approximated the posterior distribution through application of Bayes' rule to the joint probability generated from appropriate histograms, and estimated image velocity as the expected value of the posterior for a given response. Finally, we assessed decoding performance of resulting mapping functions by calculating the root-mean-square error after application to the test set. The behavioral data analysis pipeline was implemented in Python 2.7 using pandas 15.1, NumPy 1.6, SciPy 0.15, matplotlib 1.3 and Numba 0.18.

Electrophysiology. Electrophysiological *in vivo* patch-clamp recordings from lobula plate tangential cells closely followed previously described protocols^{21,22,28}. Recordings were low-pass filtered with a cut-off frequency of 3 kHz and digitized at 10 kHz. Data acquisition was based on Matlab R2011A (MathWorks). We identified cell types based on their response profile when stimulated with moving gratings. In addition, cells were dye-filled and anatomically verified whenever possible.

We visually stimulated flies using a custom-built LED arena spanning approximately 180° in azimuth and 90° in elevation of the fly's visual field with a spatial resolution of 1.5° per individual LED. The LED refresh rate was in the kHz range; stimulus images were then updated with up to 600 Hz. Maximum luminance was 80 cd m^{-2} . During offline data analysis, recorded traces were down-sampled to 2 kHz and averaged across 2–5 trials per cell. We randomized the order of stimulus presentation within trials. Cells that did not respond reliably to grating stimulation were excluded from further analysis. Before we extracted response maxima and minima for edge responses (Fig. 3), electrophysiological traces were filtered with a second-order Savitzky-Golay kernel that was 40 samples wide. The electrophysiological data analysis pipeline was implemented in Python 2.7 using pandas 15.1, NumPy 1.6, matplotlib 1.3 and Numba 0.18.

Calcium imaging. We employed a custom-built two-photon laser scanning microscope as described previously^{21,22}. We prepared flies analogously to electrophysiology experiments. Images were recorded at a resolution of 256×128 pixels and a frame rate of 3.74 Hz. Raw images were then converted into relative fluorescence change ($\Delta F/F$) series by using the mean of three frames before stimulation onset as a baseline. For summary images, the resulting images were averaged across time; for time-resolved traces, we defined relevant regions of interest and collapsed signals within the defined borders by averaging across pixels. We used the LED arena described above for visual stimulation. Data acquisition and analysis were performed in Matlab R2011a (MathWorks) using ScanImage 3.8.

Image sets. Two image sets were used throughout the study. First, for all behavioral experiments involving natural images, we generated a small library of 60 panoramic images spanning approximately 360° in azimuth using a consumer-grade camera (iPhone 5s; Apple). The resolution of each image was $10,800 \times 2,460$ pixels. Images were taken in various natural environments covering different visual statistics: woods (30%), open rural spaces (30%), urban landscapes (20%), and laboratories (20%). We used raw images without processing or calibration and converted them to gray scale by averaging across color channels. Critical image statistics such as RMS contrast (that is, the s.d. of pixel values), luminance distribution, and power spectrum were comparable to other scientific image libraries. Second, for all *in silico* experiments, we made use of calibrated images from the van Hateren natural image database⁶. No image category was excluded and we performed no further sorting, yielding 4,167 images at a resolution of $1,536 \times 1,024$ pixels. One pixel corresponded to one arc minute of visual angle. We normalized the set through subtraction of and division by the mean pixel value for each image^{12,45}. Kernel density estimates (Figs. 2 and 6) were generated using a routine in the SciPy library. Gaussian kernels were used, and we determined bandwidth via Silverman's rule.

We scaled the contrast of our in-house image set by subtracting the image's mean luminance, applying the specified multiplicative factor, and then adding the initial mean luminance (Figs. 1 and 2). Phase-scrambling of the van Hateren image set was achieved by performing a Fourier transform, replacing the phase spectrum with that of a Gaussian random image of equal mean luminance, and finally recovering the phase-randomized image via the inverse Fourier transform (Fig. 6b). The luminance-remapped scrambled set was generated by replacing each pixel value of a phase-randomized image with the value corresponding to

the same luminance-ordered rank in the original image (Fig. 6c). Analogously, we generated the luminance-remapped natural set by drawing pixel values from the corresponding phase-scrambled image (Fig. 6d).

Visual stimuli. On every trial of the closed-loop course stabilization experiment (Fig. 1), a random image was chosen from our in-house image library and projected onto a virtual cylinder surrounding the fly. In order to cover the visual field without significant distortion, the panorama was mirrored across the fly's elevation axis. Each trial lasted 5 s. The rotational component of the walking trajectory was used as a feedback signal for the azimuthal orientation of the virtual cylinder, effectively giving flies control over their angular orientation relative to the environment. Feedback gain was set to unity. Between 1.5 s and 3.5 s, we additionally rotated the virtual environment at a constant 80° s^{-1} in clockwise or counter-clockwise direction. Contrast was scaled in accordance with the procedure described above to 12.5%, 25%, 50% and 100% of the original RMS value.

For open-loop velocity estimation experiments (Fig. 2), images were chosen and projected as above while feedback gain was set to zero. On each trial, a random velocity was drawn from a Gaussian distribution centered at 0° s^{-1} with a s.d. of 50° s^{-1} . Trials lasted 3.5 s. Between 1.5 s and 2 s, the virtual environment rotated with the constant velocity drawn earlier. The border where the image on the cylinder wrapped around was placed such that it remained in the back of the fly on most trials. Here, we added the 6% contrast condition.

We used single bright and dark edges for characterizing the physiological response properties of ON and OFF channels (Fig. 3). During electrophysiology experiments, we presented edges moving at 12 constant velocities across two orders of magnitude (6.25, 12.5, 25, 50, 75, 100, 150, 200, 300, 500, 700 and 900° s^{-1}). When recording from vertical system or horizontal system cells, edges traveled along the vertical or horizontal axis, respectively, and in the preferred direction of the cell. Edges used during calcium imaging always moved at 25° s^{-1} and either downwards or from front to back (no differences between the two directions were observed). Physiology stimuli (Fig. 3) had a Michelson contrast of 100%, starting from either a dark (ON) or bright (OFF) background. For additional experiments (Supplementary Fig. 4), edges started from an equal background luminance of 10.7 cd m^{-2} . As the stimulation device only allowed discrete steps, ON edges then had a contrast of 76% and OFF edges a contrast of 100%.

The behavioral balanced motion stimulus resembled previous iterations^{19,21,23}. Briefly, we presented flies with a stationary square wave grating that had an initial spatial wavelength of 45° and Michelson contrast of 50%. Each individual trial lasted 9 s. Between 2 s and 7 s, bright and dark edges moved in opposite directions at the same velocity. In contradistinction to previous experiments, we reset the stimulus to the initial state after edges had traversed 20° of visual angle, allowing us to keep stimulus duration fixed regardless of edge velocity. After each reset, we applied a random phase shift in order to minimize the effect of initial grating position relative to the fly. This was done for six velocities (20, 40, 80, 160, 320 and 640° s^{-1}) in clockwise and counter-clockwise direction. Pulse experiments (Supplementary Fig. 5) were performed analogously, with edge movement being limited to the indicated duration (500 ms, 250 ms or 100 ms).

Glider experiments (Figs. 7 and 8) were performed as described previously¹². Briefly, the visual field was divided into vertical stripes that had an azimuthal extent of 6° (behavior) or 4.5° (electrophysiology). Each bar could either be dark or bright; Michelson contrast for these experiments was 50% (behavior) or 100% (electrophysiology). Initial bars were seeded with a random binary pattern. Depending on the glider, bars were then updated according to the corresponding deterministic rule. The glider update frequency was either 24 Hz (behavior) or 10 Hz (electrophysiology). For electrophysiological experiments, we used a single pre-generated glider sequence. Here, preferred direction was defined as the update direction that would depolarize cells for two-point gliders.

Modeling. The ON-OFF detector used in this study (Figs. 5, 6 and 8) was derived from a previously published two-quadrant model¹⁰. Briefly, we modeled photoreceptor signals as time series with a resolution of 10 ms (for optimization experiments) or 1 ms (for other experiments) per step. Lamina processing was then approximated as the linear sum of a high-pass-filtered signal (first-order RC filter with $\tau = 250 \text{ ms}$) and an unfiltered tonic component (DC) with variable weight. This was followed by a half-wave rectification step. For the pure ON detector, signals were rectified with the threshold set to exactly zero. For the pure OFF detector, the signal was inverted and then rectified with the threshold set to exactly

zero. Further processing was identical for both: The signal was first-order low-pass filtered with variable time constant τ and then multiplied with an unfiltered signal from the other spatial location. This was done twice in a mirror-symmetrical fashion, followed by subtraction, yielding a fully opponent direction-selective signal. For the full ON-OFF detector, an ON detector and an OFF detector were summed with equal weight. Unlike previous versions¹⁰, our simplified detector did not make use of shifted rectification thresholds or unequally weighted detector halves. Outside of natural image experiments, stimuli were rendered at a spatial resolution of 0.1° . We modeled the spatial acceptance profile of photoreceptors as Gaussians with a half-width at maximum of 5° . The symmetric detectors (Figs. 5 and 8) had, by definition, zero DC component and identical filter time constants for the ON and the OFF channel as determined by the optimization procedure. The asymmetric detector had DC components and time constants that were allowed to differ between ON and OFF during optimization.

The detector characterization (Fig. 5) depicts results from a combination of 20 detectors separated by 6.5° . The spatial wavelength of all gratings was 20° with velocity being defined by temporal frequency. Simulations for grating and edge tunings ran for 10 s each; output was averaged across detectors and time. For the velocity profile (Fig. 5g), we used a time series drawn from a Gaussian distribution with s.d. = 20° s^{-1} that was first-order low-pass filtered with $\tau = 500 \text{ ms}$. Units were discarded for display purposes. Modeled edge stimuli lasted for 15 s, with movement starting after 2 s. The starting condition was fixed at 1.0 and followed by a jump to 1.2 for ON edges or 0.8 for OFF edges. Detector output was averaged for the duration of edge motion, which depended on velocity. We simulated 50 velocities on a logarithmic scale from 10° s^{-1} to $1,000^\circ \text{ s}^{-1}$. Glider stimuli (Fig. 8) were rendered as idealized signals mapping 21 virtual stripes to the 21 virtual photoreceptors of an array of 20 detectors, without any spatial overlap. The array was seeded with a random combination of binary dark and bright values (arbitrarily defined as 1.0 and 3.0, respectively) and then updated according to previously described rules¹² at a frequency of 5 Hz. Glider simulations ran for 5 s each and were averaged across 500 instantiations and time (Fig. 8f–i). We approximated compressive characteristics of the visuo-motor transformation by multiplying two-point and three-point responses with slightly different gain values ($2,500^\circ \text{ s}^{-1}$ and $3,500^\circ \text{ s}^{-1}$, respectively) when translating detector output into turning tendency. All simulations were implemented in Python 2.7 using NumPy 1.6 and Numba 0.18.

Detector optimization. Optimization of detector models was based on an exhaustive cross-validated search on a two-dimensional parameter grid. We generated 50 random training-to-test splits from the 4,167 images of the van Hateren data set with a training-to-test ratio of 4:1. All images received a luminance bias of 3.0 and were clipped at zero in order to ensure that only positive signals arrived at detector inputs while keeping mean values constant. The optimization procedure was then performed independently for each training fold.

We scanned a parameter space comprising 40×21 combinations of low-pass time constants (from 10 to 400 ms in 10-ms steps) and DC contribution (from -20% to $+20\%$ in 2% steps). For each parameter set, three detectors with the corresponding parameter settings were simulated: a pure ON detector, a pure OFF detector, and a symmetric ON-OFF detector where ON and OFF channels used the same parameters. Fitness of a given detector was determined as follows, based on previous studies¹² and analogously to behavioral experiments (Fig. 2): on each iteration, we drew a random image from the training set and a random velocity from a Gaussian distribution centered at zero with s.d. = 25° s^{-1} . We then generated two time series corresponding to a simulated pair of photoreceptors separated by 6.5° traveling across the horizontal middle row of the image at the constant velocity drawn before and for a duration of 1,000 ms. The signals were fed into each of the three detectors. Detector output was averaged across time. We repeated this procedure 50,000 times per parameter set. Detector fitness was then defined as the Pearson correlation between input velocity and average detector output. During testing, we assembled two detectors per test set. The optimal symmetric detector was the best-performing detector constrained to use equal ON and OFF settings and zero DC. The optimal asymmetric detector was the linear combination of the best performing ON detector and the best performing OFF detector. The performance of both was then evaluated on the corresponding test set; here, detector evaluations were repeated 100,000 times. This was done for the natural, phase-scrambled and luminance-remapped image sets.

We implemented the optimization procedure in Python 2.7 using NumPy 1.6, SciPy 0.15, Numba 0.18, and IPython 3.0. Parallel operations were distributed across 128 CPUs on a Beowulf cluster consisting of eight physical machines.

Code availability. Python and Matlab code used throughout analysis, modeling, and optimization is available upon request to the authors.

Statistics. All statistical tests were two-tailed Student's *t* tests at a significance level of 0.05, assuming unequal variance unless stated otherwise. Where necessary, conservative Bonferroni correction was applied in order to correct for multiple hypothesis testing. Normality of data was confirmed visually and not formally tested. We did not predetermine sample sizes using statistical tests, but numbers

are in line with established work^{12,20,21,23,27}. Our confidence intervals were computed according to a bootstrapping procedure based on 1,000 re-samplings of the data set. We did not differentiate levels of significance; only single asterisks are used regardless of *P* value. Statistical procedures were used as implemented in SciPy 0.15. All experiments and data analysis were performed without blinding to conditions or genotypes.

A **Supplementary Methods Checklist** is available.

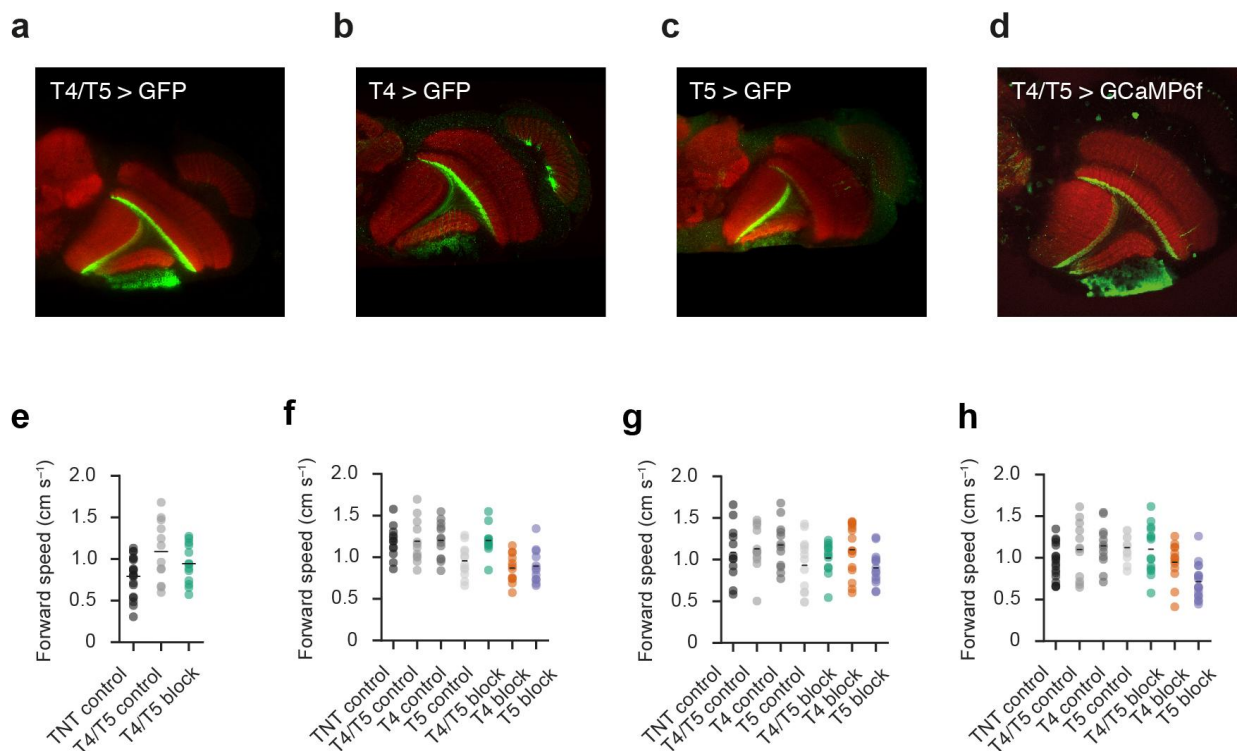
51. Yu, J.Y., Kanai, M.I., Demir, E., Jefferis, G.S.X.E. & Dickson, B.J. Cellular organization of the neural circuit that drives *Drosophila* courtship behavior. *Curr. Biol.* **20**, 1602–1614 (2010).



Erratum: Asymmetry of *Drosophila* ON and OFF motion detectors enhances real-world velocity estimation

Aljoscha Leonhardt, Georg Ammer, Matthias Meier, Etienne Serbe, Armin Bahl & Alexander Borst
Nat. Neurosci.; doi:10.1038/nn.4262; corrected online 7 March 2016

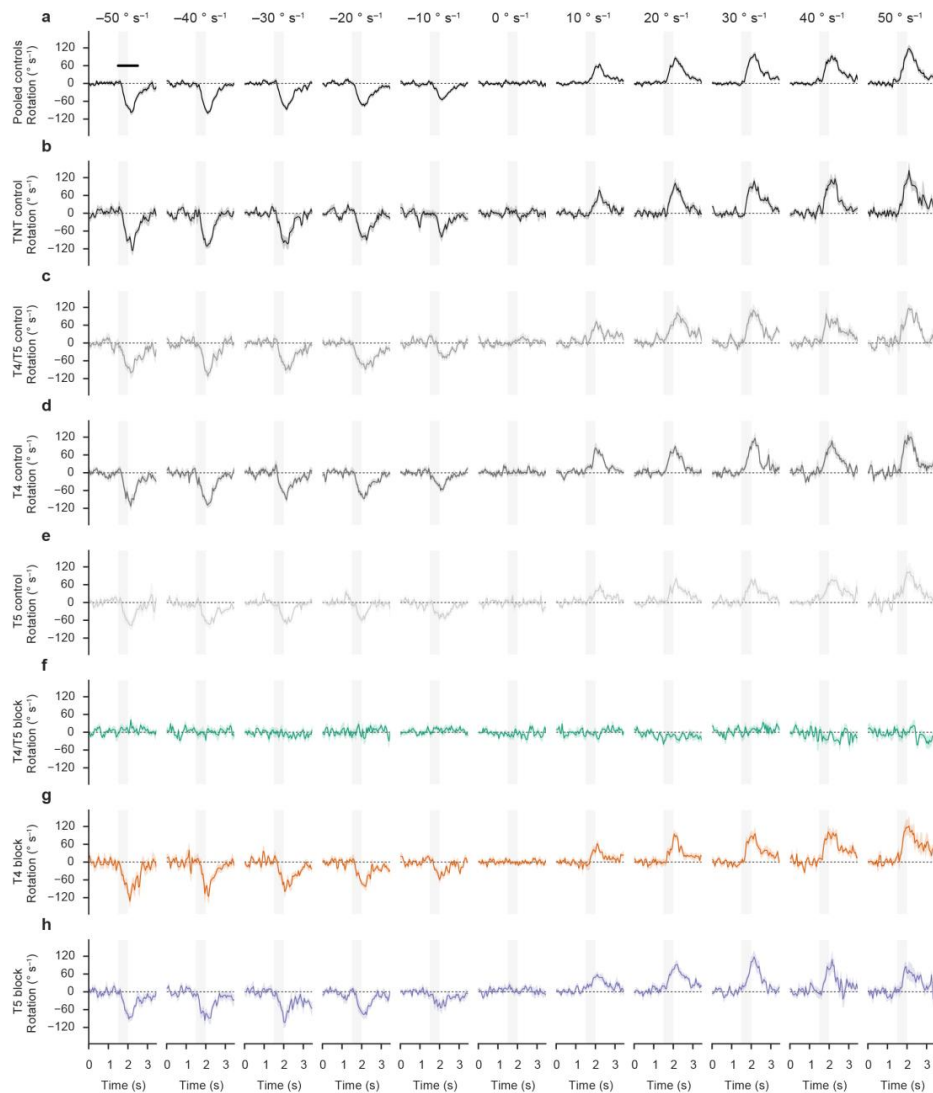
In the version of this article initially published online, the second and third authors of ref. 40, J.D. Seelig and M.B. Reiser, were replaced by the second author of ref. 39, A. Borst. The error has been corrected for the print, PDF and HTML versions of this article.



Supplementary Figure 1

Auxiliary data for Gal4 lines used throughout the study.

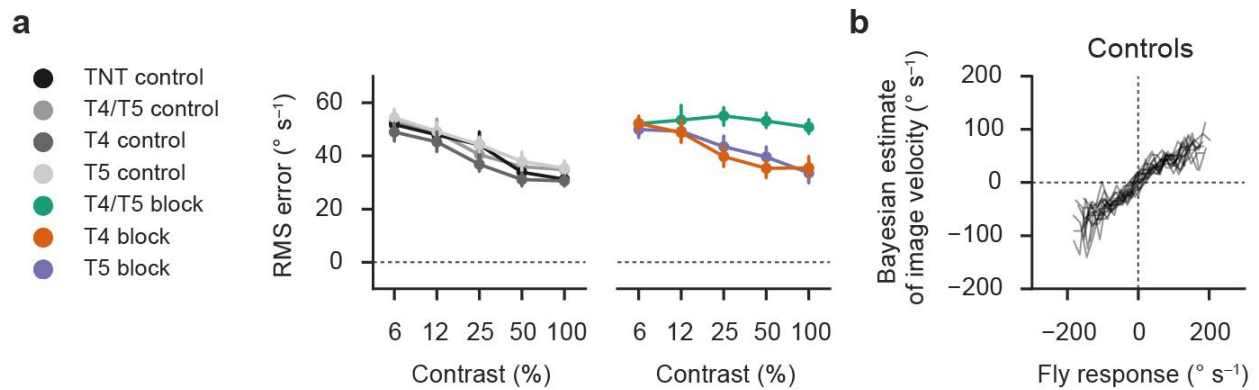
(a-d) UAS-mCD8GFP or UAS-GCaMP6f were driven by Gal4 driver lines used throughout the text and visualized using confocal images of the optic lobe. (a) GFP expression of splitGal4 line labeling T4 and T5. (b) GFP expression of Gal4 line labeling T4. (c) GFP expression of Gal4 line labeling T5. (d) GCaMP6f expression of combined Gal4 line labeling T4 and T5. See Online Methods for Gal4 line names and details of the immunohistochemistry procedures. (e-h) Locomotor integrity for each behavioral experiment was quantified as the mean forward velocity across conditions, with values close to control level indicating a general ability to respond to visual stimuli. (e) Walking speeds for closed-loop experiments (Fig. 1). (f) Walking speeds for open-loop experiments (Fig. 2). (g) Walking speeds for opposing edge experiments (Fig. 4). (h) Walking speeds for glider experiments (Fig. 8). Dots represent individual flies. Black bars mark the group mean for each genotype.



Supplementary Figure 2

Walking traces for open-loop velocity estimation experiment.

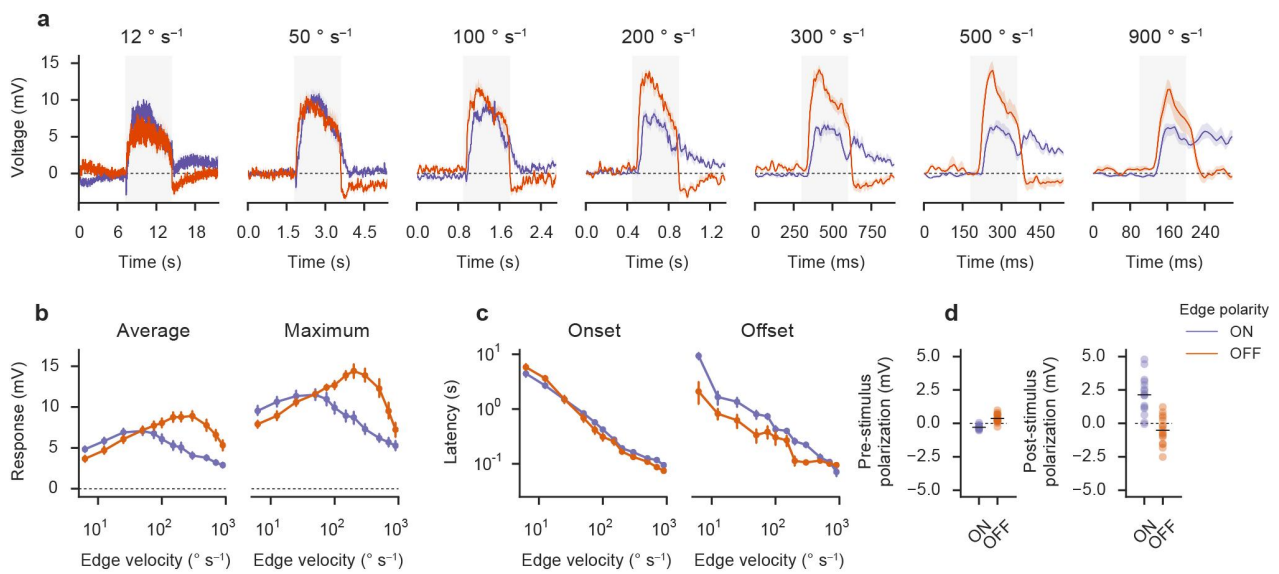
Binned response traces for all genotypes used throughout the stochastic open loop velocity estimation experiment (**Fig. 2**). In order to generate velocity-specific traces, stimulus velocities were sorted into bins spanning 5° s^{-1} centered about the value indicated above each column. The corresponding traces were then averaged for each fly. Shaded areas indicate the bootstrapped 68% confidence interval across flies (N as in main figure; **Fig. 2**). Notably, traces were not low-pass filtered and the sampling base for each fly decreases with distance from zero velocity due to the stimulus distribution. The black line in the top leftmost panel indicates the period over which we averaged in order to generate responses for main experiment (**Fig. 2**). See Online Methods for details. (a) Responses for pooled controls as in main experiment (**Fig. 2b**). (b-h) Responses for individual genotypes.



Supplementary Figure 3

Bayesian analysis of open-loop behavioral data.

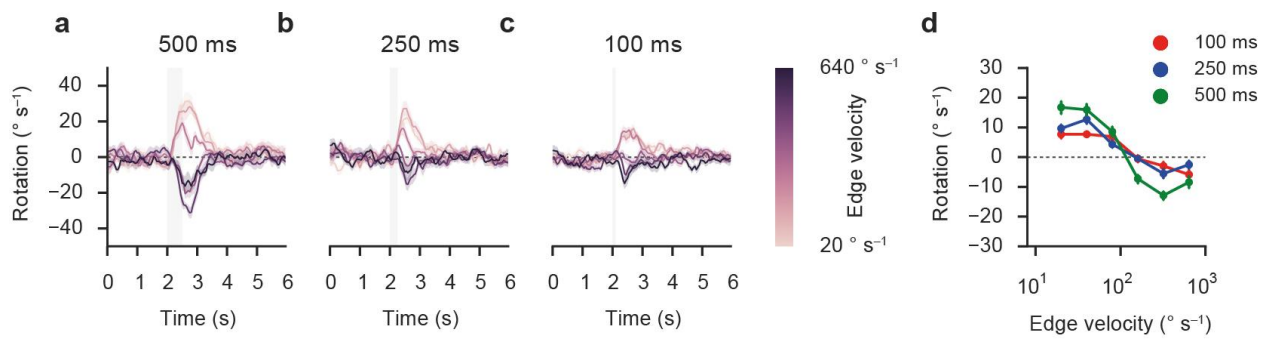
Using open-loop behavioral data (**Fig. 2**), we generated Bayesian decoders according to the procedure outlined in the Online Methods. For details about quantification and subject numbers, refer to main experiment (**Fig. 2**). **(a)** Mapping error across image contrast values, quantified as the root-mean-square error after application to the test data set. With higher contrasts, the quality of the estimate improves; this resembles results based on linear correlation. For T4/T5 block flies, the error stays flat. T4 or T5 block cannot be distinguished from wild-type behavior. **(b)** Visualization of resulting mapping functions, transforming fly responses into Bayesian estimates of input image velocity. Each line corresponds to a single fly. No significance tests were performed.



Supplementary Figure 4

Physiological edge velocity tuning for fixed starting luminance.

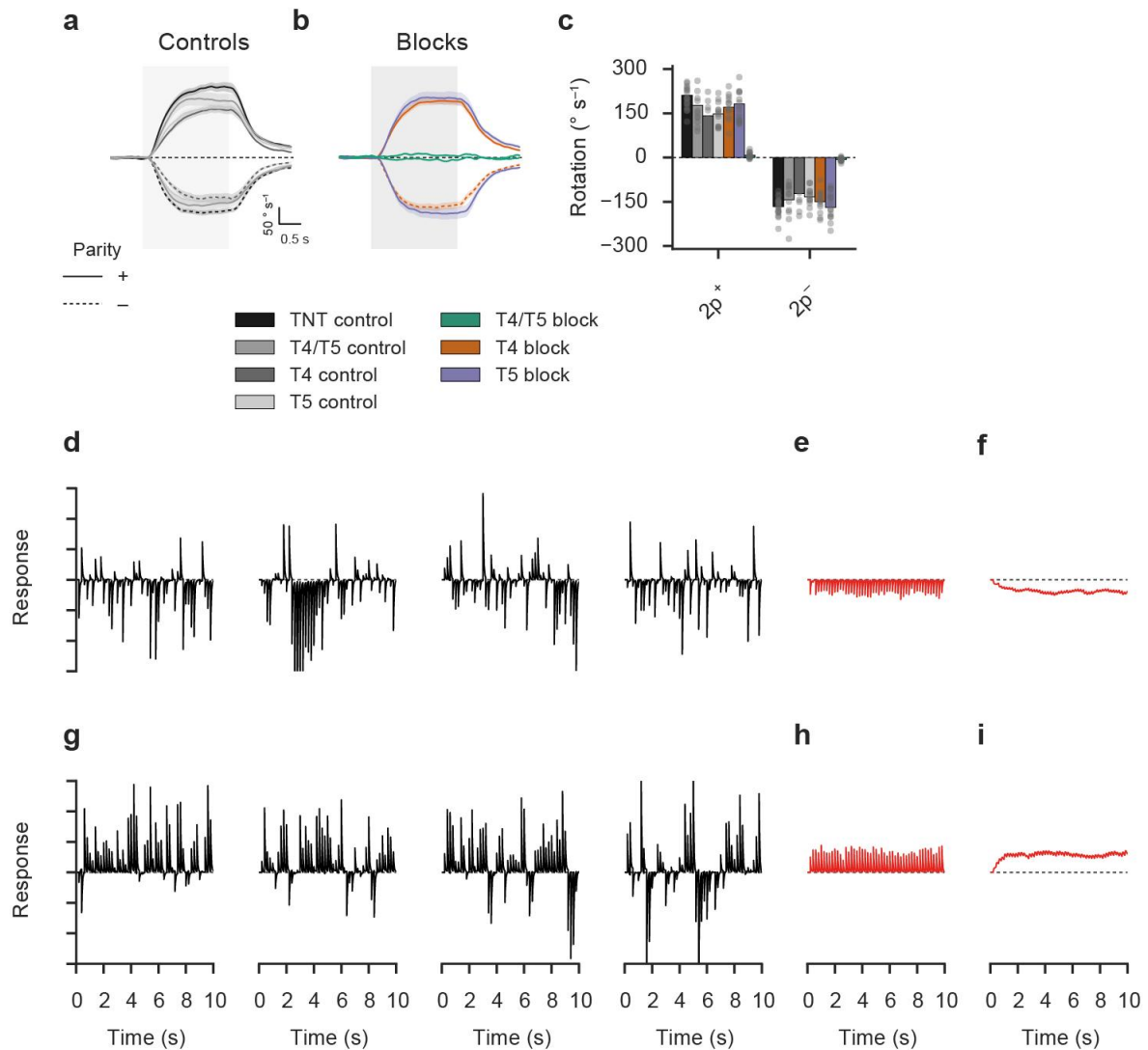
Lobula plate tangential cell responses to ON and OFF edges for equalized initial mean luminance ($N=16$ by pooling 12 vertical system/4 horizontal system cells). See legend of main experiment (**Fig. 3**) as well as Online Methods for details. **(a)** Response traces for edges moving at various velocities. Note that the timescale depends on edge velocity. **(b)** Quantification of velocity tuning. **(c)** Quantification of response dynamics (with latency being defined as the time to maximal response during stimulation for onset or time to minimal response after stimulation for offset). **(d)** Quantification of polarization before and after stimulus presentation. No significance tests were performed.



Supplementary Figure 5

Opposing edge responses for varying stimulus durations.

Presentation and quantification are analogous to main experiment (**Fig. 4**; see Online Methods and associated legend for details). Depicted flies were T4/T5 control flies. (**a-c**) Turning responses for edge pulses of 500 ms ($N=12$), 250 ms ($N=12$), and 100 ms ($N=14$) duration, respectively. (**d**) Quantification of turning responses.



Supplementary Figure 6

Extended data for higher-order motion experiments and simulations.

(a-c) T4 block flies and T5 block flies show 2-point glider responses at control level. (a) Control responses for 2-point gliders of positive or negative parity. (b) Block fly responses. (c) Summary of average turning tendency. Shaded area indicates stimulation period (see Online Methods and legend of main experiment for details; Fig. 8). (d-i) Time- and instantiation-resolved output of the asymmetric detector for converging 3-point gliders. Black traces are arbitrarily scaled detector responses for five random starting conditions of the pattern. (d) Single traces for positive parity. (e) Average time-resolved output for positive parity across 100 instantiations of the stimulus. (f) Low-pass filtered trace from e (first order with time constant of 500 ms followed by multiplicative scaling with a factor of four, approximating the behavioral response). (g) Single traces for negative parity. (h) Average time-resolved output for negative parity across 100 instantiations of the stimulus. (i) Low-pass filtered and scaled trace from h (procedure as in f).

Supplementary Table 1

Alias	Genotype	Experiments
T4/T5 block	w ⁺ /w ⁻ ; UAS-TNT-E/Gal4-R59E08-AD; +/Gal4-R42F06	Figs. 1, 2, 4, 8, S1, S2, S3, S6
T4/T5 imaging	w ⁻ ; UAS-GCaMP6f; Gal4-VT25965/Gal4-VT37588	Fig. 3, S1
T4 block	w ⁺ /w ⁻ ; UAS-TNT-E/+; +/Gal4-VT37588	Figs. 2, 4, 8, S1, S2, S3, S6
T5 block	w ⁺ /w ⁻ ; UAS-TNT-E/+; +/Gal4-R42H07	Figs. 2, 4, 8, S1, S2, S3, S6
TNT control	w ⁺ /w ⁻ ; UAS-TNT-E/+; +/+	Figs. 1, 2, 4, 8, S1, S2, S3, S6
T4/T5 control	w ⁺ /w ⁻ ; +/Gal4-R59E08-AD; +/Gal4-R42F06	Figs. 1, 2, 4, 8, S1, S2, S3, S5, S6
T4 control	w ⁺ /w ⁻ ; +/+; +/Gal4-VT37588	Figs. 2, 4, 8, S1, S2, S3, S6
T5 control	w ⁺ /w ⁻ ; +/+; +/Gal4-R42H07	Figs. 2, 4, 8, S1, S2, S3, S6
Canton S	w ⁺ ; +/+; +/+	Figs. 3, 7, S4

Supplementary Table 2

12.5% contrast			25% contrast		
Genotype		T4/T5 block (n=13)	Genotype		T4/T5 block (n=13)
UAS control	n	19	UAS control	n	19
	t	9.27		t	12.2
	p	2.83e-10		p	3.89e-13
Gal4 control	n	12	Gal4 control	n	12
	t	11.2		t	16.4
	p	1.35e-9		p	3.75e-14

50% contrast			100% contrast		
Genotype		T4/T5 block (n=13)	Genotype		T4/T5 block (n=13)
UAS control	n	19	UAS control	n	19
	t	14.4		t	12.9
	p	4.55e-13		p	3.56e-12
Gal4 control	n	12	Gal4 control	n	12
	t	13.7		t	13.9
	p	1.47e-12		p	3.36e-12

Extended statistics for Fig. 1. For each contrast condition, we determined significance by comparing the block group to both control groups (UAS control and Gal4 control) using a two-tailed Student's *t* test. Blocks were declared significantly different if and only if both control groups were significantly different at a level of 0.05. For multiple comparisons, Bonferroni correction was applied. Red fields indicate significant differences after Bonferroni correction. The number indicated by n is the number of individual flies.

Supplementary Table 3

Correlation coefficient (Fig. 2d)

c = 6.25%

Genotype		T4/T5 block (n=11)	T4 block (n=12)	T5 block (n=12)
UAS control	n	12	12	12
	t	-3.98	0.673	-0.862
	p	7.06e-4	0.508	0.398
Gal4 control	n	12	13	12
	t	-6.20	-1.95	-0.923
	p	3.89e-6	0.0631	0.368

c = 12.5%

Genotype		T4/T5 block (n=11)	T4 block (n=12)	T5 block (n=12)
UAS control	n	12	12	12
	t	-9.15	0.968	-1.49
	p	4.05e-8	0.344	0.150
Gal4 control	n	12	13	12
	t	-14.7	-2.38	-1.57
	p	2.86e-12	0.0277	0.130

c = 25%

Genotype		T4/T5 block (n=11)	T4 block (n=12)	T5 block (n=12)
UAS control	n	12	12	12
	t	-13.2	0.108	-0.545
	p	2.50e-11	0.915	0.591
Gal4 control	n	12	13	12
	t	-19.1	-2.53	0.0875
	p	7.56e-14	0.0198	0.931

c = 50%

Genotype		T4/T5 block (n=11)	T4 block (n=12)	T5 block (n=12)
UAS control	n	12	12	12
	t	-31.5	-0.499	-2.02
	p	1.42e-17	0.624	0.0608
Gal4 control	n	12	13	12
	t	-28.2	-1.49	-0.832
	p	4.00e-18	0.156	0.415

c = 100%

Genotype		T4/T5 block (n=11)	T4 block (n=12)	T5 block (n=12)
UAS control	n	12	12	12
	t	-24.0	-1.89	-2.25
	p	4.04e-13	0.0803	0.0362
Gal4 control	n	12	13	12
	t	-22.3	-2.17	-0.458
	p	6.25e-14	0.0495	0.652

Gain (Fig. 2e)

Genotype		T4/T5 block (n=11)	T4 block (n=12)	T5 block (n=12)
UAS control	n	12	12	12
	t	-4.13	0.175	-1.34
	p	5.41e-4	0.863	0.193
Gal4 control	n	12	13	12
	t	-5.99	-1.81	-0.987
	p	1.15e-5	0.0853	0.336

Genotype		T4/T5 block (n=11)	T4 block (n=12)	T5 block (n=12)
UAS control	n	12	12	12
	t	-8.66	0.0732	-1.58
	p	5.01e-7	0.942	0.129
Gal4 control	n	12	13	12
	t	-10.5	-1.55	-0.614
	p	9.04e-8	0.136	0.546

Genotype		T4/T5 block (n=11)	T4 block (n=12)	T5 block (n=12)
UAS control	n	12	12	12
	t	-11.3	-0.161	-0.828
	p	4.18e-8	0.874	0.417
Gal4 control	n	12	13	12
	t	-14.4	-1.82	0.969
	p	2.00e-9	0.0810	0.344

Genotype		T4/T5 block (n=11)	T4 block (n=12)	T5 block (n=12)
UAS control	n	12	12	12
	t	-19.3	-1.38	-2.35
	p	1.53e-10	0.185	0.0300
Gal4 control	n	12	13	12
	t	-17.3	-0.927	0.328
	p	7.31e-10	0.364	0.747

Genotype		T4/T5 block (n=11)	T4 block (n=12)	T5 block (n=12)
UAS control	n	12	12	12
	t	-16.0	-1.68	-2.00
	p	1.42e-9	0.110	0.0596
Gal4 control	n	12	13	12
	t	-19.2	-1.23	0.404
	p	4.77e-11	0.235	0.692

Extended statistics for Fig. 2. Test details were as in Supplementary Table 2. c denotes contrast. Red fields indicate significant differences after Bonferroni correction. The number indicated by n is the number of individual flies.

Supplementary Table 4

Feature		Mean (n=70)	Maximum (n=70)	Onset latency (n=70)	Offset latency (n=70)	Pre-stimulus polarization (n=70)	Post-stimulus polarization (n=70)
ON vs. OFF	t	-7.30	-5.50	5.18	5.63	-17.2	11.1
	p	3.76e-10	6.13e-7	2.13e-6	3.63e-7	1.12e-26	6.10e-17

Extended statistics for Fig. 3. We compared response features between ON and OFF edge presentation. Responses were always averaged across velocities and then tested using two-tailed Student's *t* tests at a significance level of 0.05. Red fields indicate significant differences. The number indicated by n is the number of individual cells pooled from vertical and horizontal system cells.

Supplementary Table 5

Difference from zero

$v = 20^\circ/s$

Genotype	TNT control (n=12)	T4/T5 control (n=13)	T4 control (n=12)	T5 control (n=13)
versus 0				
t	6.36	6.64	5.57	4.90
p	5.34e-5	2.39e-5	1.67e-4	3.65e-4

$v = 40^\circ/s$

Genotype	TNT control (n=12)	T4/T5 control (n=13)	T4 control (n=12)	T5 control (n=13)
versus 0				
t	4.77	5.88	5.33	6.36
p	5.77e-4	7.51e-5	2.40e-4	3.60e-5

$v = 80^\circ/s$

Genotype	TNT control (n=12)	T4/T5 control (n=13)	T4 control (n=12)	T5 control (n=13)
versus 0				
t	0.703	-0.765	-1.44	0.249
p	0.497	0.459	0.178	0.808

$v = 160^\circ/s$

Genotype	TNT control (n=12)	T4/T5 control (n=13)	T4 control (n=12)	T5 control (n=13)
versus 0				
t	-4.57	-8.74	-5.78	-7.81
p	8.02e-4	1.50e-6	1.23e-4	4.78e-6

$v = 320^\circ/s$

Genotype	TNT control (n=12)	T4/T5 control (n=13)	T4 control (n=12)	T5 control (n=13)
versus 0				
t	-5.67	-7.97	-5.44	-11.1
p	1.45e-4	3.93e-6	2.04e-4	1.14e-7

$v = 640^\circ/s$

Genotype	TNT control (n=12)	T4/T5 control (n=13)	T4 control (n=12)	T5 control (n=13)
versus 0				
t	-2.50	-1.54	-1.15	-2.64
p	0.0297	0.149	0.274	0.0216

Difference from control

Genotype	T4/T5 block (n=12)	T4 block (n=15)	T5 block (n=14)
UAS control			
n	12	12	12
t	-2.66	-14.9	6.80
p	0.0143	5.04e-13	1.32e-6
Gal4 control			
n	13	12	13
t	-2.08	-13.5	8.60
p	0.0502	2.15e-11	1.27e-7

Genotype	T4/T5 block (n=12)	T4 block (n=15)	T5 block (n=14)
UAS control			
n	12	12	12
t	-2.20	-13.1	8.85
p	0.0399	4.12e-12	2.80e-8
Gal4 control			
n	13	12	13
t	-2.90	-12.4	9.65
p	8.33e-3	1.26e-10	3.65e-8

Genotype	T4/T5 block (n=12)	T4 block (n=15)	T5 block (n=14)
UAS control			
n	12	12	12
t	-0.324	-11.8	11.3
p	0.749	1.07e-11	4.30e-10
Gal4 control			
n	13	12	13
t	0.921	-9.70	12.7
p	0.367	6.14e-10	1.86e-9

Genotype	T4/T5 block (n=12)	T4 block (n=15)	T5 block (n=14)
UAS control			
n	12	12	12
t	3.18	-6.82	12.3
p	7.32e-3	4.96e-7	7.74e-12
Gal4 control			
n	13	12	13
t	6.02	-5.98	15.0
p	1.29e-5	3.56e-6	9.84e-12

Genotype	T4/T5 block (n=12)	T4 block (n=15)	T5 block (n=14)
UAS control			
n	12	12	12
t	3.99	-6.06	14.2
p	9.22e-4	2.95e-6	1.16e-12
Gal4 control			
n	13	12	13
t	4.66	-6.45	19.0
p	1.10e-4	1.24e-6	7.84e-15

Genotype	T4/T5 block (n=12)	T4 block (n=15)	T5 block (n=14)
UAS control			
n	12	12	12
t	2.25	-2.21	4.54
p	0.0439	0.0368	1.89e-4
Gal4 control			
n	13	12	13
t	1.18	-4.80	5.05
p	0.256	1.06e-4	3.73e-5

Extended statistics for Fig. 4. For each velocity condition, we determined significance by comparing control groups to zero or block groups to both corresponding control groups (UAS control and Gal4 control) using a two-tailed Student's t test. Blocks were declared significantly different if and only if both control groups were significantly different at a significance level of 0.05. v denotes velocity. For multiple comparisons, Bonferroni correction was applied. Red fields indicate significant differences after Bonferroni correction. The number indicated by n is the number of individual flies.

Supplementary Table 6

Stimulus		Random (n=16)	3p/conv/+ (n=16)	3p/conv/- (n=16)	3p/div/+ (n=16)	3p/div/- (n=16)
versus 0	t	-0.426	-2.33	18.4	-5.44	5.73
	p	0.676	0.0341	1.02e-11	6.89e-5	3.98e-5

Extended statistics for Fig. 7. We compared glider voltage responses to zero. Responses were tested using two-tailed Student's *t* tests at a significance level of 0.05. Red fields indicate significant differences. The number indicated by *n* is the number of individual cells pooled across cells from the horizontal and vertical systems.

Supplementary Table 7

Positive parity

Negative parity

2-point

Genotype		T4/T5 block (n=14)	T4 block (n=13)	T5 block (n=17)
UAS control	n	18	18	18
	t	-16.2	-2.41	-1.33
	p	2.17e-12	0.0228	0.194
Gal4 control	n	12	12	12
	t	-7.93	1.82	1.54
	p	5.91e-6	0.0814	0.136

Genotype		T4/T5 block (n=14)	T4 block (n=13)	T5 block (n=17)
UAS control	n	18	18	18
	t	21.3	1.29	-0.169
	p	1.43e-14	0.211	0.867
Gal4 control	n	12	12	12
	t	8.08	-1.79	-1.91
	p	5.28e-6	0.0869	0.0679

3-point/conv.

Genotype		T4/T5 block (n=14)	T4 block (n=13)	T5 block (n=17)
UAS control	n	18	18	18
	t	7.82	16.7	-5.85
	p	2.73e-8	4.72e-16	1.85e-6
Gal4 control	n	12	12	12
	t	8.57	19.3	-5.49
	p	2.56e-7	2.39e-15	1.11e-5

Genotype		T4/T5 block (n=14)	T4 block (n=13)	T5 block (n=17)
UAS control	n	18	18	18
	t	-6.44	-14.0	6.83
	p	3.12e-6	1.30e-13	2.01e-7
Gal4 control	n	12	12	12
	t	-12.4	-23.7	7.00
	p	4.45e-10	1.88e-15	1.00e-6

3-point/div.

Genotype		T4/T5 block (n=14)	T4 block (n=13)	T5 block (n=17)
UAS control	n	18	18	18
	t	8.58	-3.34	10.8
	p	2.83e-8	2.32e-3	8.68e-12
Gal4 control	n	12	12	12
	t	5.36	-0.354	11.4
	p	1.85e-4	0.727	7.10e-10

Genotype		T4/T5 block (n=14)	T4 block (n=13)	T5 block (n=17)
UAS control	n	18	18	18
	t	-9.25	4.52	-8.51
	p	8.57e-9	1.01e-4	1.36e-9
Gal4 control	n	12	12	12
	t	-6.82	0.991	-9.76
	p	2.12e-5	0.335	3.33e-10

Extended statistics for Fig. 8. Test details were as in Supplementary Table 2. Red fields indicate significant differences after Bonferroni correction. The number indicated by n is the number of individual flies.

3 | DISCUSSION

Without interaction with the environment, survival is generally not possible. Information gathered by sensory systems is therefore crucial for the existence of any organism. Important features about external cues are extracted by neural networks downstream of sensory organs. Understanding their mode of operation would help to greatly improve our understanding of neural circuits and ultimately bring us closer to comprehending how the brain works. I investigated the neural network underlying the computation of direction selectivity in the visual system of the fruit fly *Drosophila melanogaster*. Here, algorithmic models, based on the differential temporal filtering of two signals originating from spatially offset inputs accurately describe the responses of both large field interneurons in the optic lobe of the brain, as well as the turning behavior of walking flies. Probing the nervous system with various physiological assays combined with transgenic manipulations of neurons resulted in a number of important findings.

Together with my colleagues, I could determine that bushy T4 and T5 cells respond to brightness increments and decrements, respectively, providing evidence for the separation into ON and OFF processing streams to be conserved at the level of the lobula plate inputs. I could furthermore show that the four subclasses of T4 and T5 cells exhibit direction selective responses tuned to the four cardinal directions. When I then investigated presynaptic elements to OFF-selective T5 cells I found that four Tm cell types each contribute to the computation of direction selectivity and that they provide a variety of temporal filter properties. Next, I characterized the transmitter system between T4/T5 and lobula plate tangential cells and found that excitatory, cholinergic signaling mediates preferred direction responses while null direction responses must be shaped by a class of – at the time unknown – inhibitory interneurons. In another study I investigated a parallel visual pathway computing contrast. Here, two columnar elements previously only linked to ON edge detection to be necessary for the detection of local and global contrast differences could be determined. Finally, combining physiology, behavior and modeling demonstrated that tuning differences between ON and OFF pathways reflect differences in the luminance distribution of natural scenes.

3.1 ALGORITHMIC MODELS FOR MOTION DETECTION

Classical algorithmic models for motion detection are based on the interaction of two differentially filtered input signals originating from two spatially offset locations (see [Borst, 2011](#); [Borst and Helmstaedter, 2015](#)). An intrinsic property of a Hassenstein-Reichardt correlator is

Hassenstein-Reichardt correlator

Barlow-Levick detector

Why four?

the enhancement of responses to visual motion in the preferred direction (Hassenstein and Reichardt, 1956). Figure 5a exemplifies a half detector tuned to rightward motion. An object moving from left to right will first excite receptor A and, with a certain temporal delay depending on the stimulus velocity, elicit a signal in receptor B. Since the signal in the left arm (blue), originating from receptor A is subject to temporal filtering (τ) it is delayed and arrives at the same time at the interaction stage (NL) as signal B (orange). At the multiplication stage (NL), the coincidence of the two signals results in a strong signal at the output of the half detector (black). For motion from right to left (null direction, ND) the non-delayed signal from receptor B will arrive before the delayed input from A, eliciting only weak responses at the multiplication stage (black). In another model, proposed by Barlow and Levick (1965), direction selectivity is achieved through null direction inhibition by divisive interaction of two signals. Figure 5b illustrates a Barlow-Levick motion detector tuned to rightward motion. Information provided by input A (blue) is directly conveyed to the interaction stage (NL), whereas the signal originating from input B (orange) experiences a temporal delay (τ). For motion in preferred direction, the signal from input A (black) elicits a positive response at the nonlinear interaction stage while the delayed signal from B has no effect on the positive output. For null direction motion the filtering in B results in temporal coincidence of both signals at the interaction stage. Due to the divisive nonlinearity, signal B suppresses the positive signal A. Even though based on different functional principles, both elementary motion detectors result in direction selective output signals. Ever since these models had been proposed, the quest for their neural correlates has motivated a great number of experimental studies. The computation underlying direction selectivity in the visual system of flies has been proposed to follow the principles of a Hassenstein-Reichardt correlator (Hassenstein and Reichardt, 1956; Eichner and Borst, 2011; Clark et al., 2011; Joesch et al., 2013; Borst and Egelhaaf, 1989, 1990; Borst and Haag, 2002). Conversely, motion estimation in the vertebrate retina has been proposed to be implemented as described by Barlow and Levick (Barlow and Levick, 1965; Wässle, 2004; Kim et al., 2014; Borst and Helmstaedter, 2015).

Both models for elementary motion detection compare the signals conveyed by two separate arms. My findings in the OFF pathway of *Drosophila* motion vision however indicate the implication of more than two cell types in the computation of direction selectivity. How can these results be mapped onto the architecture of classical algorithmic descriptions? Several possibilities including a more complex nonlinearity than a simple multiplication, the involvement of different classes of neurons for varying stimulus regimes or the implementation of temporal filtering through the interaction of two or more cell types, have been discussed (see 2.2). In addition to these hypotheses, a motion detector consisting of both a Hassenstein-Reichardt and a Barlow-Levick type detector seems possible. In this scenario preferred direction enhancement would exist alongside with null direction suppression. In a recent study, Fisher et al. (2015b) investigated this question by measuring calcium responses elicited by apparent motion stimuli. From their results they concluded that direction selectivity in the dendrites of T4

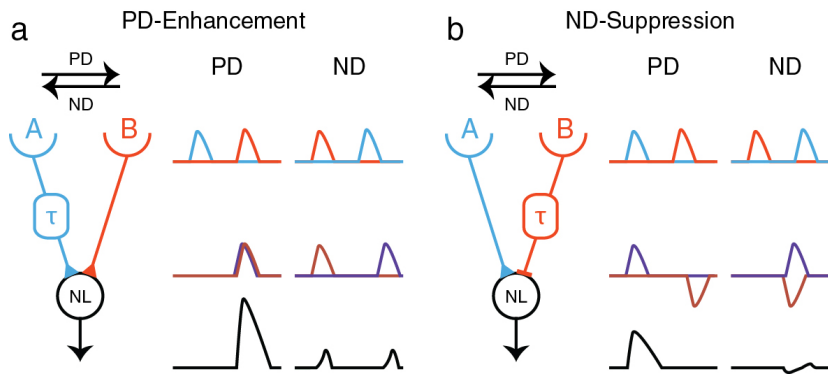


Figure 5. Two algorithmic descriptions of elementary motion detectors. (a) The Hassenstein-Reichardt correlator computes direction selective signals through the nonlinear interaction of two excitatory input signals. For motion in preferred direction (PD) the two signals (one temporally filtered, τ , the other direct) coincide on the output stage (NL) and get multiplied. For visual motion in the opposite direction (ND) the two input signals do not interact. (b) In the Barlow-Levick detector the delayed arm provides a temporally filtered inhibitory signal that cancels out a non delayed excitatory input for null direction motion (ND).

and T5 cells arises through excitatory rather than inhibitory inputs, indicating a Hassenstein-Reichardt detector like mechanism. However, their data also contained weak but significant sublinear responses of T4 cells when stimulated along the null direction. A combination of both, preferred direction enhancement and null direction suppression could help to increase the direction selectivity of local motion detectors and render their response properties more stable and less susceptible to noise. However, at the moment, a final and definite conclusion cannot yet be drawn and further experiments will have to clarify the type of motion detector present in the fly visual system.

3.2 BIOPHYSICAL IMPLEMENTATION OF LOCAL MOTION DETECTION

The two previously mentioned algorithmic descriptions for direction selectivity both rely on the nonlinear interaction of two signals (see Figure 5). My and other experimental data on the OFF pathway provide evidence for this interaction to be located on the dendrites of T4 and T5 cells (Fisher et al., 2015b, see also Borst and Helmstaedter, 2015). A prerequisite for both models is the differential temporal filtering of the two inputs. For the ON-selective pathway, anatomical as well as functional studies suggested two cell types that could implement a Hassenstein-Reichardt type motion detector. Behnia et al. (2014) electrophysiologically measured the temporal filters of Mi1 and Tm3 cells and observed small differences in the peak times. From this they concluded that Tm3 cells provide fast input, constituting the direct arm

while the slower Mi1 cells represent the slow arm. In an electron microscopy study, [Takemura et al. \(2013\)](#) found a small, direction-specific offset between Mi1 and Tm3 cells on the dendrites of T4. Here, Tm3 innervate T4 cells tuned to back to front motion in an anterior position, while Tm3 forms synapses on the proximal dendrite. Combining the two findings indicates a major problem. In a Reichardt detector tuned to back-to-front motion signals must first pass through the delayed arm before exciting the direct line. In the constellation described by [Takemura et al. \(2013\)](#) and [Behnia et al. \(2014\)](#) however, fast Tm3 cells would become activated before slow Mi1 cells. Moreover, while blocking the synaptic output of Mi1 causes strong ON-specific effects on lobula plate tangential cell responses, silencing Tm3 only seems to be important for high velocity regimes ([Ammer et al., 2015](#)). Furthermore, recent connectomic efforts have provided evidence that the spatial offset between Mi1 and Tm3 on the T4 dendrite is negligible (personal communication Lou Scheffer).

The data on the OFF pathway strongly suggest that the temporal filtering takes place at the level of the input cells. I found the four Tm cells presynaptic to T5 to exhibit a variety of temporal response properties. The outputs from any two cell types can be combined in motion detector models with frequency tunings comparable to experimentally tested values. However, the biophysical basis for the nonlinear interaction between the two input signals is currently not understood ([Borst and Egelhaaf, 1990](#); [Gabbiani et al., 2002](#); [Borst, 2011](#)). At a cellular level, several mechanisms are conceivable that result in nonlinear operations. The two inputs could be multiplied via voltage dependent ion channels, where simultaneous activation from neighboring inputs would result in an increase in membrane voltage, that in turn would acquire more voltage gated channels, resulting in a strong depolarization. However, this hypothesis is not very likely to be realized on the dendrites of T5 cells, since this probably causes a feedback loop resulting in infinite, uncontrollable excitation. Two more plausible implementations are depicted in Figure 6. Since RNA-profiling has identified both nicotinic and metabotropic acetylcholine receptors in T5 cells ([Takemura, 2014](#)), a nonlinearity could be implemented through interactions between a metabotropic receptor and a ligand gated ion channel (Figure 6a). In this scenario, a G-protein coupled receptor is activated by excitatory signaling from input A. Its activation causes the G-protein attached to the intracellular membrane to trigger a second messenger cascade. Binding of the second messenger to a neighboring ligand gated ion channel will render the channel more sensitive to activation by a neurotransmitter. Simultaneous transmitter release from input B will then lead to an opening of the channel, resulting in sodium influx and thus increase in membrane voltage. Only if both input signals temporally coincide will the cell respond with a strong depolarization. A second, related mechanism is based on calcium working as a second messenger (Figure 6b). Here, instead of a metabotropic receptor, input A activates a ligand gated calcium channel. Intracellular calcium can now bind to a sodium channel and increase its efficiency. Like previously described, temporally coinciding, excitatory transmitter release from input B will result in a strong depolarization of the postsynaptic cell. In contrast to the scenario with a metabotropic receptor, here

*Excitatory
cooperativity*

already the calcium influx will give rise to small voltage deflections. Importantly, in both cases the activation of input B alone will result in a small activation of the T5 cell. However, only the concurrent activation by both inputs will result in a supralinear increase in membrane voltage.

All mechanisms described so far are based on the interaction of two

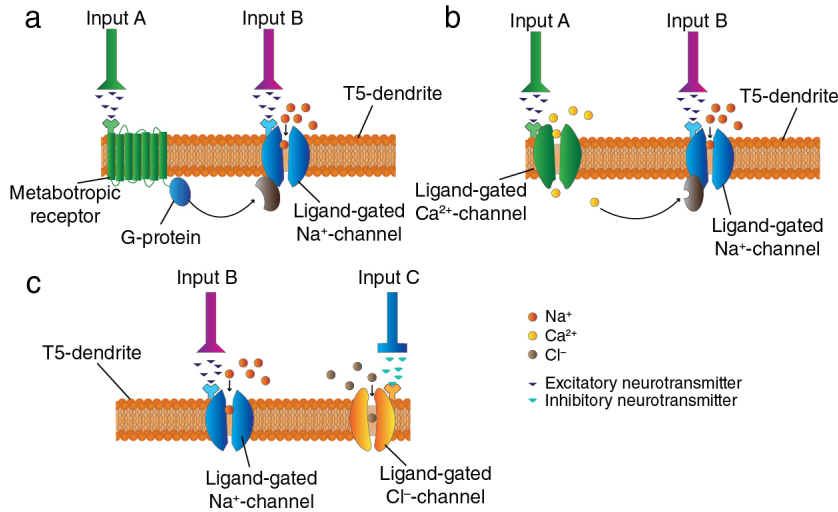


Figure 6. Potential biophysical implementation of preferred direction enhancement (a and b) and null direction suppression (c) on the dendrite of T5 cells. A Hassenstein-Reichardt type model achieves direction selectivity by comparing two temporally offset, excitatory inputs. The supralinear interaction of the two input signals can be implemented through different biophysical mechanisms. (a) Upon activation of a metabotropic receptor by excitatory input A, a G-protein attached to the internal membrane facilitates the activation of a ligand gated sodium channel that receives excitatory signaling from input B. (b) A ligand gated calcium channel, activated through binding of excitatory neurotransmitters e.g. Acetylcholine causes calcium influx. Calcium can act as a second messenger, enabling, upon binding of transmitters released through input B the opening of a ligand gated sodium channel. (c) In a Barlow-Lewick motion detector null direction signals are suppressed by inhibitory interactions. Ligand gated chloride channels open upon binding of an inhibitory transmitter, e.g. glutamate or GABA.

input lines. However, my experimental data provide strong evidence that more than two cell types are involved in the computation of direction selectivity. This raises a simple question: Why are there more than two input lines? Responses of T4 and T5 cells could not only be shaped by preferred direction enhancement (Hassenstein-Reichardt) but also by null direction suppression (Barlow-Lewick). Hence, on the dendrites of T5 cells a third, inhibitory input could inactivate the cell upon stimulation in null direction. This is likely to be implemented through inhibition via a ligand gated chloride channel (Figure 6c). In this case, input C would release an inhibitory neurotransmitter, activating the chloride channel. The coincidental activation of inhibitory input C and excitatory input B would result in a reduced response of the T5 cell. Having both, excitatory and inhibitory cooperativity

*Inhibitory
cooperativity*

would require the involvement of at least three cell types as proposed by the experimental data. One of the cells needs to release inhibitory neurotransmitters like GABA or glutamate. While Tm1, Tm2, and Tm9 cells have been identified to be cholinergic (Takemura et al., 2011; Shinomiya et al., 2014), transmitter profiling for Tm4 is still missing. For T5 cells to be motion sensitive, they need to compare signals originating from neighboring locations in space. It is thus not surprising that their dendrites are not restricted to only one column but rather sample several (7-9) columns (Shinomiya et al., 2014). In order to allocate specific roles to the different Tm cells, it is indispensable to know their spatial distribution on the T5 dendrite.

Taken together, the biophysical implementation of nonlinearities on the dendrites of T5 cells can be based on the interactions of different excitatory and inhibitory receptors. Further investigations must provide evidence for transmitter systems, receptor types, and the spatial organization of the inputs on the postsynaptic dendrite. Having this information at hand could help to shed light onto the cellular mechanisms achieving direction selectivity in local motion detectors.

3.3 FUNCTIONAL SIGNIFICANCE OF PARALLEL PROCESSING STREAMS

Separating a computational task into parallel processing streams seems to be a successful evolutionary strategy conserved across phyla. Examples for parallel circuits computing ON and OFF signals separately can be found in the olfactory system of the nematode *C. elegans* (Chalasanani et al., 2007), the electric sense of some fish species (Bennett, 1971), and the mammalian auditory cortex (Scholl et al., 2010). In the early visual system, the segregation of channels encoding light off versus light on can be observed across the whole animal kingdom; from arthropods (Joesch et al., 2010) over early vertebrates like amphibia (Werblin and Dowling, 1969; Segev et al., 2006) or fish (reviewed in Malicki, 2000), to rodents (Ghosh et al., 2004), predators like cats (reviewed in Wässle and Boycott, 1991) or ferrets (Isayama et al., 2009) up to primates (reviewed in Field and Chichilnisky, 2007) including us humans (Hashimoto et al., 2013). The independent, analogous development of parallel streams for the computation of brightness increments and decrements across phylogenetically distant species is a strong indication for an important evolutionary advantage provided through this separation. However, the functional significance of this division of labor is not yet finally resolved. Photoreceptor cells, the first stage of any visual system respond to both light on and light off. In postsynaptic neurons, the signals are rectified with respect to their contrast polarity. That is, ON-selective neurons depolarize to brightness increments whereas OFF-selective cells respond with increased activity to brightness decrements. Based on a study in the monkey visual system in the late 1980's, two theories for the existence of ON and OFF channels were proposed (Schiller et al., 1986; Schiller, 1992; Westheimer, 2007); first, it could be advantageous to convey information about both, positive as well as negative changes in luminance through

excitatory signals. This hypothesis was based on the observation that the baseline activity of retinal ganglion cells was generally low. A further decrease in firing rate would therefore be less informative than increased excitation. In order to preserve a high range of information about increases and decreases of luminance, the steady-state level of ganglion cells would have to be considerably higher. A second explanation is that the interaction between both channels somewhere downstream the visual processing cascade can increase contrast sensitivity. The visual system has to precisely detect differences of minuscule contrast as well as large discrepancies. Having two separate circuits that can interact in a push-pull manner on a higher level of visual processing will increase the dynamic range and thus provide sensitivity at various contrast regimes. A more recent study suggested that under realistic conditions, a bifurcation of ON and OFF streams increases the efficiency of neural coding (Gjorgjieva et al., 2014). The information transfer per spike is higher for ON/OFF models compared to simulations containing only ON/ON detectors. Hence, the segregation of pathways decreases metabolic effort and thereby increases evolutionary fitness. The most important aspect for the separate computation of ON and OFF motion signals lies the biophysical implementation of the nonlinearity. An ON/ON detector encodes brightness increments with increased activity, while brightness decrements elicit negative responses. Implementing a multiplicative nonlinearity with only this one input is biophysically implausible. Splitting the visual input into two streams that respond positively to ON and OFF components, respectively, provides the multiplication stage with two nonnegative (excitatory) signals that can interact as previously described (see 3.2, Eichner et al., 2011)

In *Drosophila* the two parallel visual pathways differ with respect to their temporal tuning. This difference reflects asymmetries in the visual scenery naturally occurring in the fly's habitat. This finding points out an additional advantage of the separation between ON and OFF channels. Systems encoding for increases and decreases in luminance with one and the same set of neurons can not be specifically tuned to intrinsic characteristics of their visual environment. The lack in adaptability would reduce their performance and introduce an evolutionary disadvantage. Flies, just like all other visual animals can simply not afford missing important information about approaching predators or potential mates.

3.4 CELLULAR MECHANISMS OF MOTION OPPONENCY

Both, the output of a Reichardt detector and the responses of lobula plate tangential cells are fully motion opponent. That is, visual motion in preferred direction elicits positive signals, while stimulation in null direction results in negative responses. At the level of the tangential cells this can be observed by depolarizations and hyperpolarizations, respectively. While this physiological particularity had first been ob-

*Lobula plate
interneurons*

*Functional
significance of
motion opponency*

served in house flies more than 30 years ago (Hausen, 1984; Joesch et al., 2008), its functional significance has remained unclear. When investigating the neural mechanism underlying the biphasic responses of tangential cells in *Drosophila*, I found that fast, monosynaptic, cholinergic input from T₄ and T₅ cells underlies the increase in membrane potential, whereas slower, inhibitory signaling via another interneuron most likely causes the null direction component of tangential cell responses. The identity of that, at the time unknown cell type could be revealed only two years later, when Mauss et al. (2015) discovered neurons connecting layer three and four of the lobula plate. This subpopulation of lobula plate intrinsic neurons (LPis) turned out to receive excitatory synaptic input from both T₄ and T₅ cells tuned to upward motion in layer three and send their axonal arborizations into the adjacent layer, where tangential cells of the vertical system tuned to downward motion reside. Here they provide glutamatergic inhibitory input onto lobula plate tangential cells. Functional characterization of two classes of LPis – projecting from layer three to four and vice versa – revealed directional tuning in agreement with their dendritic input; i.e. cells with dendrites in layer three were tuned to visual motion moving upward while LPis that receive input from layer four exhibited tuning to downward motion. Moreover, blocking the synaptic output of intrinsic neurons specifically impaired null direction responses in VS cells, leaving responses to preferred direction stimulation unaffected. The authors could thus provide experimental proof for the cellular mechanism underlying null direction responses in lobula plate tangential cells of *Drosophila melanogaster*. Presenting visual stimuli with opposing motions they could furthermore provide evidence for the functional significance of motion opponency. Lobula plate tangential cells in wild type flies respond overall weakly to these stimuli. However, blocking the output of layer 3/4 LPis, thereby eliminating the null direction response of layer four tangential cells, resulted in strong responses in VS cells. From this Mauss et al. (2015) concluded that null direction suppression cancels responses to expanding flow fields and thereby increases flowfield selectivity in lobula plate tangential cells. Transcript profiling revealed expression of the vesicular glutamate transporter vGluT in LPis and glutamate gated chloride channel GluCl in lobula plate tangential cells. Hence, the null direction inhibition seems to be provided directly onto the dendrites of tangential cells. Since also T₄ cells express glutamate gated chloride channels (Fendl, 2014) it is furthermore possible that lobula plate intrinsic neurons additionally inhibit T₄ and T₅ cells tuned to opposite directions. Characterizing the localization of glutamate receptors on the dendrites of either tangential cells or T₄/T₅ neurons with high spatial resolution would be one possibility to address this question. Investigating the directional tuning of T₄ and T₅ cells under transgenic silencing of one subclass of lobula plate intrinsic neurons could also help to unravel the exact mechanism responsible for null direction suppression.

3.5 LOBULA PLATE AND OPTOMOTOR RESPONSE

Flies, like other insects and also vertebrates respond to moving large field stimuli by stabilizing the shifting image on the retina. A process called optomotor response in insects (Hassenstein, 1951; Kunze, 1961; Götz, 1964; Neuhauss et al., 1999) and optokinetic reflex in species with movable eyes (Easter and Johns, 1974; Hess et al., 1985). In both, *Drosophila* as well as larger fly species this well described behavior has been proposed to be controlled by a group of wide field tangential cells in the lobula plate (Bishop and Keehn, 1967; Dvorak et al., 1975). This assumption is based on several observations: first, lobula plate tangential cells integrate motion across extensive areas of the fly's visual field, a prerequisite for the control of responses to wide field motion (Krapp et al., 1998; Schnell et al., 2010; Hopp et al., 2014). Second, the electrical properties of these neurons follow similar characteristics as the optomotor response itself and can be described by a correlation type model that was based on observations on the turning reactions of walking or flying insects (Hassenstein and Reichardt, 1956; Hausen, 1984; Schnell et al., 2010; Joesch et al., 2008). Tangential cells respond to visual motion in a fully-opponent direction-selective manner, depolarizing to motion in preferred direction and hyperpolarizing when stimulated in null direction. Furthermore, they exhibit similar temporal frequency tuning and their responses to varying contrasts resembles those of behaving animals. These functional attributes are also astonishingly well predicted by a Hassenstein-Reichardt correlator (reviewed in Borst et al., 2010). Third, several studies have suggested their involvement in controlling optomotor response using a variety of different approaches. Loss of function experiments with *Drosophila* mutants that lack large field cells in the lobula plate (Heisenberg et al., 1978) and microsurgically truncated lobula plate tangential cell axons (Hausen and Wehrhahn, 1983) revealed the necessity of functional neurons in the lobula plate for the correct execution of the optomotor reflex. Extracellular electrical stimulation of different regions of the lobula plate resulted in direction-specific yaw movements (Blondeau, 1981). Moreover, ventral cervical nerve motoneurons (VCNM) which are involved in head movements, have been shown to be electrically coupled to HS cells (Haag et al., 2010). Finally, cobalt coupling experiments in the blow fly *Calliphora* revealed direct connections between two out of three horizontal system cells with direction selective neck motor neurons (Strausfeld et al., 1987), further indicating an implication of tangential cells in optomotor behaviors (see also Huston and Krapp, 2008; Haag et al., 2010; Kauer et al., 2015).

The question whether and which classes of lobula plate tangential cells are sufficient for the initiation and execution of optomotor behaviors is not yet conclusively clarified. So far the only study to directly link lobula plate tangential cell activation to the initiation of both head movements and steering behavior in flying flies used optogenetic activation of horizontal system cells of tethered flying fruit flies (Haikala et al., 2013). The role of tangential cells of the vertical system, supposedly responsible for pitch movements, still awaits empirical confirmation. The experimental setup for investigating the optomotor response in the vertical axis, probing pitch movements is currently very challeng-

ing. Both, tethered walking as well as flying flies are usually attached at the back of the thorax, measuring yaw angular velocities either with a torque meter (e.g. Götz, 1964), through differences in wing beat amplitudes between left and right wings (e.g. Götz, 1987), or by monitoring the rotational velocity of a small sphere moved by the fly's legs (e.g. Buchner, 1976; Bahl et al., 2013). Since, in this configuration, only left or right turns are tracked, responses to vertical motion can not be resolved. A possible setup that could be used to overcome this limitation would be the tracking of freely flying flies in a three-dimensional environment during presentation of visual stimuli (Land and Collett, 1974; Mronz and Lehmann, 2008; Straw et al., 2011). A further problem is the lack of Gal4-lines specifically driving expression in lobula plate tangential cells. The fly strain used for optogenetic activation of HS cells contains a multitude of other cell types in its expression pattern and is therefore not suitable for other applications, such as blocking experiments (Haikala et al., 2013; Chiappe et al., 2010). Moreover, in addition to the three described HS cells and at least six VS cells (Scott et al., 2002; Joesch et al., 2008; Schnell et al., 2010), the lobula plate of *Drosophila* contains a yet unidentified number of tangential cells residing in layers two and three that may also provide input to visually evoked motor actions (Wasserman et al., 2015). Again, to date no Gal4-lines are available that drive expression in the entirety of the lobula plate circuits. Even if the contribution of lobula plate tangential cells to optomotor behaviors awaits final confirmation, the scientific evidence strongly suggests an essential role in mediating the execution of visually evoked turning responses. It seems therefore appropriate to probe the neural circuits underlying motion detection at both stages, the lobula plate tangential cells and the behavioral output.

Visuomotor
transformation

The two readouts can, nevertheless, not be used entirely interchangeably. It has been shown in *Calliphora* that descending neurons encode ego-motion more robustly than presynaptic lobula plate tangential cells (Wertz et al., 2009). The comparison of stimulus induced response fluctuations between VS cells and a postsynaptic descending neuron (DNOVS₁) revealed that signals in tangential cells contain significantly more potential fluctuations than downstream DNOVS₁, i.e. the signal is smoothed out between VS cells and their postsynaptic partners. Comparing Tm cell blocking effects on the level of tangential cells with behavioral phenotypes, revealed that the gravity of the effects differed nonlinearly between both output stages. Only severe reductions of tangential cell responses strongly affected turning responses. Both these observations can be explained by a saturating transfer function between tangential cell signalling and descending neurons and thus the behavioral output. This saturation can be implemented by a pooling of signals over several tangential cells (Weber et al., 2008). In deed, descending neurons receive input of multiple lobula plate tangential cells (Haag et al., 2007). Furthermore, VS cells in *Calliphora* are electrically coupled to neighboring VS cells via axo-axonal gap junctions (Haag and Borst, 2005; Cuntz et al., 2007). In *Drosophila*, neurobiotin injections revealed gap junctions between neighboring HS cells (Schnell et al., 2010).

Another hint for the existence of compensatory mechanisms downstream of lobula plate tangential cells becomes apparent when con-

sidering the responses of walking flies to stimulation with classical edges compared to opposing edges. Here, effects of blocking for example a combination of Tm2 and Tm9 cells did not result in strong impairments in the turning response, while the opposing edge stimulus produced a clear OFF specific phenotype (Figure 7). A possible

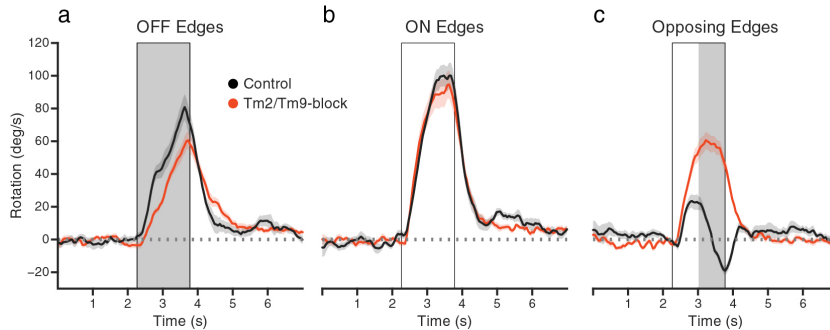


Figure 7. The strengths of behavioral phenotypes may vary depending on the visual stimulation. Probed with either multiple unidirectional OFF (a) or ON (b) edges, flies with silenced Tm2 and Tm9 cells (orange) exhibit only very mild reductions in responsiveness to moving OFF edges compared to controls (black). The same flies tested with multiple ON and OFF edges moving simultaneously into opposite directions (c, opposing edge stimulus) show strong turning tendencies in the direction of bright edge motion (positive rotation). Boxes display duration of stimulus presentation, errorshades indicate \pm s.e.m.

explanation for this observation lies in the nature of the different stimuli. Stimulation with uni-directional edges of similar polarity probes absolute effects on one of the two channels (ON or OFF). Presenting edges of complementary contrasts simultaneously moving in opposite directions, allows for an investigation of relative effects between the perception of bright and dark stimuli. For instance blocking Tm2 and Tm9 in combination leads to a strong impairment of OFF edge detection in the lobula plate. Nevertheless, the block is not 100% complete, resulting in a small response of lobula plate tangential cells to moving OFF edges. Under the stimulus conditions tested – high contrast, high luminance – this remaining response may be sufficient to elicit turning responses similar to controls. Presenting opposing edges can overcome this saturation problem. Signals from the bright and dark selective pathways are now compared and the behavioral output reflects the relative contribution of either inputs. A possible issue of this assay is that absolute effects are neglected. The turning response of wild type flies for example is not discriminable from the behavior of entirely motion blind flies. It is therefore crucial for the correct assessment of the results to combine different techniques. Absolute effects can be determined with electrophysiological recordings from tangential cells, while the relative contribution of single neural elements can be probed using the opposing edge stimulus in walking or flying flies. Taken together, lobula plate tangential cells seem to mediate visually evoked responses in behaving flies. The exact relation between the electrical signals in these wide field neurons and the behavioral output still awaits further characterization. To this end, the identity of all large field neurons of the lobula plate needs to be clarified and specific

driver lines need to be created that enable blocking the output of all lobula plate tangential cells while monitoring the response behavior of ideally freely moving *Drosophila*.

3.6 RESULTS IN THE LIGHT OF THE CURRENT LITERATURE

During the course of my PhD project, several laboratories moved their focus to the circuitry underlying visual motion detection in *Drosophila* resulting in a number of publications. While the majority of these results are in line with my findings (Tuthill et al., 2013; Behnia et al., 2014; Fisher et al., 2015b), some of them arrived at different conclusions.

Contribution of L4

Blocking the output of lamina neurons L4 using *shibire^{ts}*, resulted in a strong and specific reduction in responses of lobula plate tangential cells to moving dark edges, independent on the direction of motion. From this was concluded that L4 cells are crucial components of the OFF motion vision pathway. In contrast, when measuring the turning behavior of walking flies to moving edges, Silies et al. (2013) observed that flies lacking synaptic transmission in L4 did not exhibit similar, OFF specific phenotypes. Hence, they state that L4 is dispensable for rotational motion. However, presenting flies of a second L4 specific Gal4-line with bright and dark edges simultaneously moving in opposite directions, the same study reported significant turning responses with the direction of bright edge motion. This inconsistency makes it difficult to conclusively compare my physiological data with the results from Silies et al. (2013). Nevertheless, additionally to differences in driver line specificity and expression strength, it is also conceivable that the discrepancies emerge from similar mechanisms as discussed earlier; the saturating transfer function between the signals of lobula plate tangential cells and the behavioral output (see 3.5).

Calcium dynamics observed by fluorescence changes of genetically encoded indicators are often used as a proxy for neural activity. However, the actual membrane voltage and the detected fluorescence signal can differ quite substantially. Membrane depolarization triggers the activation of voltage-gated calcium channels which results in calcium influx. Calcium will accumulate over time in the cell. The change of the intracellular calcium concentration however, has

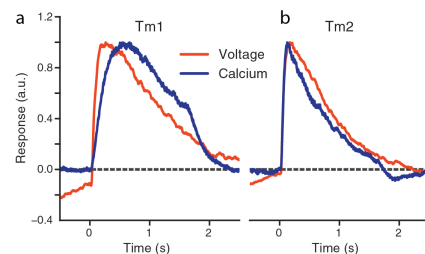


Figure 8. Voltage traces for step responses (presentation of local brightness decrements for 2s). Red traces are electrophysiological recordings from Behnia et al. (2014), blue traces depict calcium signals of Tm1 (a) and Tm2 (b) cells. Traces acquired by both techniques closely resemble each other. For Tm1, voltage signals are faster than calcium dynamics. For Tm2, the calcium signal precedes the voltage trace.

The change of the intracellular calcium concentration however, has

a slower time constant than the voltage signal (Egelhaaf and Borst, 1995). The observed calcium dynamics can therefore depict a lowpass filtered representation of the membrane voltage. This can be problematic for the interpretation of temporal response dynamics measured by calcium imaging. Interestingly, electrophysiologically measured step responses of transmedullary neurons Tm1 and Tm2 proved to be very similar to my calcium measurements (Figure 8, Behnia et al., 2014). Tm2 signals obtained with both methods are almost indistinguishable and calcium responses of Tm1 cells also closely resemble those measured with a recording electrode in the soma. The close relation between calcium and voltage signals in Tm1 and Tm2 makes us confident that our data for Tm4 and Tm9 reflect the cells' physiological properties well.

Calcium measurements using oscillating dark bars revealed small isotropic receptive fields and slow temporal dynamics. I furthermore observed strong, OFF specific effects on both lobula plate tangential cell responses and the turning behavior of walking flies when blocking the synaptic output of Tm9. In a study published in *Current Biology*, Fisher et al. (2015a) found similar characteristics for Tm9, regarding their temporal properties as well as their contribution to OFF motion vision. In contrast, they described Tm9 as wide field neurons responding to dark stimuli spanning about 60 degrees of azimuth and elevation. The stimuli used by Fisher et al. (2015a) to characterize the spatial receptive fields were different from mine. Instead of probing the responses with single bars, they used reverse correlation of a Gaussian noise stimulus identical to spike-triggered-average methods (see Dayan and Abbott, 2005). Here, neural responses are monitored while the animal is presented with a white noise stimulus. The receptive fields are then calculated by cross-correlating stimulus and response. The differing stimulation techniques could potentially explain the diverging results in spatial receptive fields. However, preliminary measurements in our laboratory, using reverse correlation of white noise stimuli, resulted in similar receptive field sizes as previously observed in my experiments using dark bars to probe receptive fields (personal communication Michael Drews). It is thus difficult to assess where these disparities originate. The Gal4 driver lines used to express GCaMP6f were different in both studies. However, expression patterns as well as the similarities regarding temporal dynamics and necessity for OFF motion computation make it highly unlikely that the inconsistencies are based on different cell populations. The spatial integration properties measured in Tm9 suggested that they receive inhibitory inputs from neighboring elements, suppressing responses to objects between approximately 10 and 70 degrees width. Measuring calcium dynamics of cells at a very dorsal position of the optic lobe, that receive input from photoreceptors facing the upper boundary of the stimulation monitor could produce indecisive results. If one imagines a circular receptive field that receives excitatory input from the center and inhibitory signals from the surround, stimulation of only one half of the center-surround field could strongly decrease the effect of lateral inhibition, resulting in larger receptive fields. The spatial integration properties of Tm9 that increase their activity for objects larger than 80 degrees speak in favor of this hypothesis.

Tm9 receptive fields

Taken together, except a few discrepancies, my data are largely in line with the recent literature in the field, creating a good basis for future experiments that can help to decipher the mechanisms for the neural implementation of motion vision in the OFF pathway and beyond.

3.7 FUTURE DIRECTIONS

During the time of my Phd project, I could contribute important new insights towards our understanding of the circuitry underlying motion detection in *Drosophila*. Nevertheless, a number of open questions still await answers. I could provide strong evidence for the involvement of four cell types (Tm₁, Tm₂, Tm₄, and Tm₉) in the computation of direction selectivity in the dark selective pathway. The mechanism underlying elementary motion detection and the role of each of these cells still need to be investigated. None of the input cells to T₅ are direction selective, thus it has been concluded that the interactions that lead to motion sensitivity must happen on the dendrites of T₄ and T₅ (see 3.2). Yet, the examination of the contribution of columnar neurons to motion detection has always happened by either measuring responses of lobula plate tangential cells or monitoring the turning behavior of walking flies. Both of these output stages are located after the summation stage of an elementary motion detector (see Figure 1). Many computational details can not be resolved on this level. For example, blocking Tm₉ resulted in a strong decrease in tangential cell responses to moving brightness decrements. This can have two underlying causes: first, T₅ cells lose their responsiveness all together and fail to provide excitatory input onto tangential cells. In a second scenario, T₅ cells lose their direction selectivity and respond to motion in all directions alike. In this case, downward motion excites T₅ cells of all four subclasses. Since inhibitory interneurons (LPis, Mauss et al., 2015) interconnect the four layers of the lobula plate this results in a similar effect on the responses of tangential cells. Due to their small size, and the resulting electrophysiological inaccessibility, responses of T₅ cells have not been characterized in the absence of any input element. Combining transgenic expression strategies one can simultaneously express a calcium indicator in T₅ cells and neuronal silencers in presynaptic elements. With this experimental approach the effects of blocking Tm cells can be investigated directly at the stage of nonlinear interaction (T₅ dendrites) and not only indirectly after spatial integration (tangential cells). This strategy can help to investigate the mechanisms behind the tuning properties of T₅ cells, determining which of the previously mentioned hypotheses for the reduction in amplitude of tangential cell responses holds true.

T₅ imaging, Tm manipulation

Besides silencing columnar elements presynaptic to T₅ insight into synaptic mechanisms can be gained by activating Tm cells and measuring responses in T₅. Again, using a combinatorial expression strategy one can express optogenetic activators like channelrhodopsin under the control of Gal4 in upstream elements and a calcium indicator controlled by LexA in postsynaptic T₅ cells. This endeavor is technically more challenging than silencing experiments. Algorithmic de-

scriptions for motion vision require two spatially offset inputs to temporally coincide on the dendrites of T5 cells. Moreover, anatomical and functional evidence point out the involvement of more than two cell types in these computations. It is therefore not very probable that simultaneously stimulating an ensemble of multiple cells of one cell type will result in responses in motion-sensitive T5 neurons. A more sophisticated stimulation system is required to allow for activating cells in a spatially and temporally defined manner. A stimulation device based on a computer driven projector recently developed in the laboratory could help to overcome this limitation. With its help it is possible to project moving patterns onto the fly's brain and thereby stimulate columnar neurons successively. Probing the contributions of Tm1, Tm2, Tm4, and Tm9 cells separately and in combinations using optogenetic activation will teach us a lot about the exact composition of the network responsible for direction selectivity.

Taken together, with this cumulative dissertation I could substantially increase the insight into the neural mechanisms of *Drosophila* motion vision. I could help to identify, in T4 and T5 cells, local motion detectors for the ON and OFF pathway, respectively. I could furthermore pinpoint the emergence of direction selectivity to the dendrites of T5 by characterizing all four presynaptic elements, thereby also describing spatial and temporal filter properties of the circuit elements involved in the computation of direction selectivity. My work provided the basis for important new experiments that have the potential to bring the deciphering of the entire neural network underlying motion detection within reach.

*Structured
illumination*

BIBLIOGRAPHY

- Alderson, T.
1965. Chemically induced delayed germinal mutation in *Drosophila*. *Nature*, 207(993):164–167. (Cited on page 6.)
- Ammer, G., A. Leonhardt, A. Bahl, B. J. Dickson, and A. Borst
2015. Functional Specialization of Neural Input Elements to the *Drosophila* ON Motion Detector Report. *Current Biology*, 25(17):2247–2253. (Cited on page 150.)
- Bahl, A., G. Ammer, T. Schilling, and A. Borst
2013. Object tracking in motion-blind flies. *Nature Neuroscience*, 16(6):730–8. (Cited on pages 2 and 156.)
- Bahl, A., E. Serbe, M. Meier, G. Ammer, and A. Borst
2015. Neural Mechanisms for *Drosophila* Contrast Vision. *Neuron*, 88:1240–1252. (Cited on page 84.)
- Baird, G. S., D. a. Zacharias, and R. Y. Tsien
1999. Circular permutation and receptor insertion within green fluorescent proteins. *Proceedings of the National Academy of Sciences of the United States of America*, 96(20):11241–11246. (Cited on page 8.)
- Barlow, H. B., R. M. Hill, and W. R. Levick
1964. Retinal Ganglion Cells Responding Selectively to Direction and Speed of Image Motion in the Rabbit. *Journal of Physiology*, 173:377–407. (Cited on page 3.)
- Barlow, H. B. and W. R. Levick
1965. The mechanism of directionally selective units in rabbit's retina. *The Journal of Physiology*, 178(3):477–504. (Cited on page 148.)
- Bausenwein, B. and K.-F. Fischbach
1992. Activity labeling patterns in the medulla of *Drosophila melanogaster* caused by motion stimuli. *Cell & Tissue Research*, 270(1):25–35. (Cited on pages 15 and 16.)
- Behnia, R., D. A. Clark, A. G. Carter, T. R. Clandinin, and C. Desplan
2014. Processing properties of ON and OFF pathways for *Drosophila* motion detection. *Nature*, 512:427–430. (Cited on pages 149, 150, 158, and 159.)
- Bellen, H. J., C. Tong, and H. Tsuda
2010. a History Lesson for the Future. *Nature Reviews Neuroscience*, 11:514–522. (Cited on page 4.)
- Bennett, M.
1971. Electrolocation in Fish. *Annals of the New York Academy of Sciences*, 188:242–269. (Cited on page 152.)

- Benzer, S.
1967. Behavioral mutants of *Drosophila* isolated by countercurrent distribution. *Proceedings of the National Academy of Sciences of the United States of America*, 58(3):1112–1119. (Cited on page 6.)
- Berndt, A., O. Yizhar, L. A. Gunaydin, P. Hegemann, and K. Deisseroth
2009. Bi-stable neural state switches. *Nature Neuroscience*, 12(2):229–234. (Cited on page 11.)
- Berni, J., A. M. Muldal, and S. R. Pulver
2010. Using Neurogenetics and the Warmth-Gated Ion Channel TRPA1 to Study the Neural Basis of Behavior in *Drosophila*. *Journal of Undergraduate Neuroscience Education*, 9(1):5–14. (Cited on page 9.)
- Bischof, J., R. K. Maeda, M. Hediger, F. Karch, and K. Basler
2007. An optimized transgenesis system for *Drosophila* using germ-line-specific phiC31 integrases. *Proceedings of the National Academy of Sciences of the United States of America*, 104(9):3312–7. (Cited on page 7.)
- Bishop, L. G. and D. G. Keehn
1967. Neural correlates of the optomotor response in the fly. *Kybernetik*, 3(6):288–295. (Cited on page 155.)
- Blondeau, J.
1981. Electrically Evoked Course Control in the Fly *Calliphora erythrocephala*. *Journal of Experimental Biology*, 92:6–10. (Cited on page 155.)
- Bloomington
2016. <http://flystocks.bio.indiana.edu/>.
- Borst, A.
1986. Time Course of the Housellies' Landing Response. *Biological Cybernetics*, 383:379–383. (Cited on page 2.)
- Borst, A.
2009. *Drosophila's* view on insect vision. *Current Biology*, 19(1):36–47. (Cited on page 10.)
- Borst, A.
2010. Neurophysiology: recording from neurons in action. *Current Biology*, 20(16):679–680. (Cited on page 3.)
- Borst, A.
2011. Fly vision: moving into the motion detection circuit. *Current Biology*, 21(24):990–992. (Cited on pages 147 and 150.)
- Borst, A.
2014a. Fly visual course control: behaviour, algorithms and circuits. *Nature Reviews Neuroscience*, 15(9):590–599. (Cited on page 17.)
- Borst, A.
2014b. In search of the holy grail of fly motion vision. *The European Journal of Neuroscience*, 40:3285–3293. (Cited on page 4.)

- Borst, A. and M. Egelhaaf
1989. Principles of visual motion detection. *Trends in Neurosciences*, 12(8):297–306. (Cited on page 148.)
- Borst, A. and M. Egelhaaf
1990. Direction selectivity of blowfly motion-sensitive neurons is computed in a two-stage process. *Proceedings of the National Academy of Sciences of the United States of America*, 87(23):9363–7. (Cited on pages 148 and 150.)
- Borst, A. and J. Haag
2002. Neural networks in the cockpit of the fly. *Journal of Comparative Physiology*, 188(6):419–437. (Cited on page 148.)
- Borst, A., J. Haag, and D. F. Reiff
2010. Fly motion vision. *Annual Review of Neuroscience*, 33:49–70. (Cited on pages 16 and 155.)
- Borst, A. and M. Helmstaedter
2015. Common circuit design in fly and mammalian motion vision. *Nature Neuroscience*, 18(8):1067–1076. (Cited on pages 147, 148, and 149.)
- Boyden, E. S., F. Zhang, E. Bamberg, G. Nagel, and K. Deisseroth
2005. Millisecond-timescale, genetically targeted optical control of neural activity. *Nature Neuroscience*, 8(9):1263–1268. (Cited on page 10.)
- Brand, A. H. and N. Perrimon
1993. Targeted gene expression as a means of altering cell fates and generating dominant phenotypes. *Development (Cambridge, England)*, 118(2):401–415. (Cited on pages 4 and 6.)
- Broca, P.
1888. *Mémoires sur le cerveau de l'homme et des primates*. Paris: C. Reinwald. (Cited on page 8.)
- Broussard, G. J., R. Liang, and L. Tian
2014. Monitoring activity in neural circuits with genetically encoded indicators. *Frontiers in Molecular Neuroscience*, 7:1–17. (Cited on pages 8 and 10.)
- Buchner, E.
1976. Elementary movement detectors in an insect visual system. *Biological Cybernetics*, 24(2):85–101. (Cited on page 156.)
- Buchner, E., S. Buchner, and I. Bülthoff
1984. Deoxyglucose mapping of nervous activity induced in *Drosophila* brain by visual movement - I. Wildtype. *Journal of Comparative Physiology A*, 155(4):471–483. (Cited on page 16.)
- Cajal, S. R. and D. Sánchez
1915. Contribución al conocimiento de los centros nerviosos de los insectos. *Trabajos del Laboratorio de Investigacionens biologicas*, 13:1–168. (Cited on pages 4 and 14.)

- Chalasan, S. H., N. Chronis, M. Tsunozaki, J. M. Gray, D. Ramot, M. B. Goodman, and C. I. Bargmann
2007. Dissecting a circuit for olfactory behaviour in *Caenorhabditis elegans*. *Nature*, 450(7166):63–70. (Cited on page 152.)
- Chalfie, M., Y. Tu, W. W. Ward, G. Euskirchen, and D. Prasher
1994. Green fluorescent protein as a marker for gene expression. *Science*, 9(2):1258–62. (Cited on pages 4 and 8.)
- Changeux, J.-P.
2010. Reflections on the origins of the human brain. In *The Newborn Brain: Neuroscience and Clinical Applications*, chapter 1. Cambridge University Press. (Cited on page 6.)
- Chen, T.-W., T. J. Wardill, Y. Sun, S. R. Pulver, S. L. Renninger, A. Bao-han, E. R. Schreiter, R. a. Kerr, M. B. Orger, V. Jayaraman, L. L. Looger, K. Svoboda, and D. S. Kim
2013. Ultrasensitive fluorescent proteins for imaging neuronal activity. *Nature*, 499(7458):295–300. (Cited on page 8.)
- Chiappe, M. E., J. D. Seelig, M. B. Reiser, and V. Jayaraman
2010. Walking modulates speed sensitivity in *Drosophila* motion vision. *Current Biology*, 20(16):1470–1475. (Cited on page 156.)
- Chuhma, N., K. F. Tanaka, R. Hen, and S. Rayport
2011. Functional connectome of the striatal medium spiny neuron. *Journal of Neuroscience*, 31(4):1183–1192. (Cited on page 11.)
- Clark, D. A., L. Bursztyn, M. A. Horowitz, M. J. Schnitzer, and T. R. Clandinin
2011. Defining the computational structure of the motion detector in *Drosophila*. *Neuron*, 70(6):1165–77. (Cited on page 148.)
- Collett, T. S. and M. F. Land
1978. How hoverflies compute interception courses. *Journal of Comparative Physiology A*, 125(3):191–204. (Cited on page 3.)
- Cruz-Martín, A., R. N. El-Danaf, F. Osakada, B. Sriram, O. S. Dhande, P. L. Nguyen, E. M. Callaway, A. Ghosh, and A. D. Huberman
2014. A dedicated circuit links direction-selective retinal ganglion cells to the primary visual cortex. *Nature*, 507:358–361. (Cited on page 3.)
- Cuntz, H., A. Borst, and I. Segev
2007. Optimization principles of dendritic structure. *Theoretical biology & medical modelling*, 4:21. (Cited on page 156.)
- Dayan, P. and L. F. Abbott
2005. *Theoretical Neuroscience: Computational and Mathematical Modelling of Neural Systems*. The MIT Press. (Cited on page 159.)
- Denk, W. and H. Horstmann
2004. Serial Block-Face Scanning Electron Microscopy to Reconstruct Three-Dimensional Tissue Nanostructure. *PLoS Biology*, 2(11):1900–1909. (Cited on page 5.)

- Denk, W., J. H. Strickler, and W. W. Webb
1990. Two-photon laser scanning fluorescence microscopy. *Science*, 248:73–76. (Cited on page 5.)
- Dvorak, D. R., L. G. Bishop, and H. E. Eckert
1975. On the identification of movement detectors in the fly optic lobe. *Journal of Comparative Physiology*, 100:5–23. (Cited on page 155.)
- Easter, S. S. and P. R. Johns
1974. Horizontal compensatory eye movements in goldfish (*Carassius auratus*). *Journal of Comparative Physiology*, 92(1):37–57. (Cited on page 155.)
- Ebrey, T. and Y. Koutalos
2001. Vertebrate Photoreceptors. *Progress in Retinal and Eye Research*, 20(1):49–94. (Cited on page 12.)
- Egelhaaf, M. and A. Borst
1995. Calcium Accumulation in Visual Interneurons of the Fly: Stimulus Dependence and Relationship to Membrane Potential. *Journal of Neurophysiology*, 73:2540–2552. (Cited on page 159.)
- Eichner, H. and A. Borst
2011. Hands-on parameter search for neural simulations by a MIDI-controller. *PloS one*, 6(10):e27013. (Cited on page 148.)
- Eichner, H., M. Joesch, B. Schnell, D. F. Reiff, and A. Borst
2011. Internal structure of the fly elementary motion detector. *Neuron*, 70:1155–1164. (Cited on page 153.)
- Fendl, S.
2014. Synaptic receptor mRNA profiling in motion-sensitive neurons of the *Drosophila* visual system. (Cited on page 154.)
- Fenko, L., O. Yizhar, and K. Deisseroth
2011. The Development and Application of Optogenetics. *Annual Review of Neuroscience*, 34(1):389–412. (Cited on page 10.)
- Field, G. D. and E. J. Chichilnisky
2007. Information processing in the primate retina: circuitry and coding. *Annual Review of Neuroscience*, 30:1–30. (Cited on page 152.)
- Fischbach, K. F. and A. P. Dittrich
1989. The optic lobe of *Drosophila melanogaster*. I. A Golgi analysis of wild-type structure. *Cell & Tissue Research*. (Cited on pages 4, 14, 15, and 17.)
- Fish, M. P., A. C. Groth, M. P. Calos, and R. Nusse
2007. Creating transgenic *Drosophila* by microinjecting the site-specific phiC31 integrase mRNA and a transgene-containing donor plasmid. *Nature Protocols*, 2(10):2325–2331. (Cited on page 7.)
- Fisher, Y. E., J. C. S. Leong, K. Sporar, M. D. Ketkar, D. M. Gohl, and T. R. Clandinin
2015a. A Class of Visual Neurons with Wide-Field Properties Is Required for Local Motion Detection. *Current Biology*, 25:1–12. (Cited on page 159.)

- Fisher, Y. E., M. Silies, and T. R. Clandinin
2015b. Orientation Selectivity Sharpens Motion Detection in *Drosophila*. *Neuron*, 88:1–14. (Cited on pages 148, 149, and 158.)
- Flight, M. H.
2013. Visual system: Mapping motion detection. *Nature Reviews Neuroscience*, 14. (Cited on page 19.)
- Gabbiani, F., H. G. Krapp, C. Koch, and G. Laurent
2002. Multiplicative computation in a visual neuron sensitive to looming. *Nature*, 420(6913):320–324. (Cited on page 150.)
- Ghosh, K. K., S. Bujan, S. Haverkamp, A. Feigenspan, and H. Wässle
2004. Types of Bipolar Cells in the Mouse Retina. *Journal of Comparative Neurology*, 469(1):70–82. (Cited on page 152.)
- Gilbert, C.
2013. Brain connectivity: Revealing the fly visual motion circuit. *Current Biology*, 23(18):R851–R853. (Cited on page 19.)
- Gjorgjieva, J., H. Sompolinsky, and M. Meister
2014. Benefits of pathway splitting in sensory coding. *Journal of Neuroscience*, 34(36):12127–44. (Cited on page 153.)
- Gollisch, T. and M. Meister
2010. Eye Smarter than Scientists Believed: Neural Computations in Circuits of the Retina. *Neuron*, 65(2):150–164. (Cited on page 2.)
- Gordon, M. D. and K. Scott
2009. Motor control in a *Drosophila* taste circuit. *Neuron*, 61(3):373–84. (Cited on page 11.)
- Götz, K. G.
1964. Optomotorische Untersuchung des visuellen Systems einiger Augenmutanten der Fruchtfliege *Drosophila*. *Kybernetik*, 2(2):77–92. (Cited on pages 4, 155, and 156.)
- Götz, K. G.
1987. Course-control, metabolism and wing interference during ultralong tethered flight in *Drosophila melanogaster*. *Journal of Experimental Biology*, 128(1):35–46. (Cited on page 156.)
- Greenspan, R. J.
2008. The origins of behavioral genetics. *Current Biology*, 18(5):192–198. (Cited on page 6.)
- Grether, M. E., J. M. Abrams, J. Agapite, K. White, and H. Steller
1995. The head involution defective gene of *Drosophila melanogaster* functions in programmed cell death. *Genes and Development*, 9(14):1694–1708. (Cited on page 9.)
- Grienberger, C. and A. Konnerth
2012. Imaging Calcium in Neurons. *Neuron*, 73(5):862–885. (Cited on page 8.)

- Gunaydin, L. A., O. Yizhar, A. Berndt, V. S. Sohal, K. Deisseroth, and P. Hegemann
2010. Ultrafast optogenetic control. *Nature Neuroscience*, 13(3):387–392. (Cited on page 10.)
- Guo, Z. V., A. C. Hart, and S. Ramanathan
2009. Optical interrogation of neural circuits in *Caenorhabditis elegans*. *Nature Methods*, 6(12):891–6. (Cited on page 11.)
- Haag, J. and A. Borst
1998. Active Membrane Properties and Signal Encoding in Graded Potential Neurons. *Journal of Neuroscience*, 18(19):7972–7986. (Cited on page 15.)
- Haag, J. and A. Borst
2001. Recurrent network interactions underlying flow-field selectivity of visual interneurons. *Journal of Neuroscience*, 21(15):5685–92. (Cited on page 5.)
- Haag, J. and A. Borst
2004. Neural mechanism underlying complex receptive field properties of motion-sensitive interneurons. *Nature Neuroscience*, 7(6):628–34. (Cited on page 15.)
- Haag, J. and A. Borst
2005. Dye-coupling visualizes networks of large-field motion-sensitive neurons in the fly. *Journal of Comparative Physiology. A*, 191(5):445–454. (Cited on page 156.)
- Haag, J., W. Denk, and A. Borst
2004. Fly motion vision is based on Reichardt detectors regardless of the signal-to-noise ratio. *Proceedings of the National Academy of Sciences of the USA*, 101(46):16333–8. (Cited on page 5.)
- Haag, J., A. Wertz, and A. Borst
2007. Integration of lobula plate output signals by DNOVS₁, an identified premotor descending neuron. *Journal of Neuroscience*, 27(8):1992–2000. (Cited on page 156.)
- Haag, J., A. Wertz, and A. Borst
2010. Central gating of fly optomotor response. *Proceedings of the National Academy of Sciences*, 107(46):20104 – 20109. (Cited on page 155.)
- Hadjikhani, N., a. K. Liu, a. M. Dale, P. Cavanagh, and R. B. Tootell
1998. Retinotopy and color sensitivity in human visual cortical area V8. *Nature Neuroscience*, 1(3):235–41. (Cited on page 2.)
- Haikala, V., M. Joesch, A. Borst, and A. S. Mauss
2013. Optogenetic control of fly optomotor responses. *Journal of Neuroscience*, 33(34):13927–34. (Cited on pages 11, 155, and 156.)
- Hamada, F. N., M. Rosenzweig, K. Kang, S. R. Pulver, A. Ghezzi, T. J. Jegla, and P. A. Garrity
2008. An internal thermal sensor controlling temperature preference in *Drosophila*. *Nature*, 454:217–220. (Cited on page 9.)

- Hardie, R. C. and M. Juusola
2015. Phototransduction in *Drosophila*. *Current Opinion in Neurobiology*, 34:37–45. (Cited on page 12.)
- Hardie, R. C. and P. Raghu
2001. Visual transduction in *Drosophila*. *Nature*, 413(6852):186–193. (Cited on page 12.)
- Hashimoto, T., S. Katai, Y. Saito, F. Kobayashi, and T. Goto
2013. ON and OFF channels in human retinal ganglion cells. *The Journal of Physiology*, 591:327–37. (Cited on page 152.)
- Hassenstein, B.
1951. Ommatidienraster und Afferente Bewegungsintegration (Versuche an dem Rüsselkäfer *Chlorophanus viridis*). *Zeitschrift für vergleichende Physiologie*, 33:301–326. (Cited on pages 2, 3, and 155.)
- Hassenstein, B. and W. Reichardt
1956. Systemtheoretische Analyse der Zeit-, Reihenfolgen- und Vorzeichenauswertung bei der Bewegungspertzeption des Rüsselkäfers *Chlorophanus*. *Zeitschrift für Naturforschung*, 11:513–524. (Cited on pages 3, 4, 148, and 155.)
- Hausen, K.
1976. Functional Characterization and Anatomical Identification of Motion Sensitive Neurons in the Lobula plate of the Blowfly *Calliphora erythrocephala*. *Zeitschrift für Naturforschung*, 31c:629–633. (Cited on pages 5, 15, and 16.)
- Hausen, K.
1984. The lobula-complex of the fly: structure, function and significance in visual behaviour. In *Photoreception and Vision in Invertebrates*, M. Ali, ed., volume 74, Pp. 523–559. New York: Plenum Press. (Cited on pages 154 and 155.)
- Hausen, K. and C. Wehrhahn
1983. Microsurgical Lesion of Horizontal Cells Changes Optomotor Yaw Responses in the Blowfly *Calliphora erythrocephala*. *Proceedings of the Royal Society B: Biological Sciences*, 219(1215):211–216. (Cited on page 155.)
- Heim, R., D. C. Prasher, and R. Tsien
1994. Wavelength mutations and posttranslational autoxidation of green fluorescent protein. *Proceedings of the National Academy of Sciences*, 91:12501 – 12504. (Cited on page 8.)
- Heisenberg, M., R. Wonneberger, and R. Wolf
1978. Optomotor-blindH31-a *Drosophila* mutant of the lobula plate giant neurons. *Journal of Comparative Physiology*, 124(4):287–296. (Cited on pages 15 and 155.)
- Helmstaedter, M., K. L. Briggman, S. C. Turaga, V. Jain, H. S. Seung, and W. Denk
2013. Connectomic reconstruction of the inner plexiform layer in the mouse retina. *Nature*, 500(7461):168–74. (Cited on pages 5 and 11.)

- Hengstenberg, R., K. Hausen, and B. Hengstenberg
1982. The number and structure of giant vertical cells (VS) in the lobula plate of the blowfly *Calliphora erythrocephala*. *Journal of Comparative Physiology A*, 149:163–177. (Cited on page 15.)
- Herz, R. S., J. Eliassen, S. Beland, and T. Souza
2004. Neuroimaging evidence for the emotional potency of odor-evoked memory. *Neuropsychologia*, 42(3):371–378. (Cited on page 1.)
- Hess, B. J. M., W. Precht, A. Reber, and L. Cazin
1985. Horizontal optokinetic ocular nystagmus in the pigmented rat. *Neuroscience*, 15(1):97–107. (Cited on page 155.)
- Hille, B.
2001. *Ion Channels of Excitable Membranes*, 3 edition. Sunderland, MA: Sinauer Associates Inc. (Cited on page 8.)
- Hodgkin, A. and A. Huxley
1952. A quantitative description of membrane current and its application to conduction and excitation in nerve. *Bulletin of Mathematical Biology*, 52(1-2):25–71. (Cited on page 5.)
- Hopp, E., A. Borst, and J. Haag
2014. Subcellular mapping of dendritic activity in optic flow processing neurons. *Journal of Comparative Physiology A*, 200(5):359–70. (Cited on page 155.)
- Hubel, D. H. and T. N. Wiesel
1968. Receptive Fields and Functional Architecture. *Journal of Physiology*, 195:215–243. (Cited on pages 2 and 3.)
- Huberman, A. D., W. Wei, J. Elstrott, B. K. Stafford, M. B. Feller, and B. a. Barres
2009. Genetic identification of an On-Off direction-selective retinal ganglion cell subtype reveals a layer-specific subcortical map of posterior motion. *Neuron*, 62(3):327–34. (Cited on page 3.)
- Huston, S. J. and H. G. Krapp
2008. Visuomotor transformation in the fly gaze stabilization system. *PLoS Biology*, 6(7):1468–1478. (Cited on page 155.)
- Isayama, T., B. J. O'Brien, I. Ugalde, J. F. Muller, A. Frenz, V. Aurora, W. Tsiaras, and D. M. Berson
2009. Morphology of Retinal Ganglion Cells in the Ferret (*Mustela putorius furo*). *Journal of Comparative Neurology*, 27(52):14299–14307. (Cited on page 152.)
- Janelia, R. C.
2015. http://emanalysis.janelia.org/flyem_tables.php.
- Jenett, A., G. M. Rubin, T.-T. B. Ngo, D. Shepherd, C. Murphy, H. Dionne, B. D. Pfeiffer, A. Cavallaro, D. Hall, J. Jeter, N. Iyer, D. Fetter, J. H. Hausenfluck, H. Peng, E. T. Trautman, R. R. Svirskas, E. W. Myers, Z. R. Iwinski, Y. Aso, G. M. DePasquale, A. Enos, P. Hulamm, S. C. B. Lam, H.-H. Li, T. R. Laverty, F. Long, L. Qu, S. D. Murphy, K. Rokicki, T. Safford, K. Shaw, J. H. Simpson, A. Sowell, S. Tae,

- Y. Yu, and C. T. Zugates
2012. A GAL4-driver line resource for *Drosophila* neurobiology. *Cell Reports*, 2(4):991–1001. (Cited on page 7.)
- Joesch, M., J. Plett, A. Borst, and D. F. Reiff
2008. Response properties of motion-sensitive visual interneurons in the lobula plate of *Drosophila melanogaster*. *Current Biology*, 18(5):368–74. (Cited on pages 5, 16, 17, 154, 155, and 156.)
- Joesch, M., B. Schnell, S. V. Raghun, D. F. Reiff, and A. Borst
2010. ON and OFF pathways in *Drosophila* motion vision. *Nature*, 468(7321):300–304. (Cited on pages 9, 16, and 152.)
- Joesch, M., F. Weber, H. Eichner, and A. Borst
2013. Functional specialization of parallel motion detection circuits in the fly. *Journal of Neuroscience*, 33(3):902–905. (Cited on page 148.)
- Johns, D. C., R. Marx, R. E. Mains, B. O'Rourke, and E. Marbán
1999. Inducible genetic suppression of neuronal excitability. *Journal of Neuroscience*, 19(5):1691–1697. (Cited on page 9.)
- Johnson, W. G. and H. E. Wildman
1983. Influence of external and covert food stimuli on insulin secretion in obese and normal persons. *Behavioral Neuroscience*, 97(6):1025–1028. (Cited on page 1.)
- Kastner, S., P. De Weerd, and L. G. Ungerleider
2000. Texture segregation in the human visual cortex: A functional MRI study. *Journal of Neurophysiology*, 83:2453–2457. (Cited on page 2.)
- Kauer, I., A. Borst, and J. Haag
2015. Complementary motion tuning in frontal nerve motor neurons of the blowfly. *Journal of Comparative Physiology A*. (Cited on pages 5 and 155.)
- Kim, J. S., M. J. Greene, A. Zlateski, K. Lee, M. Richardson, S. C. Turaga, M. Purcaro, M. Balkam, A. Robinson, B. F. Behabadi, M. Campos, W. Denk, and H. S. Seung
2014. Space-time wiring specificity supports direction selectivity in the retina. *Nature*, 509(7500):331–6. (Cited on pages 5 and 148.)
- Kitamoto, T.
2001. Conditional modification of behavior in *Drosophila* by targeted expression of a temperature-sensitive *shibire* allele in defined neurons. *Journal of Neurobiology*, 47(2):81–92. (Cited on pages 4 and 9.)
- Kleinfeld, D., A. Bharioke, P. Blinder, D. D. Bock, K. L. Briggman, D. B. Chklovskii, W. Denk, M. Helmstaedter, J. P. Kaufhold, W.-C. A. Lee, H. S. Meyer, K. D. Micheva, M. Oberlaender, S. Prohaska, R. C. Reid, S. J. Smith, S. Takemura, P. S. Tsai, and B. Sakmann
2011. Large-scale automated histology in the pursuit of connectomes. *Journal of Neuroscience*, 31(45):16125–38. (Cited on page 11.)
- Knoll, M. and E. Ruska
1932. Das Elektronenmikroskop. *Zeitschrift für Physik*, 79(9-10):699. (Cited on page 5.)

- Krapp, H. G., B. Hengstenberg, and R. Hengstenberg
1998. Dendritic structure and receptive-field organization of optic flow processing interneurons in the fly. *Journal of Neurophysiology*, 79(4):1902–1917. (Cited on page 155.)
- Kunze, P.
1961. Untersuchung des Bewegungssehens fixiert fliegender Bienen. *Zeitschrift für vergleichende Physiologie*, 44:656–684. (Cited on page 155.)
- Lai, S.-L. and T. Lee
2006. Genetic mosaic with dual binary transcriptional systems in *Drosophila*. *Nature Neuroscience*, 9(5):703–709. (Cited on page 7.)
- Land, M. F. and T. S. Collett
1974. Chasing Behavior of Houseflies (*Fannia canicularis*): A description and Analysis. *Journal of Comparative Physiology A*, 89:331–357. (Cited on pages 3 and 156.)
- Land, M. F. and D.-E. Nilsson
2012. *Animal Eyes*, second edition. Oxford Animal Biology Series. (Cited on pages 2 and 12.)
- Lee, T. and L. Luo
1999. Mosaic analysis with a repressible cell marker for studies of gene function in neuronal morphogenesis. *Neuron*, 22(3):451–61. (Cited on page 7.)
- Leonhardt, A., G. Ammer, M. Meier, E. Serbe, A. Bahl, and A. Borst
2016. Asymmetry of *Drosophila* ON and OFF motion detectors enhances real-world velocity estimation. *Nature Neuroscience*, 19(5):706–715. (Cited on page 119.)
- Lichtman, J. W., H. Pfister, and N. Shavit
2014. The big data challenges of connectomics. *Nature Neuroscience*, 17(11):1448–1454. (Cited on page 11.)
- Lima, S. Q. and G. Miesenböck
2005. Remote control of behavior through genetically targeted photostimulation of neurons. *Cell*, 121:141–152. (Cited on page 9.)
- Lin, J. Y., P. M. Knutsen, A. Muller, D. Kleinfeld, and R. Y. Tsien
2013. ReaChR: a red-shifted variant of channelrhodopsin enables deep transcranial optogenetic excitation. *Nature Neuroscience*, 16(10):1499–508. (Cited on page 10.)
- Lindsley, D. L. and G. G. Zimm
1992. *The New Redbook. The Genome of Drosophila melanogaster*. Academic Press. (Cited on page 7.)
- Luan, H., N. C. Peabody, C. R. Vinson, and B. H. White
2006. Refined Spatial Manipulation of Neuronal Function by Combinatorial Restriction of Transgene Expression. *Neuron*, 52(3):425–436. (Cited on page 7.)

- Luo, L., E. M. Callaway, and K. Svoboda
2008. Genetic Dissection of Neural Circuits. *Neuron*, 57(5):634–660. (Cited on page 6.)
- Maisak, M. S., J. Haag, G. Ammer, E. Serbe, M. Meier, A. Leonhardt, T. Schilling, A. Bahl, G. M. Rubin, A. Nern, B. J. Dickson, D. F. Reiff, E. Hopp, and A. Borst
2013. A directional tuning map of *Drosophila* elementary motion detectors. *Nature*, 500(7461):212–6. (Cited on page 19.)
- Malicki, J.
2000. Harnessing the power of forward genetics - Analysis of neuronal diversity and patterning in the zebrafish retina. *Trends in Neurosciences*, 23(11):531–541. (Cited on page 152.)
- Mank, M., D. F. Reiff, N. Heim, M. W. Friedrich, A. Borst, and O. Griesbeck
2006. A FRET-based calcium biosensor with fast signal kinetics and high fluorescence change. *Biophysical Journal*, 90(5):1790–6. (Cited on page 8.)
- Mank, M., A. F. Santos, S. Direnberger, T. D. Mrsic-Flogel, S. B. Hofer, V. Stein, T. Hendel, D. F. Reiff, C. Levelt, A. Borst, T. Bonhoeffer, M. Hübener, and O. Griesbeck
2008. A genetically encoded calcium indicator for chronic in vivo two-photon imaging. *Nature Methods*, 5(9):805–811. (Cited on page 8.)
- Masland, R. H.
2001. Neuronal diversity in the retina. *Current Opinion in Neurobiology*, 11(4):431–436. (Cited on page 2.)
- Masland, R. H.
2013. Accurate maps of visual circuitry. *Nature*, 500:4–5. (Cited on page 19.)
- Mauss, A., K. Pankova, A. Arenz, A. Nern, G. Rubin, and A. Borst
2015. Neural Circuit to Integrate Opposing Motions in the Visual Field. *Cell*, 162(2):351–362. (Cited on pages 154 and 160.)
- Mauss, A. S., M. Meier, E. Serbe, and A. Borst
2014. Optogenetic and pharmacologic dissection of feedforward inhibition in *Drosophila* motion vision. *Journal of Neuroscience*, 34(6):2254–2263. (Cited on page 72.)
- Meier, M., E. Serbe, M. S. Maisak, J. Haag, B. J. Dickson, and A. Borst
2014. Neural circuit components of the *Drosophila* OFF motion vision pathway. *Current Biology*, 24(4):385–392. (Cited on page 30.)
- Miyawaki, A., J. Llopis, R. Heim, J. M. McCaffery, J. a. Adams, M. Ikura, and R. Y. Tsien
1997. Fluorescent indicators for Ca²⁺ based on green fluorescent proteins and calmodulin. *Nature*, 388:882–887. (Cited on page 8.)

- Moffat, K. G., J. H. Gould, H. K. Smith, and C. J. O’Kane
 1992. Inducible cell ablation in *Drosophila* by cold-sensitive ricin A chain. *Development (Cambridge, England)*, 114(3):681–687. (Cited on page 9.)
- Morgan, T. H.
 1910. Sex limited inheritance in *Drosophila*. *Science*, 32(812):120–122. (Cited on page 4.)
- Mronz, M. and F.-O. Lehmann
 2008. The free-flight response of *Drosophila* to motion of the visual environment. *The Journal of Experimental Biology*, 211(13):2026–2045. (Cited on page 156.)
- Muller, H. J.
 1928. The production of mutations by X-Rays. *Proceedings of the National Academy of Sciences*, 14:714–726. (Cited on page 6.)
- Nagel, G., M. Brauner, J. F. Liewald, N. Adeishvili, E. Bamberg, and A. Gottschalk
 2005. Light Activation of Channelrhodopsin-2 in Excitable Cells of *Caenorhabditis elegans* Triggers Rapid Behavioral Responses. *Current Biology*, 15(24):2279–2284. (Cited on page 10.)
- Neuhauss, S. C., O. Biehlmaier, M. W. Seeliger, T. Das, K. Kohler, W. A. Harris, and H. Baier
 1999. Genetic disorders of vision revealed by a behavioral screen of 400 essential loci in zebrafish. *Journal of Neuroscience*, 19(19):8603–8615. (Cited on page 155.)
- Nordström, K.
 2012. Neural specializations for small target detection in insects. *Current Opinion in Neurobiology*, 22(2):272–278. (Cited on page 3.)
- Nüsslein-Volhard, C. and E. Wieschaus
 1980. Mutations affecting segment number and polarity in *Drosophila*. *Nature*, 287:795–801. (Cited on page 4.)
- Ohkura, M., M. Matsuzaki, H. Kasai, K. Imoto, and J. Nakai
 2005. Genetically encoded bright Ca²⁺ probe applicable for dynamic Ca²⁺ imaging of dendritic spines. *Analytical Chemistry*, 77(18):5861–5869. (Cited on page 8.)
- Osorio, D. and J. P. Bacon
 1994. A Good Eye for Arthropod Evolution. *BioEssays*, 16(6):419 – 424. (Cited on page 12.)
- Portugues, R. and F. Engert
 2009. The neural basis of visual behaviors in the larval zebrafish. *Current Opinion in Neurobiology*, 19(6):644–647. (Cited on page 12.)
- Pulver, S. R., S. L. Pashkovski, N. J. Hornstein, P. a. Garrity, and L. C. Griffith
 2009. Temporal dynamics of neuronal activation by Channelrhodopsin-2 and TRPA₁ determine behavioral output in *Drosophila* larvae. *Journal of Neurophysiology*, 101(6):3075–3088. (Cited on page 9.)

- Quian Quiroga, R., L. Reddy, G. Kreiman, C. Koch, and I. Fried
2005. Invariant visual representation by single neurons in the human brain. *Nature*, 435(7045):1102–1107. (Cited on page 2.)
- Rajashekhar, K. P. and V. R. Shamprasad
2004. Golgi analysis of tangential neurons in the lobula plate of *Drosophila melanogaster*. *Journal of Biosciences*, 29(1):93–104. (Cited on page 17.)
- Ready, D. F., T. E. Hanson, and S. Benzer
1976. Development of the *Drosophila* retina, a neurocrystalline lattice. *Developmental Biology*, 53(2):217–240. (Cited on page 12.)
- Reichardt, W. and H. Wenking
1969. Optical detection and fixation of objects by fixed flying flies. *Die Naturwissenschaften*, 56(8):424. (Cited on page 2.)
- Reiff, D. F. and A. Borst
2008. Advances in studying neural circuit function with genetic probes for calcium. *Cell Science Reviews*, 5(2). (Cited on page 8.)
- Reiff, D. F., J. Plett, M. Mank, O. Griesbeck, and A. Borst
2010. Visualizing retinotopic half-wave rectified input to the motion detection circuitry of *Drosophila*. *Nature Neuroscience*, 13(8):973–8. (Cited on page 8.)
- Rivera-Alba, M., S. N. Vitaladevuni, Y. Mishchenko, Y. Mischenko, Z. Lu, S.-Y. Takemura, L. Scheffer, I. A. Meinertzhagen, D. B. Chklovskii, and G. G. de Polavieja
2011. Wiring economy and volume exclusion determine neuronal placement in the *Drosophila* brain. *Current Biology*, 21(23):2000–5. (Cited on page 14.)
- Rubin, G. M. and a. C. Spradling
1982. Genetic transformation of *Drosophila* with transposable element vectors. *Science*, 218(4570):348–353. (Cited on page 6.)
- Sakmann, B. and E. Neher
1984. Patch Clamp Techniques Ionic Channels in Excitable Membranes. *Annual Reviews Physiology*, 46:455–472. (Cited on page 5.)
- Sarthy, P. V.
1991. Histamine: a neurotransmitter candidate for *Drosophila* photoreceptors. *Journal of Neurochemistry*, 57(5):1757–68. (Cited on page 12.)
- Schiller, P. H.
1992. The ON and OFF channels of the visual system. *Trends in Neurosciences*, 15(3):86–92. (Cited on page 152.)
- Schiller, P. H., J. H. Sandell, and J. H. R. Maunsell
1986. Functions of the ON and OFF channels of the visual system. *Nature*, 322:824–825. (Cited on page 152.)

- Schnell, B., M. Joesch, F. Forstner, S. V. Raghu, H. Otsuna, K. Ito, A. Borst, and D. F. Reiff
2010. Processing of horizontal optic flow in three visual interneurons of the *Drosophila* brain. *Journal of Neurophysiology*, 103(3):1646–57. (Cited on pages 16, 155, and 156.)
- Schobert, B. and J. K. Lanyi
1982. Halorhodopsin is a light-driven chloride pump. *Journal of Biological Chemistry*, 257(17):10306–10313. (Cited on page 11.)
- Scholl, B., X. Gao, and M. Wehr
2010. Nonoverlapping Sets of Synapses Drive On Responses and Off Responses in Auditory Cortex. *Neuron*, 65(3):412–421. (Cited on page 152.)
- Scott, E. K., T. Raabe, and L. Luo
2002. Structure of the vertical and horizontal system neurons of the lobula plate in *Drosophila*. *Journal of Comparative Neurology*, 454(4):470–481. (Cited on page 156.)
- Segev, R., J. Puchalla, and M. J. Berry
2006. Functional organization of ganglion cells in the salamander retina. *Journal of Neurophysiology*, 95:2277–2292. (Cited on page 152.)
- Serbe, E., M. Meier, A. Leonhardt, and A. Borst
2016. Comprehensive Characterization of the Major Presynaptic Elements to the *Drosophila* OFF Motion Detector. *Neuron*, 89:829–841. (Cited on page 44.)
- Shimomura, O., F. H. Johnson, and Y. Saiga
1962. Extraction, purification and properties of aequorin, a bioluminescent protein from the luminous hydromedusan, *Aequorea*. *Journal of Cellular and Comparative Physiology*, 59(165):223–239. (Cited on page 8.)
- Shinomiya, K., T. Karuppudurai, T. Y. Lin, Z. Lu, C. H. Lee, and I. A. Meinertzhagen
2014. Candidate neural substrates for off-edge motion detection in *Drosophila*. *Current Biology*, 24(10):1062–1070. (Cited on pages 17 and 152.)
- Silies, M., D. M. Gohl, Y. E. Fisher, L. Freifeld, D. A. Clark, and T. R. Clandinin
2013. Modular use of peripheral input channels tunes motion-detecting circuitry. *Neuron*, 79(1):111–27. (Cited on page 158.)
- Strausfeld, N. J. and J. K. Lee
1991. Neuronal basis for parallel visual processing in the fly. *Visual Neuroscience*, 7:13–33. (Cited on pages 5 and 15.)
- Strausfeld, N. J., H. S. Seyan, and J. J. Milde
1987. The neck motor system of the fly *Calliphora erythrocephala* - I. Muscles and motor neurons. *Journal of Comparative Physiology A*, 160(2):205–224. (Cited on page 155.)

- Straw, A. D., K. Branson, T. R. Neumann, and M. H. Dickinson
2011. Multi-camera real-time three-dimensional tracking of multiple flying animals. *Journal of the Royal Society, Interface*, 8(56):395–409. (Cited on page 156.)
- Sun, W., Z. Tan, B. D. Mensh, and N. Ji
2015. Thalamus provides layer 4 of primary visual cortex with orientation- and direction-tuned inputs. *Nature Neuroscience*, 19:308–315. (Cited on page 3.)
- Suster, M. L., L. Seugnet, M. Bate, and M. B. Sokolowski
2004. Refining GAL4-driven transgene expression in *Drosophila* with a GAL80 enhancer-trap. *Genesis*, 39:240–245. (Cited on page 7.)
- Sweeney, S. T., K. Broadie, J. Keane, H. Niemann, and C. J. O’Kane
1995. Targeted expression of tetanus toxin light chain in *Drosophila* specifically eliminates synaptic transmission and causes behavioral defects. *Neuron*, 14(2):341–351. (Cited on page 9.)
- Takemura, S.-y.
2014. Connectome of the fly visual circuitry. *Microscopy*, 64:37–44. (Cited on page 150.)
- Takemura, S.-y., A. Bharioke, Z. Lu, A. Nern, S. Vitaladevuni, P. K. Rivlin, W. T. Katz, D. J. Olbris, S. M. Plaza, P. Winston, T. Zhao, J. A. Horne, R. D. Fetter, S. Takemura, K. Blazek, L.-A. Chang, O. Ogundeyi, M. a. Saunders, V. Shapiro, C. Sigmund, G. M. Rubin, L. K. Scheffer, I. A. Meinertzhagen, and D. B. Chklovskii
2013. A visual motion detection circuit suggested by *Drosophila* connectomics. *Nature*, 500(7461):175–81. (Cited on pages 5, 17, and 150.)
- Takemura, S.-y., T. Karuppudurai, C.-Y. Ting, Z. Lu, C.-H. Lee, and I. A. Meinertzhagen
2011. Cholinergic circuits integrate neighboring visual signals in a *Drosophila* motion detection pathway. *Current Biology*, 21(24):2077–2084. (Cited on pages 15, 16, and 152.)
- Tuthill, J. C. and B. G. Borghuis
2016. Four to Foxtrot: How Visual Motion Is Computed in the Fly Brain. *Neuron*, 89:677–680. (Cited on page 44.)
- Tuthill, J. C., A. Nern, S. L. Holtz, G. M. Rubin, and M. B. Reiser
2013. Contributions of the 12 neuron classes in the fly lamina to motion vision. *Neuron*, 79(1):128–40. (Cited on page 158.)
- Wasserman, S. M., J. W. Aptekar, P. Lu, J. Nguyen, A. L. Wang, M. F. Keles, A. Grygoruk, D. E. Krantz, C. Larsen, and M. A. Frye
2015. Olfactory Neuromodulation of Motion Vision Circuitry in *Drosophila*. *Current Biology*, 25:467–472. (Cited on page 156.)
- Wässle, H.
2004. Parallel processing in the mammalian retina. *Nature Reviews Neuroscience*, 5(10):747–757. (Cited on pages 3 and 148.)
- Wässle, H. and B. B. Boycott
1991. Functional architecture of the mammalian retina. *Physiological Reviews*, 71(2):447–480. (Cited on page 152.)

- Weber, F., H. Eichner, H. Cuntz, and a. Borst
2008. Eigenanalysis of a neural network for optic flow processing. *New Journal of Physics*, 10(1):015013. (Cited on page 156.)
- Werblin, F. and J. Dowling
1969. Organization of the retina of the mudpuppy, *Neturus maculosis*. II. Intracellular recording. *Journal of Neurophysiology*, 32:339–355. (Cited on page 152.)
- Wertz, A., A. Borst, and J. Haag
2008. Nonlinear integration of binocular optic flow by DNOVS2, a descending neuron of the fly. *Journal of Neuroscience*, 28(12):3131–40. (Cited on page 16.)
- Wertz, A., B. Gaub, J. Plett, J. Haag, and A. Borst
2009. Robust coding of ego-motion in descending neurons of the fly. *Journal of Neuroscience*, 29(47):14993–5000. (Cited on page 156.)
- Westheimer, G.
2007. The ON-OFF dichotomy in visual processing: From receptors to perception. *Progress in Retinal and Eye Research*, 26(6):636–648. (Cited on page 152.)
- White, J., E. Southgate, J. Thomson, and F. Brenner
1986. The structure of the nervous system of the nematode *Caenorhabditis elegans*. *Philosophical transactions of the Royal Society of London. Series B, Biological sciences*, 314:1–340. (Cited on page 5.)
- Wilson, R. I., G. C. Turner, and G. Laurent
2004. Transformation of Olfactory Representations in the *Drosophila* Antennal Lobe. *Science*, 303:366–371. (Cited on page 5.)
- Yamaguchi, S., R. Wolf, C. Desplan, and M. Heisenberg
2008. Motion vision is independent of color in *Drosophila*. *Proceedings of the National Academy of Sciences of the United States of America*, 105(12):4910–5. (Cited on page 13.)
- Yarfitz, S. and J. B. Hurley
1994. Transduction mechanisms of vertebrate and invertebrate photoreceptors. *Journal of Biological Chemistry*, 269(20):14329–14332. (Cited on page 12.)
- Yeomans, M. R.
2006. Olfactory influences on appetite and satiety in humans. *Physiology and Behavior*, 89(1):10–14. (Cited on page 1.)
- Yonehara, K. and B. Roska
2013. Motion detection: neuronal circuit meets theory. *Cell*, 154(6):1188–9. (Cited on page 19.)
- Zhang, F., L.-P. Wang, M. Brauner, J. F. Liewald, K. Kay, N. Watzke, P. G. Wood, E. Bamberg, G. Nagel, A. Gottschalk, and K. Deisseroth
2007. Multimodal fast optical interrogation of neural circuitry. *Nature*, 446(7136):633–639. (Cited on page 11.)

LIST OF FIGURES

Figure 1	Hassenstein-Reichardt correlator	3
Figure 2	<i>Drosophila</i> genetics	10
Figure 3	Compound eyes	14
Figure 4	The fly visual system	17
Figure 5	Models for direction selectivity	149
Figure 6	Biophysical implementation of nonlinearity	151
Figure 7	Edges and opposing edges	157
Figure 8	Comparison between voltage and calcium signals	158

ACKNOWLEDGEMENTS

First of all I would like to thank Axel Borst for being a very helpful, understanding and inspiring supervisor throughout my time in his lab. He provided me with the fruitful combination of scientific guidance and experimental freedom that ensured successful academic results but also a very enjoyable working atmosphere. I could develop my own strategies, pursue my ideas aside beaten tracks but also count on support in times of doubt. The cooperative and amicable environment in our lab made every day from my bachelors thesis until the end of my PhD thesis a positive and formative experience.

I would furthermore like to express my gratitude to many people I could interact with on a scientific level. Very importantly I want to thank Etienne, my good friend and collaborator with whom I have spent a lot of time already during our undergraduate studies. With him I have shared office space, setups and publications. Max introduced me to the lab as a young and inexperienced Bachelor student, supervised my lab thesis and taught me a lot about science and the associated life. Friedrich, Hubert and Jones shared a considerable amount of technical and computational expertise that greatly eased the early years of my time in the lab. Moreover I want to thank Aljoscha and Armin for deep, thought-provoking discussions, revitalizing breaks and great companionship. Further, I would like to thank Bulle for supporting me with his incredible experimental knowledge and experience and being an excellent "Neben-Chef" at conferences. I am grateful to Georg, Alexander and Micky-D for many fruitful conversations about confusing data and future experiments. Michi, Stefan, Wolfgang, Chrissy, and Romina for help with fly-work, electrical engineering, immunostainings and other technical assistance. In general I want to thank the whole Borst lab for an unforgettable time, scientific success, great Happy Hours, retreats and sports events. I would also like thank my TAC members Alex and Lars for important scientific input, and especially Alex and Alison for reading and improving this manuscript.

Finally I want to thank my entire family, all of my friends and most importantly Marion for their unconditional support also during difficult times. Without you these past years would not have been such a meaningful and enjoyable episode.

Curriculum Vitae

Matthias Meier

Date of birth: 14.12.1987

Education

- Max Planck Institute for Neuroscience Martinsried, Germany – PhD 2011 - 2016
 - PhD Thesis "Functional characterization of the neural components in *Drosophila* motion vision"
 - Department: Circuits – Computations – Models, Prof. Alexander Borst
- Ludwig Maximilian Universität Munich, Germany – BSc 2007 - 2011
 - Fakultät für Biologie, BSc 240 ECTS
- Aventinus Gymnasium Burghausen, Germany – Highschool diploma 2007

Conferences and meetings

- Jul 2012 – **FENS meeting**, Barcelona attendance
- Oct 2012 – **SFB 870 retreat**, Kloster Seon attendance
- Aug 2013 – **International conference on invertebrate vision**, Bäckaskog, Sweden . . . poster
- Oct 2013 – **Munich fly retreat**, Ringberg castle oral presentation
- Jul 2014 – **FENS meeting**, Milan poster
- Oct 2015 – **MCN-QBI meeting**, Brisbane oral presentation

Personal information

- Nationality
 - German
- Personal interests
 - Sports
 - Football, rock climbing, skiing, mountaineering
- Languages
 - German — native
 - English — fluent
 - French — fluent

Publications

- Matthew S. Maisak, Jürgen Haag, Georg Ammer, Etienne Serbe, **Matthias Meier**, Aljoscha Leonhardt, Tabea Schilling, Armin Bahl, Gerald M. Rubin, Aljoscha Nern, Barry J. Dickson, Dierk Reiff, Elisabeth Hopp, and Alexander Borst (2013) A directional tuning map of *Drosophila* elementary motion detectors. *Nature* 500:212-216
- Alex S. Mauss, **Matthias Meier**, Etienne Serbe, and Alexander Borst (2014) Optogenetic and pharmacologic dissection of feedforward inhibition in *Drosophila* motion vision. *J Neurosci* 34:2254-2263
- **Matthias Meier**, Etienne Serbe, Matthew S. Maisak, Jürgen Haag, Barry J. Dickson, and Alexander Borst (2014) Neural Circuit Components of the *Drosophila* OFF Motion Vision Pathway. *Curr Biol* 24:385-392
- Armin Bahl, Etienne Serbe, **Matthias Meier**, Georg Ammer, and Alexander Borst (2015) Neural Mechanisms for *Drosophila* Contrast Vision. *Neuron* 88:1240-1252
- Etienne Serbe, **Matthias Meier**, Aljoscha Leonhardt, and Alexander Borst (2016) Comprehensive Characterization of the Major Presynaptic Elements to the *Drosophila* OFF Motion Detector. *Neuron* 89:829-841
- Aljoscha Leonhardt, Georg Ammer, **Matthias Meier**, Etienne Serbe, Armin Bahl, and Alexander Borst (2016) Asymmetry of *Drosophila* ON and OFF motion detectors enhances real-world velocity estimation. *Nature Neurosci* 19:706-715

Eidesstattliche Versicherung/Affidavit

Hiermit versichere ich an Eides statt, dass ich die vorliegende Dissertation "**Functional characterization of the neural components in *Drosophila* motion detection**" selbständig angefertigt habe, mich außer der angegebenen keiner weiteren Hilfsmittel bedient und alle Erkenntnisse, die aus dem Schrifttum ganz oder annähernd übernommen sind, als solche kenntlich gemacht und nach ihrer Herkunft unter Bezeichnung der Fundstelle einzeln nachgewiesen habe.

I hereby confirm that the dissertation "**Functional characterization of the neural components in *Drosophila* motion detection**" is the result of my own work and that I have only used sources or materials listed and specified in the dissertation.

.....
München, den
Munich, date

.....
Unterschrift
Signature

List of publications and author contributions

- Maisak MS¹, Haag J¹, Ammer G, Serbe E, **Meier M**, Leonhardt A, Schilling T, Bahl A, Rubin GM, Nern A, Dickson BJ, Reiff DF, Hopp E and Borst A. (2013) A Directional Tuning Map of *Drosophila* Elementary Motion Detectors. *Nature* 500: 212-216.
 - M.S.M. and J.H. jointly performed and, together with A.Bo., evaluated all calcium imaging experiments. G.A., E.S. and **M.M.** recorded from tangential cells. A.L., T.S. and A.Ba. performed the behavioral experiments. G.M.R., B.J.D. and A.N. generated the driver lines and characterized their expression pattern. D.F.R. performed preliminary imaging experiments. E.H. helped with programming and developed the PMT shielding for the two-photon microscope. A.Bo. designed the study and wrote the manuscript with the help of all authors.
- Mauss AS, **Meier M**, Serbe E and Borst A. (2014) Optogenetic and Pharmacologic Dissection of Feedforward Inhibition in *Drosophila* Motion Vision. *Journal of Neuroscience* 34(6): 2254-2263.
 - A.S.M. and A.B. designed research; A.S.M., **M.M.**, and E.S. performed research; A.B. contributed unpublished reagents/-analytic tools; A.S.M., **M.M.**, E.S., and A.B. analyzed data; A.S.M. and A.B. wrote the paper.
- **Meier M**¹, Serbe E¹, Maisak MS, Haag J, Dickson BJ and Borst A. (2014) Neural Circuit Components of the *Drosophila* OFF Motion Vision Pathway. *Current Biology* 24: 385-392.
 - **M.M.**, E.S. and A.B. designed the study. **M.M.** and E.S. performed electrophysiological recordings. **M.M.**, E.S., M.S.M., and J.H. performed calcium imaging experiments. B.J.D. provided unpublished Gal4-lines. **M.M.**, E.S. and A.B. wrote the paper with help of the other authors.
- Bahl A, Serbe E, **Meier M**, Ammer G and Borst A (2015). Neural Mechanisms for *Drosophila* Contrast Vision. *Neuron* 88(6): 1240-1252.
 - A.Ba. and A.Bo. designed the study. E.S. and **M.M.** performed electrophysiological recordings. G.A. provided the Mi1, Tm3, and Mi1/Tm3-Gal4 lines and did the immunostainings. A.Ba. built the behavioral setup, programmed the visual stimuli, performed the behavioral experiments, and analyzed the data. A.Ba. wrote the paper with help from the other authors.

- Serbe E¹, **Meier M**¹, Leonhardt A and Borst A (2016). Comprehensive characterization of the major presynaptic elements to the *Drosophila* OFF motion detector. *Neuron* 89(4): 829-841.
 - E.S. and **M.M.** jointly performed and evaluated all calcium imaging and electrophysiology experiments. A.L. performed and evaluated the behavioral experiments. A.L. and A.B. performed computer simulations. A.B., E.S., and **M.M.** designed the study. E.S. and **M.M.** wrote the manuscript with the help of the other authors.

- Leonhardt A¹, Ammer G¹, **Meier M**, Serbe E, Bahl A and Borst A (2016). Asymmetry of *Drosophila* ON and OFF motion detectors enhances real-world velocity estimation. *Nature Neuroscience* 19(5): 706-715
 - A.L., G.A. and A.Bo. designed the study. A.L. performed behavioral experiments, associated data analysis and all modeling work. G.A., **M.M.**, and E.S. performed electrophysiological experiments. G.A. performed calcium imaging. A.L. and G.A. analyzed physiological data. A. Ba. designed the behavioral apparatuses and performed behavioral experiments. A.L. wrote the manuscript with help from all of the authors.

.....

Matthias Meier	Prof. Dr. Alexander Borst	Etienne Serbe
	Supervisor	Co-first author

¹ equal contribution